University of Natural Resources and Life Sciences
Department of Forest and Soil Sciences
Institute of Forest Ecology

Supervisor:
Ao.Univ.Prof. Dipl.-Ing. Dr.nat.techn.
Torsten Winfried Berger

A modeling framework for temperate deciduous forest ecosystems with special emphasis on drought assessment and sulfur biogeochemistry at beech (*Fagus sylvatica* L.) stands in the Vienna Woods

Modellierung von Phänologie, Wasserbilanz, Bodentemperatur und Schwefelhaushalt auf ausgewählten Buchenstandorten (*Fagus sylvatica* L.) des Wienerwalds

Dissertation
to obtain a doctoral degree (Dr.nat.techn.)
at the University of Natural Resources and Life Sciences, Vienna

Submitted by
Dipl.-Ing. Klaus Dolschak

Vienna, July 2020

Acknowledgements

This doctoral thesis could not have been done without the help of many persons and institutions:

- First, I want to thank my supervisor and co-author Torsten W. Berger for his support during my thesis. I thank him for confidently granting me an excessive amount of freedom and trust in the way I was purchasing this goal.
- I thank him and Pétra Berger for working in the field and collecting solute samples over a 2-years period.
- I thank my colleges Alexander Muras, Michael Kaliwoda and Selina Türtscher for their help in the lab and support during the field campaign.
- Representative to all lab members of the Institute of Forest Ecology, I thank Marcel Hirsch for conducting various chemical analyses.
- I want to thank Ondřej Hanousek for conducting complex experiments, which brought priceless insights regarding the investigated forest stands' S biogeochemistry.
- For mentoring and encouragement, I want to thank Robert Jandl, Klaus Katzensteiner, and Douglas Godbold.
- Then, I want to thank my co-author Karl Gartner from the Austrian Research Centre for Forests.
- For the provision of data, I thank Helmut Schume, Thomas Bauer, Wolfgang Schöpp, Maximilian Posch, Sophia Mylona, and Matti Johansson.
- At last, I want to thank my partner Michaela Liedler for persistently encouraging me to finish this work.

This study was funded by the Austrian Science Fund (FWF, project number P23861-B16) and the Commission for Interdisciplinary Ecological Studies (KIÖS) at the Austrian Academy of Sciences (project number 2010-05), both granted to T.W. Berger. The Austrian Federal Ministry of Labor, Social Affairs and Consumer Protection provided financial support to me during a sabbatical for education.

Kurzfassung

In dieser Dissertation werden mehrere unterschiedliche Modelle vorgestellt, die zur Beschreibung biologischer, physikalischer und geochemischer Elemente des Systems Pflanze-Boden-Atmosphäre von Laubwaldstandorten der gemäßigten Zone dienen. Mehrere praktische Fallbeispiele illustrieren mögliche Anwendungsgebiete. Finales Hauptziel dieser Arbeit ist die modellhafte Beschreibung des Schwefelhaushalts bzw. der biogeochemischen Schwefeldynamik auf Buchenstandorten des Wienerwalds.

Im ersten Teil wird ein dynamisches Modell beschrieben, welches die Bodentemperatur von Waldstandorten in unterschiedlicher Bodentiefen vorhersagt. Als Input dient eine Zeitreihe der Lufttemperatur (Tagesmittelwerte). Um den Simulator an unterschiedliche Standorte anzupassen werden Punktmessungen der Bodentemperatur benötigt. Neun empirische Parameter werden über inverse Modellierung ermittelt. Der Simulator berücksichtigt den Effekt von Bodenfrost, sowie einer möglichen Schneebedeckung. Das Modell, welches ursprünglich für Waldstandorte konzipiert wurde, lässt sich auch an andere pflanzenbewachsene Standorte anpassen.

Das nächste Modul befasst sich mit der Phänologie von Buchenstandorten in Österreich. Die Schlüsselereignisse Blattaustrieb und Blattfall (Blattverfärbung) werden als Funktionen von Tageslänge und Lufttemperatur beschrieben.

Im folgenden Schritt wird ein hydrologisches Box-Modell für Buchenstandorte vorgestellt. Das *Wasserbilanz Modell* (WBM) verwendet meteorologische Parameter auf Tagesbasis, um den Wasseraustausch zwischen Pflanze, Boden und Atmosphäre zu quantifizieren. Ein Modul behandelt überirdische Prozesse wie Nebelniederschlag, Interzeption und Schneefall bzw. Schneeschmelze. Das Zweite beschäftigt sich mit bodenbezogenen Prozessen wie Infiltration, Oberflächenabfluss, Versickerung, Evaporation und Transpiration.

Neben den meteorologischen Kenngrößen benötigt das WBM das Resultat des phänologischen Modells als Input, um Schlüsselereignisse der Vegetationsperiode der untersuchten Waldstandorte zu quantifizieren. Das WBM wurde anhand von Zeitreihen der Bodenfeuchte an unterschiedlichen Buchenstandorte in Wien und Niederösterreich angepasst. Im nächsten Schritt wurde die ermittelte Parametrisierung genutzt, um eine Sensitivitätsanalyse durchzuführen. Dabei wurde die Lufttemperatur schrittweise erhöht, um einen möglichen Effekt einer Klimaerwärmung auf den Bodenwasserhaushalt zu prognostizieren. Eine Erwärmung um einen Grad Celsius bedingt eine ungefähre Verlängerung der Vegetationsperiode um 4,5 Tage. Der Blattaustrieb reagiert stärker aus der Blattfall. Durch längere Vegetationsperioden und höhere Bodenevaporation führt eine Erwärmung zu mehr Trockenstress im Hochsommer. Eine Verringerung der Transpiration in Sommermonaten wird über eine Steigerung dieser zu Beginn und am Ende einer verlängerten Vegetationsperiode kompensiert. Eine längere Vegetationsperiode bedeutet mehr Zeit für Assimilation. Gleichzeitig ist die modellierte Brutto-Primärproduktion bei Trockenstress im Sommer stark eingeschränkt. Verlängerte Vegetationsperioden können diese Einbuße nicht ausreichend kompensieren.

Im letzten Schritt wird ein Modell vorgestellt, mit dem sich die S-Biogeochemie von Buchenwald-Standorten beschreiben lässt (*Sulfur Dynamics Model*, SDM). Der Simulator baut auf dem Ergebnis der vorherigen Schritte auf. Das Ziel war die Identifikation und Quantifizierung aller Prozesse, welche unabdinglich für das Verständnis des S-Kreislaufs von Waldökosystemen sind. Betrachtet werden biotische sowie abiotische Austauschprozesse zwischen Pflanze Boden und Atmosphäre. Das SDM wurde an zwei Buchenstandorte im Wienerwald angepasst, die in einem Zeitraum von zwei Jahren engmaschig beprobt wurden. Ermittelt wurde, neben physikalischen Bodenparametern wie Bodenfeuchte und Bodentemperatur, die chemische Zusammensetzung von Bodenlösung sowie der atmosphärischen Deposition. Inverse Modellierung lieferte brauchbare Ergebnisse für beide Standorte: Es war nicht nur möglich die beobachtete zeitliche Dynamik der Sulfat-Konzentration in Bodenlösung nachzubilden. Auch das aktuelle Ungleichgewicht zwischen atmosphärischem Input und Versickerung bzw. Fließgewässer Output wird durch die Simulationen abgebildet. Das

Wechselspiel aus mikrobieller Immobilisation und Mineralisierung von organischem S wurde als wichtigster Treiber der kurzfristigen S-Dynamik in Bodenlösung ermittelt. Hingegen ist die langsame Mineralisation eines großen Pools von historisch akkumulierten S aus pflanzlicher Herkunft verantwortlich für den aktuell auf vielen Standorten beobachteten Export Überschuss. Adsorption bzw. Desorption spielt in den Simulationen an den untersuchten Standorten nur eine untergeordnete Rolle. Abschließend kann man sagen, dass ein Modell, welches auf gängigen Annahmen zum S-Kreislauf basiert, ausreichend ist, um die beobachtete S Dynamik der Buchenstandorte mit zufriedenstellender Genauigkeit zu beschreiben

Abstract

In this work, a set of hierarchical models is introduced, aiming to describe biological, physical and biogeochemical aspects of the plant-soil-atmosphere system of temperate, deciduous forest stands. Every presented simulator has applications on its own. As a digression, a drought assessment is performed for north-eastern Austrian beech forest stands. In the end, the presented simulators form the framework to describe the biogeochemical S dynamics of beech stands in the Vienna Woods.

In the first step, the setup and the application of an empirical model, based on Newton's law of cooling, capable to predict daily mean soil temperature (T_{soil}) under vegetated surfaces, is described. The only input variable, which is necessary to run the model, is a time series of the daily mean air temperature. The simulator employs nine empirical parameters, which were estimated by inverse modeling. The model, which primarily addresses forested sites, incorporates the effect of snow cover and soil freezing on soil temperature. It was applied to several temperate forest sites, managing the split between Central Europe (Austria) and the United States (Harvard Forest, Massachusetts; Hubbard Brook, New Hampshire), aiming to cover a broad range of site characteristics. Investigated stands differ fundamentally in stand composition, elevation, exposition, annual mean temperature, precipitation regime, as well as in the duration of winter snow cover. At last, to explore the limits of the formulation, the simulator was applied to non-forest sites (Illinois), where soil temperature was recorded under short cut grass. The model was parameterized, specifically to site and measurement depth. After calibration of the model, an evaluation was performed, using approximately 50 % of the available data. In each case, the simulator was capable to deliver a feasible prediction of soil temperature in the validation time interval. To evaluate the practical suitability of the simulator, the minimum amount of soil temperature point measurements, necessary to yield expedient model performance was determined. In the investigated case 13 to 20 point observations, uniformly distributed within an 11-year timeframe, have been proven sufficient to yield sound model performance (root mean square error <0.9 °C, Nash–Sutcliffe Efficiency >0.97). This makes the model suitable for the application on sites, where the information on soil temperature is discontinuous or scarce.

In the second step, a set of functions is presented to describe the inter-annual variation of beech phenology. Leaf sprouting and leaf senescence are calculated as functions of day-length and air temperature.

In the next step, an eco-hydrological box model is presented to quantify the water exchange between plant soil and atmosphere. The *Water Balance Model* (WBM) uses standard meteorological parameters as input variables and runs on a daily time step. It consists of two modules. The aboveground module (i) comprises routines for fog precipitation generation, precipitation interception and snowfall/snowmelt dynamics. Covered belowground processes (ii) are bypass flow, percolation, soil evaporation and transpiration, where the latter two processes are treated separately.

Subsequently, the output of the phenological simulator is fed into the WBM. It is then applied to four European beech dominated forest stands in the northeastern part of Austria. They are located on a gradient of declining annual precipitation (from west to east). The two easterly sites are located close to the dry limit of the natural distribution of beech. Records of soil moisture were used for the adjustment of 26 parameters. On all sites the calibration process (*simulated annealing*) delivered good predictions of soil moisture (Nash-Sutcliffe Efficiency ≥ 0.925).

Then, the obtained parameterization was used to perform a sensitivity analysis. Different scenarios of global warming were applied. The temperature was increased step-wisely up to 4°C. All scenarios were run (i) with present phenological conditions and (ii) with phenology responding to higher temperatures. This way the effect of higher temperatures and longer growing seasons on the water dynamics of the forest stands was assessed. A warming of one °C corresponded roughly to an elongation of the growing season of 4.5 days, where the start

of the growing season was affected more strongly than the end. Apparently, higher temperatures led to drier soils. The strongest change was observed in early summer, also amplified by an earlier start of the growing season. Rising temperatures led to lower export fluxes of liquid water, simultaneously increasing evapotranspiration (ET). The gain in ET was almost entirely assignable to increased soil evaporation. Drier soils led to a sharp depression of transpiration during summer months. This decline was compensated by the effect of elongated growing seasons. The risk of severe drought was increased by higher temperatures, but here the contribution of growing season length was negligible. Drier soils seem to hamper the stands' productivity. For all warming scenarios, the estimated increase of the gross primary production, caused by longer periods of assimilation, is nullified by the effect of soil water deficit in mid-summer.

This work culminates in the description of the stands S biogeochemistry: All presented simulators are put to use by forming the framework to run the *Sulfur Dynamics Model* (SDM). In the final step, the set up and the application of the SDM are described. The aim was the identification plus quantification of processes, which are crucial for the understanding of the biogeochemical S cycle of forest ecosystems. The simulator takes into account abiotic processes as well as biotic interactions between atmosphere, plant and soil. The model was applied to two Austrian beech stands where deposition of S and soil solution chemistry were monitored closely over a two-year period. Under consideration of high historic loads and the more recent recession of atmospheric S deposition, a suitable model configuration was found: It was possible to assign both (i) intra annual fluctuations in the SO_4-S in soil solution, as well as (ii) long time trend in the stream discharge to specific S transformation processes. The interplay of microbial immobilization and mineralization was identified as key driver of short-term fluctuations in the soil solution. In the long term, the delayed release of historically accumulated S is driven mainly by the slow mineralization of S rich plant biomass, recalcitrant to decomposition. Desorption processes seem to play only a negligible role on the explored plots. It can be concluded, that a model, based on the current understanding of S biogeochemistry, is sufficient to provide a useful description of S dynamics on the investigated forest stands.

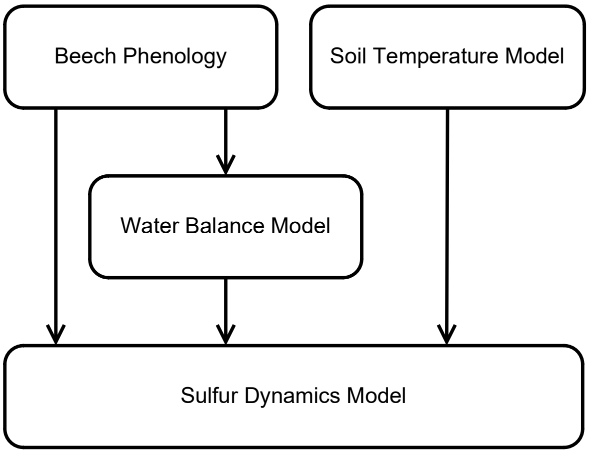

Figure 1: The dependencies of all four presented modules

Table of Contents

1 Introduction, Aim and Scope

1.1 Soil Temperature

Various biotic, as well as abiotic processes in the soil are temperature dependent (Rankinen et al., 2004). Usually, these dependencies are assumed to have a non-linear nature (Bond-Lamberty et al., 2005; Davidson et al., 2006; Macdonald et al., 1995; Wagle and Kakani, 2014), meaning that the response of the process to changes of temperature, strongly depends on the temperature range it is occurring in. Especially for high temperatures, small changes in temperature might yield big changes in the process's response. For the assessment of temperature dependent soil processes, it is therefore crucial to have expedient knowledge about spatial, as well as temporal fluctuations of soil temperature (Bond-Lamberty et al., 2005). The most reliable source of information would be the permanent monitoring of subsurface ground temperature. But in practice it is often hard to measure continuously. Usually, the modeler has to deal with fragmentary timelines of soil temperature, scarce point observations or even no records of T_{soil} at all (Lei et al., 2011). To fill these gaps or to extend the timeline beyond the measurement timeframe, the researcher must consider the application of a soil temperature model.

The approaches to predict subsurface ground temperature can be coarsely divided in two categories; (i) process based models, and (ii) empirical models (Kang et al., 2000). Process based approaches to predict soil temperature generally use meteorological input variables (primarily temperature and solar radiation) to calculate energy balance of the soil surface, and heat transport in the soil, by solving the heat equation (Paul et al., 2004). The applicability of these models is often limited by their high complexity, high demand of input data, and specific model parameters which are often not available for the investigated site (Lei et al., 2011; Svensson et al., 2008). Empirical models, presented in the work of Brown et al. (2000), Kang et al. (2000) or Paul et al. (2004) rely on the statistical relationship between meteorological parameters and soil temperature. More recently, there have been successful attempts to predict T_{soil} using combinations of artificial neural networks and fuzzy logic (Bilgili et al., 2013; Kim and Singh, 2014; Kisi et al., 2015; Talaee, 2014).

Soil thermal regimes are controlled by various environmental drivers. The most important meteorological factors are air temperature and radiation, laying the base for heat exchange at the soil surface (Hu and Feng, 2003). In the latter, forested sites differ substantially from other types of land cover: The radiation driven heat exchange between soil surface and atmosphere, is limited due to the shielding effect of the canopy (Paul et al., 2004). Therefore, forested sites show strongly dampened T_{soil} fluctuations, compared to sites with sparse vegetation or bare soil (Balisky and Burton, 1993). Only a few models exist, which explicitly address the soil thermal conditions of forested ecosystems.

Zheng et al. (1993) set up a dynamical model based on Newton's law of cooling, assuming the change of T_{soil} proportional to the temperature difference between air and soil. The fact, that the vegetation cover limits radiation driven heat flux, is taken into account by utilizing a heat transfer coefficient, which depends on the stands leaf area. They assume, that the canopy's damping effect is more pronounced for incoming radiation, than for emission from the ground. This is incorporated, by applying different heat transfer coefficients, whether the soil is warming or cooling. The damping term, dependent on LAI, only comes into effect for soil warming conditions. Based on this work, Kang et al. (2000) set up a spatially resolved T_{soil} model. To describe the soil thermal regimes of South Korean forest sites, they extended the latter approach by introducing a more *mechanistic* element, based on Fourier's law of heat transport. Besides the spatial and temporal variability of the leaf area, this approach also accounts for the effect of the stands litter layer on soil heat flux. The authors assumed, that T_{soil} does not fall below freezing for most Korean forest sites. As well as in the latter approach, T_{soil} estimates below 0°C were replaced with 0°C.

Brown et al.(2000), predicted daily mean T_{soil} of four different Northern Hardwood stands, utilizing a statistical relationship between T_{soil} and the average air temperature of the previous day. As a correction term, accounting for the phase shift or *lagging behind* of the annual course of T_{soil} compared to air temperature, they introduced a cosine function of the Julian day. Despite the simple model structure, the predictions of T_{soil} were quite precise (disregarding the cold season).

To predict daily T_{soil} of various Australian forest sites, Paul et al. (2004) used daily average air temperature and stand parameters like leaf area, understory growth, and litter mass. They assumed T_{soil} oscillating around an annual mean soil temperature, which is calculated from annual mean air temperature, modified with a correction factor, derived from information about the stands' vegetation cover and litter layer. The resulting temperature wave is then offset by a term describing daily fluctuations of T_{soil}, which again, is derived from air temperature. The model specifically addresses the thermal conditions of the topsoil. Therefore, phase shift and attenuation of the temperature oscillation, which become relevant with increasing soil depth, were not considered.

Bond-Lamberty et al. (2005) examined the spatiotemporal dynamics of soil thermal regimes during stand development of a disturbed boreal forest. To accompany this investigation and for laying the base to simulate forest dynamics, they implemented an empirical T_{soil} model. Accounting for the influence of recent past air temperature conditions on present T_{soil}, they calculate running averages of the daily mean air temperature. T_{soil} is then calculated as a linear function of multiple running averages, centered to different days in the past. The authors report difficulties to predict T_{soil} close to the freeze/thaw transition.

To evaluate the suitability of T_{soil} as a predictor for the treeline position in the Swiss Alps, Gehrig-Fasel et al. (2008) presented an approach, which strongly differs from others described in this section. To satisfy the statistical requirements for regression modeling, the data was first detrended and then transformed for first differences. After performing the regression analysis, the data was transformed back. Considering that daily mean air temperature was the only input parameter, the model showed high performance in the validation timeframe. Assuming only an insignificant influence of winter soil temperatures on the treeline position (Körner and Paulsen, 2004), the validation could be limited to the warm season.

Most approaches presented here disregard T_{soil} dynamics of the cold season. The decoupling of the soil from the atmosphere by a fluctuating snowpack (Betts et al., 2001), the heat transformation processes at the phase change from liquid to frozen (Beltrami, 2001; Viterbo et al., 1999) or changes in heat capacity and conductivity seem difficult to be captured in the framework of an empirical approach. In cases where winter T_{soil} is assumed to reach or fall below 0°C, process based approaches, presented by e. g. Rankinen et al. (2004), should be preferred. But even though this model could be described 'simple' from a mechanistic point of view, solely the empirical snow accumulation/melt module, upstream to the T_{soil} model, requires the assignment of 11 free parameters. An alternative might be the semi-empirical model presented by Katterer and Andren (2009). Making the approach suitable for colder temperature conditions, the formulation presented by Kang et al.(2000) was modified. They interposed a surface temperature term, which acts as link between air and soil temperature. In this term the influence of air temperatures below 0°C is attenuated by a constant factor. This way, they account for the low thermal conductivity of snow.

The objective of this work is the presentation of a model to predict soil temperature of forest stands, which aims to perform like a 'well-tuned' mechanistic simulator, using the straight-forwardness of an empiric formulation. The model enables the transformation of fragmentary records of forest soil temperature, into a complete time series of T_{soil}, using average daily air temperature as only input. In this specific case, the created time series is laying the base for the modeling of temperature dependent, biogeochemical soil processes. Due to the fact that many biotic soil processes are sensitive to winter conditions (Campbell et al. 2005), emphasis is laid on an expedient representation of the temperature dynamics of the cold season.

Running the simulation requires the adjustment of nine empirical parameters, which are not defined in a strict physical sense. This is making it hard to deduce parameter values directly from site information. For a proper site-specific parameterization, at least some snapshot measurements of T_{soil} are recommended. Therefore, this model primarily aims to sites were T_{soil} data is available, but the time series are inconsistent, or have to be extended beyond the timeframe of measurement.

1.2 Climate Change, Phenology and Water Balance of Beech Stands

Climate change is assumed to have a strong impact on Central European forest ecosystems. Over the last 140 years, South Europe and the Alps experienced a temperature increase of 2°C (Mayer et al., 2005). Current climate estimations point to a further rise of the global surface temperature of 2°C in the next 40 years (Field et al., 2014); it seems likely that the alpine region will experience a temperature elevation which will even be stronger (Eea, 2015). Beech is a dominant tree species in Central and Western European forests (Dittmar et al., 2003); the natural distribution is associated to the Atlantic to sub-continental climate (Sutmöller et al., 2008). As a species with a broad eco-physiological amplitude, it seems adequately adapted to resist climate change in the (humid and cool) Atlantic areal of distribution (Kölling et al., 2007). Especially on the southern limit of the species' distribution a different picture is expected. There, the occurrence of beech is mainly restricted by the soil water availability (Ellenberg and Leuschner, 1996). European Beech is a species which is particularly vulnerable to soil drought (Bolte et al., 2009). Dry and hot conditions have been known to restrict net primary production of beech forests significantly (Ciais et al., 2005). Higher temperatures are assumed to increase the frequency and intensity of soil drought due to the forcing effect on potential evapotranspiration (Bergh et al., 2003). In contrast to rising temperatures, annual precipitation sums are assumed to retain the present level, but there might be a shift in the seasonal pattern. Current estimations point towards increasing late-winter to spring precipitation, hand in hand with decreased precipitation during summer months (Geßler et al., 2007; Kunstmann et al., 2004), exacerbating soil water deficit.

Warmer conditions will lead to a temporal elongation of the growing season of beech (Vitasse et al., 2009). Under optimal conditions this would result in an increased productivity (Lindner et al., 2010). Under water limitation the opposite effect seems possible. High temperatures in spring favor growth at first. Later in the season they accelerate the soil water depletion, resulting in a sharp drop of carbon fixation by mid-summer (Dittmar et al., 2003; Kljun et al., 2007; Richardson et al., 2013).

A future increase of frequency and duration of drought periods during the growing season might alter the productivity and competitive and regenerative abilities of beech stands, especially on shallow soils (Geßler et al., 2007; Rennenberg et al., 2004). On these sites, it seems likely that beech stands will be replaced by drought resilient Oak-Hornbeam forest associations (Theurillat and Guisan, 2001).

In this work, I set up a model, describing the water balance of deciduous forest stands. The routing of modeled water fluxes is illustrated in Figure 10. Due to a strong connection of processes such as light extinction, precipitation interception or the stands water demand to the stands leaf area (van Wijk and Williams, 2005) I see the need to describe the temporal dynamics of the vegetation cover. Preceding to the WBM, a phenological routine is introduced, consisting of two elements: (i) the calculation of inter-annual variations of leaf emergence and leaf senescence, and (ii) a quantitative measure, describing the stands seasonal development of the leaf area.

This way the soil moisture dynamics of four beech stands are assessed, which are located in the north-easterly part of Austria, close to the dry distribution limit of European beech. The effect of climate change on the sites' water balance is analyzed. In that context, possible changes in CO_2 air concentration or the precipitation pattern are neglected; the focus lies solely on the impact of rising temperatures on the stands' soil moisture regime. This way, I assess temperature driven changes of the frequency and intensity of soil water deficit. At last, I try to identify factors which were influencing the stands' vulnerability and resilience towards soil drought.

1.3 Sulfur Biogeochemistry of Beech

During the 20th century, Central European forest ecosystems received high loads of atmospheric S. Several reasons led to a sharp decrease of S emissions and accordingly deposition, starting in the late 1980s. From 1990 to 2016, S emissions could be reduced by 81% in Austria (Umweltbundesamt, 2018). This decrease was assignable to policy driven shifts in the energy sector, mainly the reduction in the use of S rich fossil fuel, coupled with the installation of end-of-pipe technology. With declining emission, also the deposition load to forest ecosystems decreased. In the period from 1984 to 2013 throughfall (plus stemflow) fluxes for an Austrian beech stand declined from 2.3 to 0.6 g m^{-2} $year^{-1}$ (Berger and Muras, 2016). However, the observed drop was only poorly reflected in the catchment output of most forest sites (Alewell, 2001; Alewell et al., 2001; Pannatier et al., 2011; Prechtel et al., 2001). Similar patterns were also reported from Northern America: The observed decline of acid deposition was, in most cases, not accompanied with a decline of acidifying agents in the stream output of the investigated catchments (Watmough et al., 2005). This was in strong contrast to the prediction of, at that time, state of the art ecosystem simulators, which forecasted a relatively fast response of solution and stream chemistry after a change in the deposition regime. Likens et al. (2002) postulated four mechanisms, explaining a negative input/output balance of S. (i) The release of S by bedrock weathering, (ii) a net release from the ion adsorber, (iii) the excess mineralization of historically accumulated organic S, or (iv) the underestimation of dry S deposition. Studies of the isotopic composition of the atmospheric S input and the catchment S output clearly pointed towards an organic source (Novák et al., 2000). Especially for catchments, which received high historic loads of anthropogenic S, the isotopic composition of the stream discharge showed higher portions of ^{32}S than the atmospheric input. Plants and soil microflora generally prefer the lighter ^{32}S isotope towards the heavier, less abundant ^{34}S (Mitchell et al., 2001; Zhang et al., 1998). Sulfur, which was biologically incorporated into organic material during phases of high deposition, was now being released steadily, in form of SO_4-S by mineralization. Novák et al. (2000) state, that a considerable amount of the atmospherically deposed S is cycled through the biosphere before being given off to the soil solution and the stream discharge. Ecosystem models such as MAGIC, SMART, SAFE or CHESS describe S storage and release based solely on sorption isotherms (compare Alewell, 2001). They share their neglect in the possibility of biotic S cycling and the storage of S incorporated in an organic pool. In an attempt to model the stream chemistry of the output of a forested catchment in Germany with the MAGIC model, it was necessary to introduce an additional S source (968 mg m^{-2} yr^{-1}) to match the simulated with the observed stream discharge (Prechtel et al., 2003). Gbondo-Tugbawa et al. (2001) found that the introduction of a plant S uptake and a mineralization module considerably increased the performance of the PnET-BGC model in describing the SO_4-S output of a forested catchment. In this work, I introduce a biogeochemical model to describe biogeochemical S dynamics of temperate deciduous forest stands. Besides the assessment of geochemical dynamics, I lay emphasis on biotic interactions: In addition to plant uptake, litterfall and the release of S via mineralization of plant organic material, I try to assess microbial immobilization (the microbial conversion of soil solution sulfate to organically bond S) in the forest soil as a crucial part of the biogeochemical S cycle. The model is applied to two beech stands in eastern Austria where deposition and solution chemistry were monitored closely over a two-year period. In this work, I try to answer the following questions:

- Is it possible to derive a model configuration that delivers a plausible representation of the current state of the investigated sites and of the observed temporal pattern in the soil solution?
- Does this model configuration provide insight, which biogeochemical processes are the key drivers of the observed intra-annual pattern in the SO_4-S soil solution?

- Furthermore, is the simulator, which is calibrated on data from a very narrow timeframe, capable to provide a reasonable perspective regarding the future development of the stands' S budget and balance? How long does it take for the stream discharge of S to decline to a pre-industrial level? Is a new steady state (balance between S input and S output) foreseeable within the model timeframe?

2 Material and Methods

2.1 Study Sites

2.1.1 Soil Temperature

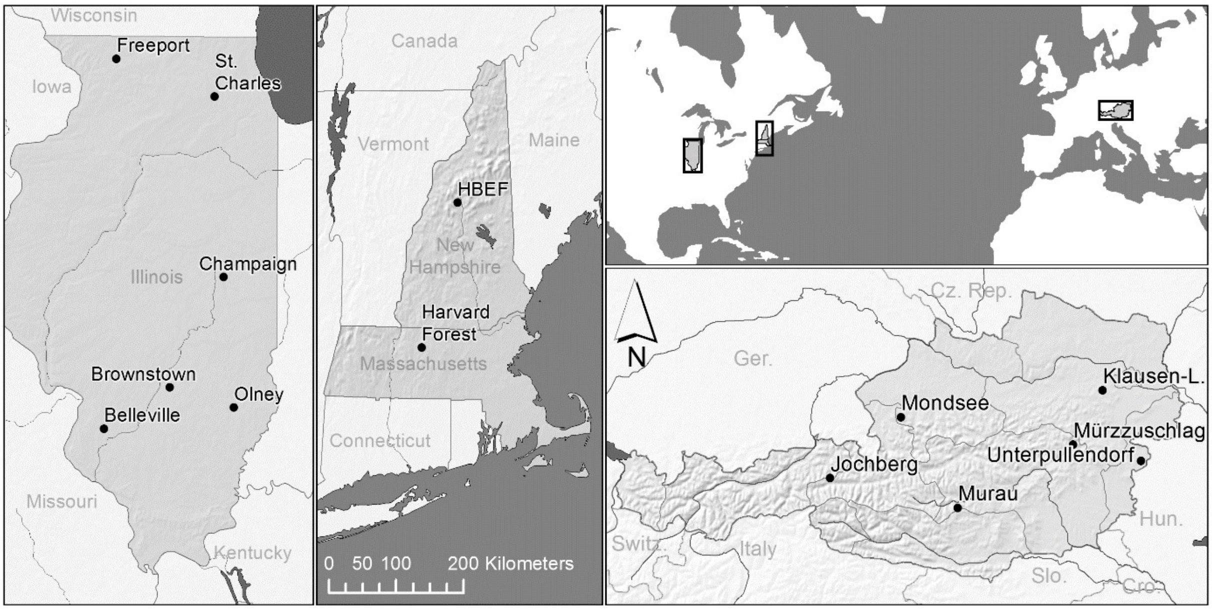

Figure 2: Location of soil temperature study sites in the United States and in Austria. The sites used for parameterization of the forest soil temperature simulator cover a broad range of characteristics. For a brief site description, see Table 1.

2.1.1.1 Austria (Level II)

In the framework of the *International Co-operative Programme on Assessment and Monitoring of Air Pollution Effects on Forests (ICP Forests)*, the *Austrian Research Centre for Forests* operates several, intensively monitored, forest sites *(Level II)* (Neumann et al., 2001). In addition to various other environmental parameters, meteorological conditions are monitored continuously. Soil temperature records exist for soil depths, ranging from 5 - 60 cm.

The soil temperature model was originally set up on data from the Level II Plot Klausen-Leopoldsdorf (KL), which is located in the Vienna Woods (48°07'16"N, 16°02'52"E), at an elevation of 510 m a. s. l. The research site is a pure beech (*Fagus sylvatica* L.) stand, which was planted in the late thirties of the last century. The location is facing NE with an inclination of 20%. The actual forest vegetation coincides with the potential natural one, and can be classified as *Hordylemo-Fagetum* (Mucina et al., 1993). For a more detailed site description see (Neumann et al., 2001).

Table 1: Investigated locations cover a broad range of site characteristics and distinct climatic and altitudinal gradients.

		Elevation [m a. s. l.]	**Exp.**	**Slope** [°]	**MAT*** [°C].	**MAP*** [mm]	**Dominant species**	**Soil type**
Level II	**Jochberg**	1050	NE	4	5.7	1358	*Picea abies*	Dystric C.
	Mondsee	860	SE	14	~5.7	1521	*Picea abies*	Eutric C.
	Murau	1540	N	33	5.0	918	*Picea abies*	Dystric C.
	Mürzzuschlag	715	S	10	6.0	933	*Picea abies*	Eutric C.
	Klausen-Leo.	510	NE	11	8.2	804	*Fagus sylvatica*	Stagnic C.
	Unterpullend.	290	-	0	9.6	630	*Quer. petraea/cerris*	Planosol
HBEF	**High Elev. Plots**	560	N	~13	5.0	1400	*Betula alleghaniensis*	Podzol
	Low Elev. Plots	430	S	~11	6.1	1400	*Acer saccharum*	Podzol
Harvard	**Prospect Hill**	365	-	0	8.5	1080	*Quer. rubra*	Dystric C.
	Barre Woods	305	-	0	8.5	1080	*Quer. rubra/velutina*	Dystric C.
ICN	**Freeport**	265	-	0	~9.1	~860	*Sod covered ground*	
	St. Charles	226	-	0	~9.3	~780	*Sod covered ground*	
	Champaign	219	-	0	~11.3	~1020	*Sod covered ground*	
	Belleville	133	-	0	~12.7	~960	*Sod covered ground*	
	Brownstown	177	-	0	~12.3	~960	*Sod covered ground*	
	Olney	134	-	0	~12.5	~1010	*Sod covered ground*	

* MAT= Mean annual temperature, MAP=Mean annual precipitation sum, C.=Cambisol, Quer.=Quercus

Subsequently, data from 5 other *Level II* forest stands were accessed. The selection aims to cover a broad range of site characteristics. Investigated sites show a strong altitudinal and climatic gradient. The elevation of the investigated stands ranges from 290 (Unterpullendorf) to 1540 m a.s.l. (Murau), leading to annual mean temperatures from 9.6 to 5°C, respectively. Austria lies in the transition zone between oceanic and continental climate. Progressing from west to east, investigated locations therefore experience a strong decline in annual precipitation sums, ranging from 1521 mm for mountainous stands in the north-west, affected by orographic precipitation (Mondsee), to 630 mm in the continentally influenced east of the country (Unterpullendorf).

To fill gaps in the record of average daily air temperature, data were accessed, provided by the European Climate Assessment (ECA&D; Tank et al., 2002). Missing values were replaced, using linear regression with available neighboring stations.

2.1.1.2 New England

Intending to test the soil temperature model's over-regional validity, I moved to another continent. Data were accessed from two intensive long-term ecological research areas in New England; (i) the Hubbard Brook Experimental Forest (HBEF), and (ii) Harvard Forest.

The HBEF lies in the White Mountain National Forest in north-central New Hampshire (43°56'N, 71°42'W). The elevation of the investigated watershed ranges from 250 m to 1000 m. The forest type can be classified as Northern Hardwood, dominated by Sugar maple (*Acer saccharum* Marsh). The climate is cool, continental, and humid, with mean annual precipitation sums around 1400 mm (Bailey et al., 2003). Approximately one third of the precipitation is falling as snow, leading to a snowpack, typically lasting from December to April. Soils can be classified as well-drained Spodosols (WRB: Podzol), developed on glacial till (Campbell et al., 2010).

Daily T_{soil} (depth: 5 cm) data, recorded within the framework of the project *Snow Depth & Soil Freezing as a Regulator of Microbial Processes* (Duran et al., 2014), were obtained. Data of three intensive high elevation plots (mean elevation: 560 m, exposition: north) and three intensive low elevation plots (mean elevation: 430 m, exposition: south) were used. For each altitude class, one mean time-series of T_{soil} was calculated.

Because of their proximity to the investigated stands, records of air temperature (Bailey et al., 2003) from meteorological station 23 and 1, for high and low elevation plots respectively were obtained. Missing data were replaced, using offset temperatures of highly correlated neighboring stations. To fill remaining gaps in the air temperature record, the GHCN-Daily dataset was accessed, provided by the NOAA (Menne et al., 2012a; Menne et al., 2012b), utilizing data from the station Wentworth, New Hampshire (43°52'22"N, 71°54'31"W).

The *Harvard Forest Research Station* is located in Central Massachusetts (42°32'N, 72°11'W). The climate is cool, temperate, and humid. Precipitation is distributed evenly through the year, with annual sums in the range of 1080 mm. The annual mean temperature is 8.5°C (Berbeco et al., 2012). The elevation of the investigated locations is approximately 350 m a. s. l. Soils can be classified as Typic Dystrudepts (WRB: Dystric Cambisol). After a severe disturbance in the beginning of the last century, the forest regrew naturally, resulting in an even aged stand of mixed hardwood species, with Red oak (*Quercus rubra* L.) dominating (Butler et al., 2012).

Within the forest site, the simulator was applied to two sub-sites: (i) Barre Woods (Melillo et al., 2003), and (ii) Prospect Hill (Melillo et al., 1999). Both locations were set up to study the effect of soil warming on carbon and nitrogen turnover by artificially heating the ground (Berbeco et al., 2012; Melillo et al., 2002). The model was adjusted to the topsoil (depth 5 cm) of the undisturbed control plots, whereat on the Prospect Hill site data from 6 control plots were combined, calculating a mean time-series of T_{soil}. Daily air temperature was obtained from the EMS tower (Munger and Wofsy, 1999), where the record 7.6 m above ground was selected. Data gaps were closed, using offset temperature measurements at other heights, or data from the Fisher meteorological station (Boose, 2001). If no other source was available, the *GHCN-Daily* dataset was again accessed, applying offset air temperature data from the Municipal Airport station at Orange, Massachusetts (42°33'46"N, 72°16'59"W).

2.1.1.3 Non-Forested Sites in Illinois

At last, to explore the limits of the formulation, the model was applied to 6 sites which lack the shielding properties of a dense forest canopy. Therefore, data were obtained from the *Illinois Climate Network, (ICN)*, which operates several open field meteorological stations in Illinois. Air temperature was measured two meters above ground. Gaps in the air temperature record were closed, using offset temperature measurements of, highly correlated, and neighboring stations. Soil temperature was recorded in 10 cm and 20 cm depth (Hollinger et al., 1994) under sod covered ground. Soil texture was assessed as silt loam, throughout all studied locations. The elevation of the investigated sites ranges from 133 – 265 m a. s. l.

Illinois' climate is typically continental with cold winters and warm summers. Moving from north to south, mean annual air temperatures increase from 8.9°C to 14.5°C. Also annual precipitation sums reveal a strong north-south gradient, ranging from 810 mm to 1220 mm. Stations in the north-west of the state are climatically influenced by Lake Michigan, which is attenuating temperature extremes and enhancing winter precipitation (lake effect snow) (Changnon et al., 2008).

2.1.2 Beech Phenology Water Balance and S Biogeochemistry

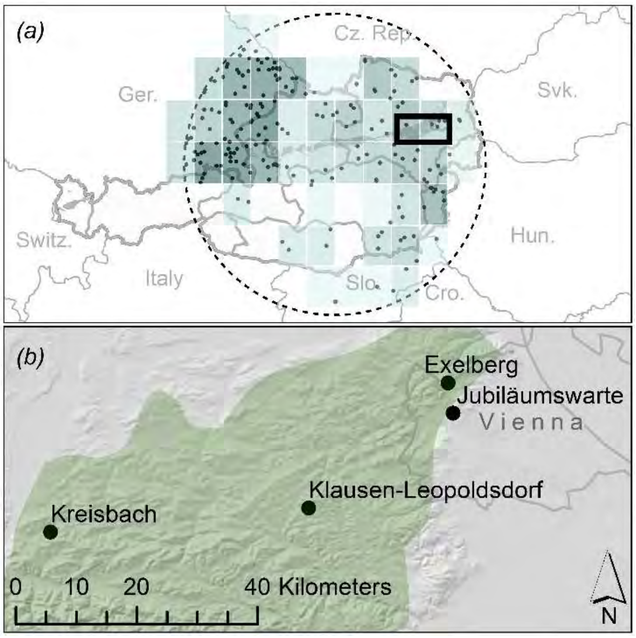

Figure 3: (a) For calibration of the phenological model, *PEP725 (Pan European Phenology Data)* beech stands (small black dots) were accessed within a radius of 200 km centred to 47°42'00"N, 14°30'00"E. One average time series of air temperature was calculated, using data from the *E-OBS* gridded dataset (Tank et al., 2002) (0.5° resolution, turquoise rectangles). The frequency of selected sites within one grid cell defines the relative weight the cell receives in the calculation of the average; darker cells correspond to higher weightings. (b) Locations used in the calibration of the WBM (black dots). All sites are beech dominated stands and share their geological bedrock (Flysch). The green area represents the natural distribution of European Beech according to the Map of the Natural Vegetation of Europe (Bohn et al., 2004).

The investigated forest stands are located in the north-easterly part of Austria in the foothills of the Northern Calcareous Alps (see Figure 3b). The parent material for soil formation is Flysch, which consists of old tertiary and mesozoic sandstones and clayey marls of maritime origin. Due to high clay content, the saturated hydraulic conductivity is low, leading to frequent episodes of waterlogging. Therefore, the soil type can be classified as stagnic cambisol according to the WRB soil classification (IUSS Working Group, 2006) throughout all studied sites. The mean annual temperature in the study area is approximately 9°C. Precipitation declines from west to east, with average annual sums ranging from 820 mm (Kreisbach) to 652 mm (Vienna).

In the framework of the *International Co-operative Programme on Assessment and Monitoring of Air Pollution Effects on Forests (ICP Forests)*, the Austrian Research Centre for Forests operates several intensively monitored forest sites (Level II; Neumann et al., 2001). In addition to other environmental parameters, meteorological conditions are monitored continuously. Soil moisture (Campbell CS615 FDR probe) is recorded at three different depths (15, 30, 60 cm). The Water Balance Model was originally set up on data from the Level II plot Klausen-Leopoldsdorf (KL), which is also used in the soil temperature assessment. The site description can be found in section 2.1.1.1.

The Kreisbach (KB) site, which is located south of St. Pölten (48°05'50"N, 15°39'50"E) at an elevation of 470 m a. s l., is a mixed European beech-Norway spruce (*Picea abies* L.) stand, with beech dominating. The stand is facing NNE with an inclination of 19 %. The natural plant association can be classified as *Asperulo odoratae-Fagetum*. From 1998 to 2003 the site was monitored meteorologically within the framework of a special research program on Forest

Ecosystem Restoration. Soil moisture records (Trase1 TDR probe) exist for four different depths (10, 20, 40, 55 cm). For a more detailed site description see Schume et al. (2003).

The third site (Exelberg, EX; 48°14'40"N, 16°15'18"E) site is located in Lower Austria close to the border to Vienna. This site is also a pure beech stand. The stands' age was estimated to approximately 100 years. The site is also facing SE with an inclination of 22%. Two years of bi-weekly observations of soil moisture exist for 10, 30 and 60 cm depth.

The last site (Jubiläumswarte, JU) is located within the municipal area of Vienna at the eastern edge of the Vienna Woods (48°13'12"N, 16°15'56"E) which is 2.8 km southeast of EX, at an elevation of 440 m a. s. l. The site, which is a pure beech stand with an estimated age of 125-150 years, is facing SSE with an inclination of 15%. As a matured stand it is showing signs of collapse but also strong natural regeneration. Different to the other investigated sites, the bedrock contains calcareous material, reflected in higher base saturation and soil pH.

The latter two sites are located at the dry distribution limit of beech (see Bohn et al., 2004). They receive significantly less precipitation than the first two. Due to their location at upper hill slopes and their exposition, they seem prone to soil drought. It is also the latter two sites to which the SDM is applied (see Figure 4). Due to their south-easterly exposition and their location close to the hilltop they are very susceptible to SO_2 enriched air flow, coming from the urban area of Vienna. Further details about forest site, stand and soil characteristics are given in Hanousek et al. (2017). The mean annual temperature for EX and JU is approximately 9 °C. The average annual precipitation amounts to approximately 660 mm (Wien – Hohe Warte).

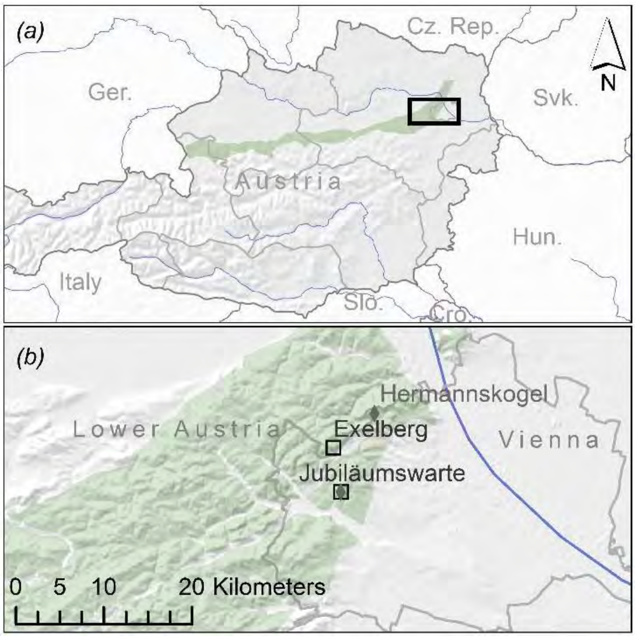

Figure 4: (a) Location of the forest stands where the SDM was applied. Both sites are located in Lower Austria and accordingly Vienna. They share the bedrock Flysch (darker band area, crossing Northern Austria) and several other site characteristics. (b) Both forest stands (squares) are located at upper hill slopes, close to the ridge, facing SE. Due to the sites' micro-relief, in combination with the immediate proximity to the urban area of Vienna, they are deemed very susceptible for pollution enriched air flow from south to easterly directions. Weather Information and SO_2 data (diamonds) was obtained mainly from Jubiläumswarte and Hermannskogel.

2.2 Data Sources

2.2.1 Beech Phenology and Water Balance

The WBM runs on a daily time step and uses standard meteorological data on a daily base as input. Time series of minimum (T_{min}, °C), mean (T_{mean}) and maximum (T_{max}) temperature, the daily averages of relative humidity (rH), global radiation (gR, wm^{-2}), and wind speed at two meters above ground (u_2, ms^{-1}), as well as the observed 24 h precipitation sum (P_{obs}, mm) are required. The phenological module utilizes daily T_{mean} and T_{max}.

For gap filling purposes, data were accessed from the Austrian Meteorological Agency (ZAMG) as well as from the Austrian Hydrographic Service (eHYD). For the EX site, precipitation records from a private weather station were used. Missing data were replaced, using simple regression techniques, with data from highly correlated, neighboring stations.

For calibration of the phenological module, data were retrieved from the PEP725 database (PEP725 Pan European Phenology Data, data set accessed on 06/06/2015 at http://-www.zamg.ac.at/pep725/). Two phenological stages were considered. (i) BBCH-11: leaf unfolding (LU) on the first visible leaf stalk, represents the onset of the growing season. (ii) BBCH-94: autumnal leaf coloring (50% of leaves colored; LC), marking the end of the growing season. In this work, phenological phases are calculated as functions of day-length and air temperature. Therefore the gridded E-OBS dataset (a daily gridded observational dataset for meteorological parameters) was accessed (0.5°, regular grid), provided by the European Climate Assessment (ECA&D; Tank et al., 2002).

Due to strong site variations of phenological events, the set-up of the phenological model was conducted, utilizing multiple phenological sites within a radius of 200 km, centered to 47°42'00"N, 14°30'00"E (see Figure 3 a). The phenological dataset was scanned for outliers using Tukey's test. Parallel data was checked for month-mistakes (Schaber and Badeck, 2002). Only time series with 10 or more annual observations were considered in the calculation. To overcome site specific effects, the influence of phenotypic plasticity (Capdevielle-Vargas et al., 2015), or divergences in the assessment of phenological stages (Estrella and Menzel, 2006), the calibration of the model was performed on an assembled time-series. To generate this assembled time-series, I implemented the 3rd method which was proposed in (Häkkinen et al., 1995). To each DoY of each time-series a site wise offset (Os) was applied. The aim was to minimize the residual between site-wise time-series and the mean time-series over all sites.

$$\min_{O_s}\left[\sum_{y}\sum_{s}\left(\left(DoY_{sy}-O_s\right)-\frac{\sum_s\left(DoY_{sy}-O_s\right)}{n_y}\right)^2\right] \tag{1.}$$

To achieve this, the classical hill climber algorithm was applied. 40 000 iterations were used to adapt Os for all considered sites. The sum of squared residuals could be reduced to approximately 55% of its initial value. To ensure that the residual sum equals zero, the overall mean before and after the optimization was calculated; the difference between both means stated a second offset which was applied to DoY_{sy}.

$$o_n=-\frac{\sum_{sy}O_s}{n_{sy}} \tag{2.}$$

Parallel, a time-series of the average T_{min}, T_{mean} and T_{max} was calculated over all E-OBS grid cells, comprising selected phenological sites, whereat the number of sites within the cell defined the relative weighting the cell received in the calculation of the average.

2.2.2 Sulfur Biogeochemistry

The simulator, outlined in this work, runs on a daily timestep. Therefore, all input data must be provided in daily resolution. Sulfur enters and leaves the soil system mainly in aqueous solute form. To describe the short-term dynamics of S in the soil, water balance and water fluxes are simulated, using the formulation of the Water Balance Model (WBM) presented in 2.3.3. I ran the WBM using meteorological input data from the weather station Jubiläumswarte (100 m distant from JU) obtained from the *Zentralantalt für Meteorologie und Geodynamik* (ZAMG). The meteorological record of the mentioned station starts in 2011. For the timeframe before that year, a synthetic weather time series was created using neighbouring stations with longer records; outside the timeframe with measured data, a weather generator was applied to create a synthetic record. The daily mean air temperature and snapshot measurements of soil temperature were used to generate a continuous record of soil temperature. The approach plus its parameterization is described in section 2.3.1. To determine the timing of the stands' phenological key events, the phenological module was used, which is presented in section 2.3.2.1.

Both investigated sites were monitored from April 2010 to June 2012 in a biweekly interval. Precipitation water was collected in the open field (bulk precipitation), as well as after the passage through the canopy (throughfall). A funneling apparatus was installed on one tree per site to collect stemflow. Soil solution lysimeters were installed at 10, 30 and 50 cm soil depth, each in 5 replications per site. Snapshot measurements of soil moisture (TDR-Trase) and soil temperature were taken in the course of the biweekly sample collection. Water samples (precipitation and soil solution) were analyzed for SO_4-S content via ion chromatography (Dionex DX 500, USA). All field work was done by Torsten and Pétra Berger.

Daily mean values of the aerial SO_2 concentration were obtained from the Umweltbundesamt (Wiener Umweltschutzabteilung – MA 22 Luftmessnetz), for the site Hermannskogel, ranging back to the year 1988. To extrapolate this data to the pre-industrial era, a time series of the estimated SO_4-S deposition is used (Figure 5a, EMEP), derived by Schöpp et al. (2003). This time series was normalized to a value of one for the period with existing data.

Outside the timeframe the normalized estimate was multiplied with the Day of Year (DoY) mean from the measured period. The data estimates range back to 1880. The EMEP dataset also comprises estimates for the near future. Here, the CLE (Current Legislation Emission) scenario was chosen. Outside the defined timeframe, the time series was extended, assuming static conditions before the first and after the last year of prognosis (see Figure 5b).

On both sites, bulk precipitation deposition of SO_4-S (open field) was sampled from April 2010 to June 2012 in a bi-weekly interval. To achieve a daily resolution, the collected amount was prorated proportionally to the measured amount of daily precipitation. For the extension of deposition to the time period before measured data was available, a similar approach was used as with the extrapolation of the SO_2 air concentration (Figure 5c).

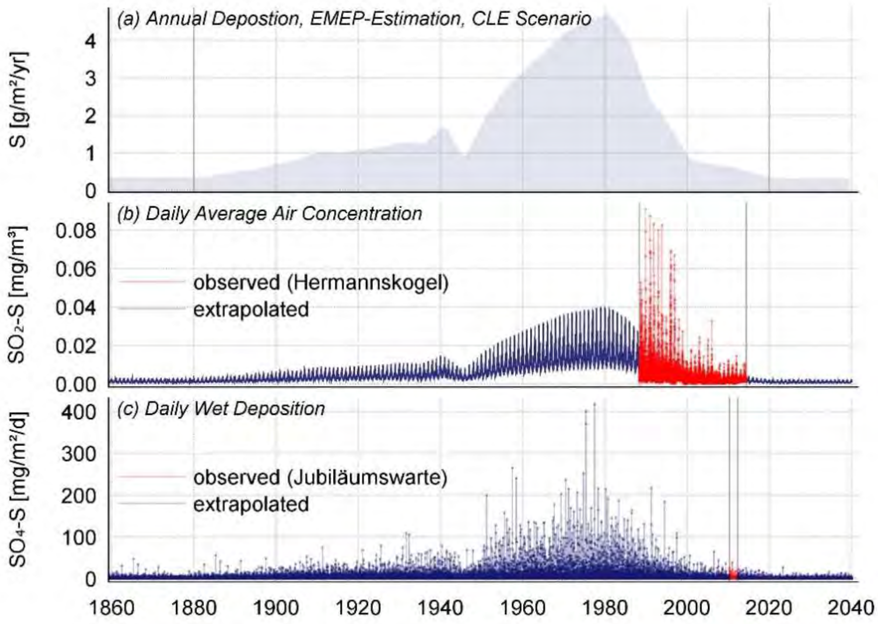

Figure 5: Extrapolation of observed depostion data to the model timeframe. The model timeframe spans from year 1770 to 2100. (a) Observatios of S Deposition and air concentration were availalble only for the very recent past. (a) To extend the input data timeseries beyond the observed timeframes a dataset of SO_4-S deposition estimates was used (EMEP), generated by (Schöpp et al., 2003). The data estimates range back to 1880.The set also comprises two scenarios for the near future. The CLE (Current Legislation Emission) scenario was chosen. Outside the defined timeframe, the time series was extended, assuming steady conditions. (b) Daily mean values of the aerial SO_2 concentration for the site Hermannskogel, were available, ranging back to the year 1988. Due to the fact that SO_2 concentrations exhibit a strong seasonal pattern, extrapolation was performed by calculating average values on a Day of Year base, which were then extended beyond the available timeframe. Here, the normalized EMEP timeseries served as a mulitplier to scale the aereal concentration to historic and future conditions. (c) For daily wet deposition, an approach was applied, similar to the extension of the aerial concentration. Annual deposition sums where partitioned proportionally to daily precipitation events.

2.3 Mathematical Representation

2.3.1 Soil Temperature Model

The model describes T_{soil} as a function of daily mean air temperature ($T_{\text{air},t}$). It employs a daily time step. The formulation is based on Newton's law of cooling (Bergman et al., 2011), which is applied two times consecutively.

Utilizing a relatively small heat transfer coefficient (λ_{shift}), the first application of Newton's law provides a phase shifted temperature time series ($T_{\text{shift},t}$) which lacks the high frequency fluctuations of $T_{\text{air},t}$.

$$T_{\text{shift},t} = T_{\text{air},t} + (T_{\text{shift},t-1} - T_{\text{air},t})\exp(-\lambda_{\text{shift}}) \qquad (3.)$$

A fictive environmental temperature ($T_{\text{env},t}$) is postulated as the weighted mean of the elements $T_{\text{air},t}$, $T_{\text{shift},t}$, and a constant correction temperature (T_{corr}). pc_{air}, pc_{shift}, and pc_{corr} are partitioning coefficients, which define the relative weight of the specific element.

$$T_{\mathrm{env},t} = T_{\mathrm{air},t} pc_{\mathrm{air}} + T_{\mathrm{shift},t} pc_{\mathrm{shift}} + T_{\mathrm{corr}} pc_{\mathrm{corr}} \qquad (4.)$$

The partitioning coefficients sum up to 1, so two must be defined as model parameters, the third can be deduced.

$$pc_{\mathrm{corr}} = 1 - (pc_{\mathrm{air}} + pc_{\mathrm{shift}}) \qquad (5.)$$

ΔT states the difference of the soil temperature to $T_{\mathrm{env},t}$.

$$\Delta T = T_{\mathrm{env},t} - T_{\mathrm{soil},t-1} \qquad (6.)$$

Taking into account the insulating effect of the snow cover and the heat release/consumption due to the phase change of soil water from liquid to solid and vice versa (Beltrami, 2001), a variable heat transfer coefficient (λ_{eff}) is implemented. λ_{max} represents the transfer coefficient above the upper threshold temperature (T_1). Below T_1 λ_{eff} gets reduced, reaching the minimum (λ_{min}) at the lower threshold (T_0), where different λ_{min} are applied for soil warming and cooling.

$$\lambda_{\mathrm{min}} = \begin{cases} \lambda_{\mathrm{thaw}}, & \Delta T > 0 \\ \lambda_{\mathrm{frost}}, & \Delta T \leq 0 \end{cases} \qquad (7.)$$

The transition of the transfer coefficient in between T_1 and T_0 is described, using a third order polynomial.

$$\lambda_{\mathrm{eff}} = \begin{cases} \lambda_{\mathrm{min}}, & T_{\mathrm{soil},t-1} \leq T_0 \\ \lambda_{\mathrm{min}} + (\lambda_{\mathrm{max}} - \lambda_{\mathrm{min}})(3x^2 - 2x^3), & T_0 < T_{\mathrm{soil},t-1} < T_1 \\ \lambda_{\mathrm{max}}, & T_{\mathrm{soil},t-1} \geq T_1 \end{cases} \qquad (8.)$$

For that, $T_{\mathrm{soil},t-1}$ has to be transformed into an auxiliary variable inside the interval 0 to 1.

$$x = \frac{T_{\mathrm{soil},t-1} - T_0}{T_1 - T_0} \qquad (9.)$$

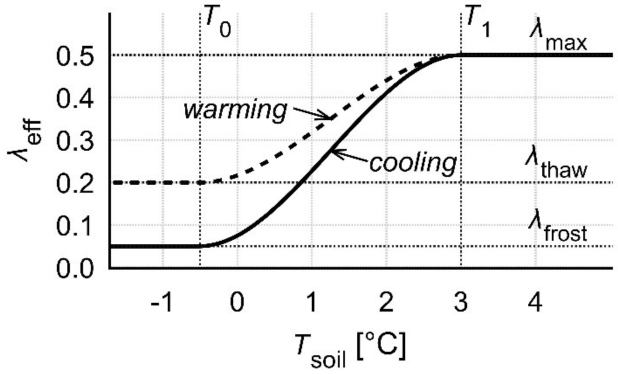

Figure 6: Polynomial transition of the heat compensation coefficient (λ_{eff}), between two threshold soil temperatures (T_0, T_1), close to soil freezing. The reduction of the coefficient pays respect to the energy release/demand of phase changes, from liquid to solid and vice versa. High model performance was achieved, using different minimal compensation coefficients for soil cooling (λ_{frost}) (solid line) and warming (λ_{thaw}) (dashed line) respectively.

At last, Newton's law is applied the 2nd time. The actual daily mean soil temperature calculates as:

$$T_{\mathrm{soil},t} = T_{\mathrm{env},t} - \Delta T \exp(-\lambda_{\mathrm{eff}}) \qquad (10.)$$

2.3.2 Phenology and Leaf Area

2.3.2.1 The Timing of Phenological Key Events

Beech can be considered a late flushing species (Vitasse and Basler, 2013). By that, it is following a rather conservative strategy, aiming to decrease the risk of late frost exposure (Caffarra and Donnelly, 2011; Körner and Basler, 2010). There are several environmental signals involved in the triggering of the start of the growing season. Of high relevance is the seasonal course of the photoperiod (Basler and Körner, 2012), meaning the day length has to exceed a critical threshold in spring before bud burst might occur (Körner and Basler, 2010). According to (Laube et al., 2014), an environmental trigger which is weighted even more strongly, is the chilling demand, meaning winter temperatures, undershooting a threshold for a certain time, are promoting dormancy release in spring. Furthermore, leaf sprouting is accelerated by high spring temperatures (Caffarra and Donnelly, 2011; Vitasse et al., 2009).

Compared to spring phenology, the environmental triggering of beech senescence is less understood (Estrella and Menzel, 2006; Vitasse et al., 2009). Especially the role of temperature is discussed controversially. For European beech stands, (Estrella and Menzel, 2006) reported positive correlation of the August and September mean air temperature, with the date of leaf coloring. Surprisingly, the authors found also a negative correlation with temperature in May and June, meaning low average temperatures in late summer and high temperatures in late spring promote the temporal occurrence of leaf senescence. Whether the latter was a direct temperature effect, or the effect of (temperature correlated) drought during critical phenological stages, was not examined.

In this section, a model is presented, describing the onset of the growing season as function of daily air temperature. Assuming the chilling demand generally over-satisfied for central European forest stands (Fu et al., 2012), only the forcing effect of air temperature is considered.

A common approach to quantify the forcing effect of air temperature on spring development requires the definition of a threshold temperature; below this temperature no forcing is taking place, above the temperature forcing is assumed proportional to the temperature difference between actual and threshold temperature (Cannell and Smith, 1983). To achieve a more gradual transition of the forcing response to air temperature, a piecewise combination of a first and second order polynomial is presented in this work. The full formulation of the function, which is optically resembling the shape of a hockey stick, is stated in 8 Appendix (Eq. A1, A6, A7). Below the threshold temperature ($T_{0,\mathrm{LU}}$) the response is assumed to be zero. The onset is described with a 2nd order polynomial. A second key temperature ($T_{1,\mathrm{LU}}$) defines the transition from quadratic to linear response, where m_{LU} sets the forcing rate at $T_{1,\mathrm{LU}}$. Most approaches for predicting spring phenology as a function of air temperature make use the daily mean temperature. In this work, it was found that the average of daily T_{mean} and T_{max}, aiming to represent the average daytime temperature (T_{day}), displayed higher force of expression in the prediction of LU.

$$f_{\mathrm{T}} = hockey\left(T_{\mathrm{day}}, T_{0,\mathrm{LU}}, T_{1,\mathrm{LU}}, 0, m_{\mathrm{LU}}\right) \qquad (11.)$$

Analogue to (Blümel and Chmielewski, 2012), a day length term is included, accounting for the photoperiodic influence on spring development. The day length (*dl*, hours) was calculated as function of the day of the year (*DoY*) and the geographical latitude, analogue to Swift (1976). A model parameter in the exponent (x_{LU}) adds one degree of freedom. Preventing vast values in the photoperiod term, day length is normalized by dividing by 14 hours.

$$f_{\mathrm{dl}} = \left(\frac{dl}{14h}\right)^{x_{\mathrm{LU}}} \qquad (12.)$$

The daily forcing is described as the product of a function of air temperature and day length.

$$f_{\mathrm{LU}} = f_{\mathrm{T}} f_{\mathrm{dl}} \tag{13.}$$

The temperature accumulation starts with $DoY_{0,\mathrm{LU}}$. LU is triggered after the accumulation of 10 forcing units.

$$Sf_{DoY1,\mathrm{LU}} = \sum_{DoY=DoY_{0,\mathrm{LU}}}^{DoY_{1,\mathrm{LU}}} f_{\mathrm{LU,DoY}} = 10 \tag{14.}$$

The calibration of the model was conducted on the assembled time-series, described in section 2.2.1. The phenological data which was used in this work was provided in discrete daily resolution but calculating means over several sites led to non-integer values for the day of the year of the phenological event. A model, which is treating phenological events as discrete in time, cannot overcome the residual caused by the decimal places. To surmount this minor but unnecessary flaw, another function is introduced: The difference of the sum, necessary to trigger budburst and the sum of the day prior to budburst, divided by the difference of the sum, achieved on the budburst day and the prior day, minus a half day is calculated:

$$c_{\mathrm{LU}} = \frac{10 - Sf_{DoY1,\mathrm{LU}-1}}{Sf_{DoY1,\mathrm{LU}} - Sf_{DoY1,\mathrm{LU}-1}} - \frac{1}{2} \tag{15.}$$

A distinct exceeding of the temperature sum which is necessary to trigger the event on $DoY_{1,\mathrm{LU}}$ will result in a negative value of c_{LU}. Therefore, DoY_{LU} will be shifted to a slightly earlier point in time. A weak overshooting will result in a delay of the event. The DoY of leaf unfolding is finally calculated.

$$DoY_{\mathrm{LU}} = DoY_{1,\mathrm{LU}} + c_{\mathrm{LU}} \tag{16.}$$

The approach for modeling the annual variability of the end of the growing season, is based on the findings of Estrella and Menzel (2006). A linear model is set up, utilizing averaged T_{mean} of two seasonal periods ($DoY_{0,\mathrm{LC}}$-$DoY_{1,\mathrm{LC}}$, $DoY_{2,\mathrm{LC}}$-$DoY_{3,\mathrm{LC}}$): (i) late spring and (ii) late summer to early autumn. Within these periods, a parabolic function assigns weight (w_{LC}) to the observed T_{mean}.

$$w_{\mathrm{LC}} = \begin{cases} 0, & DoY \leq DoY_{0,\mathrm{LC}} \\ 4h_{\mathrm{LC}} \dfrac{(DoY_{1,\mathrm{LC}} - DoY)(DoY - DoY_{0,\mathrm{LC}})}{(DoY_{1,\mathrm{LC}} - DoY_{0,\mathrm{LC}})^2}, & DoY_{0,\mathrm{LC}} < DoY < DoY_{1,\mathrm{LC}} \\ 0, & DoY_{1,\mathrm{LC}} \leq DoY \leq DoY_{2,\mathrm{LC}} \\ 4\dfrac{(DoY_{3,\mathrm{LC}} - DoY)(DoY - DoY_{2,\mathrm{LC}})}{(DoY_{3,\mathrm{LC}} - DoY_{2,\mathrm{LC}})^2} & DoY_{2,\mathrm{LC}} < DoY < DoY_{3,\mathrm{LC}} \\ 0 & DoY \geq DoY_{3,\mathrm{LC}} \end{cases} \tag{17.}$$

Due to the fact that senescence dates correlate negatively with T_{mean} in late spring, the parabolic function in the first period yields negative values, with a minimum of h_{LC}. The weighted average T_{mean} (wA_{LC}) inside the temporal window is calculated. Figure 7 states a graphical representation of the assessment of spring and autumn phenology.

$$wA_{\mathrm{LC}} = \frac{\sum_{i=DoY_{3\mathrm{LC}}}^{DoY_{0\mathrm{LC}}} T_{\mathrm{mean},i} w_{\mathrm{LC},i}}{\sum_{i=DoY_{3\mathrm{LC}}}^{DoY_{0\mathrm{LC}}} |w_{\mathrm{LC},i}|} \tag{18.}$$

The annual *DoY* of LC is then calculated in a linear equation.

$$DoY_{\mathrm{LC}} = k_{\mathrm{LC}} wA_{\mathrm{LC}} + d_{\mathrm{LC}} \tag{19.}$$

2.3.2.2 Seasonal Leaf Area Development

In this section a function is presented, describing relative leaf area (Kc_{LAI}) in an interval from zero to one (see Figure 8). Five phenological stages are distinguished: (i) Dormancy, (ii) a linear onset of the growing season, (iii) a polynomic convergence with the maximum, (iv) a plateau stage, and (v) senescence, which is described, using a third order polynomial (*smoothstep function*, compare 8 Appendix) Five parameters define the shape of the function. Four key *DoYs* (DoY_{LU}: Leaf unfolding, DoY_{CC}: Canopy closure, DoY_{LC}: Leaf coloring, DoY_{LE}: Litterfall end) define the seasonal development; the parameter ID_{LAI} accounts for a relative fraction of indeciduous trees.

$$Kc_{\mathrm{LAI}} = ID_{\mathrm{LAI}} + (1 - ID_{\mathrm{LAI}}) \begin{cases} 0 & DoY \leq DoY_{\mathrm{LU}} \lor DoY > DoY_{\mathrm{LE}} \\ \dfrac{4t_{\mathrm{LU}}}{3} & DoY_{\mathrm{LU}} < DoY \leq DoY_{2/3} \\ \dfrac{8t_{\mathrm{LU}} - 4{t_{\mathrm{LU}}}^2 - 1}{3} & DoY_{2/3} < DoY \leq DoY_{\mathrm{CC}} \\ 1 & DoY_{\mathrm{CC}} < DoY \leq DoY_{\mathrm{LC}} \\ 1 - 3{t_{\mathrm{LC}}}^2 + 2{t_{\mathrm{LC}}}^3 & DoY_{\mathrm{LC}} < DoY \leq DoY_{\mathrm{LE}} \end{cases} \tag{20.}$$

The temporal center of the unfolding period marks the transition from linear increment to polynomic flattening.

$$DoY_{2/3} = \frac{DoY_{\mathrm{LU}} + DoY_{\mathrm{CC}}}{2} \tag{21.}$$

The end of the growing season is calculated as the sum of the mean start of senescence and the length of the litterfall event.

$$DoY_{\mathrm{LE}} = DoY_{\mathrm{LC}} + l_{\mathrm{LC}} \tag{22.}$$

The *DoY* is normalized inside the corresponding interval by following equations:

$$t_{\mathrm{LU}} = \frac{DoY - DoY_{\mathrm{LU}}}{DoY_{\mathrm{CC}} - DoY_{\mathrm{LU}}} \tag{23.}$$

$$t_{\mathrm{LC}} = \frac{DoY - DoY_{\mathrm{LC}}}{l_{\mathrm{LC}}} \tag{24.}$$

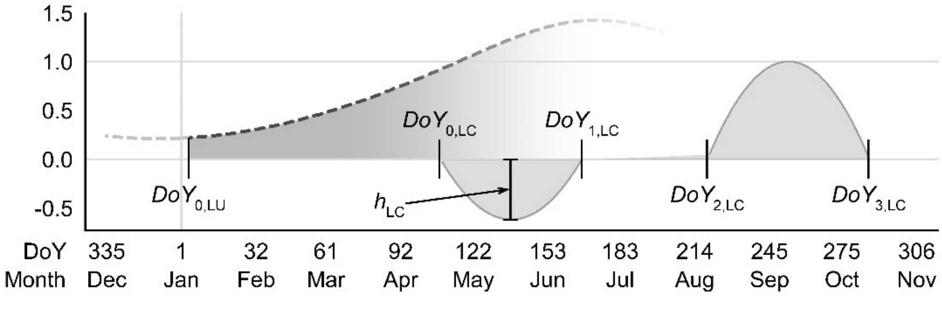

Figure 7: Air temperature multipliers, utilized in the assessment of LU and LC. The factor f_{dl} (dashed line), calculated as function of day-length, serves in the determination of the onset of the growing season. $DoY_{0,\mathrm{LC}}$ marks the potential start of the temperature accumulation in winter. For the calculation of the timing of LC, T_{mean} is weighted by a parabolic shaped function, within two intervals. Assuming a negative influence of high spring temperatures on the timing on senescence, the parabolic function in the first interval takes negative values. Due to a positive effect of high late summer on growing season length, the multiplier of the second interval is also positive. Utilizing the weighted average of both temporal windows combined, the timing of LC is calculated in a simple linear model.

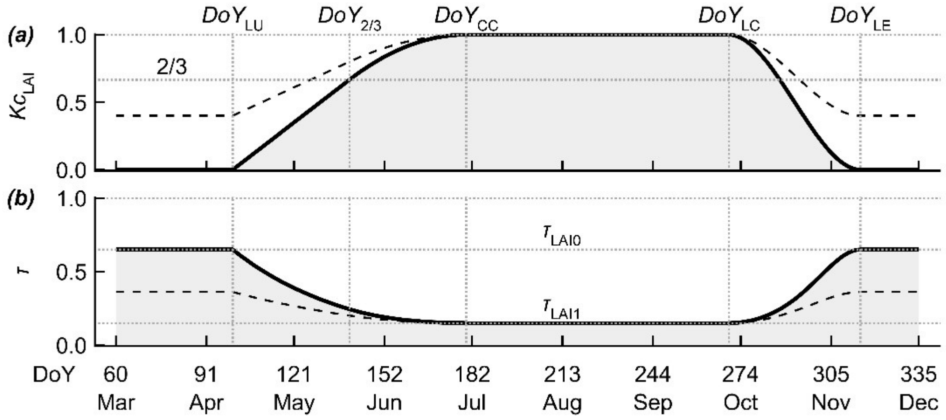

Figure 8: (a) Construction of the relative LAI index (Kc_{LAI}) with parameters DoY_{LU} =100, DoY_{CC}=180, DoY_{LC}=270, DoY_{LE}=315. The first half of the leaf unfolding period (DoY_{LU}- $DoY_{2/3}$) is described utilizing a linear equation. The second half ($DoY_{2/3}$- DoY_{CC}) is described using a second order polynomial. Leaf senescence (DoY_{LC}- DoY_{LE}) is modeled with the *smoothstep function*. Solid and the dashed line account for an indeciduous fraction (IC_{LAI}) of 0% and 40%, respectively. (b) Definition of the relative radiation transmission (τ) as a function of Kc_{LAI} using τ_{LAI0}=0.65 for the dormant season and τ_{LAI1}=0.15 at full vegetation cover. The solid and the dashed line again account for an evergreen fraction of 0% and 40%, respectively.

2.3.3 Water Balance Model

2.3.3.1 Fog Interception Precipitation

This very simple static model employs three parameters. Input variables are *rH* (daily average), daily mean temperature and wind speed. The mean temperature is used to calculate saturation vapor pressure (E_{sat}, kPa), and subsequently the saturation water content of the air (ρ, kg m^{-3}). Having available only observations of daily mean *rH*, there is no direct information on the temporal frequency within one day, saturation vapor pressure is actually reached and thus conditions might be suitable for the generation of fog precipitation. Therefore, the dimensionless model variable f_{sat} is introduced, which enables conversion of *rH* into an estimate of the relative frequency of saturation events within one day. The calculation utilizes the *smoothstep function* (see 8 Appendix). It assumes values in a range from zero to one. The parameter (rH_0) defines a supposed minimum of the daily average *rH*, where fog is occurring. At *rH* =100, fog is supposed to occur the entire day.

$$f_{\mathrm{sat}} = smooth(rH, rH_0, 100,0,1) \tag{25.}$$

As a simple analytical model, fog drip can be described as the product of liquid water content (*LWC*, kg m^{-3}) and deposition velocity of aerosol particles (Slinn, 1982), where deposition velocity is assumed to be almost proportional to the wind speed above the canopy. Due to unavailability of *LWC* measurement, proportionality of f_{sat} and the mean daily liquid water content is assumed.

$$f_{\mathrm{sat}} \sim LWC \tag{26.}$$

Therefore, the resulting model can be written as the product of the relative frequency of daily saturation events, the water content at saturation, the mean wind speed (u_2, m s^{-1}), and a coefficient f_c, which scales this product to actual daily fog precipitation sums [mm].

$$P_{\mathrm{fog}} = f_{\mathrm{sat}} f_{\mathrm{c}} u_2 \tag{27.}$$

The fog precipitation module is very sensitive to humidity data. Minor differences in the measurement of relative humidity will yield highly different results in the amount of modeled fog precipitation. If no data for validation is available, and accordingly the data quality of humidity measurement in the range close to saturation water content is poor, the impact of whole module can be reduced by setting f_c to a low value, or even zero. The sum of observed precipitation and fog precipitation states the input at the canopy.

$$P_{\mathrm{sum}} = P_{\mathrm{obs}} + P_{\mathrm{fog}} \tag{28.}$$

2.3.3.2 Precipitation Interception

In this section, I present an analytical precipitation interception module, which can be interpreted as an analogue to the Langmuir adsorption isotherm, where interception (I) and throughfall (Tf) are replacing occupied sorption sites and solution concentration, respectively. K_i corresponds to the Langmuir adsorption constant. The latter defines the impermeability of the canopy at low precipitation intensity. C_{max} [mm] sets the maximum possible charge of the canopy.

$$I = \frac{K_{\mathrm{i}} C_{\mathrm{max}} Tf}{1 + K_{\mathrm{i}} Tf} \tag{29.}$$

The solving of the equation for Tf, is described in the Appendix (Eq. A8 – A11). The determination of throughfall utilizes the sum of observed precipitation and modeled fog precipitation, the shape parameters of the Langmuir type equation, plus two auxiliary variables (Tf_h, P_h) which are derived, from the canopy storage of the previous day (C_{t-1}).

$$Tf_{\mathrm{h}} = \frac{C_{t-1}}{K_{\mathrm{i}}(C_{\mathrm{max}} - C_{t-1})} \tag{30.}$$

$$P_{\mathrm{h}} = Tf_{\mathrm{h}} + C_{t-1} \tag{31.}$$

Actual throughfall is determined.

$$Tf = tru(P_{\mathrm{sum}} + P_{\mathrm{h}}, C_{\mathrm{max}}, K_{\mathrm{i}}) - Tf_{\mathrm{h}} \tag{32.}$$

Actual interception is calculated as the difference of incoming precipitation and throughfall:

$$I = P_{\mathrm{sum}} - Tf \tag{33.}$$

Canopy storage prior to canopy evaporation is defined as:

$$C_{\mathrm{init}} = C_{t-1} + I \tag{34.}$$

The determination of the canopy interception evaporation (E_I) utilizes the FAO-Penman Monteith reference evapotranspiration (ET_o) (Allen et al., 1998), modified with an empirical coefficient (Kc_{canopy}).

$$E_{\mathrm{I}} = \begin{cases} ET_{\mathrm{o}} Kc_{\mathrm{canopy}}, & C_{\mathrm{init}} \geq ET_{\mathrm{o}} Kc_{\mathrm{canopy}} \\ C_{\mathrm{init}}, & C_{\mathrm{init}} < ET_{\mathrm{o}} Kc_{\mathrm{canopy}} \end{cases} \tag{35.}$$

At last, the actual canopy storage is calculated.

$$C_t = C_{\mathrm{init}} - E_{\mathrm{I}} \tag{36.}$$

As this model focuses on deciduous forest stands, it seems indispensable to consider a change of interception characteristics with the change of canopy cover throughout the year. Analogue to Bastiaanssen et al. (2012) and van Dijk and Bruijnzeel (2001), a linear relationship of leaf area index and canopy storage capacity is assumed. This is implemented by defining two parameters: (i) a minimum value at $Kc_{\mathrm{LAI}}=0$, is reflecting winter conditions with only stems and bare branches intercepting precipitation, and (ii) a maximum value at full vegetation cover ($Kc_{\mathrm{LAI}}=1$). For transition periods in between minimum and maximum a linear equation is employed, using both parameters.

$$C_{\max} = Kc_{\mathrm{LAI}}\left(C_{\max,\mathrm{LAI1}} - C_{\max,\mathrm{LAI0}}\right) + C_{\max,\mathrm{LAI0}} \qquad (37.)$$

Besides a change of $C_{\max}$, I hypothesize also a change in the permeability of the canopy throughout the season. In this work, the permeability of the canopy is controlled by the parameter K_i. Analogue to canopy storage capacity, it is assumed that a dense vegetation cover is leading to low permeability. The dependency of this shape parameter on leaf area is set analogue to the dependency of canopy storage capacity.

$$K_{\mathrm{i}} = Kc_{\mathrm{LAI}}\left(K_{\mathrm{i,LAI1}} - K_{\mathrm{i,LAI0}}\right) + K_{\mathrm{i,LAI0}} \qquad (38.)$$

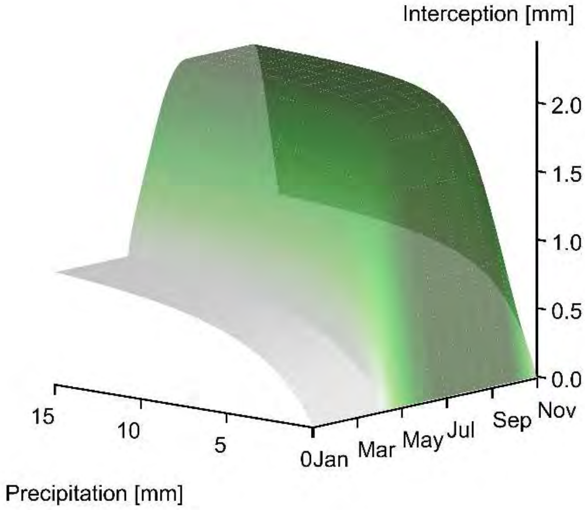

Figure 9: Seasonal course of precipitation dependent interception. For the parameters, used in the construction of Kc_{LAI} see **Figure 8**. Utilized interception parameters were: $C_{\max,\mathrm{LAI0}}=1$ mm, $C_{\max,\mathrm{LAI1}}=2.2$ mm, $K_{\mathrm{i,LAI0}}=0.3$, $K_{\mathrm{i,LAI1}}=4$. A high K_i value is leading to low permeability of the canopy at low precipitation sums. Note that the displayed response surface only applies to canopies, which were dry prior to the precipitation event!

2.3.3.3 Snow Dynamics

In the presented work, potential snowfall and snowmelt are processes which depend on daily temperature. In both cases, a critical temperature is defined, which allows the decision whether incoming precipitation falls as snow or rain, as well as snowmelt is taking place. Temperature threshold models might have shortcomings when working with mean temperatures on a daily base. In this case it is possible that the actual temperature crosses the threshold during the day, resulting in a transition of the state (rain/snow, frost/melt), undetected by the model (Hock, 2003). One possibility to tackle this problem would be the replacement of the threshold with a transition interval (Feiccabrino and Lundberg, 2008), or more resource demanding, the utilization of temperature data with a higher temporal resolution to cover temperature fluctuations within the day (Hock, 2003). There are possibilities to circumvent this necessity. For calculating relative partitions of snow and rain precipitation, (Willen et al., 1971) first presented an approach, using observed T_{min} and T_{max} and a critical temperature (T_{snow}).

$$p_{\text{snow}} = \begin{cases} 0, & T_{\text{snow}} \leq T_{\text{min}} \\ \dfrac{T_{\text{snow}} - T_{\text{min}}}{T_{\text{max}} - T_{\text{min}}}, & T_{\text{min}} < T_{\text{snow}} < T_{\text{max}} \\ 1, & T_{\text{snow}} \geq T_{\text{max}} \end{cases} \tag{39.}$$

This way the probability of a complete misjudgment of the precipitation phase is reduced (Federer, 1995). Actual rainfall and snowfall are then calculated as:

$$P_{\text{rain}} = Tf(1 - p_{\text{snow}}) \tag{40.}$$

$$P_{\text{snow}} = Tf p_{\text{snow}} \tag{41.}$$

In this work, the liquid water equivalent (LWE, mm) is the unit, used in all snow calculations. The determination of potential snowmelt is based on the classical degree-day method (Rango and Martinec, 1995), where snowmelt is assumed to occur, when the actual temperature exceeds a threshold (T_{melt}). The amount is assumed proportional to the difference of both temperatures. Dealing with T_{min} and T_{max}, the approach is modified. The variable f_{melt} can be described as temporal fraction of a day, the critical temperature for snowmelt is exceeded.

$$f_{\text{melt}} = \begin{cases} 1, & T_{\text{melt}} \leq T_{\text{min}} \\ \dfrac{T_{\text{max}} - T_{\text{melt}}}{T_{\text{max}} - T_{\text{min}}}, & T_{\text{min}} < T_{\text{melt}} < T_{\text{max}} \\ 0, & T_{\text{melt}} \geq T_{\text{max}} \end{cases} \tag{42.}$$

The mean temperature for the temporal fraction above the threshold (m_{melt}) is calculated.

$$m_{\text{melt}} = \begin{cases} \dfrac{T_{\text{max}} + T_{\text{min}}}{2}, & T_{\text{melt}} \leq T_{\text{min}} \\ \dfrac{T_{\text{max}} + T_{\text{melt}}}{2}, & T_{\text{min}} < T_{\text{melt}} < T_{\text{max}} \end{cases} \tag{43.}$$

Potential snowmelt (pot_{melt}) is then described, as product of the temporal fraction above the threshold, the temperature difference, and an empirical degree-day factor (DDF_{melt}, mm°C^{-1}d^{-1}).

$$pot_{\text{melt}} = f_{\text{melt}}(m_{\text{melt}} - T_{\text{melt}})DDF_{\text{melt}} \tag{44.}$$

The snowpack storage (mm liquid water equivalent), prior to snowmelt is calculated:

$$SP_{\text{init}} = SP_{t-1} + P_{\text{snow}} \tag{45.}$$

Actual snowmelt is defined.

$$P_{\text{melt}} = \begin{cases} pot_{\text{melt}}, & SP_{\text{init}} \geq pot_{\text{melt}} \\ SP_{\text{init}}, & SP_{\text{init}} < pot_{\text{melt}} \end{cases} \tag{46.}$$

Finally, the actual snowpack storage is determined.

$$SP_t = SP_{\text{init}} - P_{\text{melt}} \tag{47.}$$

2.3.3.4 Soil Moisture Dynamics

At the soil surface, the pathway for incoming water is branching up into bypass flow and soil infiltration. In this work, bypass flow is defined as the fraction of incoming water which hits the forest ground surface but is not coming in closer contact with the soil matrix. In the presented formulation, bypass flow is generated two ways. The first bypass partition (B_1) is calculated by multiplying the sum of rainfall and snowmelt with a constant factor (f_{BY}) taking values from zero to one.

$$B_1 = f_{\mathrm{BY}}(P_{\mathrm{rain}} + P_{\mathrm{melt}}) \tag{48.}$$

The remaining water states the available input (A) to the soil box.

$$A = (P_{\mathrm{rain}} + P_{\mathrm{melt}})(1 - f_{\mathrm{BY}}) \tag{49.}$$

In this work, a zero-dimensional box model approach for modeling soil moisture dynamics is presented, meaning the formulation lacks vertical or horizontal resolution within the soil column. Therefore, the soil could be considered as a box with a basal area of one m^2 and a chosen soil depth (z_r, mm), with uniform characteristics throughout the entire profile. The calculated soil moisture aims to resemble the observed mean water content [LL^{-1}]; calculated input/output fluxes equal sums [Lm^{-2}], vertically integrated over z_r. So called box models have been reviewed and tested for their applicability in works by Baudena et al. (2012) and Kumagai et al. (2009).

The net soil water balance can be reduced to an ordinary differential equation were z_r resembles the active soil depth [mm], and θ the volumetric water content [LL^{-1}].

$$z_{\mathrm{r}}\frac{d\theta}{dt} = (A - B_2) - (E_{\mathrm{C}} + E_{\mathrm{S}} + P_{\mathrm{S}}) \tag{50.}$$

The change of soil water storage can therefore be described as the difference of infiltrating water (available water minus saturation excess overflow) and the sum of transpiration, soil evaporation, and percolation. The presented formulation neglects the possibility of capillary rise, lateral flow and moisture diffusion.

While the aboveground module handles processes in a sequential way, in the soil module several nonlinear processes, which both influence and depend on the soil water content, occur simultaneously. To linearize this set of nonlinear equations the classical 4th order Runge-Kutta method was implemented.

2.3.3.5 Saturation Excess Overflow (B_2)

When the entire pore spaced is filled with water, the excess water (forming the second bypass partition) is calculated as:

$$B_2 = \begin{cases} z_{\mathrm{r}}\theta + A - z_{\mathrm{r}}\theta_{\mathrm{sat}}, & \theta + A/z_{\mathrm{r}} \geq \theta_{\mathrm{sat}} \\ 0, & \theta + A/z_{\mathrm{r}} < \theta_{\mathrm{sat}} \end{cases} \tag{51.}$$

2.3.3.6 Evapotranspiration (*ET*)

In the presented approach, the *FAO-Penman-Monteith equation* (Allen et al., 1998) serves as the centerpiece for the determination of actual evapotranspiration rates. After calculation of the reference evapotranspiration (ET_{O}), using daily averages of radiation, humidity, wind speed and temperature, it is scaled to the actual evaporation, e.g. transpiration rates, using several coefficients. Possible energy inputs by ground flux are neglected. In this work, no detailed description of the calculation of ET_{O} is given. The following section should just highlight the parts where the applied procedure differs from the standard procedures of the computation of the reference *ET*.

2.3.3.7 Canopy Transpiration (**E_C**)

Three coefficients influence the response of transpiration to the forest stand. (i) With all other controlling factors kept constant, proportionality of the relative leaf area (Kc_LAI) to E_C is assumed. (ii) Further, a site-specific crop coefficient (Kc_tree) for the selected forest stand is introduced. (iii) A soil moisture dependent stress coefficient ($Kc_\mathrm{s,tree}$) defines the response of E_C to soil drought.

$$Kc_\mathrm{s,tree} = msmooth(\theta, \theta_\mathrm{pwp}, \theta^*, 0{,}1, ET_\mathrm{m}) \qquad (52.)$$

Above a critical soil moisture content *(θ^*),* transpiration is assumed unlimited, with stomata fully opened. In this case model transpiration is defined solely as the product of ET_O the Crop Coefficient for the stand and the relative stage of the growing season. Undershooting θ^* plants begin to respond to reduced water availability by closing stomata. At soil moisture levels below the wilting point (θ_pwp), all stomata are assumed fully closed, resulting in a complete shut-down of transpiration. Consistent with this behavior, a relative stress coefficient is introduced, which declines in between θ^* and θ_pwp from one to zero. Many authors describe this transition using a linear relationship (Laio et al., 2001). In this work, the *modified smoothstep function* is applied with the shape parameter ET_m. Its derivation is defined in the Appendix (Equation A1, A4, A5). Actual canopy transpiration (E_C) is then calculated as the product of the reference evapotranspiration and three coefficients.

$$E_\mathrm{C} = ET_\mathrm{o} Kc_\mathrm{tree}\, Kc_\mathrm{LAI}\, Kc_\mathrm{s,tree} \qquad (53.)$$

2.3.3.8 Soil Evaporation (**E_S**)

The calculation of E_S differs slightly from the calculation of E_C: For determination of reference evapotranspiration below the plant cover (ET_soil*)* global radiation below the canopy *(R_soil)* is used. Therefore, the relative radiation transmittance (τ) is estimated as function of the actual state of vegetation cover, using Beer-Lamberts law.

$$\tau = \tau_\mathrm{LAI0} \exp\,(\ln \frac{\tau_\mathrm{LAI1}}{\tau_\mathrm{LAI0}} Kc_\mathrm{LAI}) \qquad (54.)$$

τ_LAI1 and τ_LAI0 define transmittance at vegetation period extremes Kc_LAI = 1 and Kc_LAI =0, respectively*.* Global radiation below the canopy is calculated as product of the transmittance and the net radiation above the canopy.

$$R_\mathrm{soil} = \tau R_\mathrm{n} \qquad (55.)$$

The calculations of the stress coefficients for evaporation ($Kc_\mathrm{s,soil}$) and transpiration share two of three parameters. In the determination of E, θ_pwp is replaced with the residual water content (θ_res), which is assumed to lie below the wilting point.

$$Kc_\mathrm{s,soil} = msmooth(\theta, \theta_\mathrm{res}, \theta^*, 0{,}1, ET_\mathrm{m}) \qquad (56.)$$

In the absence of a snow cover, soil evaporation is defined as the product of ET_soil, the stress coefficient, and a crop coefficient for soil evaporation *(Kc_soil)*. A present snowpack is assumed to suppress E_S completely.

$$E_\mathrm{S} = \begin{cases} ET_\mathrm{soil} Kc_\mathrm{s,soil}\, Kc_\mathrm{soil}, & SP_\mathrm{t} = 0 \\ 0, & SP_\mathrm{t} > 0 \end{cases} \qquad (57.)$$

2.3.3.9 Percolation (**P_s**)

Comparable to evapotranspiration, I describe drainage as a threshold process. Below water holding capacity *(θ_fc)*, gravitational potential is assumed to be fully compensated by the soil matrix potential, resulting in no change in soil water storage due to leakage. Exceeding this critical value, percolation is initiated, reaching its maximum rate *(k_{sat})* at soil water saturation *(θ_{sat})*. For modeling the transition of leakage losses between θ_{fc} and θ_{sat}, Laio et al. (2001) use an exponential relationship.

$$P_{\mathrm{S}} = k_{\mathrm{sat}} \frac{e^{\beta(\theta-\theta_{\mathrm{fc}})} - 1}{e^{\beta(\theta_{\mathrm{sat}}-\theta_{\mathrm{fc}})} - 1} \tag{58.}$$

The parameter β defines the shape of the transition from θ_{fc} to θ_{sat}. Also, in this work percolation is formulated in exponential form. The parameter θ_{m} marks the relative position between θ_{fc} and θ_{sat} where the conductivity reaches 50% of k_{sat}.

$$P_{\mathrm{S}} = z_{\mathrm{r}} k_{\mathrm{sat}} \begin{cases} 0, & \theta \leq \theta_{\mathrm{fc}} \\ \left(\dfrac{\theta - \theta_{\mathrm{fc}}}{\theta_{\mathrm{sat}} - \theta_{\mathrm{fc}}}\right)^{\frac{\ln 0.5}{\ln \theta_{\mathrm{m}}}}, & \theta_{\mathrm{fc}} < \theta < \theta_{\mathrm{sat}} \\ 1, & \theta \geq \theta_{\mathrm{sat}} \end{cases} \tag{59.}$$

Finally, the stream discharge can be determined as the sum of two bypass fractions and percolation.

$$D = B_1 + B_2 + P_{\mathrm{S}} \tag{60.}$$

2.3.4 Sulfur Biogeochemistry

Disregarding S inputs from dry deposition and gaseous losses, S enters and leaves the undisturbed forest ecosystem mainly in form of aqueous solute SO_4^{2-} (Likens et al., 2002). Consequently, there is a strong link between net S balance and the hydrologic balance. Also the S uptake by plants, the mineralization of S containing biomass (Moyano et al., 2012; Sierra et al., 2015), as well as other microbially mediated S transformations in the soil are assumed to show a strong response to soil moisture (Aulakh et al., 2002; Janzen and Bettany, 1987; Solberg et al., 2005). Therefore, an expedient description of the water balance seems crucial for modeling the S dynamics of a forest stand.

The simulator, which is outlined in this section, works as an extension to the WBM. Running the *Sulfur Dynamics Model* (SDM) requires the output of the WBM. Additional to that, the simulator requires daily information about SO_4-S inputs via wet deposition above the canopy. To calculate the amount of dry and occult deposition, the daily mean SO_2 air concentration is required. For the calculation of biological S transformations in the soil, the mean daily soil temperature is required. All other necessary input data is derived from the output of the WBM simulation. Fluxes, associated to the solute phase of S (canopy interception, snow dynamics, infiltration, bypass flow, percolation) are fully controlled by the associated water fluxes, defined through the WBM. All these processes are calculated, using the following scheme. The change in the content of the solute [mg/m^2] of the desired pool, is defined as the product of content and the relative change of the water content of the pool during the timestep.

$$\frac{dCont}{dt} = Cont \frac{\frac{dWater}{dt}}{Water} \tag{61.}$$

Analog to the WBM, the SDM can be divided into an aboveground and a belowground module. A flowchart of both formulations is given in Figure 10. Only two aboveground processes are explicitly modeled in the SDM: Occult (fog) deposition and dry (stomatal) deposition. Here I assume the SO_4-S concentration in fog precipitation proportional to the SO_2 concentration in the air. The amount of daily fog deposition [mg/m^2] is calculated as the product of fog precipitation [mm], the average daily SO_2-S air concentration [mg/m^3], multiplied with a specific enrichment factor.

$$occult = SO_2Sf_{\text{occult}}FOG \tag{62.}$$

The determination of stomatal deposition also utilizes the SO_2-S air concentration. As proxy for the degree of stomatal opening I use the soil moisture dependent stress coefficient ($Kc_{\text{s,tree}}$, see also section 2.3.3.6). A value of one would correspond to fully opened stomata, whereat a value of zero would result in a complete shutdown of the stomatal gas exchange. The stands relative leaf area (Kc_{LAI}) serves as proxy for the foliage surface (or the relative number of stomata), exposed to sulfur dioxide. The function is stated as a product of the SO_2-S air concentration [mg/m^3], a specific enrichment factor, the stress coefficient, the relative leaf area and the daily mean wind speed [m/s], measured two meters above ground.

$$dry = SO_2Sf_{\text{dry}}Kc_{\text{s,tree}}Kc_{\text{LAI}}u_2 \tag{63.}$$

Belowground and biotic S fluxes and transformations are stated as a system of five ordinary differential equations which are solved simultaneously using the 4th order explicit Runge-Kutta scheme. The temporal dynamics of SO_4-S (*Sol*) in the soil solution are formulated, using following equation. Infiltration (*Inf*) and the leaching (*Leac*) of sulfate-S are fluxes, driven by the WBM. M_{stable} and M_{labile} state the input to the soil solution via mineralization of the stabile organic and labile organic sulfur pool, respectively. U_{plant} and U_{micro} state the uptake of S by plants and soil microbes, respectively. *Ads* accounts for the adsorbed amount of SO_4-S.

$$\frac{dSol}{dt} = (Inf + M_{\text{stable}} + M_{\text{labile}}) - \left(Leac + U_{\text{plant}} + U_{\text{micro}} + \frac{dAds}{dt}\right) \tag{64.}$$

Foliage S (*Fol*) dynamics are described as the difference of plant uptake, multiplied with a constant fraction, describing the partition of plant uptake, routed to the foliage, plus dry deposition input to the canopy, minus the autumnal litterfall loss of S. The simulator neglects the possibility of S washout from the canopy. The seasonal foliage S pool is the only explicitly defined biomass pool in the SDM. As the interest does not lie in tree growth, I do not assume a change in S storage during stand development. It could be claimed, that living biomass S storage is incorporated in the labile as well as the stabile soil organic S pool.

$$\frac{dFol}{dt} = f_{\text{fol}}U_{\text{plant}} + dry - litter \tag{65.}$$

In this model, two pools are used to describe the dynamics of organic soil sulfur: A stable pool accounts for recalcitrant organosulfur compounds, a labile pool accounts for more transitory organic sulfur species. The first pool could be viewed as corresponding to carbon-bond S, the second could be assigned to ester-bond sulfate (McGill and Cole, 1981). As a simplification, it is assumed that microbial S immobilization is only contributing to the labile pool. The balance of the labile organosulfur pool can be stated as the difference of the labile partition of plant uptake, which is not routed to the foliage, and litterfall, plus the microbial S assimilation, and the loss via mineralization. As a simplification, I assume a steady state forest with an unchanging S content in the living woody biomass.

$$\frac{dLabile}{dt} = f_{\text{labile}}\left((1 - f_{\text{fol}})U_{\text{plant}} + litter\right) + U_{\text{micro}} - M_{\text{labile}} \tag{66.}$$

The stable pool is formulated analog to the labile pool. The stabile fraction of plant uptake and litterfall is formulated as 1-f_{labile}.

$$\frac{dStable}{dt} = (1 - f_{\text{labile}})\left((1 - f_{\text{fol}})U_{\text{plant}} + litter\right) - M_{\text{stable}} \tag{67.}$$

Sulfate adsorption is modeled, using the *Langmuir Isotherm*. M_{ads} and K_{ads} are site specific model parameters, *Conc* states the SO_4-S concentration in the soil solution. To express the kinetics of the process, it is coupled with a first order decay function.

$$\frac{dAds}{dt} = \lambda_{\text{ads}}\left(\frac{M_{\text{ads}}K_{\text{ads}}Conc[mg/L]}{1 + K_{\text{ads}}Conc[mg/L]} - Ads\right) \tag{68.}$$

The concentration of SO_4-S in the soil solution is calculated as the storage in soil solution, divided by the product of soil depth and soil moisture.

$$Conc[mg/L] = \frac{Sol[mg/m^2]}{z_{\mathrm{r}}\theta} \tag{69.}$$

The lambda value is derived from the process' half-life.

$$\lambda_{\mathrm{ads}} = -\frac{\ln 0.5}{HL_{\mathrm{ads}}} \tag{70.}$$

The function stated below describes the response ($resp_{\mathrm{Q10}}$) of microbial S transformations to soil temperature. A base temperature of 8°C should resemble the annual average soil temperature at the investigated stands. The factor f_{Q10} describes the relative increase of the response when soil temperature rises by 10°C.

$$resp_{\mathrm{Q10}} = e^{\frac{\ln f_{\mathrm{Q10}}}{10}(T_{\mathrm{soil}} - 8°C)} \tag{71.}$$

In the WBM, the autumnal decrease of the LAI inside the interval DoY_{LC}- DoY_{LE} (compare section 2.3.2.2) is described using the *smoothstep function* (see 8 Appendix). To define the relative amount of sulfur in the litterfall (*litter*) at first the relative amount of daily litterfall (f_{litter}) is calculated.

$$f_{\mathrm{litter}} = \begin{cases} 0, & DoY < DoY_{\mathrm{LC}} \\ 1 - \frac{LAI_{\mathrm{Kc,DoY}}}{LAI_{\mathrm{Kc,DoY-1}}}, & DoY_{\mathrm{LC}} \le DoY < DoY_{\mathrm{LE}} \\ 1, & DoY = DoY_{\mathrm{LE}} \end{cases} \tag{72.}$$

To calculate the amount of sulfur in the litter fall this value is multiplied with the sulfur content in the foliage pool.

$$litter = f_{\mathrm{litter}} fol \tag{73.}$$

The latter function describes the response ($resp_{\theta}$) of microbial S transformations to soil moisture (see Sverdrup et al., 2007). At soil moisture levels below (θ_0) and above a certain threshold (θ_3), all microbial transformations are assumed to come to a halt ($resp_{\mathrm{opt}}$=0). At medium soil moisture between θ_1 and θ_2 conditions are assumed to be optimal ($resp_{\mathrm{opt}}$). In between θ_0 and θ_1 and accordingly in between θ_{moist} and θ_{drown} a linear transition is set.

$$resp_{\theta} = resp_{\min} + \left(resp_{\mathrm{opt}} - resp_{\min}\right) \begin{cases} 0, & \theta \le \theta_0 \vee \theta < \theta_3 \\ \frac{\theta - T_0}{T_1 - T_0}, & \theta_0 < \theta \le \theta_1 \\ 1, & \theta_1 < \theta \le \theta_2 \\ 1 - \frac{\theta - T_2}{T_3 - T_2}, & \theta_2 < \theta \le \theta_3 \end{cases} \tag{74.}$$

$$V_{\mathrm{m}} = \frac{V_{\max} Conc[mg/L]}{K_{\mathrm{m}} + Conc[mg/L]} \tag{75.}$$

The formulation of microbial S immobilization utilizes the *Michaelis-Menten equation*.

$$V_{\mathrm{m,immobil}} = \frac{V_{\mathrm{max,immobil}} Conc[mg/L]}{K_{\mathrm{m,immobil}} + Conc[mg/L]} \tag{76.}$$

The maximal assimilation rate depends on soil temperature and soil moisture.

$$V_{\mathrm{max,immobil}} = V_{\mathrm{coeff,immobil}} resp_{\mathrm{Q10,immobil}} resp_{\mathrm{\theta,immobil}} \tag{77.}$$

The mineralization of stable organic S is stated as first order decay process, dependent on soil temperature and soil moisture.

$$M_{\mathrm{stable}} = Stable\lambda_{\mathrm{stable}} resp_{\mathrm{Q10,mineral}} resp_{\theta\mathrm{,mineral}} \tag{78.}$$

The release of labile organic S (ester-bond) is also described as first order decay process dependent on soil temperature and soil moisture. In addition, the rate of mineralization is also dependent on the SO_4-S soil solution concentration.

$$M_{\mathrm{labile}} = Labile\lambda_{\mathrm{sulfatase}} resp_{\mathrm{Q10,mineral}} resp_{\theta\mathrm{,mineral}} \tag{79.}$$

The simulator comprises the effect of microbial sulfatase release on the kinetics of the labile organic S. A low SO_4 concentration in the soil solution promotes the microbial release of sulfatase, thus accelerating the mineralization release of ester-bond sulfate (Scherer, 2009). This is implemented by making the process' half-life linearly dependent on the soil solution concentration. To set the linear dependence, half-lives are defined for two key solution concentrations (0 and 10 [mg SO_4-S /L]).

$$k_{\mathrm{sulfatase}} = \frac{HL_{\mathrm{sulfatase.10}} - HL_{\mathrm{sulfatase.0}}}{10} \tag{80.}$$

The linear equation takes the form:

$$HL_{\mathrm{sulfatase}} = k_{\mathrm{sulfatase}} C[mg/L] + HL_{\mathrm{sulfatase.0}} \tag{81.}$$

The half-life is used to calculate the lambda value of the first order decay process.

$$\lambda_{\mathrm{sulfatase}} = -\frac{\ln 0.5}{HL_{\mathrm{sulfatase}}} \qquad (82.)$$

The S uptake of deciduous trees is mediated through two distinct active carrier systems (Herschbach and Rennenberg, 2001). Kreuzwieser and Rennenberg (1998) postulate high affinity and low affinity uptake systems. Low sulfate level in the aqueous phase of forest soils, point to the dominance of the high affinity system (Herschbach and Rennenberg, 2001). The uptake of S beech trees is simulated using Michaelis-Menten kinetics. The assumption is that plant uptake is only taking place during the growing season.

$$U_{\mathrm{plant}} = \begin{cases} \dfrac{V_{\mathrm{max,plant}} Conc[mg/L]}{K_{\mathrm{m,plant}} + Conc[mg/L]}, & Kc_{\mathrm{LAI}} > 0 \\ 0, & Kc_{\mathrm{LAI}} = 0 \end{cases} \qquad (83.)$$

It is also claimed that plants only take up a certain amount of S during the season. After a specific demand is met (ACU_{starve}), plants start to throttle the uptake. After a second threshold is met (ACU_{sat}), plants shut down the uptake of S completely. The accumulated uptake is calculated on a Day o Year base.

$$ACU_{\mathrm{DoY}} = \begin{cases} 0, & DoY = 1 \\ U_{\mathrm{plant}} + ACC_{\mathrm{DoY-1}}, & DoY > 1 \end{cases} \qquad (84.)$$

The transition of the demand is modeled under the usage of the *smoothstep function* (see Appendix).

$$V_{\mathrm{max,plant}} = smooth\left(ACU_{\mathrm{DoY}}[g/m^2], ACU_{starve}, ACU_{sat}, V_{\mathrm{starve,plant}}, V_{\mathrm{sat,plant}}\right) \qquad (85.)$$

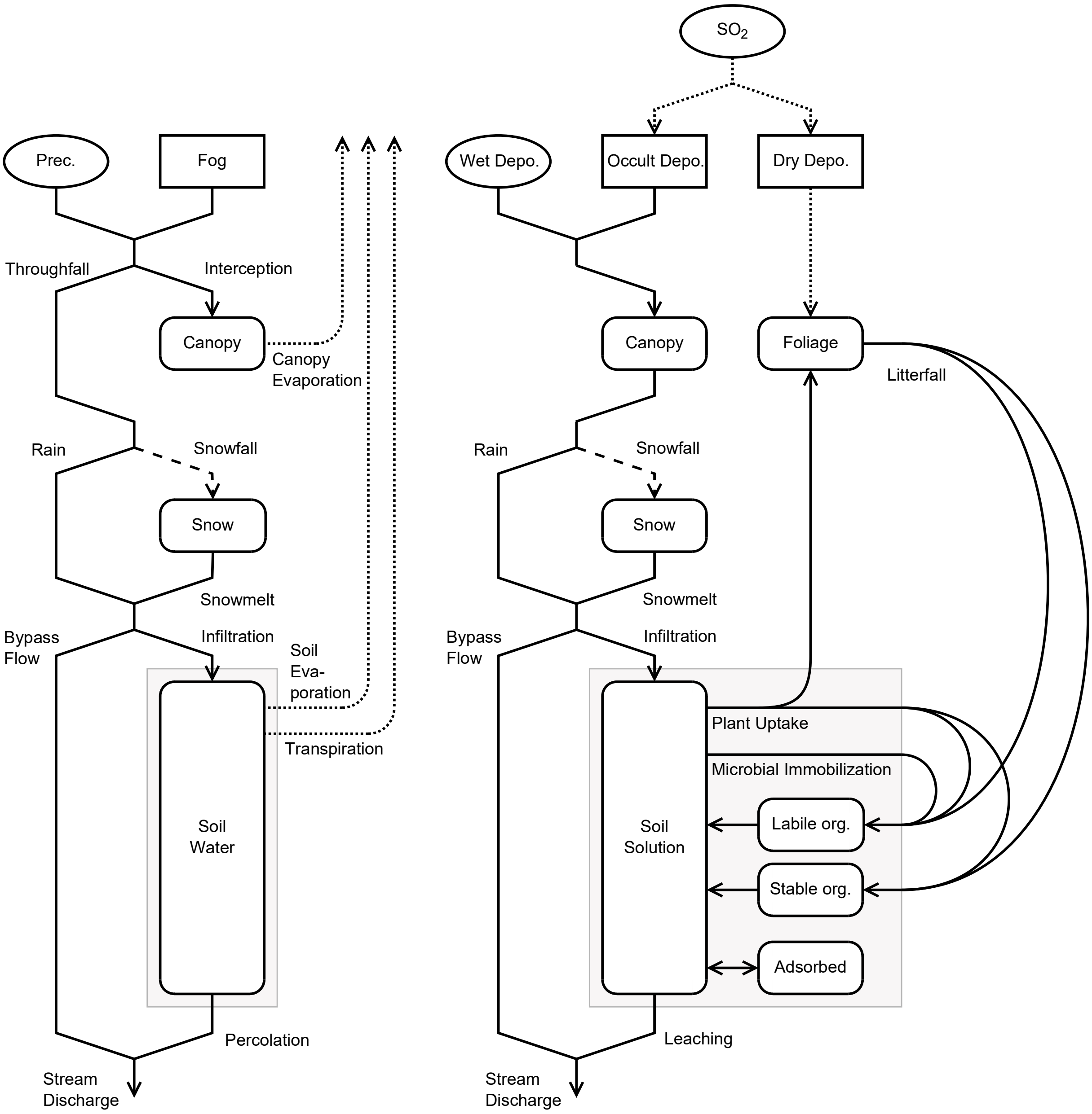

Figure 10: Flowchart of the WBM (left) and the SDM (right)

2.4 Model Application

2.4.1 Parameterization of the Soil Temperature Model

The model for soil temperature was applied to each site and depth specifically. Emphasis was laid on its application on longest possible records of T_{soil}, to cover the broadest possible range of different environmental states, which might have a potential influence on soil thermal regimes. On the other hand it seems obvious, that due to changes in leaf area, undergrowth, litter layer, water consumption, etc., forest T_{soil} regimes undergo a certain shift during stand development (compare: Kang et al., 2000). In cases where, for reasons unknown, an obvious change in the soil thermal regime was observed, the time frame of the investigation was manually narrowed down. Both $T_{\mathrm{soil},t}$ and $T_{\mathrm{shift},t}$ were initialized at 8°C. The simulator ran a 150-day spin-up prior to the analysis time frame. For model parameterization a *simulated annealing* algorithm (Kirkpatrick et al., 1983) was applied, selecting an exponential cooling schedule. Optimization/evaluation criterion was in every case the *Nash-Sutcliffe Efficiency* (NSE) (Nash and Sutcliffe, 1970); a function, which is generally used to evaluate hydrological models.

$$NSE = 1 - \frac{\sum_{i=1}^{n}\left(T_{\text{soil},obs,i} - T_{\text{soil},sim,i}\right)^2}{\sum_{i=1}^{n}\left(T_{\text{soil},obs,i} - \overline{T_{\text{soil},obs}}\right)^2} \tag{86.}$$

Enabling a balanced split, the calibration was conducted on data from odd years, data from even years served in the evaluation. Making the simulation result comparable to other works, other performance indices like Root Mean Squared Error (RMSE), mean absolute error (MAE) and mean bias error (MBE) were calculated.

$$RMSE = \left[n^{-1}\sum_{i=1}^{n}\left(T_{\text{soil},obs,i} - T_{\text{soil},sim,i}\right)^2\right]^{1/2} \tag{87.}$$

$$MAE = n^{-1}\sum_{i=1}^{n}\left|T_{\text{soil},obs,i} - T_{\text{soil},sim,i}\right| \tag{88.}$$

$$MBE = n^{-1}\sum_{i=1}^{n} T_{\text{soil},obs,i} - T_{\text{soil},sim,i} \tag{89.}$$

2.4.1.1 Parameterization on limited input data

To test the simulators practical suitability to cope with limited input data, the T_{soil} record of Klausen-Leopoldsdorf (15 cm depth) was used, ranging from November 2001 to June 2013 (~11 years, 4053 valid observations). The dataset was split into n sectors of approximately equal size. The parameterization (simulated annealing) was performed, drawing only one random observation per sector. The remaining observations served in the evaluation. This step was repeated 12 times per n, each time with different random observations, to generate a distributed result. After 12 iterations, n was incremented, starting with $n = 4$, gradually progressing to $n = 2000$. This way, the minimum number of point observations was determined, necessary to yield satisfactory model performance.

2.4.2 Parameterization of the Phenological Module

The parameterization was conducted on the assembled timeseries, presented in section 2.2.1. The optimization was performed, using a combination of simulated annealing and the Gauss-Newton algorithm. Performance criterion was the Nash-Sutcliffe Efficiency.

2.4.3 Parameterization of the Water Balance Model

The simulator was parameterized, using time-series of observed soil moisture. Records of different depths were used to calculate a mean time-series, aiming to reflect the integrated volumetric soil moisture over soil depth (z_r). Averages over a soil depth of 500 mm were calculated for all sites. Both canopy and the snowpack storage were initialized at 0 mm. Soil water storage was initialized at the product of soil depth and the water content at field capacity ($z_r\theta_{fc}$). The model ran a 200 day spin up, prior to the performance analysis timeframe. Twenty-six parameters (compare **Table 6**) were optimized by inverse modeling; a simulated annealing algorithm was applied. Performance criterion was the Nash-Sutcliffe Efficiency (see section 2.4.1). The parameterization was performed over the entire investigation timeframe.

2.4.3.1 Water stress assessment

The obtained parameterization was used to run the model over a reference climate period of 30 years. The timeframe was set from Jan. 1983 to Dec. 2012. Then, eight scenarios of climate warming were applied. Temperatures were increased from 0 to 4°C in one-degree steps. Four scenarios were run under the assumption that (i) phenology retains the values of the reference climate; four scenarios were run with (ii) phenology responding to warmer conditions. This way, it was possible to quantify the influence of elongated growing seasons on the stands' water consumption and soil water deficit.

Different levels of water stress were calculated. The transpiration index (*Ti)* states the daily ratio between simulated actual transpiration and potential transpiration (transpiration which would occur under optimal root water supply) (Clausnitzer et al., 2011; Vilhar, 2016). In this formulation, it corresponds to the water stress coefficient ($Kc_{\mathrm{s,tree}}$) in the calculation of the actual transpiration rate.

$$Ti = Kc_{\mathrm{s,tree}} \tag{90.}$$

A level of one corresponds to unlimited transpiration, a level of zero would correspond to a complete shutdown of transpiration. Investigating beech stands, Schwärzel et al. (2009) found indications of noteworthy water stress when Ti fell below 70%. Therefore, a threshold for (at least) moderate soil water deficit of 0.7 seemed reasonable. According to Bréda et al. (2006), xylem embolism occurs when stomatal conductance drops below 10% of its initial value. Therefore, a second stress level was calculated: If Ti falls below 0.1, the stand is affected by severe drought.

According to Granier et al. (1999), water stress occurs when the *relative extractable water content* (REW) drops below the critical value of 0.4. REW is calculated by normalizing theta to the interval from the wilting point to field capacity. The formulation, which is presented here, allows soil moisture below the wilting point (θ_{pwp}) and above field capacity (θ_{fc}). Therefore, REW can take values below zero and above one!

$$REW = \frac{\theta - \theta_{\mathbf{pwp}}}{\theta_{\mathbf{fc}} - \theta_{\mathbf{pwp}}} \tag{91.}$$

Then, the number of days during the growing season with *Ti* or REW below the defined threshold was calculated. In this assessment, the growing season is considered as interval from the 25th of March (DoY=84) to the 11th of November (DoY=315). Years with more than 120 growing season days of *Ti* > 0.7 were defined as dry years. The threshold for drought years was reached with a minimum of 31 growing season days with *Ti* below 0.1. At last, to gain information about the stands' photosynthetic activity, the *gross primary production* (GPP, $\mathrm{gm^{-2}d^{-1}}$) is estimated as the product of *water-use efficiency* (WUE) and the transpiration rate.

$$GPP = E_C WUE \tag{92.}$$

To estimate the WUE, an empirical relationship was used, which was proposed by Tang et al. (2006). The water-use efficiency was calculated as function of the vapor pressure deficit (VPD).

$$WUE = 4.4 + 15.69 e^{-5.94\, VPD} \tag{93.}$$

2.4.4 Parameterization of the Sulfur Dynamics Model

Before running the SDM, three target criteria are defined, which mark a successful simulation:

- To bootstrap the SDM, a model spin-up was run, starting in the year 1770. As a primary requisite, the model has to achieve steady state conditions before atmospheric deposition starts to rise in 1880.

- The plots were sampled and analysed in 2010; the total S stock in forest floor and mineral soil (0-50 cm) was determined (EX: 78 gm^{-2}, JU: 102.6 gm^{-2}). The sum of all modeled soil S pools (adsorbed, stable organic, labile organic, soil solution) in 2010 has to be in a close range to the measured value.
- The simulator has to deliver a satisfactory reproduction of the observed timeline of the SO_4-S concentration in the monitored soil solution.

Plausible ranges for 25 parameters (Table 8) were defined. The SDM was calibrated via *Simulated Annealing* (Kirkpatrick, 1984). Performance criterion was the *Nash-Sutcliffe Model Efficiency* (Nash and Sutcliffe, 1970).

3 Results and Discussion

3.1 Soil Temperature

The model was applied to various sites and depths. In this work, a representative selection of 36 simulation runs is displayed. The simulator delivered good estimates of T_{soil} on all investigated forest sites. NSE values above 0.979 and RMSE consistently below 1 °C underline the outcome (compare Table 2), whereat good results were not limited to the topmost soil horizons. Increasing phase shift and the attenuation of the temperature wave with increasing soil depth, were also captured by the simulation (Figure 12b). Winter T_{soil} dynamics are strongly affected by (i) heat transformations at the freeze/thaw transition and (ii) the insulating by the snowpack (Beltrami, 2001). The presented model does not specifically address these effects, but it is capable, to account for both effects combined. In most cases, the description of the winter soil thermal regime was successful. Figure 11a, 12a, and 12d clearly show the decoupling of ground temperature from air temperature under snow cover. The simulator was able to track this behavior, where in some cases it failed to predict the exact time when soil temperature rises in spring (Figure 11a): The melting of the snow cover causes a sharp increase in T_{soil} due to the ceasing insulating effect, hand in hand with an abrupt decrease in surface albedo, making the forest ground susceptible for short wave radiation inputs, which are already considerably high in early spring. Rankinen et al. (2004) solved this problem by incorporating a snow dynamics routine into the calculations, but this would require the embedding of more model parameters and meteorological input data. In consideration of the model's practical applicability, this was set aside.

Compared to forested locations, the biotic site components at the open field meteorological stations are kept intentionally constant. This enabled the successful prediction of T_{soil} over a long timeframe. On two sites in the northern part of the state (Freeport, St Charles) good results were accomplished over 24 years of calibration and evaluation. But the best performance (evaluation NSE ≥ 0.99 over several years) was achieved on comparatively warm locations, located at low elevations, in the south of Illinois (Belleville, Brownstown, Olney). In contrast to forested sites, open field sites, lack the attenuating properties of a dense canopy, or a thick litter layer. Especially for cold, but snow-free winters, these locations were prone to soil frost (Figure 11c, St. Charles). Temperature fluctuations in early winter indicate the absence of a thick insolating snowpack. When in midwinter all latent heat is released, due to the freezing of soil water, T_{soil} suddenly drops. Due to the structure of the model, this behavior could not be tracked: In the presented formulation the transfer coefficient below the lower threshold temperature (T_0) remains constant at a reduced level, suppressing further soil cooling. This model limitation could be tackled by letting the transfer coefficient rise at temperatures below T_0. On the other hand, that would require the segregation of the effects of freeze/thaw processes and snow cover insulation, making the model again more complex and input data demanding.

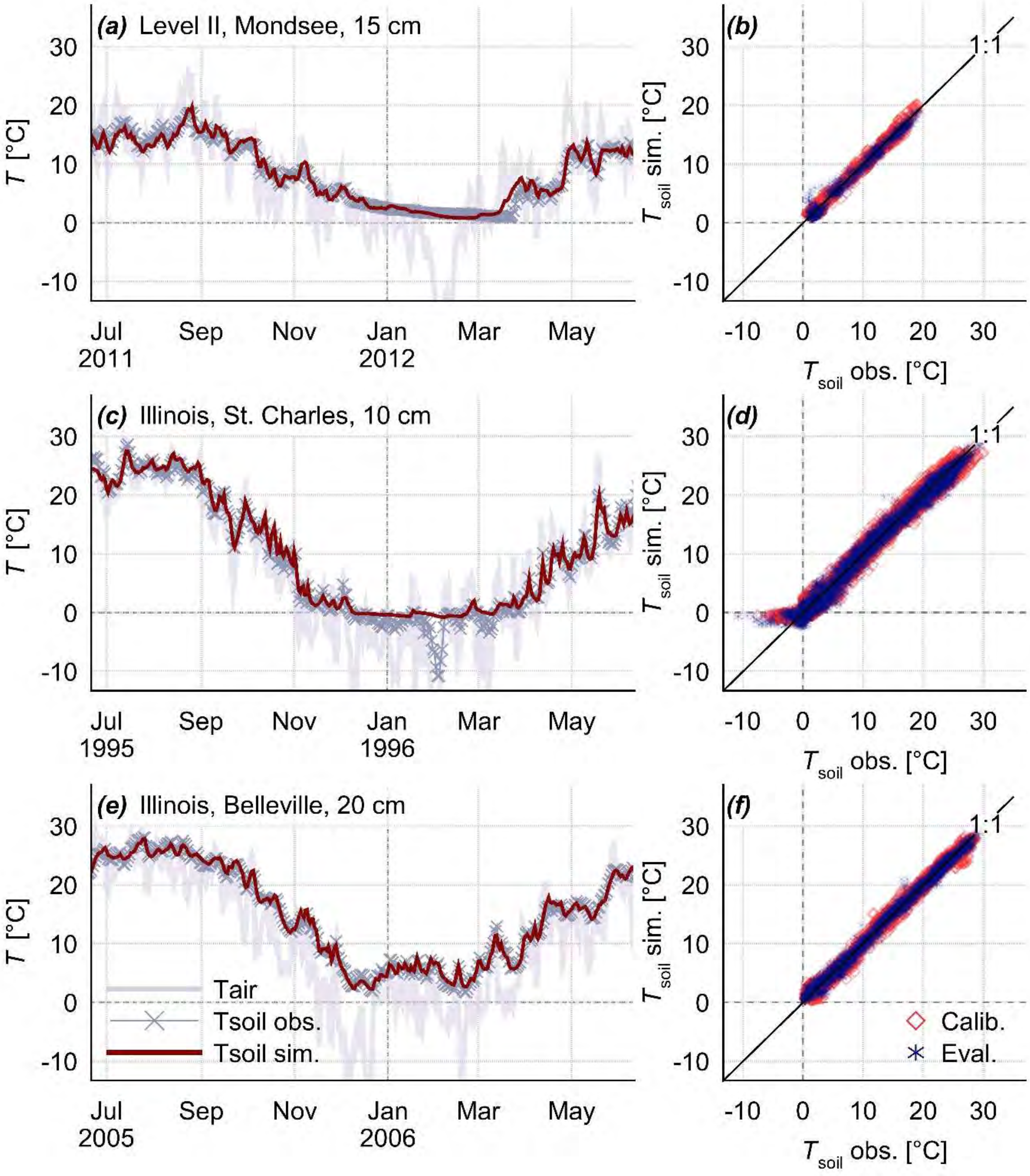

Figure 11: One-year section of observed and simulated T_{soil} time series plus the corresponding performance scatterplot. Note that the scatterplots cover the whole investigation timeframe! *(a, b)* winter snow cover decouples the course of air and soil temperature. The melting of the snowpack in the end of March causes T_{soil} to escalate, due to the ceasing insulation plus the abrupt decrease in surface albedo, making the soil susceptible for short wave radiation inputs, which are already considerably high in early spring. As the snowpack is not modeled explicitly, the simulator fails to predict the exact time when T_{soil} rises in spring. *(c, d)*. Failure to predict a major soil frost event, due to limitations in the model structure: Temperature fluctuations in early winter indicate the absence of a snowpack. When in midwinter all latent heat is released due to the freezing of soil water, T_{soil} suddenly drops. In the formulation the transfer coefficient below the lower threshold temperature (T_0) remains constant. As a consequence, this formulation applies best, to sites where severe soil frost plays only a subordinate role *(e, f)*.

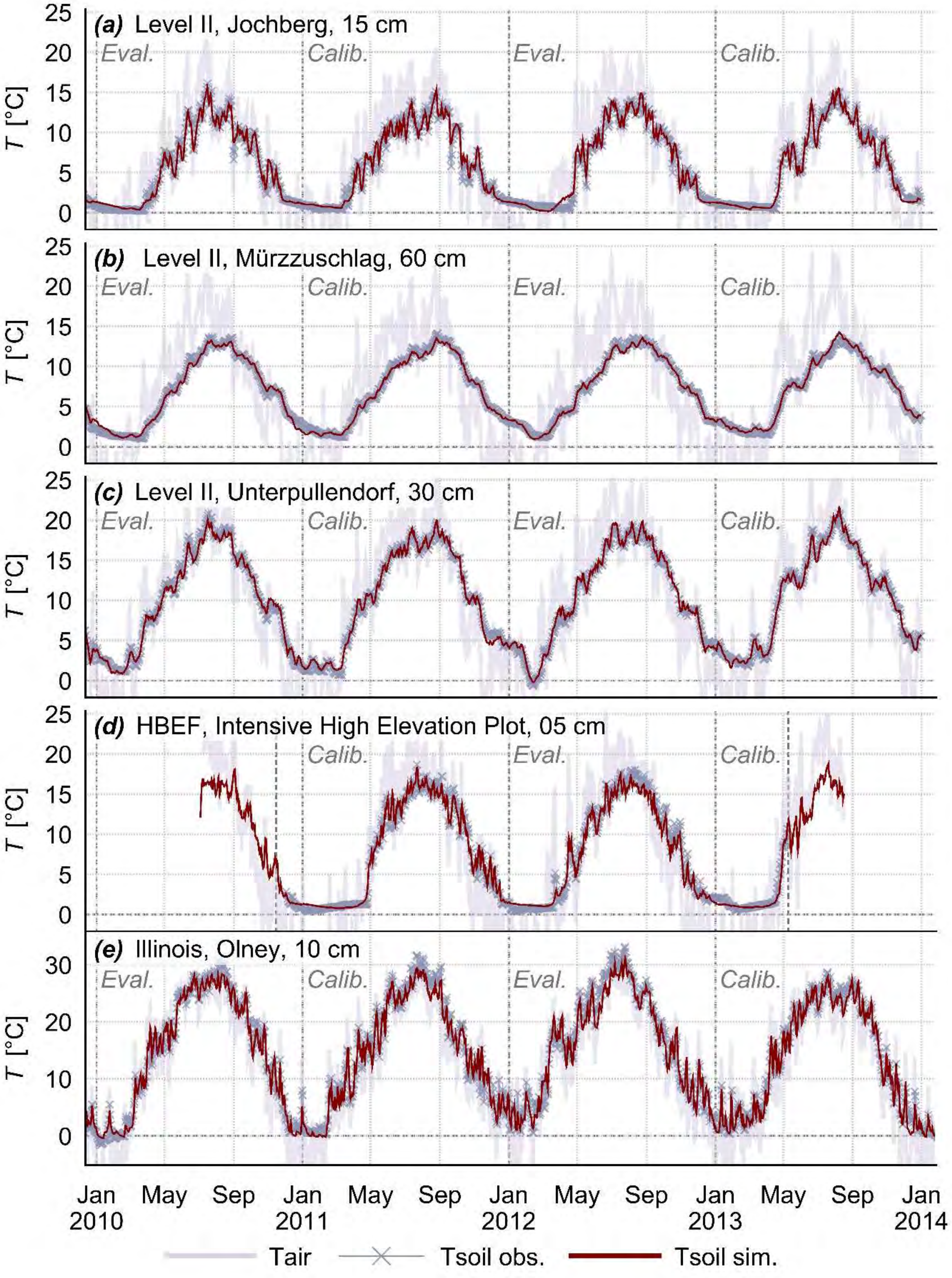

Figure 12: Four years of observed air and soil temperature overlaid with simulated T_{soil}. Calibration was performed on odd years, performance evaluation on even ones. Plot *(a)* and *(d)* clearly show the effect of snow cover on winter soil thermal regimes. In both cases the trend was successfully captured by the simulator. Also increasing phase shift and attenuation of the soil temperature wave with increasing soil depth *(b)* were captured. Stronger fluctuations

of T_{soil} under open-field conditions *(e)*, where the heat exchange might be dominated by radiation fluxes, did also not limit the simulators capability.

The examination, to determine the minimum amount of point observations of soil temperature, necessary to yield suitable results, was performed on, an 11-year time series, of air and soil temperature at the Level II plot Klausen-Leopoldsdorf (15 cm depth). The time frame was divided in *n* sectors. Only one observation was selected randomly by sector. All other observations served in the evaluation. Disregarding single outlier runs, good results (NSE > 0.97, RMSE < 0.9°C) were achieved with $n \leq 13$. Having available 50 or more daily observations, there was only little difference to the result, compared to utilizing ~ 50% (n = 2000) of the available data in the calibration process (Figure 13).

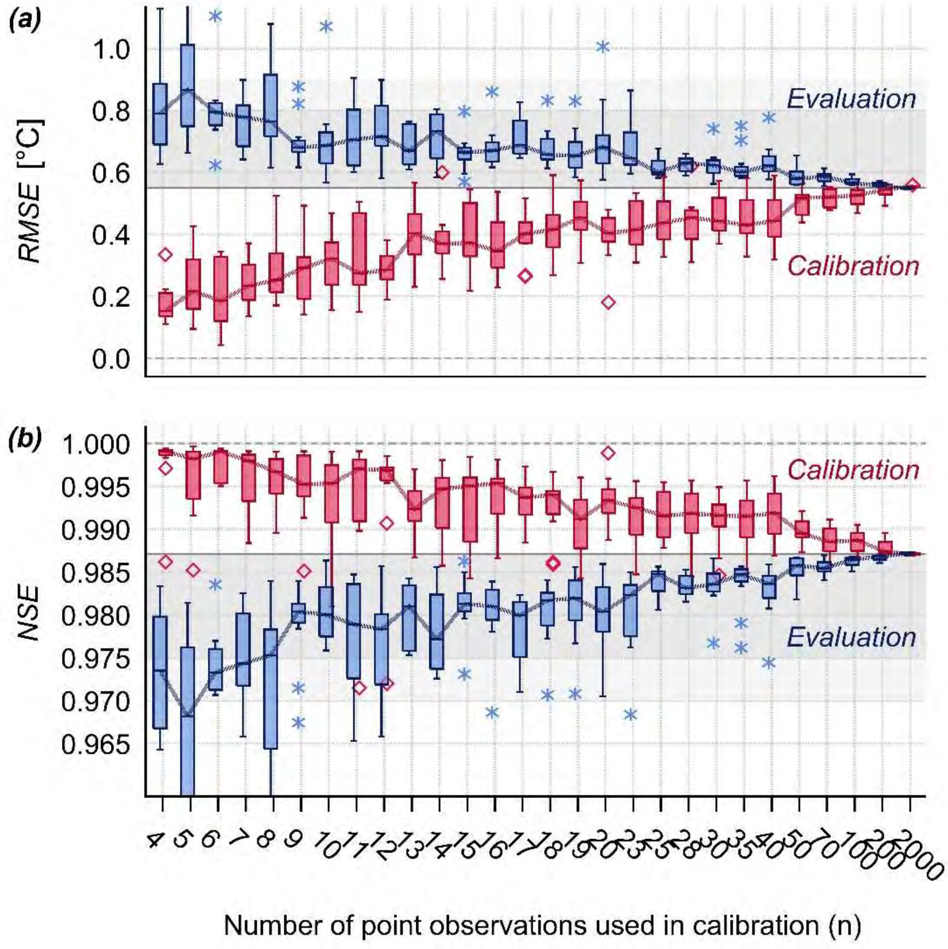

Figure 13: Model optimization result for Klausen-Leopoldsdorf, 15 cm: To determine the amount of point observations necessary to achieve sound model performance, the investigated time series was divided into *n* intervals of equal size, drawing one random point observation each. These *n* observations were used to optimize the model *(simulated annealing)*. The remaining observations were used to validate model performance. For each *n*, the procedure was repeated 12 times with different random observations, to generate a distributed result. Performance measures shown are *(a)* root mean squared error, and *(b) Nash-Sutcliffe Efficiency*. Both indices show high performance (RMSE ≤ 0.9 °C, NSE ≥ 0.97) with $n \geq 13$. For $n \geq 50$ there was only little difference in performance, compared to optimization utilizing the full calibration timeframe (n = 2000, horizontal, grey line).

Two considerations led to the implementation of decreasing transfer coefficients with decreasing soil temperature: (i) The heat release/consumption at the freeze/thaw transition (Beltrami, 2001), and (ii) the insulating effect of the winter snow cover. So intentionally, values for T_0 and T_1 were searched around 0°C. Surprisingly, in most cases the optimization process led to T_1 values much higher, meaning that the attenuation of the transfer coefficient starts already at higher temperatures. The idea behind utilizing different responses for soil warming and cooling, was the assumption, that soil warming in spring is strongly driven by incoming solar radiation, which is accelerating the temperature rise.

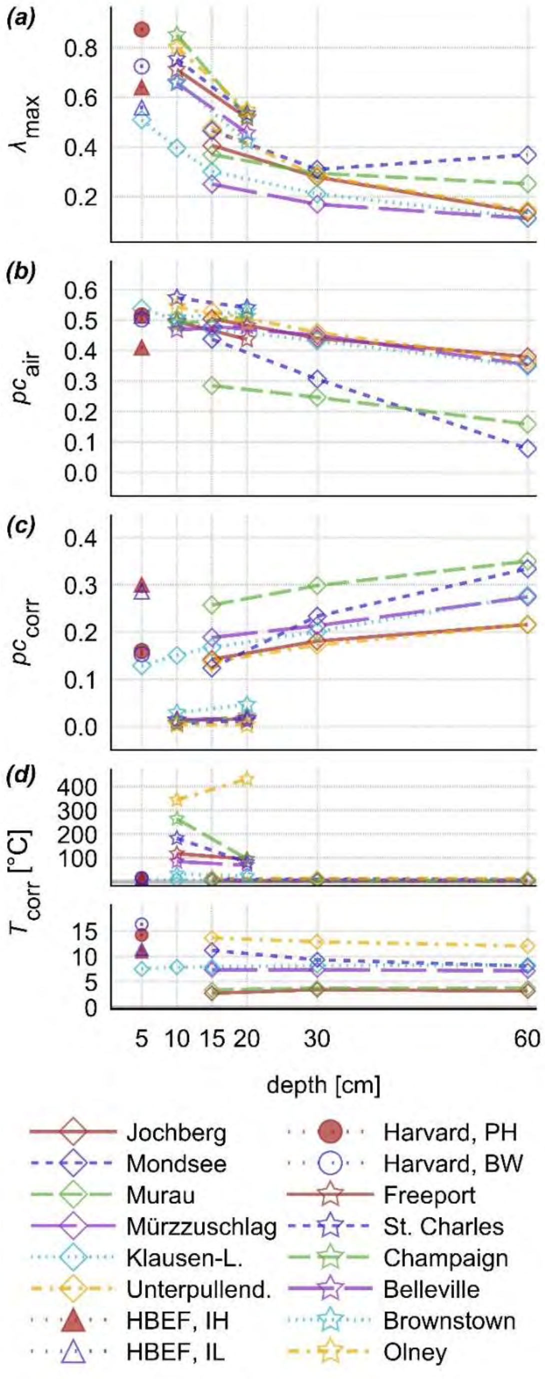

Figure 14: Four selected parameters and their change with increasing soil depth. (a) Transfer coefficient values showed a clear decreasing trend with increasing soil temp. (b) Also the fraction of the air temperature in the calculation of the environmental temperature showed, almost linear, decrement. (d) Where the correction temperature on forested sites was in a close range to the annual mean air temperature, the open field locations (star symbol) revealed much higher values. On the other hand, the relative weighting (c) of these temperatures was much smaller on non-forested sites. It is assumed, that on these locations, both parameters combined compensate for direct shortwave radiation inputs.

As this model is primarily of an empirical nature, used parameters lack a specific meaning, in a strict physical sense. Nevertheless, it was noted that parameter values were strongly affected by certain site characteristics: λ_{max} values clearly decreased with increasing soil depth (Figure 14a). Meaning, the time demand, to compensate a fraction of the temperature difference between soil layer and air, rose with increasing soil depth. Also the relative partition of the correction temperature (pc_{corr}), in the calculation of the environmental temperature, increased in deeper soil layers (Figure 14c). In contrast, the direct influence of air temperature (pc_{air}) showed a decrease downwards.

Investigated open field sites differed strongly from forest sites in parameter values of the correction temperature (T_{corr}). Where on forest locations T_{corr} resided closely to the stands annual mean air temperature, open field sites revealed T_{corr} values, around and above 100°C (Figure 14d). On the other hand, their relative weight (pc_{corr}) in the calculation of the environmental temperature, is much lower than on forested sites. It is assumed, that in these cases, they correct for direct radiation energy inputs, which are obviously much higher without the presence of a shielding canopy. The reason that, even under such conditions, the simulator (which does not particularly address radiative heat flux) delivers good estimates of T_{soil}, might be found in the strong correlation between energy balance components, and the air temperature itself (Hock, 2003).

Table 2: Parameterization result for 36 sites and depths. Optimization was performed, using a simulated annealing algorithm. Performance criterion was the Nash-Sutcliffe Efficiency.

		Parameter								
	z	λ_{max}	λ_{aux}	λ_{frost}	λ_{thaw}	T_0	T_1	T_{corr}	pc_{corr}	pc_{air}
	[cm]					[°C]	[°C]	[°C]		
Jochberg	15	.4059	.0365	.0041	.0568	1.3	3.6	2.7	.142	.505
	30	.2781	.0327	.0044	.0806	1.5	5.6	3.5	.181	.440
	60	.1349	.0273	.0008	.0942	1.0	9.2	3.2	.216	.380
Mondsee	15	.4653	.0708	.0026	.0700	0.9	7.6	11.2	.124	.438
	30	.3090	.0541	.0056	.0616	1.2	8.3	9.3	.234	.306
	60	.3672	.0419	.0084	.2010	1.7	12.0	8.1	.334	.078
Murau	15	.3686	.0447	.0000	.0285	0.6	7.0	3.4	.257	.285
	30	.2934	.0424	.0005	.0296	0.8	7.0	3.8	.298	.247
	60	.2514	.0379	.0037	.0498	1.5	6.7	3.8	.350	.158
Mürzzuschlag	15	.2494	.0208	.0028	.0140	0.3	2.7	7.4	.188	.480
	30	.1687	.0184	.0130	.0244	0.9	2.7	7.4	.213	.451
	60	.1119	.0177	.0031	.0321	-0.3	6.4	7.1	.274	.353
Klausen-Leopoldsdorf	05	.5092	.0261	.0131	.1840	1.5	5.4	7.5	.129	.538
	10	.3949	.0244	.0130	.1374	1.6	6.2	7.9	.151	.500
	15	.3006	.0229	.0123	.1287	1.5	7.6	7.9	.168	.471
	30	.2104	.0214	.0147	.0947	2.0	8.3	8.2	.201	.432
	60	.1138	.0204	.0021	.0590	0.9	9.3	8.3	.278	.349
Unterpullendorf	15	.4752	.0383	.0360	.0541	-2.3	12.5	13.6	.137	.528
	30	.2824	.0313	.0177	.0191	-3.2	12.3	12.9	.172	.460
	60	.1443	.0254	.0091	.0101	-2.6	9.3	12.0	.216	.366
HBEF, Intensive High Elevation	05	.6399	.0418	.0024	.0133	1.1	5.3	10.9	.300	.411
HBEF, Intensive Low Elevation	05	.5584	.0355	.0001	.0075	0.9	3.1	11.4	.286	.515
Harvard Forest, Prospect Hill	05	.8723	.0447	.0000	.0116	-0.4	9.2	14.2	.160	.516
Harvard Forest, Barre Woods	05	.7238	.0467	.0000	.0357	0.4	7.0	16.3	.153	.502
Freeport	10	.7111	.0974	.0009	.1094	-0.8	7.3	118.1	.012	.495
	20	.5157	.0808	.0014	.1598	-0.4	10.2	94.5	.016	.437
St. Charles	10	.7541	.0915	.0045	.1397	-0.5	7.1	182.4	.007	.573
	20	.5323	.0771	.0035	.2367	-0.7	10.7	80.4	.012	.540
Champaign	10	.8515	.1215	.0000	.3250	0.2	6.0	264.2	.008	.487
	20	.5223	.0822	.0000	.3130	0.5	8.8	95.2	.022	.512
Belleville	10	.6570	.0722	.0072	.6131	-0.1	11.0	83.8	.014	.468
	20	.4561	.0598	.0044	.4558	-0.1	11.3	68.9	.017	.481
Brownstown	10	.6627	.0916	.0003	.4320	-0.4	13.3	32.6	.029	.508
	20	.4212	.0754	.0036	.2782	-0.3	13.2	22.6	.046	.528
Olney	10	.8012	.1035	.0010	.4226	-0.7	7.7	343.5	.003	.544
	20	.5477	.0909	.0015	.4373	-0.4	10.0	431.5	.003	.492

Table 3: Performance indices for calibration and evaluation intervals. Calibration was performed on odd years, evaluation on even ones. A long evaluation timeframe (high *n*) adds significance to the results.

		Calibration					**Evaluation**					**Timeframe**	
	z [cm]	***n***	**NSE**	**RMSE** [°C]	**MAE** [°C]	**MBE** [°C]	***n***	**NSE**	**RMSE** [°C]	**MAE** [°C]	**MBE** [°C]	**Start**	**End**
Jochberg	15	780	**.991**	.416	.300	.003	731	**.989**	.496	.364	-.03	03/01/2009	12/31/2013
	30	780	**.991**	.385	.281	.003	731	**.990**	.444	.327	-.01	03/01/2009	12/31/2013
	60	780	**.992**	.320	.234	.003	731	**.991**	.351	.266	.013	03/01/2009	12/31/2013
Mondsee	15	761	**.986**	.641	.513	-.00	731	**.979**	.806	.626	.249	12/01/2009	12/31/2013
	30	761	**.988**	.518	.409	-.00	731	**.981**	.678	.559	.275	12/01/2009	12/31/2013
	60	761	**.990**	.396	.301	-.00	731	**.980**	.570	.473	.254	12/01/2009	12/31/2013
Murau	15	1037	**.974**	.604	.487	-.00	718	**.986**	.434	.325	.017	01/01/2009	12/31/2013
	30	1037	**.974**	.565	.451	.002	718	**.987**	.399	.299	.045	01/01/2009	12/31/2013
	60	1037	**.970**	.542	.434	.001	718	**.989**	.330	.235	.037	01/01/2009	12/31/2013
Mürzzuschlag	15	761	**.994**	.381	.284	.003	731	**.993**	.441	.352	.014	12/01/2009	12/31/2013
	30	761	**.994**	.348	.261	.004	731	**.992**	.415	.314	.073	12/01/2009	12/31/2013
	60	761	**.994**	.312	.237	.010	731	**.994**	.332	.254	.079	12/01/2009	12/31/2013
Klausen-Leopoldsdorf	05	1927	**.986**	.625	.478	-.00	1770	**.986**	.615	.482	.165	11/08/2001	07/01/2013
	10	1927	**.987**	.585	.448	.000	1770	**.986**	.581	.454	.176	11/08/2001	07/01/2013
	15	1927	**.987**	.550	.425	-.00	2126	**.987**	.562	.438	.103	11/08/2001	07/01/2013
	30	1927	**.988**	.499	.386	.000	2126	**.987**	.527	.402	.105	11/08/2001	07/01/2013
	60	1914	**.989**	.418	.330	-.00	2126	**.985**	.490	.375	.106	11/08/2001	07/01/2013
Unterpullendorf	15	829	**.994**	.492	.384	-.00	711	**.992**	.559	.451	-.08	09/19/2009	12/31/2013
	30	829	**.995**	.419	.335	.004	720	**.994**	.471	.384	-.05	09/19/2009	12/31/2013
	60	829	**.995**	.371	.293	-.00	720	**.994**	.401	.317	-.01	09/19/2009	12/31/2013
HBEF, Intensive High	05	489	**.991**	.549	.402	-.00	390	**.986**	.704	.554	.198	12/01/2010	05/10/2013
HBEF, Intensive Low	05	493	**.986**	.726	.560	-.00	396	**.979**	.943	.781	-.68	12/01/2010	05/10/2013
Harvard, Prospect Hill	05	1477	**.989**	.717	.534	-.01	1556	**.986**	.811	.621	.141	06/01/1991	05/31/2000
Harvard, Barre Woods	05	1290	**.990**	.673	.513	.002	1013	**.990**	.664	.500	-.18	05/21/2003	04/20/2010
Freeport	10	4568	**.985**	1.16	.864	.014	4389	**.986**	1.07	.821	-.06	01/01/1991	07/31/2015
	20	4571	**.989**	.956	.702	.001	4389	**.989**	.909	.703	-.04	01/01/1991	07/31/2015
St. Charles	10	4524	**.985**	1.12	.870	.013	4389	**.982**	1.19	.884	.180	01/01/1991	07/31/2015
	20	4551	**.990**	.875	.684	.010	4384	**.987**	.973	.742	.160	01/01/1991	07/31/2015
Champaign	10	2190	**.983**	1.25	.984	-.01	1828	**.982**	1.24	.991	-.20	01/01/1995	12/31/2005

		Calibration					**Evaluation**					**Timeframe**	
	z	***n***	**NSE**	**RMSE**	**MAE**	**MBE**	***n***	**NSE**	**RMSE**	**MAE**	**MBE**	**Start**	**End**
	[cm]			[°C]	[°C]	[°C]			[°C]	[°C]	[°C]		
	20	2190	**.991**	.846	.686	-.01	1828	**.989**	.916	.727	-.13	01/01/1995	12/31/2005
Belleville	10	2033	**.992**	.784	.615	.003	2187	**.991**	.844	.659	.098	01/01/2004	07/31/2015
	20	2033	**.991**	.789	.601	.002	2193	**.992**	.753	.584	.048	01/01/2004	07/31/2015
Brownstown	10	3610	**.985**	1.04	.820	-.02	3652	**.990**	.845	.662	.079	01/01/1991	12/31/2010
	20	3610	**.987**	.950	.754	.014	3652	**.990**	.816	.636	.070	01/01/1991	12/31/2010
Olney	10	2035	**.989**	.990	.763	-.00	2192	**.988**	1.02	.776	-.02	01/01/2004	07/31/2015
	20	2034	**.992**	.787	.615	.009	2192	**.992**	.809	.621	-.01	01/01/2004	07/31/2015

NSE=Nash-Sutcliffe Efficiency, RMSE=Root Mean Squared Error, MAE=Mean Absolute Error, MBE= Mean Bias Error. A positive MBE indicates that the observed mean soil temperature exceeds the predicted mean soil temperature and vice versa.

3.2 The Timing of Phenological Key Events

Both, spring and autumn phenology showed high intra-annual plasticity. Nevertheless, after transforming the data to an assembled time-series, LU revealed a distinct pattern, with a recent trend towards an earlier onset of the growing season (see Figure 16). On the contrary to very high intra-annual plasticity, the year to year variations of the assembled means of LC were smaller compared to LU. The reason, no trend towards a delaying of senescence was observed, might be found in the counteracting effect of late spring and late summer temperatures.

The parameterization of the LU module led to a good fit between observed and modeled onset of the growing season (compare **Table 4**; NSE > 0.89, RMSE < two days). A very low modeled $T_{0,LU}$ (< -11°C) seems to be non-meaningful in a plant physiological sense. On the other hand, the simulated effect of temperature forcing at cold conditions is partially nullified by low multiplier values from the day-length term, at the beginning of the forcing period, in early winter (see Figure 15).

The regression approach, to predict the end of the growing season, utilizing the mean temperature of two temporal windows, was also suitable to reproduce the observed pattern to a sufficient degree (NSE > 0.73, RMSE < two days). The mechanism behind the acceleration of senescence by high temperatures in late spring was not elaborated in this work. Nevertheless, two explanatory assumptions are stated: High temperatures is spring point to an early onset of the growing season. This, and the high temperature itself might increase the water consumption, (i) inducing drought during critical phenological stages. (ii) High temperatures in late spring might support the development of specific pest or pathogens, leading to stress induced, premature leaf coloring (see also Menzel et al., 2008).

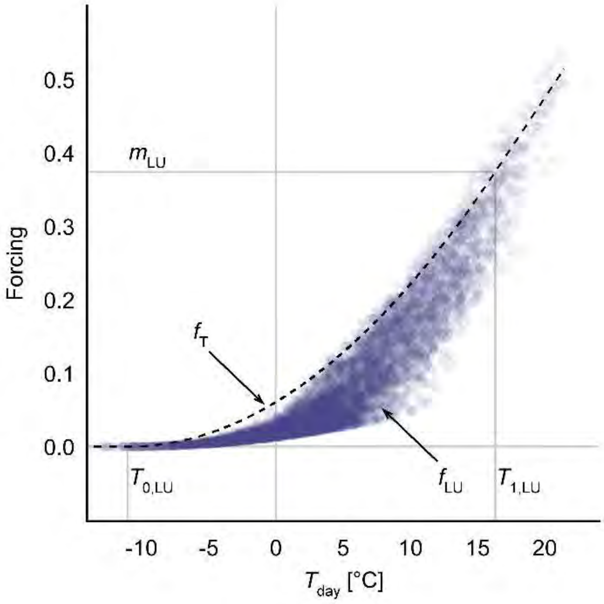

Figure 15: Modeled temperature driven forcing (f_T: dashed line) and the daily actual forcing (f_{LU}: point cloud) in relation to daytime temperature. The onset of f_T at very low temperatures, is partially nullified by the photoperiod term, taking low values early in the year.

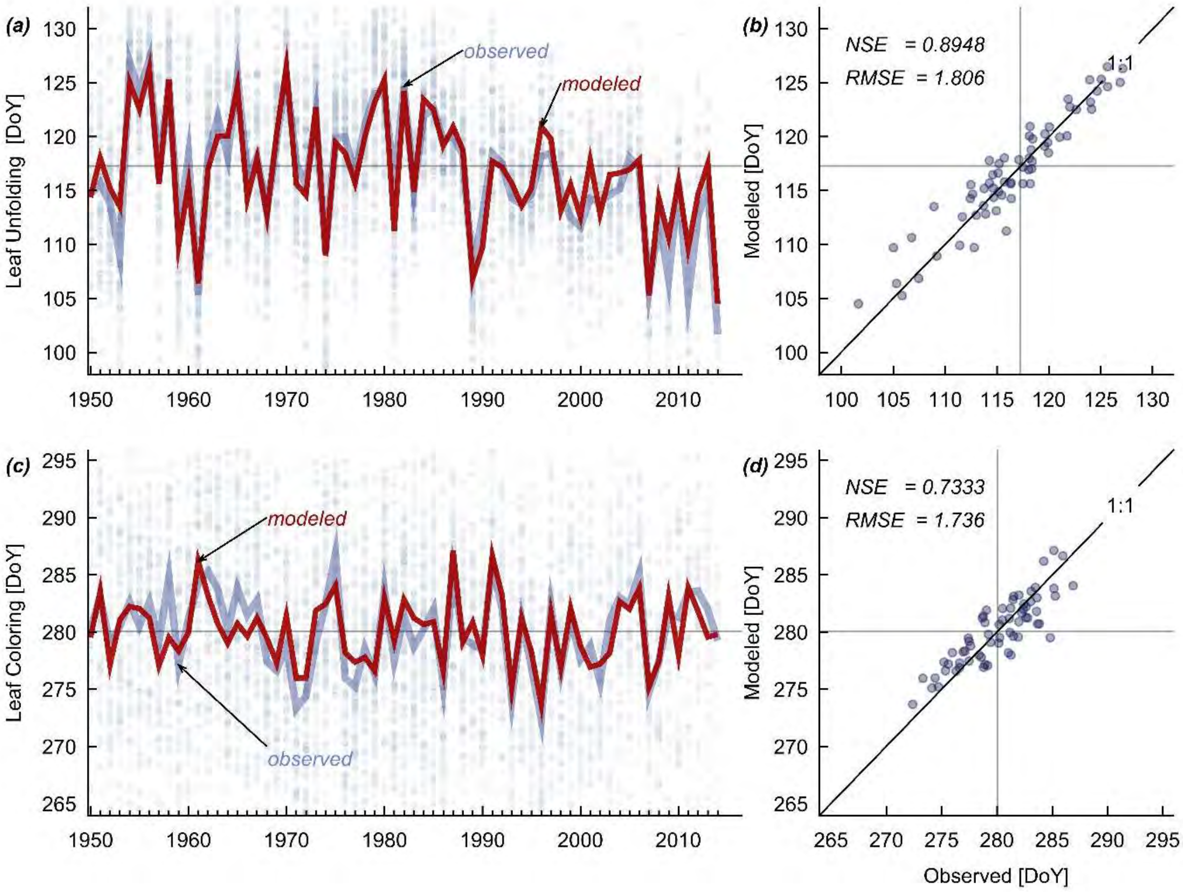

Figure 16: (a,c) The model was fitted to an assembled time-series of annual DoYs (pale solid lines), which were calculated, if more than 10 annual observations (small dots) were available. Leaf unfolding and coloring data were processed analogously (a) Where LU clearly shows a trend towards earlier onsets of the growing season in last decades, LC (c) reveals no such pattern. The reason for this might be found in the counteracting effect of late spring and late summer temperatures. (b,d) Observed assembled time-series mean of leaf unfolding and leaf coloring vs. the modeled timing of the event. Details about calculations of NSE (Nash-Sutcliffe Efficiency) and RSME (root mean squared error in days) are given in the text.

Table 4: Parameterization results of the phenological module. Optimization was conducted, using a combination of simulated annealing and the Gauss-Newton algorithm. Performance criterion was the Nash-Sutcliffe Model Efficiency.

Leaf unfolding		**Leaf coloring**	
$DoY_{0,LU}$	4.353	$DoY_{0,LC}$	108.451
$T_{0,LU}$	-10.820	$DoY_{1,LC}$	167.207
$T_{1,LU}$	30.747	$DoY_{2,LC}$	219.214
m_{LU}	0.362	$DoY_{3,LC}$	286.441
x_{LU}	2.921	h_{LC}	-0.618
		k_{LC}	4.002
		d_{LC}	261.107
n	65	***n***	65
NSE	**0.895**	**NSE**	**0.733**
RMSE	1.806	**RMSE**	1.736

3.3 Water Balance

The approaches to describe fog precipitation, precipitation interception, as well as the responses of evapotranspiration and percolation to soil moisture, presented in this work are novel. Therefore, their parameterization cannot be deduced from literature data. Due to unavailability of direct measurements, they were determined by model optimization, applying broad search ranges. In cases where literature values existed (e. g. degree day factors for snowmelt, field capacity), parameter values were searched in the close proximity of values stated in the literature. On both investigated sites, the optimization process lead to a good fit between the observed and predicted soil water content (NSE < 0.92.5); the simulator was capable to track the temporal dynamics of the daily average soil moisture (θ, L L^{-1}), over the whole investigation timeframe (Figure 18).

In the following section, the parameterization of the WBM is discussed. For the parameter configuration of all four sites, see Table 6. On the sites KR and KL, the fog precipitation module had no improving effect on the model's performance. In both cases, the optimization process led to fog coefficient (f_c) values close to zero. The amount, fog is contributing to the total precipitation, seems insignificant at these locations. An explanation might be found in the sites' relief; both investigated stands are located at lower hill slopes, partially shielded from (at least) two directions. A different picture was found on the EX and JU site; they are both located at upper hill slopes, close to the hilltop, leaving them much more exposed to direct air flow.

The optimization process leads to relatively high parameters values, describing the maximum capacity of canopy storage (C_{max}). For a Central European beech stand, (Gerrits et al., 2010) reported a canopy C_{max} ranging from 0.4 mm for winter conditions to 0.9 mm in summer. In this work, the parameterization led to a maximum storage capacity of 4.3 and 2.7 mm for the KB and the KL site, respectively. For the beech stand mentioned above, (Gerrits et al., 2010) calculated a litter layer storage capacity with a yearly average of 1.8 mm, temporally peaking in autumn (2.8 mm). So, it seems possible, that high C_{max} might be explained by the contribution of the litter layer to precipitation interception. Soil moisture records, utilized in the calibration process, existed for a minimum depth of 10 cm and 15 cm, for Kreisbach and Klausen-Leopoldsdorf, respectively. It seems also plausible that the canopy interception module accounts for soil water storage/interception, caused by the topmost layer of the mineral soil. An alternative to explain high values for C_{max} arises from the assessment of precipitation on a daily time-step: The possibility of multiple storms within one day is neglected. In such a case, the formulation might underestimate canopy storage (compare Pearce and Rowe, 1981). Here, high values for C_{max} would have a compensating effect. High values for the coefficient, scaling the reference evapotranspiration (ET_O) to canopy evaporation (Kc_{canopy}), could be explained by the low surface resistance of the wet canopy (Herbst et al., 2008). The combination of high Kc_{canopy} and high C_{max} values is leading to high interception evaporation (E_I) fluxes. On the KB site, deposition chemistry was monitored from the beginning of May 2002 to the end of October 2003 (Berger et al., 2008). In this course, also canopy evaporation fluxes were estimated as the difference between observed open area precipitation and the sum of throughfall and stemflow. A determined annual interception sum of 238 mm (26% of the open area precipitation) is in close resemblance to the estimate of the mean annual interception, presented in this work. On the KL site, throughfall was monitored in a bi-weekly interval from 2006 to 2010. For dormant and growing season, 5.8% and 11.9%, of the observed precipitation was intercepted by the canopy, respectively. For the same temporal interval, the simulation delivered canopy evaporation percentages of 8 and 11.9 for the dormant and growing season, respectively. For different beech stands, (Peck and Mayer, 1996) reported rainfall interception ranging from 5 to 48% of total precipitation, with a mean of 20%. On the investigated sites, modeled annual rainfall interception (canopy evaporation), was found to be on the low end of these estimates. Precipitation interception decreased from west to east, reaching its lowest value on the EX site (Table 6).

The calibration process led to an unremarkable parameterization of the module, describing snow accumulation and snowmelt. Threshold temperatures for snowfall and snowmelt, as well as the degree day factors for snowmelt, were in the range of literature values. For a summary on threshold temperatures for snowfall see Feiccabrino and Lundberg (2008), a summary on snowmelt degree-day factors for various catchments is given in Hock (2003).

On the KR forest location, an assessment of physical soil characteristics revealed a pore volume 52%, and a volumetric water content of 18.85% at one MPa (Schume et al., 2004). The parameterization for this site delivered values for saturation water content (θ_{sat}) and θ_{pwp}, which are located in the close vicinity of the measured ones.

For different beech stands, Peck and Mayer (1996) reported annual transpiration (E_C) sums ranging from 268 to 601 with a mean of 363 mm. The estimations of annual E_C were below these values, on all sites (Table 7). Especially on the KR and KL plot, is seems possible that transpiration water fluxes were slightly underestimated in the simulation outcome. On the KR plot, beech roots were found at a soil depth of 85 cm (Schmid, 2002). On the KL plot, an assessment of the sites soil characteristics revealed medium to strong root penetration down to 65 cm soil depth (Neumann et al., 2001). Due to reasons of soil moisture data availability, only the topmost 50 cm of the mineral soil were considered in this work, neglecting the possible contribution of deeper soil layers to the trees' water supply.

On the KR and especially on the EX plot, the simulator delivered high relative fractions of bypass flow (Table 7). Analogue to the underestimation of E_C fluxes, the disregarding of the influence of deeper soil layers on the stands' water balance might result in an overestimation of bypass flow.

High transpiration rates during the growing season, in contrast to low evaporative water consumption during the leafless period of the year, are leading to a distinct seasonal pattern of soil moisture. Where in the growing season, θ above field capacity occurs only exceptional, in the cold part of the year field capacity is rarely undershot, determining percolation through the soil profile as phenomenon of the dormant season (Figure 17c,d).

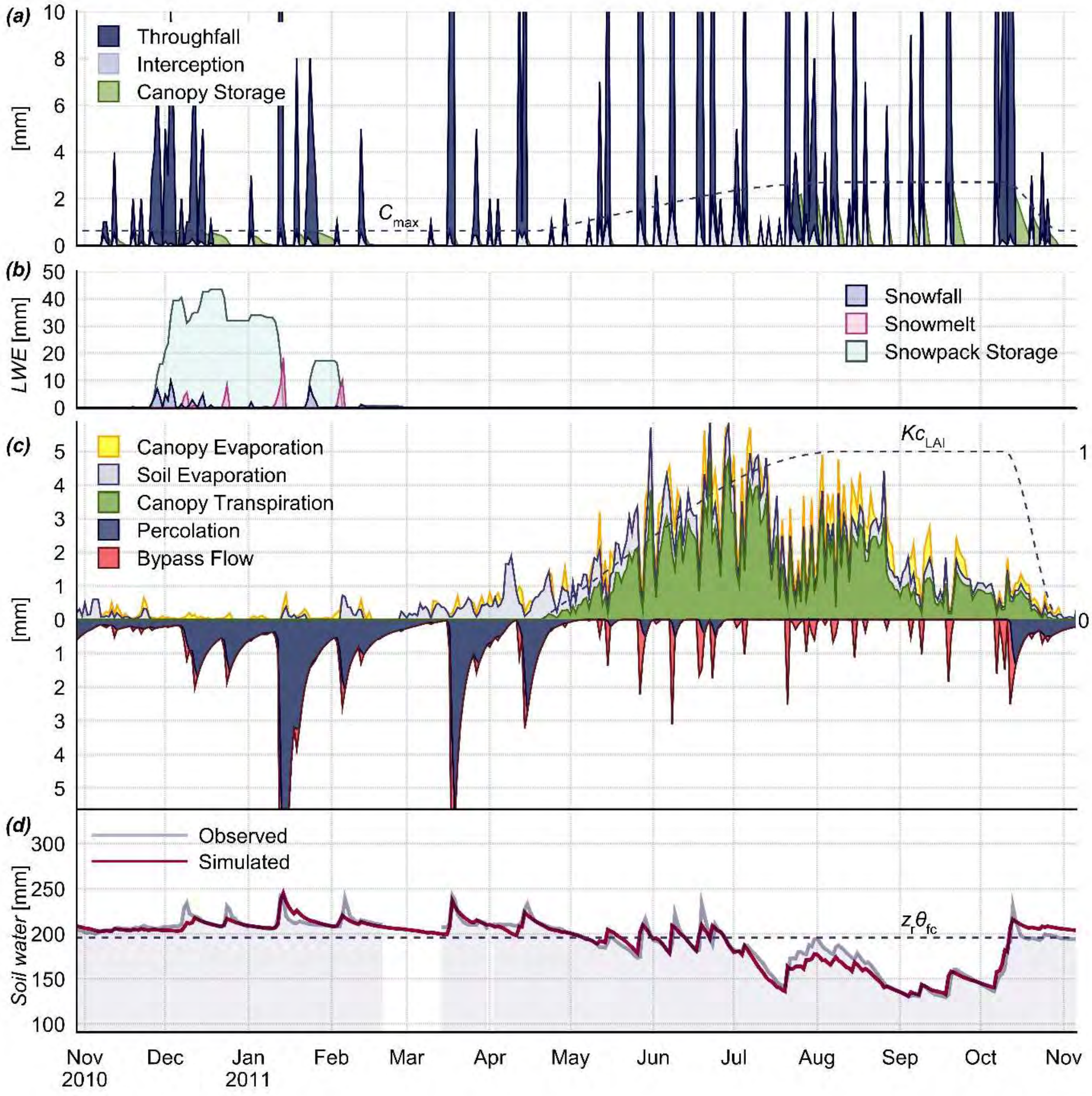

Figure 17: Breakdown of daily modeled pools and fluxes for a one-year section of the Klausen-Leopoldsdorf plot. (a) Due to the nullity of the fog precipitation module on this site, the sum of throughfall and interception equals the observed precipitation. (c) Export fluxes: Gaseous and liquid exports are stated as positive and negative values, respectively. The high interception capacity of the canopy, combined with a high canopy specific crop coefficient (Kc_{canopy}), sets canopy evaporation as the dominant pathway for gaseous losses. Compared to canopy evaporation and transpiration, the fraction soil evaporation is contributing to gaseous exports, is negligible. (d) Soil moisture, almost constantly above the field capacity (θ_{fc}) during the dormant season, clearly states (c) percolation through the soil profile as a phenomenon of the cold part of the year.

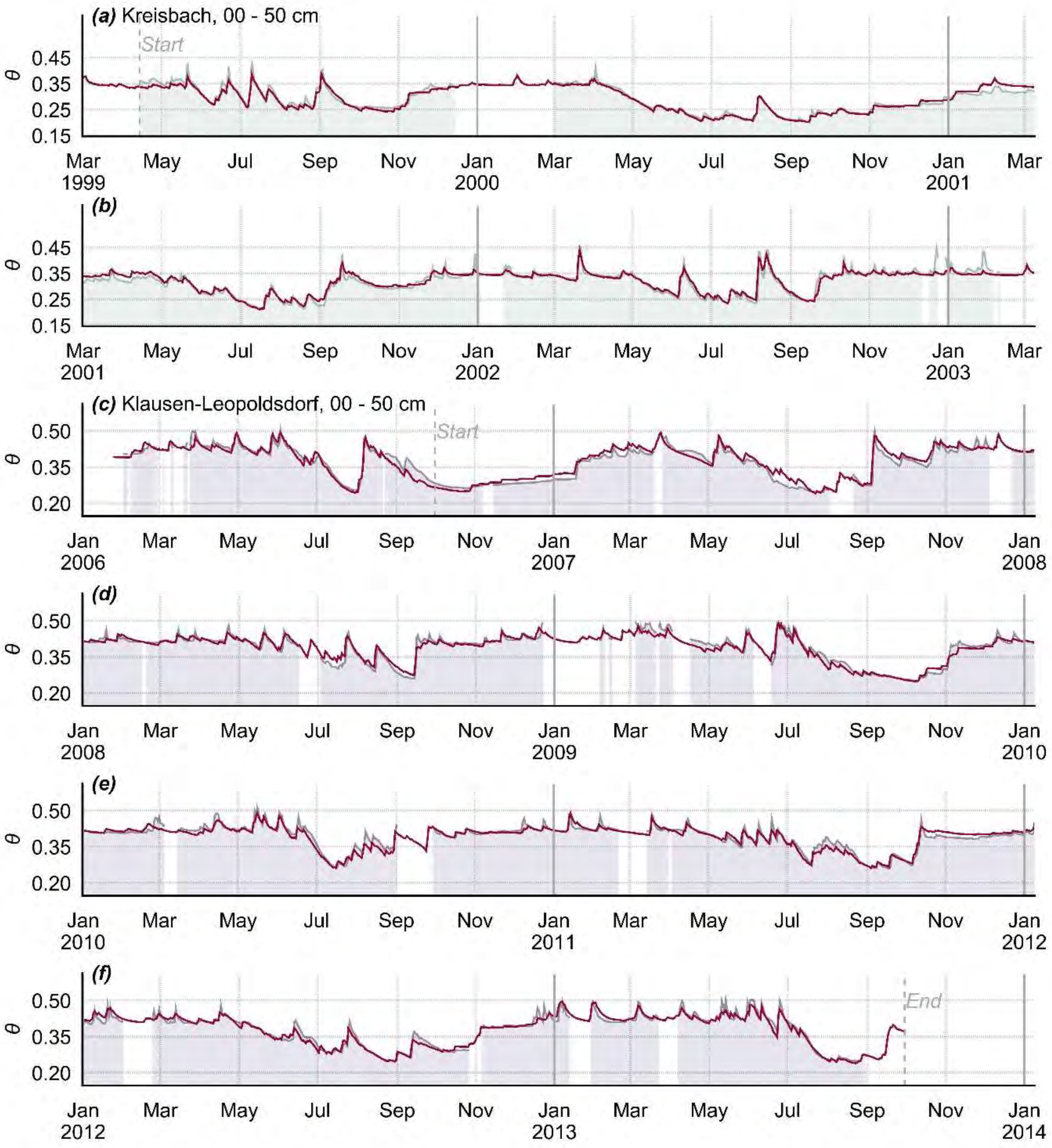

Figure 18: Time series of observed (pale bands) and modeled (solid line) soil moisture. The calibration delivered an expedient estimate for 4 years of observed θ on the Kreisbach site (a, b). On the Klausen Leopoldsdorf site (c – f) the simulator was able to track θ over an almost seven-year period.

Table 5: The model calibration was conducted, utilizing soil moisture records of the entire model timeframe. Optimization was performed, using a simulated annealing algorithm. Performance criterion was the Nash-Sutcliffe Efficiency.

Site	Timeframe	z [cm]	*n*	NSE	RMSE
Kreisbach	04/14/1999 - 02/10/2003	00 - 50	1294	0.9262	0.0132
Klausen-Leopoldsdorf	10/01/2006 - 09/30/2013	00 - 50	2262	0.9303	0.0163
Exelberg	10/01/2009 - 09/30/2012	00 - 50	33	0.9148	0.0152
Jubiläumswarte	10/01/2009 - 09/30/2012	00 - 50	33	0.9225	0.0176

n=Number of utilized observations, NSE=Nash-Sutcliffe Efficiency, RMSE=Root Mean Squared Error (LL^{-1}).

Table 6: Parameter optimization results for all 4 investigate sites.

Parameter	**Description**	**Unit**	**KB**	**KL**	**EX**	**JU**
rH_0	Lower relative humidity threshold for fog	rH	99.99	99.99	94.34	93.93
f_c	Fog coefficient		0	0	0.516	0.494
DoY_{CC}	Canopy closure	DoY	221.4	222.9	173.3	180.5
l_{LC}	Duration of leaf senescence	Days	22.88	20.94	25.14	13.60
ID_{LAI}	Indeciduous fraction of leaf area at canopy closure		0.079	0	0	0
$C_{max,LAI0}$	Canopy interception capacity at Kc_{LAI}=0	mm	2.221	0.632	0.325	0.309
$C_{max,LAI1}$	Canopy interception capacity at Kc_{LAI}=1	mm	4.326	2.701	0.678	1.230
$K_{i,LAI0}$	Interception function shape parameter at Kc_{LAI}=0		4.354	3.777	2.665	2.832
$K_{i,LAI1}$	Interception function shape parameter at Kc_{LAI}=1		5.342	6.712	4.678	5.339
Kc_{canopy}	Crop coefficient for canopy evaporation		1.102	0.472	0.787	0.822
τ_{LAI0}	Maximum radiation transmittance coefficient at		0.742	0.701	0.802	0.805
τ_{LAI1}	Minimum radiation transmittance coefficient at		0.390	0.321	0.319	0.291
T_{snow}	Upper threshold temperature for snowfall	°C	1.388	0.203	1.706	1.509
T_{melt}	Lower threshold temperature for snowmelt	°C	1.972	1.508	1.897	0.938
DDF_{melt}	Degree day factor for snowmelt	mm°C^{-1}	2.165	2.982	0.813	0.686
f_{by}	Water fraction, bypassing the soil box		0.362	0.083	0.437	0.112
k_{sat}	Saturated conductivity	LL^{-1} d^{-1}	0.071	0.038	0.017	0.021
θ_m	Shape parameter for percolation response		0.528	0.728	0.753	0.748
θ_{sat}	Saturated water content	LL^{-1}	0.502	0.520	0.369	0.420
θ_{fc}	Field capacity	LL^{-1}	0.344	0.392	0.285	0.362
θ^*	Upper threshold water content for	LL^{-1}	0.344	0.410	0.270	0.348
θ_{pwp}	Permanent wilting point, lower threshold for	LL^{-1}	0.189	0.228	0.085	0.155
θ_{res}	Residual water content, lower threshold for soil	LL^{-1}	0.008	0.003	0.012	0.003
ET_m	Shape parameter for evapotranspiration response		0.488	0.391	0.422	0.424
Kc_{tree}	Crop coefficient for vegetation at canopy closure		1.361	1.783	0.526	0.857
Kc_{ground}	Crop coefficient for soil evaporation		0.364	0.517	0.209	0.398

Table 7: Breakdown of modeled export fluxes, given as mean annual sums and in percent of the observed precipitation.

Site	**Kreisbach**		**Klausen-Leo.**		**Exelberg**		**Jubiläumswarte**	
***n* (Years)**	30		30		30		30	
Unit	**mm a^{-}**	**%**	**mm a^{-}**	**%**	**mm a^{-1}**	**%**	**mm a^{-}**	**%**
Precipitation (+Fog)	961.0	100	831.1	100	751.5	100	654.5	100
Fog	0	0	0	0	6.0	0.8	6.8	1.1
Canopy	202.8	21.7	88.4	10.8	54.4	7.4	68.4	10.7
Infiltration	480.8	49.7	656.4	79.1	386.1	51.5	492.4	75.7
Soil evaporation	106.6	11.6	127.1	15.6	100.1	13.8	189.0	30.1
Transpiration	189.1	19.8	246.3	29.8	174.4	23.5	180.9	27.6
Bypass flow	277.6	28.6	85.5	10	311.1	41.4	93.9	13.9
Percolation	185.1	18.4	283.0	33.7	111.8	14.6	122.9	18.6

3.4 Temperature sensitivity assessment

Step-wisely increased temperatures led to a proportional elongation of the growing season. One °C roughly corresponded to an elongation of 4.7 days. The modeled relationship between warming and lengthening of the growing season was almost linear. All sites responded with a similar pattern (Figure 19a-d). Spring phenology showed stronger reaction than autumn phenology. One °C warming corresponds to leaf unfolding, 3.5 days earlier. Regarding leaf senescence, the delaying effect of warmer late-summer temperatures was not fully compensated by the accelerating effect of high late-spring temperatures. A temperature increase of 1°C corresponded to a delay of LC of 1.2 days.

The simulated temperature rise had a strong effect on the stands' water balance. Apparently, higher temperatures during the growing season led to drier soils (Figure 21a-d). Gaseous water exports increased, while liquid exports decreased. Overall, the soil evaporation partition was affected positively, the percolation water fraction was affected negatively by warmer conditions (Figure 20a-d). Increased ET was shifting soil moisture to lower levels, favoring the evaporation partition of ET, which is capable to deplete soil water at moisture levels below the wilting point, inducing severe drought.

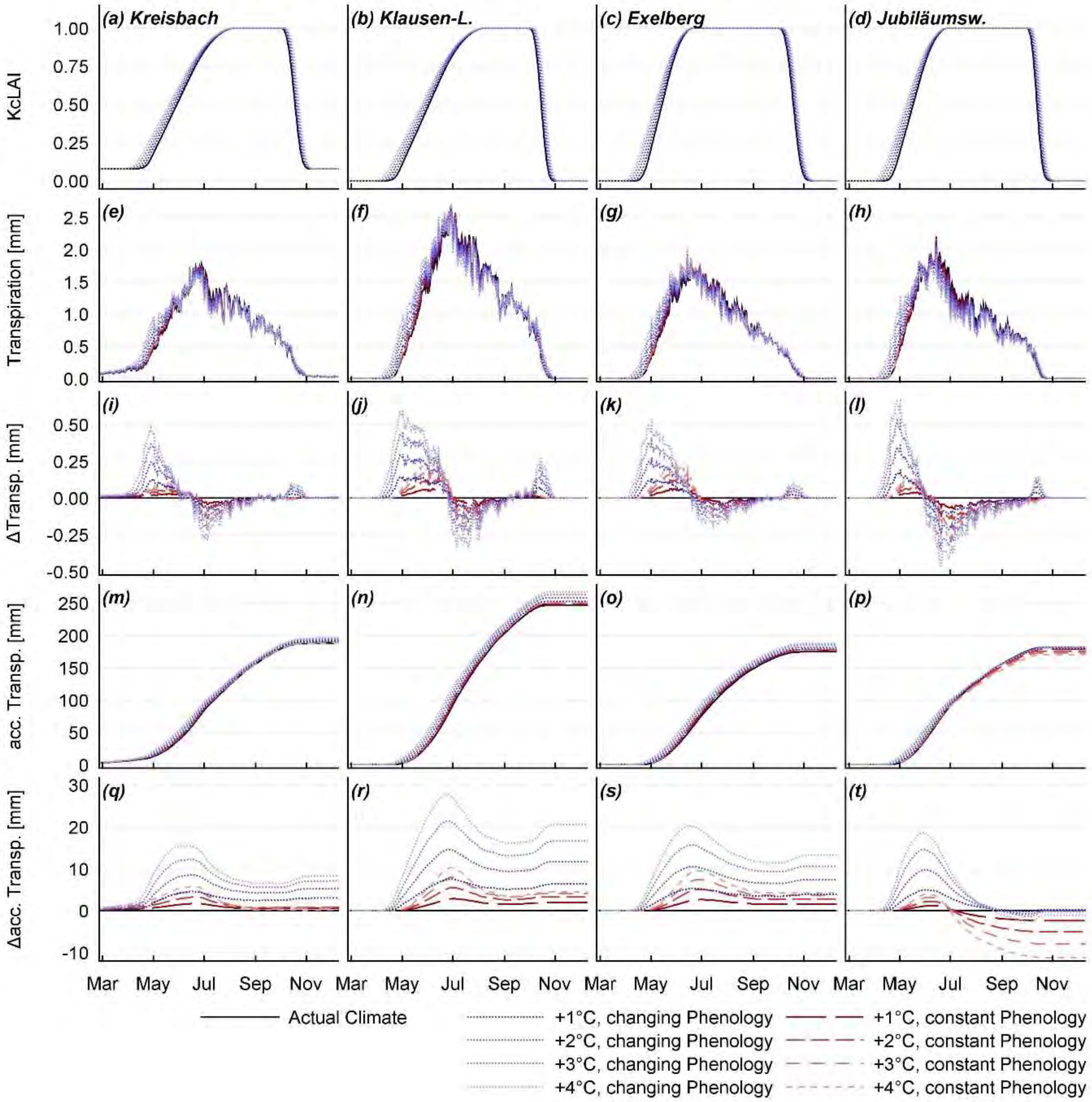

Figure 19: Result of the temperature sensitivity analysis on day of year base. (a-d) Relative leaf area: One degree temperature rise corresponds roughly to an increase of 4.7 days in growing season length, whereat LU is affected more strongly than LC. (e-h) Mean daily transpiration for all four sites: Transpiration is modeled highest at the beginning of summer. The KL site experiences the highest transpiration rates. (i-l) Change of daily transpiration compared to the actual climate: The increase of transpiration at the beginning of the growing

season caused by higher temperatures and earlier LU is followed by a marked decrease in summer, due to soil water depletion. (m-p) Accumulated transpiration: The KL site displays the highest annual sums. (q-t) Change of the accumulated transpiration compared to the present climate. Without consideration of elongated growing seasons, the JU site responds with a decline of transpiration due to soil drought in mid-summer. This decline is compensated by the effect of the elongated growing seasons.

Under current conditions, the KR and JU site experience frequent dry and drought years (Figure 20i,l). Here, rising temperatures might lead to a drastic exacerbation of the situation. The reason that the KR site (which is receiving the highest amount of precipitation) shows a similar behavior as the JU site (which is receiving the lowest annual precipitation sums), can be found in an unfavorable combination of high canopy evaporation rates with high bypass water fluxes (**Table 7**). At the end, only a small partition of the incoming water is available for plant consumption.

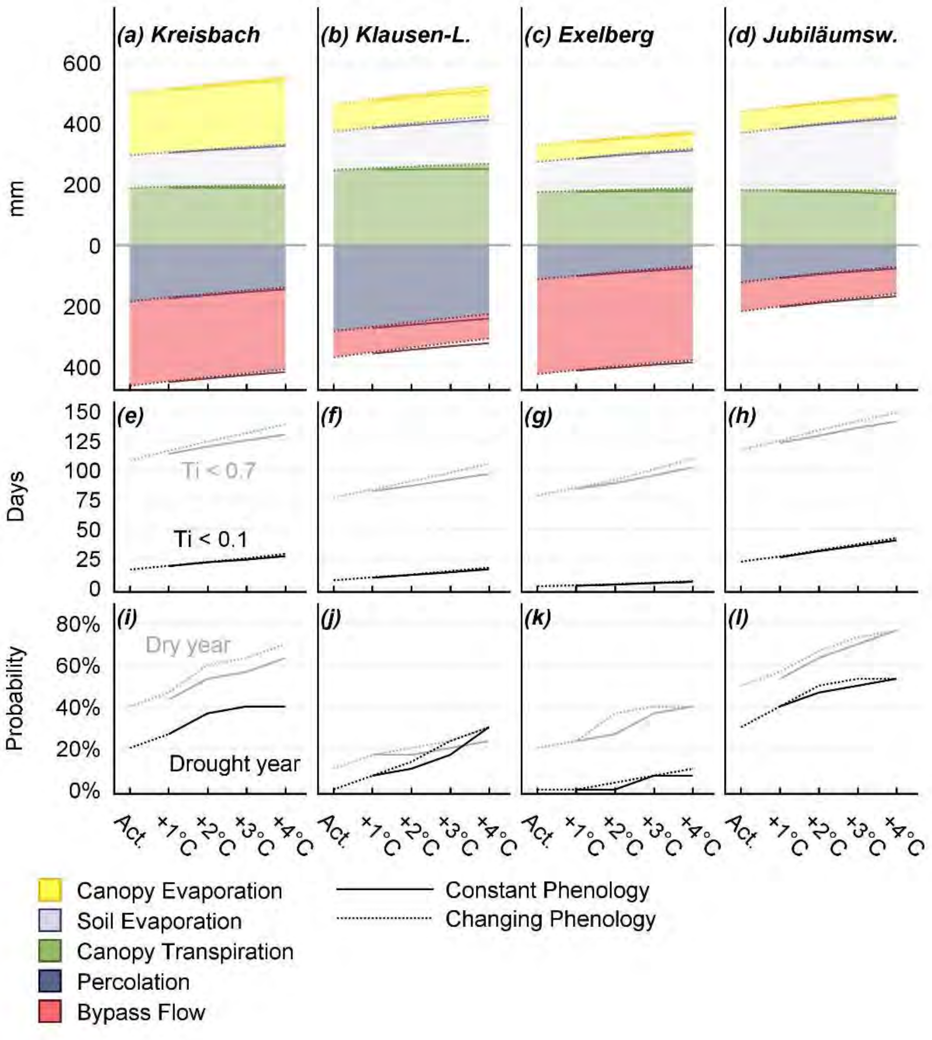

Figure 20: (a-d) The influence of rising temperatures on the stands' annual export flux sums. Liquid and gaseous fluxes are displayed below and above zero, respectively. Warmer temperatures decrease the fraction of percolation, while (unproductive) soil evaporation rises. Although potential evapotranspiration rises, annual transpiration shows almost no response to higher temperature. The reason for this can be found in drier soils, which are favoring soil evaporation. (e-h) Days with water stress (defined as Ti < 0.7: grey line) and soil drought (Ti < 0.1: black line) within the growing season (from 25th March to 11th November): With rising temperature all sites display a distinct increase of dry days per year. Except on the EX site,

higher temperatures lead also to an increased frequency of drought days per year. In both cases, the effect of elongated growing seasons is almost negligible. (i-l) Dry years are defined as years with more than 120 days of Ti < 0.7 during the growing season; drought years are defined as years with more than 30 days of Ti < 0.1 during the growing season. Under current climate the risk for drought years does not exceed 20%, meaning drought years occur roughly every 5th year. On the KL and EX site, no year fulfilled the criteria for drought years, within the reference climate period. On the EX site, 4 °C warming lead also to no noteworthy increase of drought years. Under current conditions, the KB and JU site are facing the highest risk of severe soil water deficit. Considering an exacerbation due to rising temperatures, it seems possible that these stands might undergo future changes in species composition and productivity.

Under current conditions, drought is a rare phenomenon on the KL and EX site (Figure 20f,g): The KL stand receives relatively high annual precipitation sums. Only a small percentage is lost by interception (Table 7). Paired with a high infiltration capacity, this has a beneficial effect on the stands' water supply. But also here, rising temperatures led to an increase of dry and drought years. Due to the favorable current state, the impact seemed to be less pronounced. It appears paradox, that the driest site experiences the lowest risk for severe soil drought, but the EX forest benefits from a very low modeled wilting point (see Table 6). This is enabling plant water supply at low soil moisture levels (Figure 23). On this site, severe soil drought does only occur infrequently under present conditions and also rising temperatures lead to no significant increase of the drought risk (Figure 21s,w).

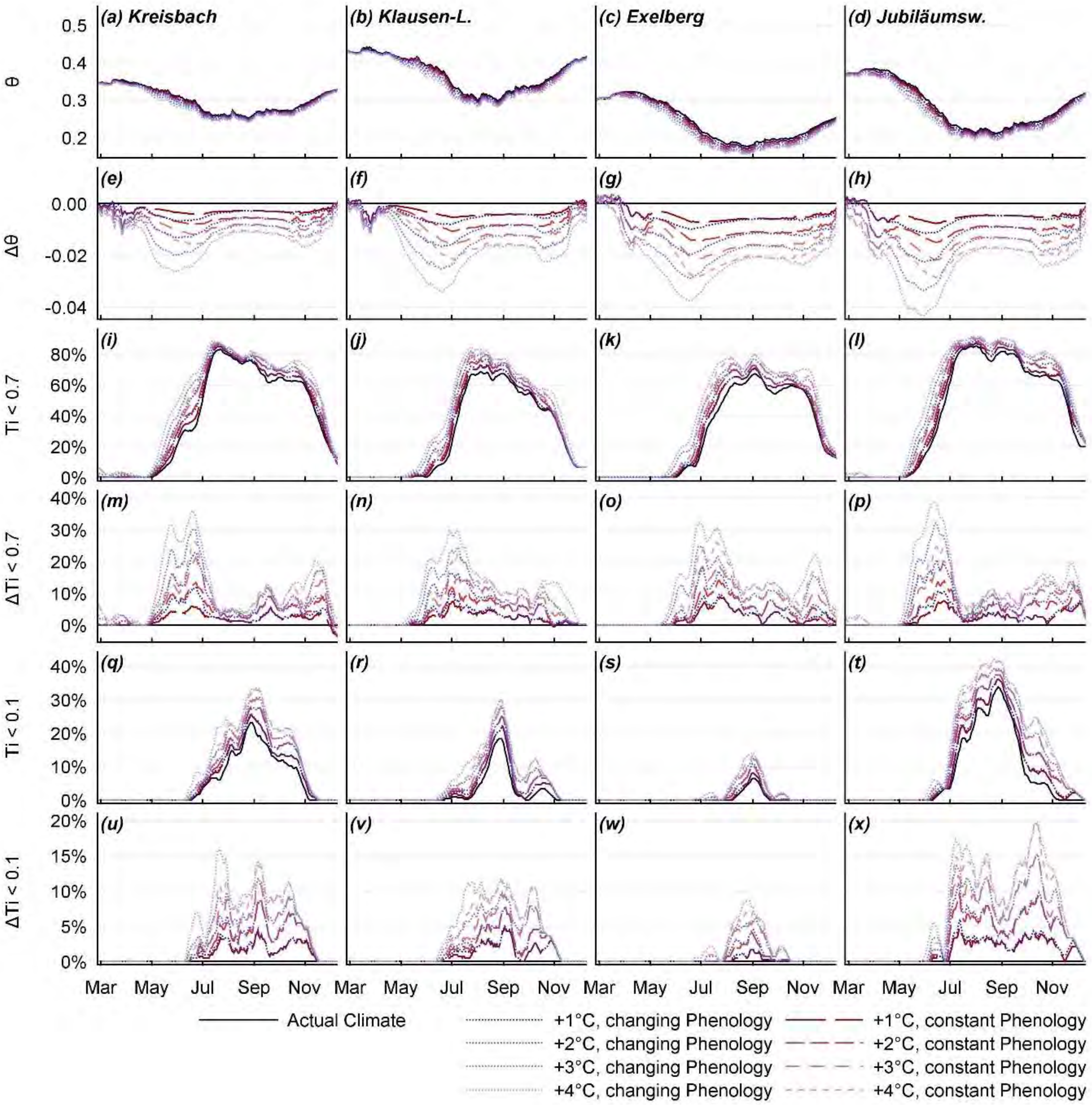

Figure 21: Result of the temperature sensitivity analysis on day of year base. (a-d) Seasonal course of the relative water content: All sites display the same seasonal dynamics with lowest soil moisture during the growing season. The EX site appears to be strikingly drier than the other sites. (e-h) Changes of soil moisture compared to the present climate: All investigated forest stands are apparently getting drier. The KB and KL site seem to be affected slightly weaker than the other sites. The reduction of soil moisture is most pronounced at the beginning of summer, also amplified by an earlier LU. (i-l) Probability of water stress (defined as Ti < 0.7): On all sites, water stress is the usual soil state during the warm season. The highest probability is found in mid-summer. (m-p) Change of the water stress probability, compared to the present state. Warmer temperatures e. g. longer growing seasons increase the risk of soil water stress, especially in early summer. An earlier LU amplifies the probability of water stress, especially at the beginning of summer. (q-t) Risk of severe soil drought (defined as Ti < 0.1): All sites show the highest probability of severe drought at the end of August. Although the EX site appears to be the driest site, the risk for severe water stress is strikingly low. The reason can be found in the low wilting point (see Figure 23, Table 6), allowing transpirative water consumption at low soil moisture. (u-x) Change of drought risk, compared to present conditions: Higher temperatures increase the risk of severe drought on all sites. The KB and JU site show the highest vulnerability. On these sites, a temperature rise of 4°C more than doubles the probability for severe drought. On the other hand, the elongation of the growing

season has almost no impact on the drought risk. The driest site (EX) exhibits the weakest increase in the risk of severe drought.

An earlier start of the growing season let to higher E_C water fluxes from spring to early summer (Figure 19i-l). The effect was amplified by high rates of potential evapotranspiration during this period. Early LU had an intensifying effect on soil water stress in summer. As a consequence, the scenarios which considered changes in spring phenology experienced a drastic transpiration drop in mid-summer. On the contrary to soil water stress, extended growing seasons had almost no effect on the frequency and duration of severe drought. On all sites, there was a high probability for moderate soil water deficit (Ti < 07) during the entire growing season, with a weakly pronounced maximum at the beginning of summer. On the other hand, the risk for severe drought (Ti < 0.1) shows a very distinct peak at the end of August (Figure 21q-t).

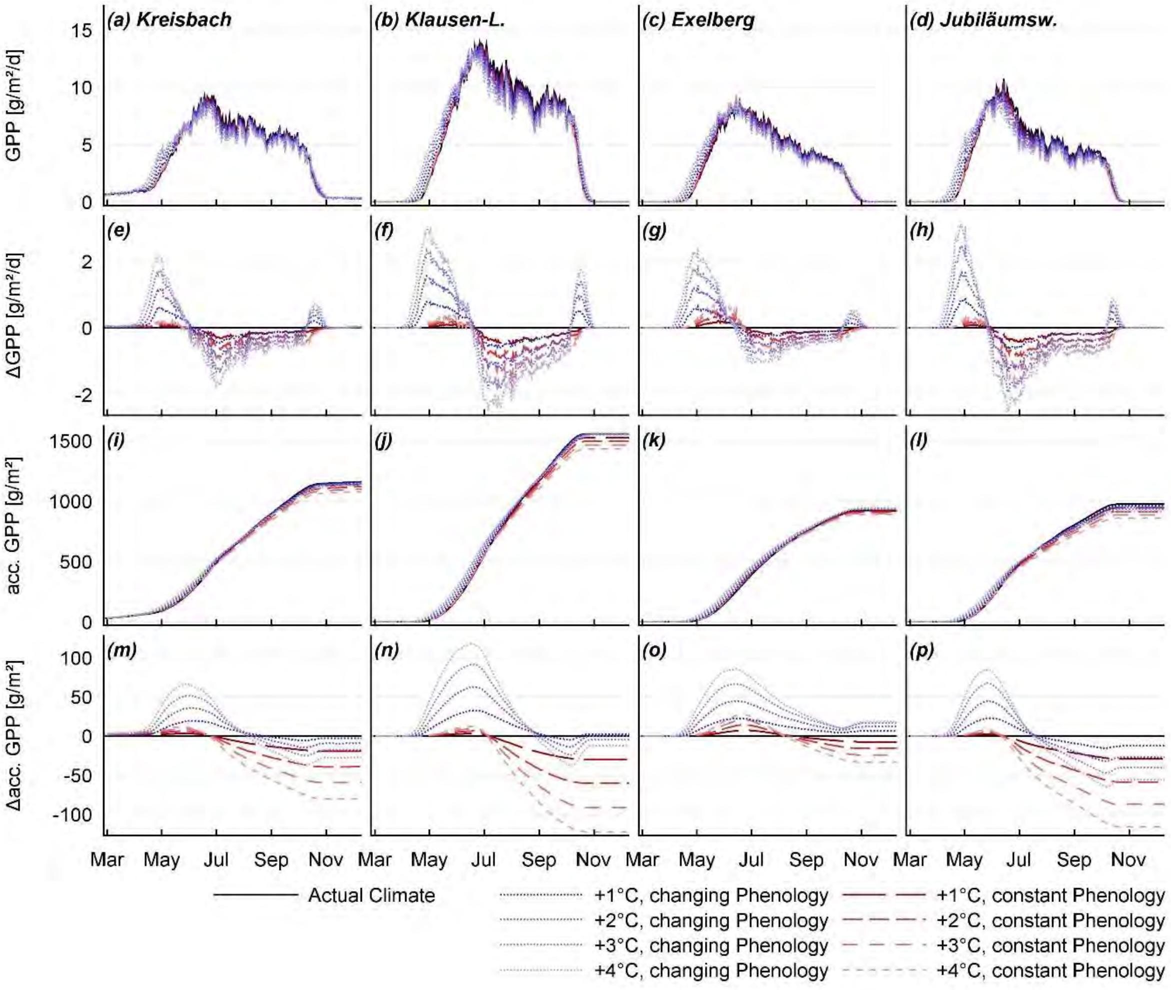

Figure 22: Gross primary production on a day of year base: GPP was calculated as the product of transpiration water fluxes and the estimated water use efficiency. (a-d) GPP shows a pattern, very similar to transpiration. (e-h) Change of daily GPP compared to the reference scenario: Higher temperatures in spring and earlier LU accelerate the assimilation early in the season, before soil moisture deficit hampers primary production in mid-summer. (i-l) Accumulated GPP over the year: Analogue to annual transpiration, the KL plot (j) shows the highest productivity. (m-p) Change of the accumulated primary production to the reference climate period: All warming scenarios show an advance in production in late spring, which dissipates in summer. Without consideration of a change in the growing season length, all warming scenarios respond with decreased annual assimilation. Due to a compensating effect of elongated growing seasons, rising temperatures lead to no net change of the stands' annual primal

production. Again, the EX stand represents an exception. It appears paradox that the driest site seems to be also the only site, which might benefit from higher temperatures!

Longer growing seasons are assumed to widen the timeframe for potential carbon assimilation (Gunderson et al., 2012; Vitasse et al., 2009). Without consideration of the growing season elongation caused by higher temperatures, all sites responded with decreased annual GPP due to water stress in mid-summer (Figure 22e-h). In this simulation, prolonged growing seasons led to a marked increase of productivity at early stages of the growing season, followed by a significant depression from July to September (compare also Bergh et al., 2003). Growing season elongations were hardly sufficient to compensate for the productivity drop in mid-summer, caused by soil water stress. Only the EX site exhibits a net gain of GPP due to the combination of higher temperatures and longer growing seasons (Figure 22o).

Falling in a time of high potential productivity, the extension at the start of the growing season had a stronger effect than the delay of autumn senescence (compare Gunderson et al., 2012).

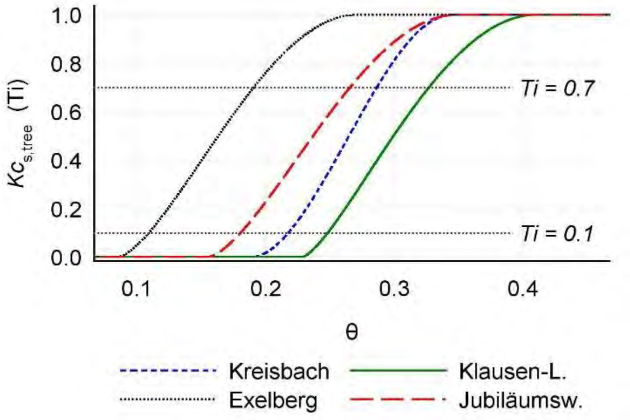

Figure 23: The transpiration stress coefficient is dependent on soil moisture. The transition between θ_{pwp} and θ^* is modeled utilizing the modified *smoothstep function* (8 Appendix, Equation A4, A5). Severe water stress is assumed when Ti drops below 0.1. At the EX forest stand, this corresponds to relative soil moisture levels below ~11%.

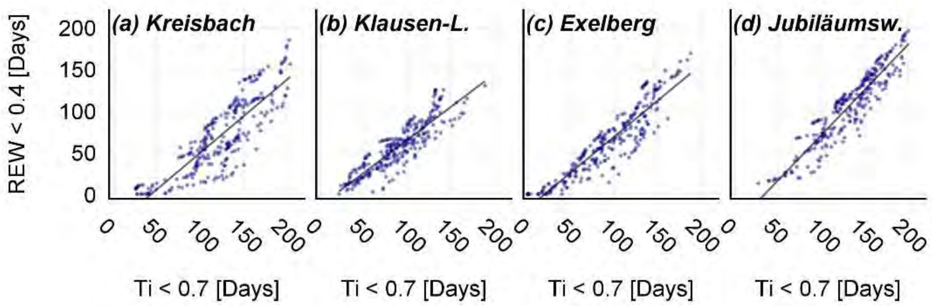

Figure 24: Site-wise comparison of water stress indices: Number of days per growing season, where actual transpiration falls below 70% of the potential evaporation vs. days per growing season, the relative extractable water soil water content (REW) falls below 0.4. The growing season is considered as period from the 25th of March to the 11th of November. Generally, both indices deliver similar results; the easterly sites (EX, JU) exhibit higher correlation.

3.5 Evaluation of the SDM

Soil solution chemistry was monitored in a bi-weekly interval, on each site in 15 replications (Figure 25a,b). This enables the calculation of robust site wise mean SO_4-S soil solution concentrations per sampled event. The resulting timelines of both forest stands reveal a very similar pattern (Figure 25c). The observed correlation gives a hint, that sulfate solution chemistry might be driven by the same processes, on both stands.

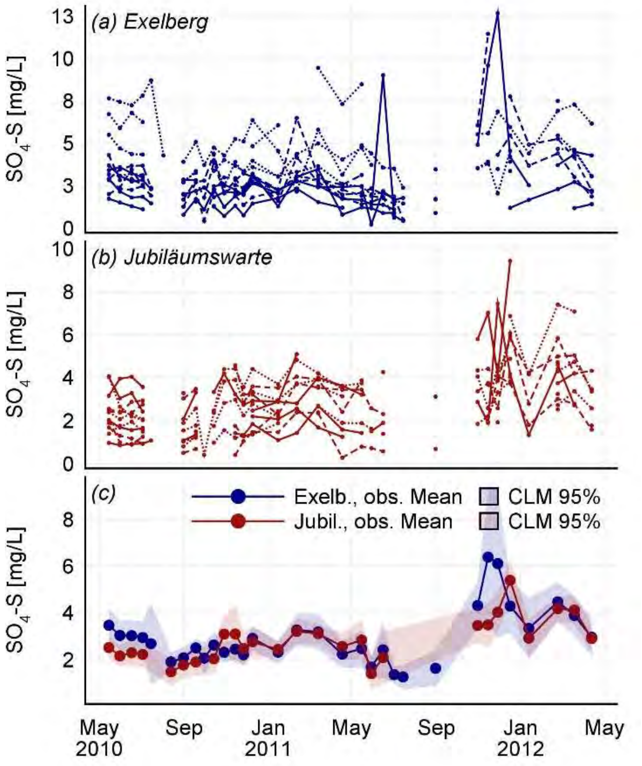

Figure 25: (a, b) Time-series of SO_4-S concentration, observed in soil solution. Each line represents one lysimeter. Eighteen lysimeters were installed per plot (6 repetitions and three depth classes). To overcome the noise in the data, the SDM was fitted to site-wise mean concentrations (c). After calculating the mean, both sites reveal a very similar pattern regarding the temporal development of the soil solution concentration. This is leading to the assumption, that soil S dynamics are controlled by similar processes on both sites.

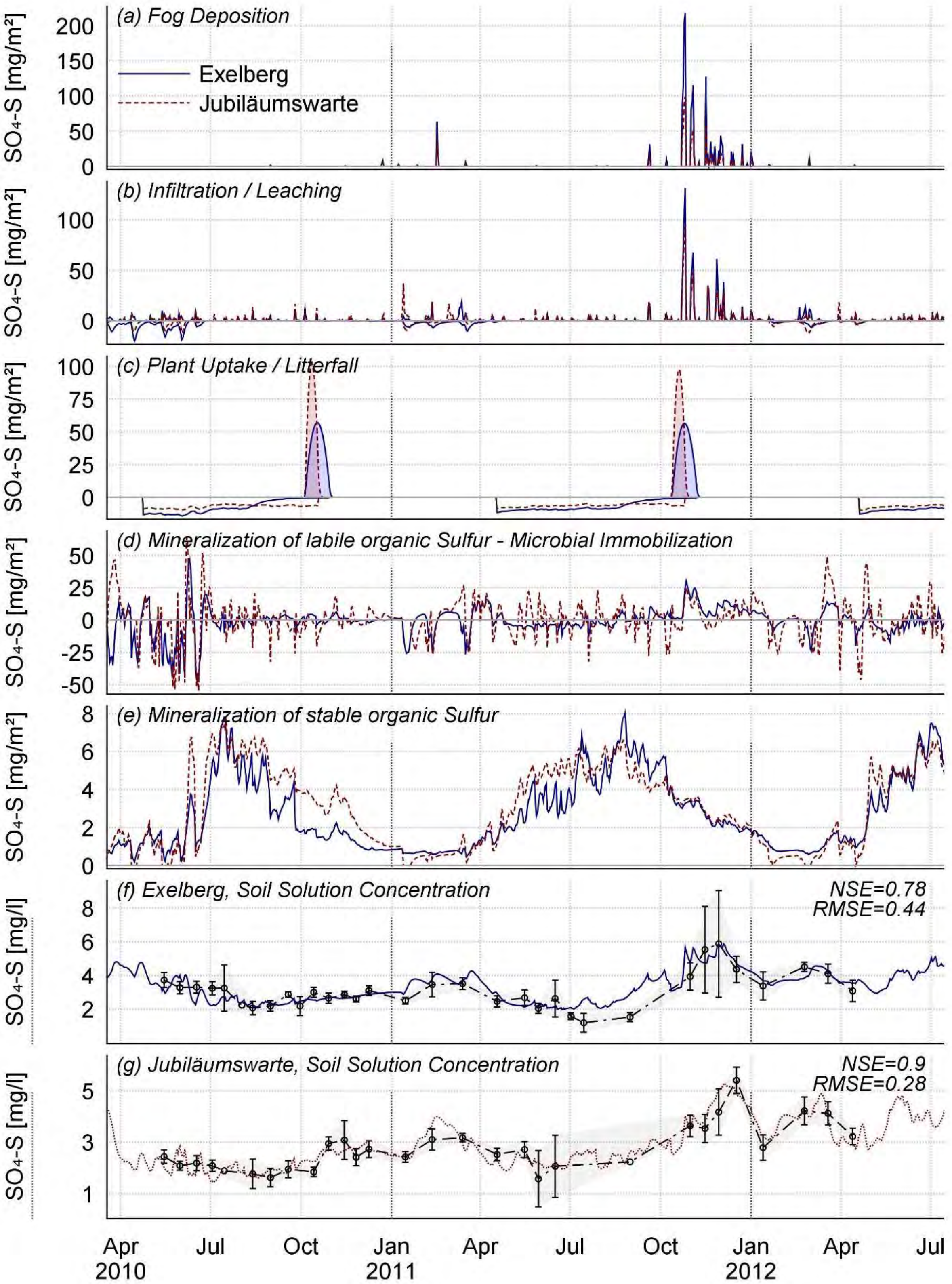

Figure 26: S fluxes during two years of field campaign. (a) Both stands experience a prolonged fog event in the autumn of 2011. During this period, observed occult deposition loads ranged between 200 to 500 mg SO_4-S/m^2. The simulation outcome suggests much higher values: From mid-October to the end of December 2011, the simulator predicts occult deposition sums of 1800 and 900 mg SO_4-S/m^2, for the EX and JU site respectively. (b) During the field campaign, atmospheric inputs were dominated by the occult deposition event in the fall of

2011. Due to the coupling with percolation, leaching of SO_4-S only takes place, when soil moisture is above water holding capacity. This happens predominantly during the dormant season when evapotranspiration water fluxes are low. (c) Plant uptake is assumed to take place only during the growing season. Because plant uptake is driven by their demand in this simulation, highest rates of S assimilation are achieved relatively early in the growing season. As the annual demand is met in late summer, plants start to throttle the uptake of S. During autumnal litterfall, the S, which is stored in leaf biomass is transferred to the soil organic pool. (d) In this graph, the difference of mineralization of labile organosulfur and microbial immobilization is displayed. Positive values represent inputs to the soil solution meaning that mineralization is dominating. The erratic pattern is caused by shifted Θ optima for both processes (compare Figure 28, Figure 29). Mineralization slightly favours higher Θ values than immobilization. (e) Mineralization is driven by substrate availability, Θ, and soil temperature. Maximal values are achieved at moderate Θ, and high soil temperature (see Figure 28, Figure 29). (f, g) Observed and modeled timeline of the SO_4-S concentration in the soil solution. The dash-dotted line illustrates the stands mean concentration at given time, the error bars display the 95% confidence limit for the mean. The calibration led to sufficiently good results for both investigated forest stands. Both sites exhibit a peak in the solution concentration in late autumn of 2011. This is assignable to (i) high input loads via fog deposition and (ii) mineralization excess during this period.

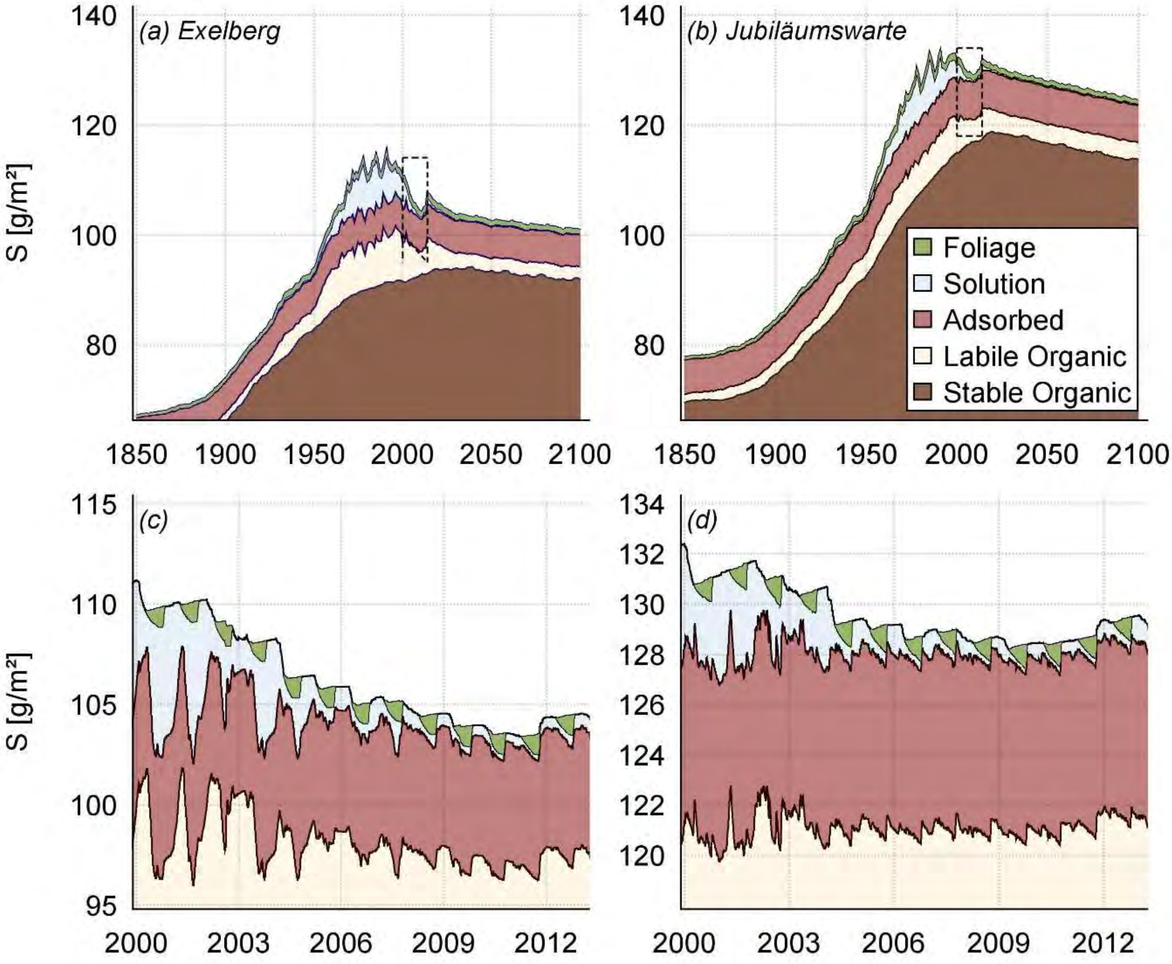

Figure 27: Temporal development of S pools over the whole model timeframe (a, b) and focused on the recent past (c, d). (a, b) The model displays a rise in the stands' overall S stock, which is mainly assignable to the stable organosulfur pool (dark brown). Interestingly, this

increase still has not tapered in the present decade. Form the 1960s to the late 1980s S deposition peaked; high S loads are reflected in altered labile organosulfur and solute SO_4-S in the soil. The amount of SO_4-S, adsorbed in the soil, shows the lowest variability. Simulated sorption (EX: 6 g, JU: 6.8 g) is during most periods close to the (modeled) maximum sorption capacity on both sites ($K_{max,ads}$ = 6.1 g SO_4-S m^{-2} EX, 7.1 g SO4-S m^{-2} JU). Both stands' total soil S pool was estimated in 2010. On the Exelberg site, an estimated amount of 78 g/m^2 corresponds to a simulated soil S pool of 103 g/m^2. The Jubiläumswarte soil S pool was estimated to 102 g/m^2 in June 2010, 128 g/m^2 were simulated. Both sites exhibit two peaks of the total S pool; one at the end of the 1980s and one at the end of the monitoring period. The second peak might be caused by a high recurrence of deposition rich fog events in this period. After 2020 both sites display a slow recession of S pools which does not reach steady state until the end of the prediction timeframe in 2100. (c, d) The model does not explicitly account for S, stored in non-green living plant biomass. The S uptake fraction, which is not assigned to foliage S, is routed to the soil organic S pool, where it is instantaneously exposed to mineralization. The simulated S content of foliage lies in the range of one g/m^2. S is modeled, to be taken up steadily during the growing season. Autumnal litterfall leads to a sharp increase in the soil organic S pools.

Regarding the timeline of SO_4-S in soil solution, the SDM yields feasible results for both investigated stands: The simulations capture the observed timeline to a satisfactory degree (Exelberg: NSE=0.78, Jubiläumswarte: NSE=0.9) (compare Figure 26f,g,

Table 8). The SDM overestimates the amount of total soil-S, which was quantified in 2010. For the EX and JU plot, the observed mean of the total soil-S pool down to a depth of 50 cm was 78 g/m^2 and 102.6 g/m^2 (Hanousek et al., 2017). The SDM delivers an estimate of 103 and 128 g/m^2 (see Figure 27c,d). Therefore, it overestimates both sites' pools, each by approximately 25 g/m^2. Given the fact, that the presented model does not explicitly account for organic S, bond in living tree biomass other than foliage, one could argue that a portion of the modeled organic pool is contained in the aboveground plant tissue. For a beech rich Northern Hardwood forest (Hubbard Brook Experimental Forest), Likens et al. (2002) give an estimate for the S, bound in aboveground living biomass, of 8.5 g/m^2 roughly. Subtracting one g representing foliage S this narrows the gap, reducing the overestimation to approximately 17.5 g/m^2.

Soil samples from both investigated sites were analysed for S fractions by Hanousek et al. (2017). Additionally, they used material from a third site to create pooled samples. Adsorbed S was determined to a fraction of 6.4% of total soil S. The organic fraction accounted for 89%. The modelling work, which is presented here, delivers similar values. On both locations, adsorbed and organic fraction account for roughly 6% and 93.5% (Figure 27c,d).

The organic fraction can further be divided into carbon bonded S and ester-sulfates. For a nearby beech stand on similar bedrock the ester fraction was determined by Hanousek et al (2017) via HI-reduction (described in Kulhánek et al., 2011; Tabatabai, 1996). The authors found, that ester-sulfates account for approximately 38% of the entire organic fraction, which is in contradiction to Havlin et al. (2005) who suggest that ester-sulfates account for the majority of organic soil S. The hypothesis that labile soil organosulfur corresponds to ester-sulfates must be rejected: Accounting for only 3.5% (EX) and 4.5% (JU) or organic soil S, the simulated labile pool (June 2010) is even smaller than reported by Hanousek et al. (2017).

For a Beech stand on similar bedrock, Berger et al. (2009) reported an annual litterfall S flux of 0.45 g/m^2. However, the S content in green foliage tissue was more than two times higher than in litter material, indicating translocation processes before leaf senescence. In this work, the simulations exhibit values, of one g/m^2 by year. This overestimation could be explained by the neglect of plant-internal S translocations in the current version of the SDM.

3.5.1 Microbial S transformations

Compared to other soil S pools, the microbial S pool is small. According to Chowdhury et al. (1999), microbially bond S accounts only for 1- 4% of total soil S. Nevertheless, it is of great importance considering plant nutrition due to its labile nature. Kertesz and Mirleau (2004) describe the contribution of microbial activity to the plant S supply: Plants take up S primarily in form of inorganic SO_4 (Buchner et al., 2004). However, only a minor fraction of soil S is available in this form. As stated before, the majority is contained in organic material. Soil microbiota are responsible for the mineralization of organically bond S to inorganic sulfate. On the other hand, microorganisms are also driving the rapid immobilization of inorganic sulfate, first to relatively labile ester sulfates and furthermore, to more stable C-bonded S species (Ghani et al., 1993). In the presented formulation, S taken up by plants is routed to both, stabile and labile organosulfur. In contrast to plant uptake, microbial immobilization contributes only to the labile pool (compare Figure 10). Here mineralization and immobilization of the labile organic pool are described as temperature and moisture dependent. The soil moisture optima are slightly displaced (see Figure 28): Immobilization is favoured by dryer soil conditions. Immobilization also exhibits stronger response to warm conditions (compare Figure 29). Kertesz and Mirleau (2004) see immobilization and mineralization as concurrent processes, occurring simultaneously in the soil. In these simulations, it is in fact the non-congruence of soil moisture and temperature response, which is driving a large portion the observed fluctuations in the SO_4 soil solution, favouring net mineralization under cool and moist conditions, and net immobilization under warm and slightly dryer conditions.

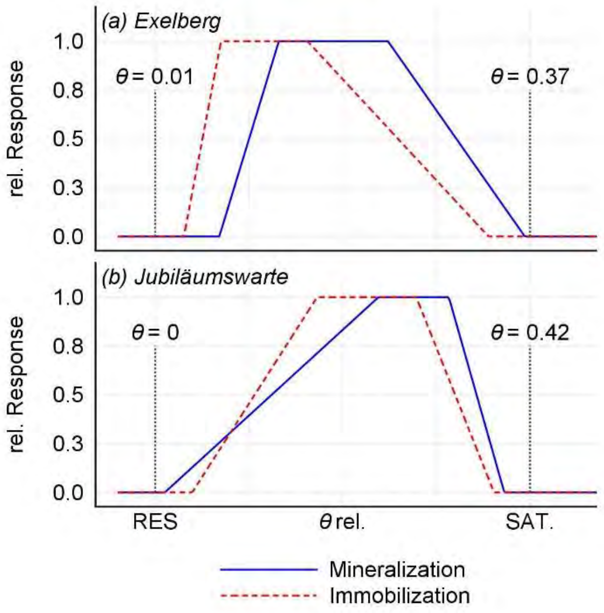

Figure 28: Response of microbial S transformations to soil moisture (*Θ*). *Θ* is displayed on a relative scale whereas 0 corresponds to the residual water content and 1 to soil saturation, respectively. The response of microbial processes to *Θ* was described using a piecewise linear function. On both sites, the calibration led to mineralization and immobilization optima at medium *Θ* where a balanced water and oxygen supply is given. Tthe range of maximal immobilization rates is slightly shifted to drier soil conditions (compare Table 8). In the simulations presented in this work, the non-congruence between the moisture response of immobilization and mineralization is responsible for short term fluctuations in the SO_4-S soil solution concentration.

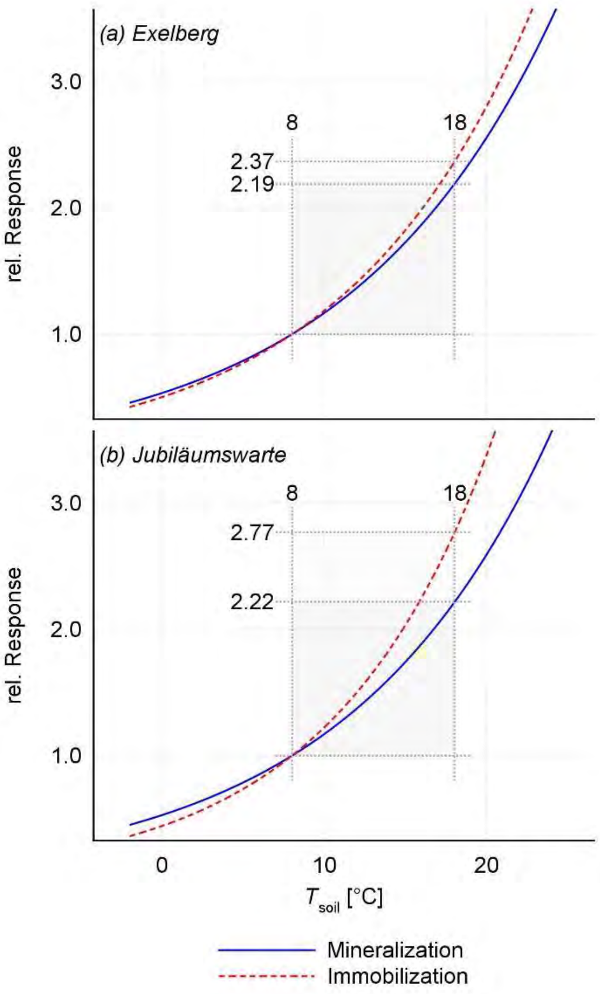

Figure 29: Response of microbial S transformations to soil temperature. The effect of soil temperature was modeled, using the Q_{10} temperature coefficient. The base temperature was set to 8°C, which is close to the annual mean soil temperature of the sites. The calibration process delivered similar Q_{10} factors for both forest stands, whereas the temperature sensitivity of immobilization was slightly higher than the sensitivity for mineralization (compare Table 8).

3.5.2 Occult deposition

During two years of field campaign, a prolonged fog event was captured in late autumn of 2011. There is a solid body of work asserting that fog water is enriched in sulfate compared to rainwater (see Fowler et al., 1989; Lange et al., 2003). Especially in mountainous regions, fog can contribute significantly to the hydrologic and nutrient balance (Klemm and Wrzesinsky, 2007). Deposition was monitored (i) in the open and (ii), below the canopy (throughfall) and in form of (iii) stemflow. The accumulated S deposition sums clearly displays significant S inputs via occult deposition during the captured fog event (compare Figure 30). The observed discrepancy between open area deposition and throughfall plus stemflow deposition indicates an extra input of approximately 500 mg SO_4-S m^{-2}. In this work, open area deposition states the input for the simulation. The derivation of fog precipitation is presented in section 2.3.3.1.To scale from the mean daily aerial SO_2-S concentration to the SO_4-S concentration in the fog precipitation water, an enrichment factor is applied (see Lange et al., 2003). From 22nd October to 5th December 2011, the simulation yields an input of 1330 and 620 mg SO_4-S m^{-2} in form of occult deposition for EX and JU, The spike in the soil solution at the end of 2011 (see Figure 25a,f,g) is mostly assignable to fog deposition inputs. The observed and predicted high loads might be a result of the stands' local conditions: In the Vienna Basin, winter fog events often coincide with south-easterly currents passing over the urban area, the air becomes enriched with pollutants. At the edge of the Vienna Woods it is forced to rise, condensation starts. The forest stands, which are located at the upper hill slope, facing south to east, are acting as a first barrier for the enriched fog, making them susceptible for the interception of high loads of atmospheric S. For a detailed description of this regional phenomenon see Auer et al. (1989).

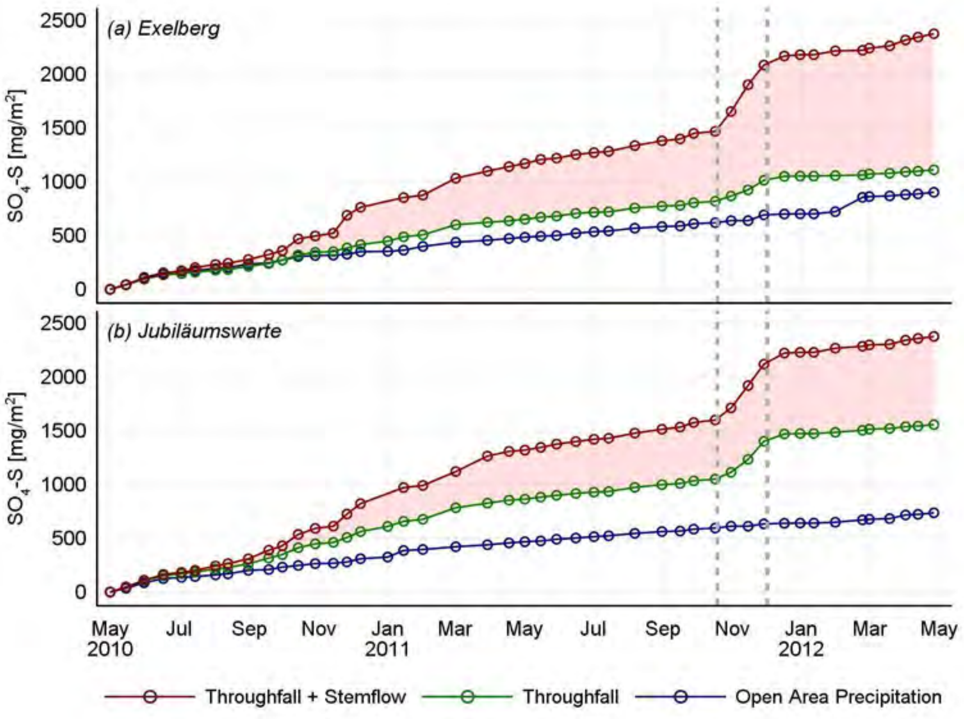

Figure 30: Accumulated SO_4–S deposition on both investigated stands. During late autumn 2011 both sites experience a sharp increase in throughfall deposition. This period coincides with a long-lasting fog event; occult deposition seems to be an important sulfate source during such events.

Table 8: Parameter optimization results for both investigated sites.

Parameter	Description	Unit	EX	JU
f_{occult}	Fog (Occult Deposition) Enrichment Factor		33922.35	15395.36
f_{dry}	Stomatal (Dry) Deposition Factor		0.00	0.00
$\Theta_{0,\text{mineral}}$	Mineralization, Lower Threshold Θ	LL^{-1}	0.07	0.01
$\Theta_{1,\text{mineral}}$	Mineralization, Lower Optimal Θ	LL^{-1}	0.13	0.25
$\Theta_{2,\text{mineral}}$	Mineralization, Upper Optimal Θ	LL^{-1}	0.23	0.33
$\Theta_{3,\text{mineral}}$	Mineralization, Upper Threshold Θ	LL^{-1}	0.36	0.39
$\Theta_{0,\text{immobil}}$	Immobilization, Lower Threshold Θ	LL^{-1}	0.04	0.04
$\Theta_{1,\text{immobil}}$	Immobilization, Lower Optimal Θ	LL^{-1}	0.07	0.18
$\Theta_{2,\text{immobil}}$	Immobilization, Upper Optimal Θ	LL^{-1}	0.16	0.29
$\Theta_{3,\text{immobil}}$	Immobilization, Upper Threshold Θ	LL^{-1}	0.33	0.38
HL_{stable}	Half-Life, Stable Soil-Organosulfur, opt.	Years	54.71	67.34
HL_{labile}	Half-Life, Labile Soil-Organosulfur, opt. Conditions	Days	21.99	13.00
$K_{\text{m,immobil}}$	Immobilization, K_{m} Parameter		1.81	1.05
$V_{\text{m,immobil}}$	Immobilization, Maximum Rate, opt. Conditions	SO$_4$-S mg m^{-2}	2.11	2.11
$f_{\text{Q10,immobil}}$	Immobilization, Q10 Factor		2.37	2.77
$f_{\text{Q10,mineral}}$	Mineralization, Q10 Factor		2.19	2.22
$V_{\text{m,starve}}$	Plant Uptake, Maximum Rate at S Starvation	SO$_4$-S mg m^{-2} d^{-1}	0.11	0.07
$V_{\text{m,sat}}$	Plant Uptake, Maximum Rate at S Saturation	SO$_4$-S mg m^{-2} d^{-1}	0.00	0.00
$K_{\text{m,plant}}$	Plant Uptake, Km Parameter		1.16	0.95
TC_{starve}	Plant Uptake, Threshold Uptake, Starvation	SO$_4$-S mg m^{-2}y^{-1}	1141.79	913.76
TC_{sat}	Plant Uptake, Threshold Uptake, Saturation	SO$_4$-S mg m^{-2}y^{-1}	1367.79	2166.95
f_{labile}	Plant Uptake, routed to Labile Soil-Organosulfur		0.18	0.07
f_{fol}	Plant Uptake, routed to Foliage Pool		0.74	0.82
HL_{ads}	Adsorption, Half-Life	Days	205.00	71.10
$K_{\text{L,ads}}$	Adsorption, Half-Saturation Concentration	SO$_4$-S mg L^{-1}	12.53	11.68
$K_{\text{max,ads}}$	Adsorption, Maximum Charge	SO$_4$-S mg m^{-2}	6085.48	7057.02
	Initialization 1770, Labile Soil-Organosulfur	SO$_4$-S mg m^{-2}	5054.55	6804.58
	Initialization 1770, Stable Soil-Organosulfur	SO$_4$-S mg m^{-2}	51175.13	61845.05
	Plant Uptake 2010	SO$_4$-S mg m^{-2}	1345.80	1245.00
	Litterfall 2010	SO$_4$-S mg m^{-2}	992.40	1017.40
NSE	Nash-Sutcliffe Efficiency		0.78	0.90
RMSE	Root Mean Square Error		0.44	0.28

3.5.3 Historic development and future prospect

Both stands display a strong rise in the total soil S pool during the 20th century (compare Figure 27a,b). This can be assigned largely to the accumulation of stable organosulfur originating from plant residuals. Interestingly, the accumulation of stable S has not fully tapered off in the present decade. In an attempt, to predict the future S output of two German catchments with the MAGIC model (Cosby et al., 2001), Prechtel et al. (2003) found that for one catchment the observed SO$_4$ release could not be explained solely by adsorption/desorption processes in the soil. It was necessary to introduce an additional S source (968 mg m^{-2} yr^{-1}) to match the simulated with the observed stream output. The authors suggested an S release from decomposition of organic soil constituents. In this work, S from mineralization of stable organosulfur adds a relatively steady annual amount between 700 and 1300 mg (1980 - 2020) to the budget. However, in these simulations, only a limited fraction of mineralized S enters the stream output. As the availability of other S sources might dwindle in the future, this fraction could further decrease. Much rather than being exported, it might be rapidly incorporated into living biomass and be cycled through the biosphere again. On the other hand, the remaining fraction which is leaving the system via seepage might hinder the achievement of a balanced input/output for many decades. Prechtel et al. (2003) point out that the investigated catchments could reach pre-industrial conditions in a few decades. They also claim that knowledge of origin and behaviour of the postulated organic sulphur is crucial for the prediction of future trend in the stream chemistry. In this work, a large organic S pool with modeled half-lives up to 67 years will allow only a slow temporal recession of the catchment S export over the coming decades (see Figure 31): Pre-industrial conditions in the stream-discharge as well as a steady state equilibrium are not reached over the whole investigation timeframe.

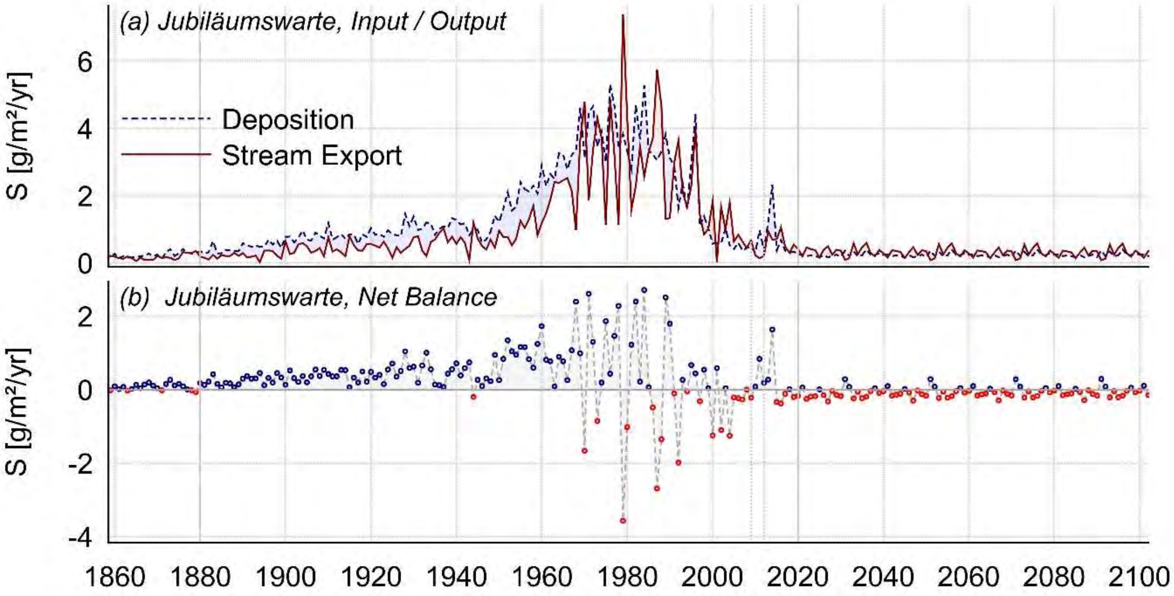

Figure 31: Annual S input vs. annual output (I/O) for the Jubiläumswarte site. After the spin-up period I/O is in steady state. With rising atmospheric deposition, the system shifts to input excess in the end of the 19th century. Highest inputs are modeled around the year 1980. In the late 1980s, the system shifts to output domination for the first time. A second smaller peak of input excess around the year 2015 is caused by a frequent occurrence of fog events in this period. After 2020 the model predicts a steady recession of input and output with output moderately dominating inputs for the remaining time period. At the end of the investigation timeframe in the year 2100, the system has still not fully restored I/O equilibrium and stream discharge of SO_4-S remains slightly above the level of the pre-industrial era, ending in 1880.

Mineralization of S containing soil constituents shows a strong response to soil moisture and soil temperature. Mitchell and Likens (2011) state the importance of the water balance in controlling the S output of forested watersheds: Soil moisture affects the net stream discharge, mineralization, desorption and weathering of S bearing minerals. High temperatures might also accelerate these processes. On the other hand, due to increase of evapotranspiration, high temperatures might lead to dryer soils conditions (as stated in section 3.4) impeding release and the export of S. Hence, how a changing climate might affect the stands' S dynamics has yet to be explored.

3.5.4 Inactive Modules

3.5.4.1 Stomatal Deposition

It is assumed, that plants take up S primarily by the roots. Additionally, it is possible that airborne SO_2 contributes to plant nutrition via the stomatal pathway (Rennenberg et al., 1990). In this work, stomatal deposition is displayed as a function of aerial SO_2 concentration, the relative leaf area, the stomatal degree of openness (see section 2.3.3.6) and the wind speed. The calibration process always leads to stomatal deposition rates close to zero. It seems possible that (i), under current atmospheric SO_2 concentration, stomatal uptake plays only a negligible role in plant nutrition or (ii) the effect of stomatal uptake is comprised in other simulated modules.

3.5.4.2 Soil Sulfatase Activity

The SDM comprises the effect of microbial sulfatase release on the kinetics of the labile organic S. Deficits in the S supply (low SO_4-S solution concentration) promote the microbial release of sulfatase, thus accelerating the mineralization of organically bond sulfate (Scherer, 2009). This is implemented by introducing half-lives of the labile organic pool, linearly dependent on the soil solution concentration. Yet during model fitting, concentration dependent half-lives did not improve the performance of the simulator. Comparable to stomatal deposition, it seems possible that (i) other modeled processes already cover the effect of microbial sulfatase release. It might also be thinkable that (ii) the observed SO_4 supply in the soil solution if sufficiently high to fully meet the needs of soil microflora. Hence, the release of exo-enzymes might be initiated only at solution concentrations much lower than observed.

4 Conclusion

In this thesis, a hierarchical set of mathematical simulators is presented with the aim to describe certain physical, biological and biogeochemical aspects of the plant-atmosphere-soil system of deciduous forest stands. A soil temperature model, a phenological model, a soil-hydrological model and an S-biogeochemistry model are presented and applied. The soil temperature module and the phenological module can be applied on their own. The application of the water balance module requires the upstream running of the phenological module. The model-based description of S balance and fluxes of deciduous forest stands, which was the final goal of this thesis; it requires output from all preceding modules (see **Figure 1**).

4.1 Soil Temperature

The primary intention of this module was the provision of a tool, which enables the transformation of fragmentary records of forest soil temperature, into a complete time series of T_{soil}, using average daily air temperature as only input. In this specific case, the created time series is laying the base for the modeling of temperature dependent, biogeochemical soil processes.

To test the resilience of this model, it was applied to various locations and depths, covering a broad amplitude of site characteristics. The simulator delivered accurate predictions of the temperature of the topsoil, as well as of deeper layers. The high performance was not limited to the warm season. The combination of the insulating effect of the snow cover plus the effect of heat transformations at the freeze/thaw transition, on soil thermal regimes were captured sufficiently. The formulation was applied to forested, as well as open to field locations, where in the open field it failed to reproduce some major soil frost events. Bearing this limitation in mind, this simulator seems to be well applicable to other land use types.

The model parameters lack a specific meaning in a strict physical sense. Therefore, currently the parameterization requires at least a modest amount of T_{soil} observations, to yield sufficient results. A challenging impulse for future work, would be the attempt to derive model parameters, directly from more easily obtainable site characteristics. This also would enable the capability of the simulator to deal with a changing soil thermal regime, during stand development.

4.2 Phenology and Water Balance

In the next steps, two simulators are presented, aiming to depict the water fluxes and the phenological dynamics of beech forest stands. Covering forest sites dominated by deciduous trees, the formulation comprises routines for the inter- and intra-annual dynamics of the vegetation cover. A routine is introduced, calculating fog precipitation as a function of air temperature, relative humidity and wind speed. Furthermore, precipitation interception is calculated, utilizing a function based on the Langmuir isotherm. Soil processes (saturation excess overflow, percolation, soil evaporation, and transpiration) are described, utilizing a zero-dimensional box model approach. Despite the strong simplification of the plant–soil system, this approach was sufficient to provide an accurate prediction of the vertically integrated soil moisture on both investigated plots. The formulation, which's set up is exhibited in this article, it then used to assess changes in the water balance, caused by increasing temperatures.

Climate change might affect Central European forests in multiple ways. Along with the rise in temperature, the sites will face the effects of changing precipitation patterns, rising atmospheric CO_2 concentration, and the change of frequency, duration and intensity of extreme weather events. On the biotic side, the increased occurrence of pathogens will put even more pressure on forest ecosystems. In this work, the focus lies solely on the effect of rising temperatures of the stands' water balance. The result of the simulation leads to the suggestion of mitigating measures.

To decrease the impact of drought on the forest stand, (Bolte et al., 2007) point out the importance of a deliberate water resource management. They claim, that reduction in the shelterwood (i) decreases the overall water consumption of the stand and the (ii) drought risk of overtopped trees. This modeling work points out the opposite: A reduction of leaf area might lead to reduced water consumption by stand transpiration. On the other hand, unproductive soil evaporation is promoted by the increased aeration and light availability at the forest ground. At soil moisture approaching the wilting point, trees respond by actively shutting down transpiration. Only soil evaporation is capable to cause a noteworthy soil water depletion at soil moisture levels close to the wilting point, inducing severe drought. A dense canopy cover might help to counteract this, by suppressing evaporative fluxes from the soil. In that context, the strict differentiation between moderate soil water deficit and severe soil drought seems reasonable. Soil water deficit during the growing season seems to be a very common state on the investigated sites. It is clearly represented through the simulations that trees decrease their productivity during periods of water stress, but overall, they seem sufficiently adapted to such conditions. Only a strong increase in the frequency of moderate soil water stress might induce a shift in the composition towards species, with higher tolerance to soil water deficit. Severe drought on the other hand, might actively lead to severe damage of the stand (compare Barigah et al., 2013), resulting in more abrupt, or even catastrophic, changes in the appearance of the forest.

4.3 Sulfur Biogeochemistry

The final target of this thesis was the description of the forest stands' sulfur biogeochemistry. Here, the objective lies less in the long-term perspective of acidification recovery of forest soils. The primary interest lies in finding a mathematical description of the forest plant-soil system, capable to reproduce observed temporal patterns of the SO_4-S in soil solution, on plot scale. Furthermore, I try to assign high-frequency fluctuations in the soil solution, observed on plot scale, to actual biogeochemical processes in the soil. After that, I venture a very cautious prognosis of the future development of the plant-soil systems' S budget on the investigated forest stands.

Microbial S transformations are identified as important driver of the short-term dynamics in the soil solution. Yet on the long run, the mineralization of plant originated soil organic S is responsible for the present input output imbalance. A large pool of historically accumulated organosulfur, which is decaying only very slowly, leads to an output excess for decades or even centuries. Pre-industrial conditions in the stream discharge are not reached over the entire model timeframe. Besides that, occult deposition still contributes considerably to the supply of S to the forest.

For each plot, one set of parameters is delivered, which yields the best calibration result. I am aware, that many different parameter configurations might lead to similar or even better outcomes. Nevertheless, the fact, that it is even possible to find an adequate parameter set for each forest plot, indicates that the current knowledge about forest soil S dynamics might be sufficient to describe the stands' dynamics to a satisfactory degree. At least in the short period that was monitored no unexplainable artefacts remain, requiring fundamental reconsideration of the assumptions about the workings of soil S dynamics. At this point, it seems like all essential processes are covered, necessary to illustrate a comprehensive picture of the stands' current S cycling.

5 Literature

Alewell, C., 2001. Predicting reversibility of acidification: the European sulfur story. Water, Air, and Soil Pollution, 130: 1271-1276.

Alewell, C. et al., 2001. Are there signs of acidification reversal in freshwaters of the low mountain ranges in Germany? Hydrology and Earth System Sciences, 5: 367-378.

Allen, R.G., Pereira, L.S., Raes, D. and Smith, M., 1998. Crop evapotranspiration-Guidelines for computing crop water requirements-FAO Irrigation and drainage paper 56. FAO, Rome, 300: 6541.

Auer, I., Böhm, R. and Mohnl, H., 1989. Klima von Wien: eine anwendungsorientierte Klimatographie. Beiträge zur Stadtforschung, Stadtentwicklung und Stadtgestaltung. Stadt Wien, Magistratsabteilung 18 - Stadtentwicklung und Stadtplanung, Vienna.

Aulakh, M.S., Jaggi, R.C. and Sharma, R., 2002. Mineralization-immobilization of soil organic S and oxidation of elemental S in subtropical soils under flooded and nonflooded conditions. Biology and fertility of soils, 35: 197-203.

Bailey, A.S., Hornbeck, J.W., Campbell, J.L. and Eagar, C., 2003. Hydrometeorological database for Hubbard Brook Experimental Forest: 1955-2000, 305. US Department of Agriculture, Forest Service, Northeastern Research Station.

Balisky, A.C. and Burton, P.J., 1993. Distinction of soil thermal regimes under various experimental vegetation covers. Canadian journal of soil science, 73: 411-420.

Barigah, T.S. et al., 2013. Water stress-induced xylem hydraulic failure is a causal factor of tree mortality in beech and poplar. Ann Bot-London, 112: 1431-1437.

Basler, D. and Körner, C., 2012. Photoperiod sensitivity of bud burst in 14 temperate forest tree species. Agr Forest Meteorol, 165: 73-81.

Bastiaanssen, W.G.M., Cheema, M.J.M., Immerzeel, W.W., Miltenburg, I.J. and Pelgrum, H., 2012. Surface energy balance and actual evapotranspiration of the transboundary Indus Basin estimated from satellite measurements and the ETLook model. Water Resour Res, 48: W11512.

Baudena, M. et al., 2012. Soil water dynamics at a midlatitude test site: Field measurements and box modeling approaches. J Hydrol, 414: 329-340.

Beltrami, H., 2001. On the relationship between ground temperature histories and meteorological records: a report on the Pomquet station. Global Planet Change, 29(3-4): 327-348.

Berbeco, M.R., Melillo, J.M. and Orians, C.M., 2012. Soil warming accelerates decomposition of fine woody debris. Plant Soil, 356(1-2): 405-417.

Berger, T.W. and Muras, A., 2016. Predicting recovery from acid rain using the micro-spatial heterogeneity of soil columns downhill the infiltration zone of beech stemflow: introduction of a hypothesis. Modeling earth systems and environment, 2(3): 154.

Berger, T.W., Untersteiner, H., Schume, H. and Jost, G., 2008. Throughfall fluxes in a secondary spruce (Picea abies), a beech (Fagus sylvatica) and a mixed spruce–beech stand. Forest Ecol Manag, 255(3): 605-618.

Berger, T.W., Untersteiner, H., Toplitzer, M. and Neubauer, C., 2009. Nutrient fluxes in pure and mixed stands of spruce (Picea abies) and beech (Fagus sylvatica). Plant and soil, 322: 317-342.

Bergh, J. et al., 2003. Modelling the short-term effects of climate change on the productivity of selected tree species in Nordic countries. Forest Ecol Manag, 183(1): 327-340.

Bergman, T.L., Incropera, F.P. and Lavine, A.S., 2011. Fundamentals of heat and mass transfer. John Wiley & Sons.

Betts, A.K., Ball, J.H. and McCaughey, J.H., 2001. Near-surface climate in the boreal forest. Journal of Geophysical Research-Atmospheres, 106: 33529-33541.

Bilgili, M., Sahin, B. and Sangun, L., 2013. Estimating soil temperature using neighboring station data via multi-nonlinear regression and artificial neural network models. Environmental Monitoring and Assessment, 185: 347-358.

Blümel, K. and Chmielewski, F.M., 2012. Shortcomings of classical phenological forcing models and a way to overcome them. Agr Forest Meteorol, 164: 10-19.

Bohn, U. et al., 2004. Map of the Natural Vegetation of Europe. Federal Agency for Nature Conservation, Bonn, Germany.

Bolte, A. et al., 2009. Adaptive forest management in central Europe: climate change impacts, strategies and integrative concept. Scandinavian Journal of Forest Research, 24: 473-482.

Bolte, A., Czajkowski, T. and Kompa, T., 2007. The north-eastern distribution range of European beech—a review. Forestry, 80(4): 413-429.

Bond-Lamberty, B., Wang, C.K. and Gower, S.T., 2005. Spatiotemporal measurement and modeling of stand-level boreal forest soil temperatures. Agricultural and Forest Meteorology, 131: 27-40.

Boose, E., 2001. Fisher meteorological station (since 2001), Harvard Forest Data Archive: HF001.

Brown, S.E., Pregitzer, K.S., Reed, D.D. and Burton, A.J., 2000. Predicting daily mean soil temperature from daily mean air temperature in four northern hardwood forest stands. Forest Science, 46: 297-301.

Bréda, N., Huc, R., Granier, A. and Dreyer, E., 2006. Temperate forest trees and stands under severe drought: a review of ecophysiological responses, adaptation processes and long-term consequences. Ann Forest Sci, 63(6): 625-644.

Buchner, P., Takahashi, H. and Hawkesford, M.J., 2004. Plant sulphate transporters: co-ordination of uptake, intracellular and long-distance transport. Journal of Experimental Botany, 55: 1765-1773.

Butler, S.M. et al., 2012. Soil warming alters nitrogen cycling in a New England forest: implications for ecosystem function and structure. Oecologia, 168(3): 819-828.

Caffarra, A. and Donnelly, A., 2011. The ecological significance of phenology in four different tree species: effects of light and temperature on bud burst. Int J Biometeorol, 55(5): 711-721.

Campbell, J.L. et al., 2010. Past and projected future changes in snowpack and soil frost at the Hubbard Brook Experimental Forest, New Hampshire, USA. Hydrol Process, 24(17): 2465-2480.

Cannell, M. and Smith, R., 1983. Thermal time, chill days and prediction of budburst in Picea sitchensis. J Appl Ecol: 951-963.

Capdevielle-Vargas, R., Estrella, N. and Menzel, A., 2015. Multiple-year assessment of phenological plasticity within a beech (Fagus sylvatica L.) stand in southern Germany. Agr Forest Meteorol, 211: 13-22.

Changnon, S.A., Angel, J.R., Kunkel, K.E. and Lehmann, C.M., 2008. Illinois Climate Atlas. Illinois State Water Survey, Prairie Research Institute of the University of Illinois, Urbana-Champaign, Illinois.

Chowdhury, M.A.H., Kouno, K. and Ando, T., 1999. Correlation among microbial biomass S, soil properties, and other biomass nutrients. Soil science and plant nutrition, 45: 175-186.

Ciais, P. et al., 2005. Europe-wide reduction in primary productivity caused by the heat and drought in 2003. Nature, 437: 529-533.

Clausnitzer, F., Köstner, B., Schwärzel, K. and Bernhofer, C., 2011. Relationships between canopy transpiration, atmospheric conditions and soil water availability—Analyses of long-term sap-flow measurements in an old Norway spruce forest at the Ore Mountains/Germany. Agr Forest Meteorol, 151(8): 1023-1034.

Cosby, B.J., Ferrier, R.C., Jenkins, A. and Wright, R.F., 2001. Modelling the effects of acid deposition: refinements, adjustments and inclusion of nitrogen dynamics in the MAGIC model. Hydrology and Earth System Sciences Discussions, 5: 499-518.

Davidson, E.A., Janssens, I.A. and Luo, Y.Q., 2006. On the variability of respiration in terrestrial ecosystems: moving beyond Q(10). Glob Chang Biol, 12: 154-164.

Dittmar, C., Zech, W. and Elling, W., 2003. Growth variations of common beech (Fagus Sylvatica L) under different climatic and environmental conditions in Europe – a dendroecological study. Forest Ecology and Management, 173: 63-78.

Duran, J. et al., 2014. Winter climate change affects growing-season soil microbial biomass and activity in northern hardwood forests. Global change biology, 20(11): 3568-3577.

Eea, 2015. Global and European temperatures.

Ellenberg, H. and Leuschner, C., 1996. Vegetation Mitteleuropas mit den Alpen. Ulmer, Stuttgart, Germany.

Estrella, N. and Menzel, A., 2006. Responses of leaf colouring in four deciduous tree species to climate and weather in Germany. Clim Res, 32(3): 253–267.

Farr, T.G. and Kobrick, M., 2000. Shuttle Radar Topography Mission produces a wealth of data. Eos Trans. AGU, 81: 583-583.

Federer, C., 1995. BROOK90: a simulation model for evaporation, soil water and streamflow. USDA Forest Service, Durham NH.

Feiccabrino, J. and Lundberg, A., 2008. Precipitation phase discrimination in Sweden. In: J. Pomeroy (Editor), 65th Eastern Snow Conference, Fairlee (Lake Morey), Vermont, USA, pp. 239-254.

Field, C.B. et al., 2014. IPCC, Summary for policymakers. Climate change 2014: impacts, adaptation, and vulnerability. Part A: global and sectoral aspects. Contribution of Working Group II to the Fifth Assessment Report of the Intergovernmental Panel on Climate Change: 1-32.

Fowler, D., Cape, J.N. and Unsworth, M.H., 1989. Deposition of atmospheric pollutants on forests. Philosophical Transactions of the Royal Society of London. B, Biological Sciences, 324(1223): 247-265.

Fu, Y.S.H., Campioli, M., Van Oijen, M., Deckmyn, G. and Janssens, I.A., 2012. Bayesian comparison of six different temperature-based budburst models for four temperate tree species. Ecol Model, 230: 92-100.

Gbondo-Tugbawa, S.S., Driscoll, C.T., Aber, J.D. and Likens, G.E., 2001. Evaluation of an integrated biogeochemical model (PnET-BGC) at a northern hardwood forest ecosystem. Water Resources Research, 37: 1057-1070.

Gehrig-Fasel, J., Guisan, A. and Zimmermann, N.E., 2008. Evaluating thermal treeline indicators based on air and soil temperature using an air-to-soil temperature transfer model. Ecological Modelling, 213: 345-355.

Gerrits, A., Pfister, L. and Savenije, H., 2010. Spatial and temporal variability of canopy and forest floor interception in a beech forest. Hydrol Process, 24(21): 3011-3025.

Geßler, A. et al., 2007. Potential risks for European beech (Fagus sylvatica L.) in a changing climate. Trees, 21: 1-11.

Ghani, A., McLaren, R.G. and Swift, R.S., 1993. The incorporation and transformations of 35 S in soil: effects of soil conditioning and glucose or sulphate additions. Soil Biology and Biochemistry, 25: 327-335.

Granier, A., Bréda, N., Biron, P. and Villette, S., 1999. A lumped water balance model to evaluate duration and intensity of drought constraints in forest stands. Ecol Model, 116(2): 269-283.

Gunderson, C.A. et al., 2012. Forest phenology and a warmer climate–growing season extension in relation to climatic provenance. Global change biology, 18(6): 2008-2025.

Hanousek, O. , Prohaska, T., Kulhanek, M., Balik, J., Tejnecky, V., Berger, T.W., 2017. Fractionation of sulfur (S) in beech (Fagus sylvatica) forest soils in relation to distance from the stem base as useful tool for modeling S biogeochemistry. Modeling earth systems and environment, 3: 1065-1079.

Havlin, J.L., Beaton, J.D. and Tisdale, S.L., 2005. Soil fertility and fertilizers an introduction to nutrient management. Pearson. New Jersey. US, Prentice Hall, Upper Saddle River.

Herbst, M., Rosier, P.T., McNeil, D.D., Harding, R.J. and Gowing, D.J., 2008. Seasonal variability of interception evaporation from the canopy of a mixed deciduous forest. Agr Forest Meteorol, 148(11): 1655-1667.

Herschbach, C. and Rennenberg, H., 2001. Sulfur nutrition of deciduous trees. Naturwissenschaften, 88(1): 25-36.

Hock, R., 2003. Temperature index melt modelling in mountain areas. J Hydrol, 282(1-4): 104-115.

Hollinger, S.E., Reineke, B.C. and Peppler, R.A., 1994. Illinois Climate Network: Site Descriptions, Instrumentation, and Data Management, 178. Illinois State Water Survey.

Hu, Q. and Feng, S., 2003. A daily soil temperature dataset and soil temperature climatology of the contiguous United States. Journal of Applied Meteorology, 42: 1139-1156.

Häkkinen, R., Linkosalo, T. and Hari, P., 1995. Methods for combining phenological time series: application to bud burst in birch (Betula pendula) in Central Finland for the period 1896–1955. Tree Physiol, 15(11): 721-726.

IUSS Working Group, W., 2006. World reference base for soil resources. World Soil Resources Report, 103.

Janzen, H.H. and Bettany, J.R., 1987. The effect of temperature and water potential on sulfur oxidation in soils. Soil science, 144: 81-89.

Kang, S., Kim, S., Oh, S. and Lee, D., 2000. Predicting spatial and temporal patterns of soil temperature based on topography, surface cover and air temperature. Forest Ecology and Management, 136: 173-184.

Katterer, T. and Andren, O., 2009. Predicting daily soil temperature profiles in arable soils in cold temperate regions from air temperature and leaf area index. Acta Agriculturae Scandinavica Section B-Soil and Plant Science, 59: 77-86.

Kertesz, M.A. and Mirleau, P., 2004. The role of soil microbes in plant sulphur nutrition. Journal of Experimental Botany, 55: 1939-1945.

Kim, S. and Singh, V.P., 2014. Modeling daily soil temperature using data-driven models and spatial distribution. Theoretical and Applied Climatology, 118: 465-479.

Kirkpatrick, S., 1984. Optimization by Simulated Annealing - Quantitative Studies. J Stat Phys, 34(5-6): 975-986.

Kirkpatrick, S., Gelatt, C.D. and Vecchi, M.P., 1983. Optimization by Simulated Annealing. Science, 220(4598): 671-680.

Kisi, O., Tombul, M. and Kermani, M.Z., 2015. Modeling soil temperatures at different depths by using three different neural computing techniques. Theoretical and Applied Climatology, 121: 377-387.

Klemm, O. and Wrzesinsky, T., 2007. Fog deposition fluxes of water and ions to a mountainous site in Central Europe. Tellus Series B-Chemical and Physical Meteorology, 59: 705-714.

Kljun, N. et al., 2007. Response of net ecosystem productivity of three boreal forest stands to drought. Ecosystems, 10: 1039-1055.

Kreuzwieser, J. and Rennenberg, H., 1998. Sulphate uptake and xylem loading of mycorrhizal beech roots. New Phytol, 140(2): 319-329.

Kulhánek, M., Černý, J., Balík, J., Vaněk, V. and Sedlář, O., 2011. Influence of the nitrogen-sulfur fertilizing on the content of different sulfur fractions in soil. Plant, Soil and Environment, 57(12): 553-558.

Kumagai, T., Yoshifuji, N., Tanaka, N., Suzuki, M. and Kume, T., 2009. Comparison of soil moisture dynamics between a tropical rain forest and a tropical seasonal forest in Southeast Asia: Impact of seasonal and year-to-year variations in rainfall. Water Resour Res, 45: W04413.

Kunstmann, H., Schneider, K., Forkel, R. and Knoche, R., 2004. Impact analysis of climate change for an Alpine catchment using high resolution dynamic downscaling of ECHAM4 time slices. Hydrology and Earth System Sciences Discussions, 8: 1031-1045.

Kölling, C., Zimmermann, L. and Walentowski, H., 2007. Klimawandel: was geschieht mit Buche und Fichte. AFZ-DerWald, 11: 584-588.

Körner, C. and Basler, D., 2010. Phenology Under Global Warming. Science, 327(5972): 1461-1462.

Körner, C. and Paulsen, J., 2004. A world-wide study of high altitude treeline temperatures. Journal of Biogeography, 31: 713-732.

Laio, F., Porporato, A., Ridolfi, L. and Rodriguez-Iturbe, I., 2001. Plants in water-controlled ecosystems: active role in hydrologic processes and response to water stress - II. Probabilistic soil moisture dynamics. Adv Water Resour, 24(7): 707-723.

Lange, C.A., Matschullat, J., Zimmermann, F., Sterzik, G. and Wienhaus, O., 2003. Fog frequency and chemical composition of fog water—a relevant contribution to atmospheric deposition in the eastern Erzgebirge, Germany. Atmospheric Environment, 37(26): 3731-3739.

Laube, J. et al., 2014. Chilling outweighs photoperiod in preventing precocious spring development. Global change biology, 20(1): 170-182.

Lei, S.G., Daniels, J.L., Bian, Z.F. and Wainaina, N., 2011. Improved soil temperature modeling. Environmental Earth Sciences, 62: 1123-1130.

Likens, G.E. et al., 2002. The biogeochemistry of sulfur at Hubbard Brook. Biogeochemistry, 60: 235-316.

Lindner, M. et al., 2010. Climate change impacts, adaptive capacity, and vulnerability of European forest ecosystems. Forest Ecology and Management, 259: 698-709.

Macdonald, N.W., Zak, D.R. and Pregitzer, K.S., 1995. Temperature Effects on Kinetics of Microbial Respiration and Net Nitrogen and Sulfur Mineralization. Soil Science Society of America Journal, 59: 233-240.

Mayer, H., Holst, T., Brugger, U. and Kirchassner, A., 2005. Trends of the forest significant climate variables air temperature and precipitation in south-west Germany from 1950 to 2000. Allgemeine Forst und Jagdzeitung, 176: 45-56.

McGill, W. and Cole, C., 1981. Comparative aspects of cycling of organic C, N, S and P through soil organic matter. Geoderma, 26(4): 267-286.

Melillo, J., Steudler, P. and Mohan, J., 1999. Prospect Hill Soil Warming Experiment at Harvard Forest since 1991, Harvard Forest Data Archive: HF005.

Melillo, J., Steudler, P. and Mohan, J., 2003. Barre Woods Soil Warming Experiment at Harvard Forest since 2001, Harvard Forest Data Archive: HF018.

Melillo, J.M. et al., 2002. Soil warming and carbon-cycle feedbacks to the climate system. Science, 298(5601): 2173-2176.

Menne, M.J. et al., 2012a. Global Historical Climatology Network - Daily (GHCN-Daily), Version 3, NOAA National Climatic Data Center.

Menne, M.J., Durre, I., Vose, R.S., Gleason, B.E. and Houston, T.G., 2012b. An Overview of the Global Historical Climatology Network-Daily Database. J Atmos Ocean Tech, 29(7): 897-910.

Menzel, A. et al., 2008. Bayesian analysis of the species-specific lengthening of the growing season in two European countries and the influence of an insect pest. Int J Biometeorol, 52(3): 209-218.

Mitchell, M.J. and Likens, G.E., 2011. Watershed sulfur biogeochemistry: shift from atmospheric deposition dominance to climatic regulation. Environmental science & technology, 45(12): 5267-5271.

Mitchell, M.J. et al., 2001. Use of stable isotope ratios for evaluating sulfur sources and losses at the Hubbard Brook Experimental Forest. Water, Air, and Soil Pollution, 130(1-4): 75-86.

Moyano, F.E. et al., 2012. The moisture response of soil heterotrophic respiration: interaction with soil properties. Biogeosciences, 9: 1173-1182.

Mucina, L., Grabherr, G. and Ellmauer, T., 1993. Die Pflanzengesellschaften Österreichs. Teil 3: Wälder und Gebüsche. Gustav-Fischer, Jena, Stuttgart, New York, 353 pp.

Munger, W. and Wofsy, S., 1999. Canopy-Atmosphere Exchange of Carbon, Water and Energy at Harvard Forest EMS Tower since 1991, Harvard Forest Data Archive: HF004.

Nash, J.E. and Sutcliffe, J.V., 1970. River flow forecasting through conceptual models part I - A discussion of principles. J Hydrol, 10(3): 282-290.

Neumann, M. et al., 2001. Waldzustandsmonitoring in Österreich: Ergebnisse der Intensivbeobachtungsflächen (Level II). Forstliche Bundesversuchsanstalt Wien.

Novák, M. et al., 2000. Sulfur isotope dynamics in two Central European watersheds affected by high atmospheric deposition of SO x. Geochimica et Cosmochimica Acta, 64: 367-383.

Pannatier, E.G., Thimonier, A., Schmitt, M., Walthert, L. and Waldner, P., 2011. A decade of monitoring at Swiss Long-Term Forest Ecosystem Research (LWF) sites: can we observe trends in atmospheric acid deposition and in soil solution acidity? Environmental Monitoring and Assessment, 174: 3-30.

Paul, K.I. et al., 2004. Soil temperature under forests: a simple model for predicting soil temperature under a range of forest types. Agricultural and Forest Meteorology, 121: 167-182.

Pearce, A.J. and Rowe, L.K., 1981. Rainfall interception in a multi-storied, evergreen mixed forest: estimates using Gash's analytical model. J Hydrol, 49(3-4): 341-353.

Peck, A. and Mayer, H., 1996. Einfluss von Bestandesparametern auf die Verdunstung von Wäldern. Forstwissenschaftliches Centralblatt vereinigt mit Tharandter forstliches Jahrbuch, 115(1): 1-9.

Prechtel, A. et al., 2001. Response of sulphur dynamics in European catchments to decreasing sulphate deposition. Hydrology and Earth System Sciences, 5: 311-325.

Prechtel, A., Armbruster, M. and Matzner, E., 2003. Modelling sulphate stream concentrations in the Black Forest catchments Schluchsee and Villingen. Hydrology and Earth System Sciences Discussions, European Geosciences Union, 7(4): 552-560.

Rango, A. and Martinec, J., 1995. Revisiting the degree-day method for snowmelt computations. JAWRA Journal of the American Water Resources Association, 31(4): 657-669.

Rankinen, K., Karvonen, T. and Butterfield, D., 2004. A simple model for predicting soil temperature in snow-covered and seasonally frozen soil: model description and testing. Hydrology and Earth System Sciences, 8: 706-716.

Rennenberg, H., Brunold, C., De Kok, L. and Stulen, I., 1990. Sulfur Nutrition and Sulfur Assimilation in Higher Plants. SPB Academic Publishing, The Hague.

Rennenberg, H., Seiler, W., Matyssek, R., Gessler, A. and Kreuzwieser, J., 2004. Die Buche (Fagus sylvatica L.)–ein Waldbaum ohne Zukunft im südlichen Mitteleuropa. Allgemeine Forst-und Jagdzeitung, 175: 210-224.

Richardson, A.D. et al., 2013. Climate change, phenology, and phenological control of vegetation feedbacks to the climate system. Agricultural and Forest Meteorology, 169: 156-173.

Schaber, J. and Badeck, F.-W., 2002. Evaluation of methods for the combination of phenological time series and outlier detection. Tree Physiol, 22(14): 973-982.

Scherer, H.W., 2009. Sulfur in soils. Journal of Plant Nutrition and Soil Science, 172: 326-335.

Schmid, I., 2002. The influence of soil type and interspecific competition on the fine root system of Norway spruce and European beech. Basic and Applied Ecology, 3(4): 339-346.

Schume, H., Jost, G. and Hager, H., 2004. Soil water depletion and recharge patterns in mixed and pure forest stands of European beech and Norway spruce. J Hydrol, 289(1): 258-274.

Schume, H., Jost, G. and Katzensteiner, K., 2003. Spatio-temporal analysis of the soil water content in a mixed Norway spruce (Picea abies (L.) Karst.) - European beech (Fagus sylvatica L.) stand. Geoderma, 112(3-4): 273-287.

Schwärzel, K. et al., 2009. A novel approach in model-based mapping of soil water conditions at forest sites. Forest Ecol Manag, 258(10): 2163-2174.

Schöpp, W., Posch, M., Mylona, S. and Johansson, M., 2003. Long-term development of acid deposition (1880-2030) in sensitive freshwater regions in Europe. Hydrology and Earth System Sciences Discussions, 7(4): 436-446.

Sierra, C.A., Trumbore, S.E., Davidson, E.A., Vicca, S. and Janssens, I., 2015. Sensitivity of decomposition rates of soil organic matter with respect to simultaneous changes in temperature and moisture. Journal of Advances in Modeling Earth Systems, 7: 335-356.

Slinn, W.G.N., 1982. Predictions for Particle Deposition to Vegetative Canopies. Atmos Environ, 16(7): 1785-1794.

Solberg, E.D., Malhi, S.S., Nyborg, M. and Gill, K.S., 2005. Temperature, Soil Moisture, and Antecedent Sulfur Application Effects on Recovery of Elemental Sulfur as SO4-S in Incubated Soils. Communications in soil science and plant analysis, 36: 863-874.

Sutmöller, J., Spellmann, H., Fiebiger, C. and Albert, M., 2008. Der Klimawandel und seine Auswirkungen auf die Buchenwälder in Deutschland The effects of climate change on beech forests in Germany. Ergebnisse angewandter Forschung zur Buche, 3: 135-158.

Svensson, M. et al., 2008. Bayesian calibration of a model describing carbon, water and heat fluxes for a Swedish boreal forest stand. Ecological Modelling, 213: 331-344.

Sverdrup, H., Belyazid, S., Nihlgård, B. and Ericson, L., 2007. Modelling change in ground vegetation response to acid and nitrogen pollution, climate change and forest management at in Sweden 1500–2100 AD. Water, Air, & Soil Pollution: Focus, 7(1-3): 163-179.

Swift, L.W., 1976. Algorithm for Solar-Radiation on Mountain Slopes. Water Resour Res, 12(1): 108-112.

Tabatabai, M.A., 1996. Sulfur. Methods of Soil Analysis Part 3. Chemical Methods. Soil Science Society of America, American Society of Agronomy, Madison.

Talaee, P.H., 2014. Daily soil temperature modeling using neuro-fuzzy approach. Theoretical and Applied Climatology, 118: 481-489.

Tang, J. et al., 2006. Sap flux–upscaled canopy transpiration, stomatal conductance, and water use efficiency in an old growth forest in the Great Lakes region of the United States. Journal of Geophysical Research: Biogeosciences, 111(G2).

Tank, A.M.G.K. et al., 2002. Daily dataset of 20th-century surface air temperature and precipitation series for the European Climate Assessment. Int J Climatol, 22(12): 1441-1453.

Theurillat, J.-P. and Guisan, A., 2001. Potential impact of climate change on vegetation in the European Alps: a review. Climatic change, 50: 77-109.

Umweltbundesamt, 2018. Emissionstrends 1990-2016: Ein Überblick über die Verursacher von Luftschadstoffen in Österreich, Umweltbundesamt GmbH, Vienna.

van Dijk, A.I.J.M. and Bruijnzeel, L.A., 2001. Modelling rainfall interception by vegetation of variable density using an adapted analytical model. Part 1. Model description. J Hydrol, 247(3-4): 230-238.

van Wijk, M.T. and Williams, M., 2005. Optical instruments for measuring leaf area index in low vegetation: Application in Arctic ecosystems. Ecological Applications, 15: 1462-1470.

Vilhar, U., 2016. Comparison of drought stress indices in beech forests: a modelling study. Iforest: e1-e8.

Vitasse, Y. and Basler, D., 2013. What role for photoperiod in the bud burst phenology of European beech. Eur J Forest Res, 132(1): 1-8.

Vitasse, Y., Porte, A.J., Kremer, A., Michalet, R. and Delzon, S., 2009. Responses of canopy duration to temperature changes in four temperate tree species: relative contributions of spring and autumn leaf phenology. Oecologia, 161(1): 187-198.

Viterbo, P., Beljaars, A., Mahfouf, J.F. and Teixeira, J., 1999. The representation of soil moisture freezing and its impact on the stable boundary layer. Quarterly Journal of the Royal Meteorological Society, 125: 2401-2426.

Wagle, P. and Kakani, V.G., 2014. Confounding Effects of Soil Moisture on the Relationship Between Ecosystem Respiration and Soil Temperature in Switchgrass. Bioenergy Research, 7: 789-798.

Watmough, S.A. et al., 2005. Sulphate, nitrogen and base cation budgets at 21 forested catchments in Canada, the United States and Europe. Environmental monitoring and assessment, 109(1-3): 1-36.

Willen, D., Shumway, C. and Reid, J., 1971. Simulation of daily snow water equivalent and melt. Proceedings 1971 Western Snow Conference, 39: 1-8.

Zhang, Y., Mitchell, M.J., Christ, M., Likens, G.E. and Krouse, H.R., 1998. Stable sulfur isotopic biogeochemistry of the Hubbard Brook experimental forest, New Hampshire. Biogeochemistry, 41(3): 259-275.

Zheng, D., Hunt Jr, E.R. and Running, S.W., 1993. A daily soil temperature model based on air temperature and precipitation for continental applications. Climate Research, 2: 183-191.

6 Tables

7 Figures

8 Appendix

To achieve sigmoid shape transitions of a variables (x) response (y) inside a window (x_0 to x_1), the *smoothstep function* was applied in several cases. y_0 and y_1 state left and right threshold responses respectively. The variable x has to be normalized into an auxiliary variable (t) inside the interval 0 to 1.

$$t = \frac{x - x_0}{x_1 - x_0} \tag{A1.}$$

The transition is described using a third order polynomial.

$$y = \begin{cases} y_0, & x \leq x_0 \\ y_0 + (y_1 - y_0)(3t^2 - 2t^3), & x_0 < x < x_1 \\ y_1, & x \geq x_1 \end{cases} \tag{A2.}$$

In the article the *smoothstep function* is stated as:

$$y = smooth(x, x_0, x_1, y_0, y_1) \tag{A3.}$$

To alter the shape of the transition, the latter function was modified, by introducing an exponent term.

$$y = \begin{cases} y_0, & x \leq x_0 \\ y_0 + (y_1 - y_0)(3t^2 - 2t^3)^{\ln 0.5/\ln m}, & x_0 < x < x_1 \\ y_1, & x \geq x_1 \end{cases} \tag{A4.}$$

The parameter m states the relative x position between x_0 and x_1 where the response (y) reaches 50% of the transition from y_0 to y_1. In the article the *modified smoothstep function* is stated as:

$$y = msmooth(x, x_0, x_1, y_0, y_1, m) \tag{A5.}$$

The description of the air temperature dependent forcing of spring phenology uses a combination of a second and first order polynomial. The variable, which is being transformed, has to be normalized to the interval x_0 to x_1, using equation A1.

$$y = y_0 + (y_1 - y_0) \begin{cases} 0, & x \leq x_0 \\ t,^{2} & x_0 < x < x_1 \\ 2t - 1, & x \geq x_1 \end{cases} \tag{A6.}$$

In the paper, the function, which is optically resembling the shape of a hockey stick, is stated as:

$$y = hockey(x, x_0, x_1, y_0, y_1) \tag{A7.}$$

Precipitation interception is calculated using a function, based on the Langmuir sorption isotherm. I states interception, $C_{\max}$ the maximum charge of the canopy, K_i the shape parameter and T throughfall.

$$I = \frac{K_\mathrm{i} C_{\max} T}{1 + K_\mathrm{i} T} \tag{A8.}$$

Substituting Interception with the difference of precipitation (R) and throughfall yields:

$$R - T = \frac{K_\mathrm{i} C_{\max} T}{1 + K_\mathrm{i} T} \tag{A9.}$$

Avoiding the intricacies of an implicit formulation, the equation for throughfall is solved:

$$T = \frac{\sqrt{{K_\mathrm{i}}^2(C_\mathrm{max} - R)^2 + 2K_\mathrm{i}(C_\mathrm{max} + R) + 1} + K_\mathrm{i}(R - C_\mathrm{max}) - 1}{2K_\mathrm{i}} \qquad \text{(A10.)}$$

In the article this 3-argmuent function is stated as:

$$T = tru(R, C_\mathrm{max}, K_\mathrm{i}) \qquad \text{(A11.)}$$

9 List of Abbreviations

WBM	Water Balance Model
SDM	Sulfur Dynamics Model
S	Sulfur
KB	Kreisbach
KL	Klausen-Leopoldsdorf
EX	Exelberg
JU	Jubiläumswarte
HBEF	Hubbard Brook Experimental Forest
LU	Leaf unfolding
LC	Leaf coloring
DoY	Day of the Year (Julian Day)
NSE	Nash-Sutcliffe Efficiency
RMSE	Root Mean Squared Error
LWC	Liquid water content of the air
LWE	Liquid water equivalent (Snow)
ET	Evapotranspiration
REW	Relative extractable water
WUE	Water use efficiency
GPP	Gross primary production
VPD	Vapor pressure deficit

10 Publications

10.1 Ad Soil Temperature: *A new approach to predict soil temperature under vegetated surfaces*

https://link.springer.com/article/10.1007/s40808-015-0041-2

Model. Earth Syst. Environ. (2015) 1:32
DOI 10.1007/s40808-015-0041-2

ORIGINAL ARTICLE

A new approach to predict soil temperature under vegetated surfaces

Klaus Dolschak[1] · **Karl Gartner**[2] · **Torsten W. Berger**[1]

Received: 10 October 2015 / Accepted: 13 October 2015 / Published online: 29 October 2015

Abstract In this article, the setup and the application of an empirical model, based on Newton's law of cooling, capable to predict daily mean soil temperature (T_{soil}) under vegetated surfaces, is described. The only input variable, necessary to run the model, is a time series of daily mean air temperature. The simulator employs 9 empirical parameters, which were estimated by inverse modeling. The model, which primarily addresses forested sites, incorporates the effect of snow cover and soil freezing on soil temperature. The model was applied to several temperate forest sites, managing the split between Central Europe (Austria) and the United States (Harvard Forest, Massachusetts; Hubbard Brook, New Hampshire), aiming to cover a broad range of site characteristics. Investigated stands differ fundamentally in stand composition, elevation, exposition, annual mean temperature, precipitation regime, as well as in the duration of winter snow cover. At last, to explore the limits of the formulation, the simulator was applied to non-forest sites (Illinois), where soil temperature was recorded under short cut grass. The model was parameterized, specifically to site and measurement depth. After calibration of the model, an evaluation was performed, using $\sim$50 % of the available data. In each case, the simulator was capable to deliver a feasible prediction of soil temperature in the validation time interval. To evaluate the practical suitability of the simulator, the minimum amount of soil temperature point measurements, necessary to yield expedient model performance was determined. In the investigated case 13–20 point observations, uniformly distributed within an 11-year timeframe, have been proven sufficient to yield sound model performance (root mean square error <0.9 °C, Nash–Sutcliffe efficiency >0.97). This makes the model suitable for the application on sites, where the information on soil temperature is discontinuous or scarce.

Keywords Empirical model · Dynamical model · Newton's law of cooling · Forest soil temperature · Freeze/thaw transition · Simulated annealing

Introduction

Various biotic, as well as abiotic processes in the soil are temperature dependent (Rankinen et al. 2004). Usually, these dependencies are assumed to have a non-linear nature (Bond-Lamberty et al. 2005; Davidson et al. 2006; Macdonald et al. 1995; Wagle and Kakani 2014), meaning that the response of the process to changes of temperature, strongly depends on the temperature range it is occurring in. Especially for high temperatures, small changes in temperature might yield big changes in the processes response. For the assessment of temperature dependent soil processes, it is therefore crucial to have expedient knowledge about spatial, as well as temporal fluctuations of soil temperature (Bond-Lamberty et al. 2005). The most reliable source of information would be the permanent monitoring of subsurface ground temperature. But in practice it is often hard to measure continuously. Usually, the modeler has to deal with fragmentary timelines of soil temperature,

---

✉ Klaus Dolschak
klaus.dolschak@boku.ac.at

[1] Department of Forest- and Soil Sciences, Institute of Forest Ecology, University of Natural Resources and Live Sciences (BOKU), Peter Jordan-Straße 82, 1190 Vienna, Austria

[2] Department of Forest Ecology and Soil, Federal Research and Training Centre for Forests, Natural Hazards and Landscape, Seckendorff-Gudent-Weg 8, 1131 Vienna, Austria

scarce point observations or even no records of T_{soil} at all (Lei et al. 2011). To fill these gaps or to extend the timeline beyond the measurement timeframe, the researcher has to consider the application of a soil temperature model.

The approaches to predict subsurface ground temperature can be coarsely divided in 2 categories; (1) process based models, and (2) empirical models (Kang et al. 2000). Process based approaches to predict soil temperature generally use meteorological input variables (primarily temperature and solar radiation) to calculate energy balance of the soil surface, and heat transport in the soil, by solving the heat equation (Paul et al. 2004). The applicability of these models is often limited by their high complexity, high demand of input data, and specific model parameters, which are often not available for the investigated site (Lei et al. 2011; Svensson et al. 2008). Empirical models, presented in the work of Brown et al. (2000), Kang et al. (2000), or Paul et al. (2004), rely on the statistical relationship between meteorological parameters and soil temperature. More recently, there have been successful attempts to predict T_{soil} using combinations of artificial neural networks and fuzzy logic (Bilgili et al. 2013; Kim and Singh 2014; Kisi et al. 2015; Talaee 2014).

Soil thermal regimes are controlled by various environmental drivers. The most important meteorological factors are air temperature and radiation, laying the base for heat exchange at the soil surface (Hu and Feng 2003). In the latter, forested sites differ substantially from other types of land-cover: The radiation driven heat exchange between soil surface and atmosphere, is limited due to the shielding effect of the canopy (Paul et al. 2004). Therefore, forested sites show strongly dampened T_{soil} fluctuations, compared to sites with sparse vegetation or bare soil (Balisky and Burton 1993). Only a few models exist, which explicitly address the soil thermal conditions of forested ecosystems.

Zheng et al. (1993) set up a dynamical T_{soil} model based on Newton's law of cooling, assuming the change of T_{soil} proportional to the temperature difference between air and soil. The fact, that the vegetation cover limits radiation driven heat flux, is taken into account by utilizing a heat transfer coefficient, which depends on the stands leaf area. They assume, that the canopy's damping effect is more pronounced for incoming radiation, than for emission from the ground. This is incorporated, by applying different heat transfer coefficients, whether the soil is warming or cooling. The damping term, dependent on LAI, only comes into effect for soil warming conditions. Based on this work, Kang et al. (2000) set up a spatially resolved T_{soil} model. To describe the soil thermal regimes of South Korean forest sites, they extended the latter approach by introducing a more 'mechanistic' element, based on Fourier's law of heat transport. Besides the spatial and temporal variability of the leaf area, this approach also accounts for the effect of the stands litter layer on soil heat flux. The authors assumed, that T_{soil} does not fall below freezing for most Korean forest sites. As well as in the latter approach, T_{soil} estimates below 0 °C were replaced with 0 °C.

Brown et al. (2000), predicted daily mean T_{soil} of 4 different Northern Hardwood stands, utilizing a statistical relationship between T_{soil} and the average air temperature of the previous day. As a correction term, accounting for the phase shift or 'lagging behind' of the annual course of T_{soil} compared to air temperature, they introduced a cosine function of the Julian day. Despite the simple model structure, the predictions of T_{soil} were quite precise (disregarding the cold season).

To predict daily T_{soil} of various Australian forest sites, Paul et al. (2004) used daily average air temperature and stand parameters like leaf area, understory growth, and litter mass. They assumed T_{soil} oscillating around an annual mean soil temperature, which is calculated from annual mean air temperature, modified with a correction factor, derived from information about the stands' vegetation cover and litter layer. The resulting temperature wave is then offset by a term describing daily fluctuations of T_{soil}, which again, is derived from air temperature. The model specifically addresses the thermal conditions of the topsoil. Therefore, phase shift and attenuation of the temperature oscillation, which become relevant with increasing soil depth, were not considered.

Bond-Lamberty et al. (2005) examined the spatiotemporal dynamics of soil thermal regimes during stand development of a disturbed boreal forest. To accompany this investigation and for laying the base to simulate forest dynamics, they implemented an empirical T_{soil} model. Accounting for the influence of recent past air temperature conditions on present T_{soil}, they calculate running averages of the daily mean air temperature. T_{soil} is then calculated as a linear function of multiple running averages, centered to different days in the past. The authors report difficulties to predict T_{soil} close to the freeze/thaw transition.

To evaluate the suitability of T_{soil} as a predictor for the treeline position in the Swiss Alps, Gehrig-Fasel et al. (2008) presented an approach, which strongly differs from others described in this section. To satisfy the statistical requirements for regression modeling, the data was first detrended and then transformed for first differences. After performing the regression analysis, the data was transformed back. Considering that daily mean air temperature was the only input parameter, the model showed high performance in the validation timeframe. Assuming only an insignificant influence of winter soil temperatures on the treeline position (Körner and Paulsen 2004), the validation could be limited to the warm season.

Most approaches presented here disregard T_{soil} dynamics of the cold season. The decoupling of the soil from the atmosphere by a fluctuating snowpack (Betts et al. 2001), the heat transformation processes at the phase change from liquid to frozen (Beltrami 2001; Viterbo et al. 1999), or changes in heat capacity and conductivity seem difficult to be captured in the framework of an empirical approach. In cases where winter T_{soil} is assumed to reach or fall below 0 °C, process based approaches, presented by e.g. Rankinen et al. (2004), should be preferred. But, even though this model could be described 'simple' from a mechanistic point of view, solely the empirical snow accumulation/melt module, upstream to the T_{soil} model, requires the assignment of 11 free parameters. An alternative might be the semi-empirical model presented by Katterer and Andren (2009). Making the approach suitable for colder temperature conditions, the formulation presented by Kang et al. (2000) was modified. They interposed a surface temperature term, which acts as link between air and soil temperature. In this term the influence of air temperatures below 0 °C is attenuated by a constant factor. This way, they account for the low thermal conductivity of snow.

The objective of this article is the presentation of a model to predict soil temperature of forest stands, which aims to perform like a 'well-tuned' mechanistic simulator, using the straightforwardness of an empiric formulation. The model enables the transformation of fragmentary records of forest soil temperature, into a complete time series of T_{soil}, using average daily air temperature as only input. In this specific case, the created time series is laying the base for the modeling of temperature dependent, biogeochemical soil processes. Due to the fact that many biotic soil processes are sensitive to winter conditions (Campbell et al. 2005), emphasis is laid on an expedient representation of the temperature dynamics of the cold season.

Running the simulation requires the adjustment of nine empirical parameters, which are not defined in a strict physical sense. This is making it hard to deduce parameter values directly from site information. For a proper site specific parameterization, at least some snapshot measurements of T_{soil} are recommended. Therefore, this model primarily aims to sites were T_{soil} data is available, but the time series are inconsistent, or have to be extended beyond the timeframe of measurement.

Materials and methods

Model description

The model describes T_{soil} as a function of daily mean air temperature ($T_{air,t}$). It employs a daily time step. The formulation is based on Newton's law of cooling (Bergman et al. 2011), which is applied 2 times consecutively.

Utilizing a relatively small heat transfer coefficient (λ_{shift}), the first application of Newton's law provides a phase shifted temperature time series ($T_{shift,t}$) which lacks the high frequency fluctuations of $T_{air,t}$.

$$T_{shift,t} = T_{air,t} + \left(T_{shift,t-1} - T_{air,t}\right)\exp(-\lambda_{shift}) \quad (1)$$

A fictive environmental temperature ($T_{env,t}$) is postulated as the weighted mean of the elements $T_{air,t}$, $T_{shift,t}$, and a constant correction temperature (T_{corr}). pc_{air}, pc_{shift}, and pc_{corr} are partitioning coefficients, which define the relative weight of the specific element.

$$T_{env,t} = T_{air,t}pc_{air} + T_{shift,t}pc_{shift} + T_{corr}pc_{corr} \quad (2)$$

The partitioning coefficients sum up to 1, so 2 have to be defined as model parameters, one can be deduced.

$$pc_{corr} = 1 - (pc_{air} + pc_{shift}) \quad (3)$$

ΔT states the difference of the soil temperature to $T_{env,t}$.

$$\Delta T = T_{env,t} - T_{soil,t-1} \quad (4)$$

Taking into account the insulating effect of the snow cover and the heat release/consumption due to the phase change of soil water from liquid to solid and vice versa (Beltrami 2001), a variable heat transfer coefficient (λ_{eff}) is implemented (Fig. 1). λ_{max} represents the transfer coefficient above the upper threshold temperature (T_1). Below T_1 λ_{eff} gets reduced, reaching the minimum (λ_{min}) at the lower threshold (T_0), where different λ_{min} are applied for soil warming and cooling.

$$\lambda_{min} = \begin{cases} \lambda_{thaw}, & \Delta T > 0 \\ \lambda_{frost}, & \Delta T \le 0 \end{cases} \quad (5)$$

The transition of the transfer coefficient in betweenT_1 andT_0 is described, using a third order polynomial.

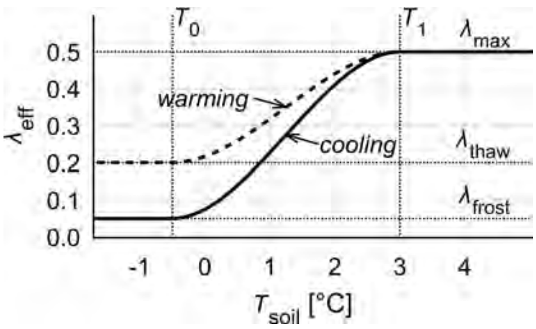

Fig. 1 Polynomial transition of the heat compensation coefficient (λ_{eff}), between 2 threshold soil temperatures (T_0, T_1), close to soil freezing. The reduction of the coefficient pays respect to the energy release/demand of phase changes, from liquid to solid and vice versa. High model performance was achieved, using different minimal compensation coefficients for soil cooling (λ_{frost}) (*solid line*) and warming (λ_{thaw}) (*dashed line*) respectively

$$\lambda_{\mathrm{eff}} = \begin{cases} \lambda_{\min}, & T_{\mathrm{soil},t-1} \leq T_0 \\ \lambda_{\min} + (\lambda_{\max} - \lambda_{\min})\,(3x^2 - 2x^3), & T_0 < T_{\mathrm{soil},t-1} < T_1 \\ \lambda_{\max}, & T_{\mathrm{soil},t-1} \geq T_1 \end{cases} \tag{6}$$

$T_{\mathrm{soil},t-1}$ has to be transformed into an auxiliary variable inside the interval 0–1.

$$x = \frac{T_{\mathrm{soil},t-1} - T_0}{T_1 - T_0} \tag{7}$$

At last, Newton's law is applied the 2nd time. The actual daily mean soil temperature calculates as:

$$T_{\mathrm{soil},t} = T_{\mathrm{env},t} - \Delta T \exp(-\lambda_{\mathrm{eff}}) \tag{8}$$

Study sites/input data

Austria

In the framework of the International Co-operative Programme on Assessment and Monitoring of Air Pollution Effects on Forests (ICP Forests), the Austrian Research Centre for Forests operates several, intensively monitored, forest sites (Level II) (Neumann et al. 2001). In addition to various other environmental parameters, meteorological conditions are monitored continuously. Soil temperature records exist for soil depths, ranging from 5 to 60 cm.

The model was originally set up on data from the Level II Plot Klausen-Leopoldsdorf, which is located in the Vienna Woods (48°07′16″N, 16°02′52″E), at an elevation of 510 m a. s. l. The research site is a pure beech (*Fagus sylvatica* L.) stand, which was planted in the late thirties of the last century. The location is facing NE with an inclination of 20 %. The actual forest vegetation coincides with the potential natural one, and can be classified as Hordylemo-Fagetum (Mucina et al. 1993).

Subsequently data from 5 other Level II forest stands were accessed (Fig. 2, Table 1). The selection aims to cover a broad range of site characteristics. Investigated sites show a strong altitudinal and climatic gradient. The elevation of the investigated stands ranges from 290 (Unterpullendorf) to 1540 m a.s.l. (Murau), leading to annual mean temperatures from 9.6 to 5 °C, respectively. Austria lies in the transition zone between oceanic and continental climate. Progressing from west to east, investigated locations therefore experience a strong decline in annual precipitation sums, ranging from 1521 mm for mountainous stands in the north-west, affected by orographic precipitation (Mondsee), to 630 mm in the continentally influenced east of the country (Unterpullendorf).

To fill gaps in the record of average daily air temperature, data were accessed, provided by the European Climate Assessment (ECA&D) (Tank et al. 2002). Missing values were replaced, using linear regression with available neighboring stations.

East Coast of the United States

Intending to test the models over regional validity, the continent was switched. Data were accessed from 2

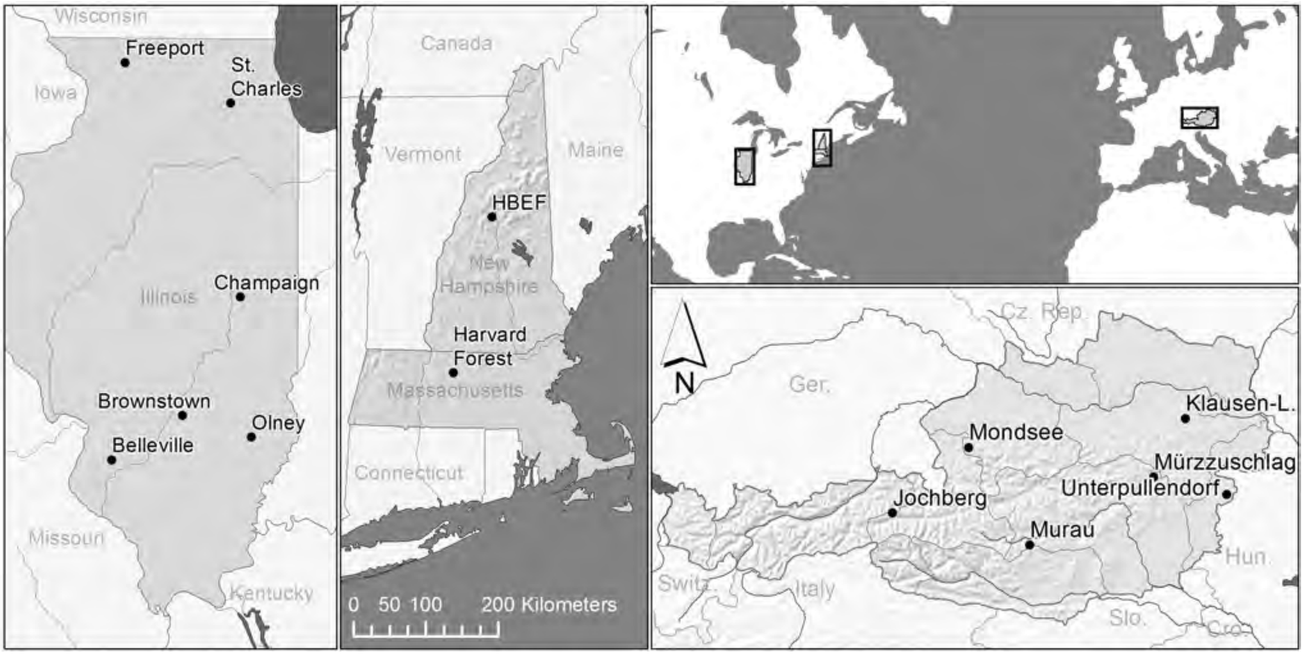

Fig. 2 Location of study sites in the United States and in Austria. The sites used for parameterization of the forest soil temperature simulator cover a broad range of characteristics. For a brief site description see Table 1

Table 1 Investigated locations cover a broad range of site characteristics and distinct climatic and altitudinal gradients

		Elevation (m a. s. l.)	Exp.	Slope (°)	MAT (°C)	MAP (mm)	Dominant species	Soil type
Level II	Jochberg	1050	NE	4	5.7	1358	*Picea abies*	Dystric Cambisol
	Mondsee	860	SE	14	~5.7	1521	*Picea abies*	Eutric Cambisol
	Murau	1540	N	33	5.0	918	*Picea abies*	Dystric Cambisol
	Mürzzuschlag	715	S	10	6.0	933	*Picea abies*	Eutric Cambisol
	Klausen-Leopoldsdorf	510	NE	11	8.2	804	*Fagus sylvatica*	Stagnic Cambisol
	Unterpullendorf	290	–	0	9.6	630	*Quercus petraea/cerris*	Planosol
HBEF	High Elevation Plots	560	N	~13	5.0	1400	*Betula alleghaniensis*	Podzol
	Low Elevation Plots	430	S	~11	6.1	1400	*Acer saccharum*	Podzol
Harvard Forest	Prospect Hill	365	–	0	8.5	1080	*Quercus rubra*	Dystric Cambisol
	Barre Woods	305	–	0	8.5	1080	*Quercus rubra/velutina*	Dystric Cambisol
ICN	Freeport	265	–	0	~9.1	~860	*Sod covered ground*	
	St. Charles	226	–	0	~9.3	~780	*Sod covered ground*	
	Champaign	219	–	0	~11.3	~1020	*Sod covered ground*	
	Belleville	133	–	0	~12.7	~960	*Sod covered ground*	
	Brownstown	177	–	0	~12.3	~960	*Sod covered ground*	
	Olney	134	–	0	~12.5	~1010	*Sod covered ground*	

MAT mean annual temperature, *MAP* mean annual precipitation sum

intensive long-term ecological research areas in New England; (1) the Hubbard Brook Experimental Forest (HBEF), and (2) Harvard Forest (Fig. 2, Table 1).

The HBEF is located in the White Mountain National Forest in north-central New Hampshire (43°56′N, 71°42′W). The elevation of the investigated watershed ranges from 250 m to 1000 m. The forest type can be classified as Northern Hardwood, dominated by Sugar maple (*Acer saccharum* Marsh). The climate is cool, continental, and humid, with mean annual precipitation sums around 1400 mm (Bailey et al. 2003). Approximately one-third of the precipitation is falling as snow, leading to a snowpack, typically lasting from December to April. Soils can be classified as well-drained Spodosols (WRB: Podzol), developed on glacial till (Campbell et al. 2010).

Daily T_{soil} (depth: 5 cm) data, recorded within the framework of the project 'Snow Depth & Soil Freezing as a Regulator of Microbial Processes' (Duran et al. 2014), were obtained. Data of 3 intensive high elevation plots (mean elevation: 560 m, exposition: North) and 3 intensive low elevation plots (mean elevation: 430 m, exposition: South) were used. For each altitude class, one mean time-series of T_{soil} was calculated.

Because of their proximity to the investigated stands, records of air temperature (Bailey et al. 2003) from meteorological station 23 and 1, for high and low elevation plots respectively were obtained. Missing data were replaced, using offset temperatures of highly correlated neighboring stations. To fill remaining gaps in the air temperature record, the GHCN-Daily dataset was accessed, provided by the NOAA (Menne et al. 2012a, b), utilizing data from the station Wentworth, New Hampshire (43°52′22″N, 71°54′31″W).

The Harvard Forest Research Station is located in Central Massachusetts (42°32′N, 72°11′W). The climate is cool, temperate, and humid. Precipitation is distributed evenly through the year, with annual sums in the range of 1080 mm. The annual mean temperature is 8.5 °C (Berbeco et al. 2012). The elevation of the investigated locations is approximately 350 m a. s. l. Soils can be classified as Typic Dystrudepts (WRB: Dystric Cambisol). After a severe disturbance in the beginning of the last century, the forest regrew naturally, resulting in an even aged stand of mixed hardwood species, with Red oak (*Quercus rubra* L.) dominating (Butler et al. 2012).

Within the forest site, the simulator was applied to 2 sub-sites: (1) Barre Woods (Melillo et al. 2003), and (2) Prospect Hill (Melillo et al. 1999). Both locations were set up to study the effect of soil warming on carbon and nitrogen turnover, by artificially heating the ground (Berbeco et al. 2012; Melillo et al. 2002). The model was adjusted to the topsoil (depth 5 cm) of the undisturbed control plots, whereat on the Prospect Hill site data from 6 control plots were combined, calculating a mean time-series of T_{soil}. Daily air temperature was obtained from the EMS tower (Munger and Wofsy 1999), where the record 7.6 m above ground was selected. Data gaps were closed, using offset temperature measurements at other heights, or data from the Fisher meteorological station (Boose 2001). If no other source was available, the GHCN-Daily dataset was again accessed, applying offset air temperature data from the Municipal Airport station at Orange, Massachusetts (42°33′46″N, 72°16′59″W).

Non-forested sites in Illinois

At last, to explore the limits of the formulation, the model was applied to 6 sites which lack the shielding properties of a dense forest canopy. Therefore, data were obtained from the Illinois Climate Network, (ICN), which operates several open field meteorological stations in Illinois (Fig. 2, Table 1). Air temperature was measured 2 m above ground. Gaps in the air temperature record were closed, using offset temperature measurements of, highly correlated, and neighboring stations. Soil temperature was recorded in 10 cm and 20 cm depth (Hollinger et al. 1994) under sod covered ground. Soil texture was assessed as silt loam, throughout all studied locations. The elevation of the investigated sites ranges from 133 to 265 m a. s. l.

Illinois' climate is typically continental with cold winters and warm summers. Moving from north to south, mean annual air temperatures increase from 8.9 to 14.5 °C. Also annual precipitation sums reveal a strong north–south gradient, ranging from 810 to 1220 mm. Stations in the north-west of the state are climatically influenced by Lake Michigan, which is attenuating temperature extremes and enhancing winter precipitation (lake effect snow) (Changnon et al. 2008).

Model application

Parameterization

The model was applied to each site and depth specifically. Emphasis was laid on its application on longest possible records of T_{soil}, to cover the broadest possible range of different environmental states, which might have a potential influence on soil thermal regimes. On the other hand it seems obvious, that due to changes in leaf area, undergrowth, litter layer, water consumption, etc., forest T_{soil} regimes undergo a certain shift during stand development (compare Kang et al. 2000). In cases where, for reasons unknown, an obvious change in the soil thermal regime was observed, the time frame of the investigation was manually narrowed down. Both $T_{\mathrm{soil},t}$ and $T_{\mathrm{shift},t}$ were initialized at 8 °C. The simulator ran a 150 day spin-up prior to the analysis time frame. For model parameterization a simulated annealing algorithm (Kirkpatrick et al. 1983) was applied, selecting an exponential cooling schedule. Optimization/evaluation criterion was in every case the Nash–Sutcliffe model efficiency (NSE) (Nash and Sutcliffe 1970).

$$NSE = 1 - \frac{\sum_{i=1}^{n}\left(T_{\mathrm{soil},obs,i} - T_{\mathrm{soil},sim,i}\right)^2}{\sum_{i=1}^{n}\left(T_{\mathrm{soil},obs,i} - \overline{T}_{\mathrm{soil},obs}\right)^2} \tag{9}$$

Enabling a balanced split, the calibration was conducted on data from odd years, data from even years served in the evaluation. Making the simulation result comparable to other works, other performance indices like Root Mean Squared Error (RMSE), mean absolute error (MAE) and mean bias error (MBE) were calculated.

$$RMSE = \left[n^{-1}\sum_{i=1}^{n}\left(T_{\mathrm{soil},obs,i} - T_{\mathrm{soil},sim,i}\right)^2\right]^{1/2} \tag{10}$$

$$MAE = n^{-1}\sum_{i=1}^{n}\left|T_{\mathrm{soil},obs,i} - T_{\mathrm{soil},sim,i}\right| \tag{11}$$

$$MBE = n^{-1}\sum_{i=1}^{n} T_{\mathrm{soil},obs,i} - T_{\mathrm{soil},sim,i} \tag{12}$$

Parameterization on limited input data

To test the simulators practical suitability to cope with limited input data, the T_{soil} record of Klausen Leopoldsdorf (15 cm depth) was used, ranging from November 2001 to June 2013 ($\sim$11 years, 4053 valid observations). The dataset was split into n sectors of approximately equal size. The parameterization (simulated annealing) was performed, drawing only one random observation per sector. The remaining observations served in the evaluation. This step was repeated 12 times per n, each time with different random observations, to generate a distributed result. After 12 iterations, n was incremented, starting with $n = 4$, gradually progressing to $n = 2000$. This way, the minimum number of point observations was determined, necessary to yield satisfactory model performance.

Results and discussion

The model was applied to various sites and depths. In this work, a representative selection of 36 simulation runs is displayed (Table 2). The simulator delivered good estimates of T_{soil} on all investigated forest sites. NSE values above 0.979 and RMSE consistently below 1 °C underline the outcome (Table 3), whereat good results were not limited to the topmost soil horizons. Increasing phase shift and the attenuation of the temperature wave with increasing soil depth, were also captured by the simulation (Fig. 3b). Winter T_{soil} dynamics are strongly affected by (1) heat transformations at the freeze/thaw transition and (2) the insulating by the snowpack (Beltrami 2001). The

Table 2 Parameterization result for 36 sites and depths

	Parameter									
	z (cm)	λ_{max}	λ_{aux}	λ_{frost}	λ_{thaw}	T_0 (°C)	T_1 (°C)	T_{corr} (°C)	pc_{corr}	pc_{air}
Jochberg	15	0.4059	0.0365	0.0041	0.0568	1.3	3.6	2.7	0.142	0.505
	30	0.2781	0.0327	0.0044	0.0806	1.5	5.6	3.5	0.181	0.440
	60	0.1349	0.0273	0.0008	0.0942	1.0	9.2	3.2	0.216	0.380
Mondsee	15	0.4653	0.0708	0.0026	0.0700	0.9	7.6	11.2	0.124	0.438
	30	0.3090	0.0541	0.0056	0.0616	1.2	8.3	9.3	0.234	0.306
	60	0.3672	0.0419	0.0084	0.2010	1.7	12.0	8.1	0.334	0.078
Murau	15	0.3686	0.0447	0.0000	0.0285	0.6	7.0	3.4	0.257	0.285
	30	0.2934	0.0424	0.0005	0.0296	0.8	7.0	3.8	0.298	0.247
	60	0.2514	0.0379	0.0037	0.0498	1.5	6.7	3.8	0.350	0.158
Mürzzuschlag	15	0.2494	0.0208	0.0028	0.0140	0.3	2.7	7.4	0.188	0.480
	30	0.1687	0.0184	0.0130	0.0244	0.9	2.7	7.4	0.213	0.451
	60	0.1119	0.0177	0.0031	0.0321	−0.3	6.4	7.1	0.274	0.353
Klausen-Leopoldsdorf	05	0.5092	0.0261	0.0131	0.1840	1.5	5.4	7.5	0.129	0.538
	10	0.3949	0.0244	0.0130	0.1374	1.6	6.2	7.9	0.151	0.500
	15	0.3006	0.0229	0.0123	0.1287	1.5	7.6	7.9	0.168	0.471
	30	0.2104	0.0214	0.0147	0.0947	2.0	8.3	8.2	0.201	0.432
	60	0.1138	0.0204	0.0021	0.0590	0.9	9.3	8.3	0.278	0.349
Unterpullendorf	15	0.4752	0.0383	0.0360	0.0541	−2.3	12.5	13.6	0.137	0.528
	30	0.2824	0.0313	0.0177	0.0191	−3.2	12.3	12.9	0.172	0.460
	60	0.1443	0.0254	0.0091	0.0101	−2.6	9.3	12.0	0.216	0.366
HBEF, intensive high	05	0.6399	0.0418	0.0024	0.0133	1.1	5.3	10.9	0.300	0.411
HBEF, intensive low	05	0.5584	0.0355	0.0001	0.0075	0.9	3.1	11.4	0.286	0.515
Harvard Forest, Prospect Hill	05	0.8723	0.0447	0.0000	0.0116	−0.4	9.2	14.2	0.160	0.516
Harvard Forest, Barre Woods	05	0.7238	0.0467	0.0000	0.0357	0.4	7.0	16.3	0.153	0.502
Freeport	10	0.7111	0.0974	0.0009	0.1094	−0.8	7.3	118.1	0.012	0.495
	20	0.5157	0.0808	0.0014	0.1598	−0.4	10.2	94.5	0.016	0.437
St. Charles	10	0.7541	0.0915	0.0045	0.1397	−0.5	7.1	182.4	0.007	0.573
	20	0.5323	0.0771	0.0035	0.2367	−0.7	10.7	80.4	0.012	0.540
Champaign	10	0.8515	0.1215	0.0000	0.3250	0.2	6.0	264.2	0.008	0.487
	20	0.5223	0.0822	0.0000	0.3130	00.5	8.8	95.2	0.022	0.512
Belleville	10	0.6570	0.0722	0.0072	0.6131	−0.1	11.0	83.8	0.014	0.468
	20	0.4561	0.0598	0.0044	0.4558	−0.1	11.3	68.9	0.017	0.481
Brownstown	10	0.6627	0.0916	0.0003	0.4320	−0.4	13.3	32.6	0.029	0.508
	20	0.4212	0.0754	0.0036	0.2782	−0.3	13.2	22.6	0.046	0.528
Olney	10	0.8012	0.1035	0.0010	0.4226	−0.7	7.7	343.5	0.003	0.544
	20	0.5477	0.0909	0.0015	0.4373	−0.4	10.0	431.5	0.003	0.492

Optimization was performed, using a simulated annealing algorithm. Performance criterion was the Nash–Sutcliffe Efficiency (NSE)

presented model does not specifically address these effects, but it is capable, to account for both effects combined. In most cases, the description of the winter soil thermal regime was successful. Figures 3a, d and 4a clearly show the decoupling of ground temperature from air temperature under snow cover. The simulator was able to track this behavior, where in some cases it failed to predict the exact time when soil temperature rises in spring (Fig. 4a): The melting of the snow cover causes a sharp increase in T_{soil} due to the ceasing insulating effect, hand in hand with an abrupt decrease in surface albedo, making the forest ground susceptible for short wave radiation inputs, which are already considerable in early spring. Rankinen et al. (2004) solved this problem by incorporating a snow dynamics routine into the calculations, but this would require the embedding of more model parameters and meteorological input data. In consideration of the models practical applicability, this was set aside.

Table 3 Performance indices for calibration and evaluation intervals

	Calibration						Evaluation					Timeframe	
	z (cm)	*n*	NSE	RMSE (°C)	MAE (°C)	MBE (°C)	*n*	NSE	RMSE (°C)	MAE (°C)	MBE (°C)	Start	End
Jochberg	15	780	0.991	0.416	0.300	0.003	731	0.989	0.496	0.364	−0.03	03/01/2009	12/31/2013
	30	780	0.991	0.385	0.281	0.003	731	0.990	0.444	0.327	−0.01	03/01/2009	12/31/2013
	60	780	0.992	0.320	0.234	0.003	731	0.991	0.351	0.266	0.013	03/01/2009	12/31/2013
Mondsee	15	761	0.986	0.641	0.513	−0.00	731	0.979	0.806	0.626	0.249	12/01/2009	12/31/2013
	30	761	0.988	0.518	0.409	−0.00	731	0.981	0.678	0.559	0.275	12/01/2009	12/31/2013
	60	761	0.990	0.396	0.301	−0.00	731	0.980	0.570	0.473	0.254	12/01/2009	12/31/2013
Murau	15	1037	0.974	0.604	0.487	−0.00	718	0.986	0.434	0.325	0.017	01/01/2009	12/31/2013
	30	1037	0.974	0.565	0.451	0.002	718	0.987	0.399	0.299	0.045	01/01/2009	12/31/2013
	60	1037	0.970	0.542	0.434	0.001	718	0.989	0.330	0.235	0.037	01/01/2009	12/31/2013
Mürzzuschlag	15	761	0.994	0.381	0.284	0.003	731	0.993	0.441	0.352	0.014	12/01/2009	12/31/2013
	30	761	0.994	0.348	0.261	0.004	731	0.992	0.415	0.314	0.073	12/01/2009	12/31/2013
	60	761	0.994	0.312	0.237	0.010	731	0.994	0.332	0.254	0.079	12/01/2009	12/31/2013
Klausen-Leopoldsdorf	05	1927	0.986	0.625	0.478	−0.00	1770	0.986	0.615	0.482	0.165	11/08/2001	07/01/2013
	10	1927	0.987	0.585	0.448	0.000	1770	0.986	0.581	0.454	0.176	11/08/2001	07/01/2013
	15	1927	0.987	0.550	0.425	−0.00	2126	0.987	0.562	0.438	0.103	11/08/2001	07/01/2013
	30	1927	0.988	0.499	0.386	0.000	2126	0.987	0.527	0.402	0.105	11/08/2001	07/01/2013
	60	1914	0.989	0.418	0.330	−0.00	2126	0.985	0.490	0.375	0.106	11/08/2001	07/01/2013
Unterpullendorf	15	829	0.994	0.492	0.384	−0.00	711	0.992	0.559	0.451	−0.08	09/19/2009	12/31/2013
	30	829	0.995	0.419	0.335	0.004	720	0.994	0.471	0.384	−0.05	09/19/2009	12/31/2013
	60	829	0.995	0.371	0.293	−0.00	720	0.994	0.401	0.317	−0.01	09/19/2009	12/31/2013
HBEF, intensive high	05	489	0.991	0.549	0.402	−0.00	390	0.986	0.704	0.554	0.198	12/01/2010	05/10/2013
HBEF, intensive low	05	493	0.986	0.726	0.560	−0.00	396	0.979	0.943	0.781	−0.68	12/01/2010	05/10/2013
Harvard, Prospect Hill	05	1477	0.989	0.717	0.534	−0.01	1556	0.986	0.811	0.621	0.141	06/01/1991	05/31/2000
Harvard, Barre Woods	05	1290	0.990	0.673	0.513	0.002	1013	0.990	0.664	0.500	−0.18	05/21/2003	04/20/2010
Freeport	10	4568	0.985	1.16	0.864	0.014	4389	0.986	1.07	0.821	−0.06	01/01/1991	07/31/2015
	20	4571	0.989	0.956	0.702	0.001	4389	0.989	0.909	0.703	−0.04	01/01/1991	07/31/2015
St. Charles	10	4524	0.985	1.12	0.870	0.013	4389	0.982	1.19	0.884	0.180	01/01/1991	07/31/2015
	20	4551	0.990	0.875	0.684	0.010	4384	0.987	0.973	0.742	0.160	01/01/1991	07/31/2015
Champaign	10	2190	0.983	1.25	0.984	−0.01	1828	0.982	1.24	0.991	−0.20	01/01/1995	12/31/2005
	20	2190	0.991	0.846	0.686	−0.01	1828	0.989	0.916	0.727	−0.13	01/01/1995	12/31/2005
Belleville	10	2033	0.992	0.784	0.615	0.003	2187	0.991	0.844	0.659	0.098	01/01/2004	07/31/2015
	20	2033	0.991	0.789	0.601	0.002	2193	0.992	0.753	0.584	0.048	01/01/2004	07/31/2015
Brownstown	10	3610	0.985	1.04	0.820	−0.02	3652	0.990	0.845	0.662	0.079	01/01/1991	12/31/2010
	20	3610	0.987	0.950	0.754	0.014	3652	0.990	0.816	0.636	0.070	01/01/1991	12/31/2010
Olney	10	2035	0.989	0.990	0.763	−0.00	2192	0.988	1.02	0.776	−0.02	01/01/2004	07/31/2015
	20	2034	0.992	0.787	0.615	0.009	2192	0.992	0.809	0.621	−0.01	01/01/2004	07/31/2015

Calibration was performed on odd years, evaluation on even ones. A long evaluation timeframe (high *n*) adds significance to the results

A positive MBE indicates that the observed mean soil temperature exceeds the predicted mean soil temperature and vice versa

NSE Nash–Sutcliffe efficiency, *RMSE* root mean squared error, *MAE* mean absolute error, *MBE* mean bias error

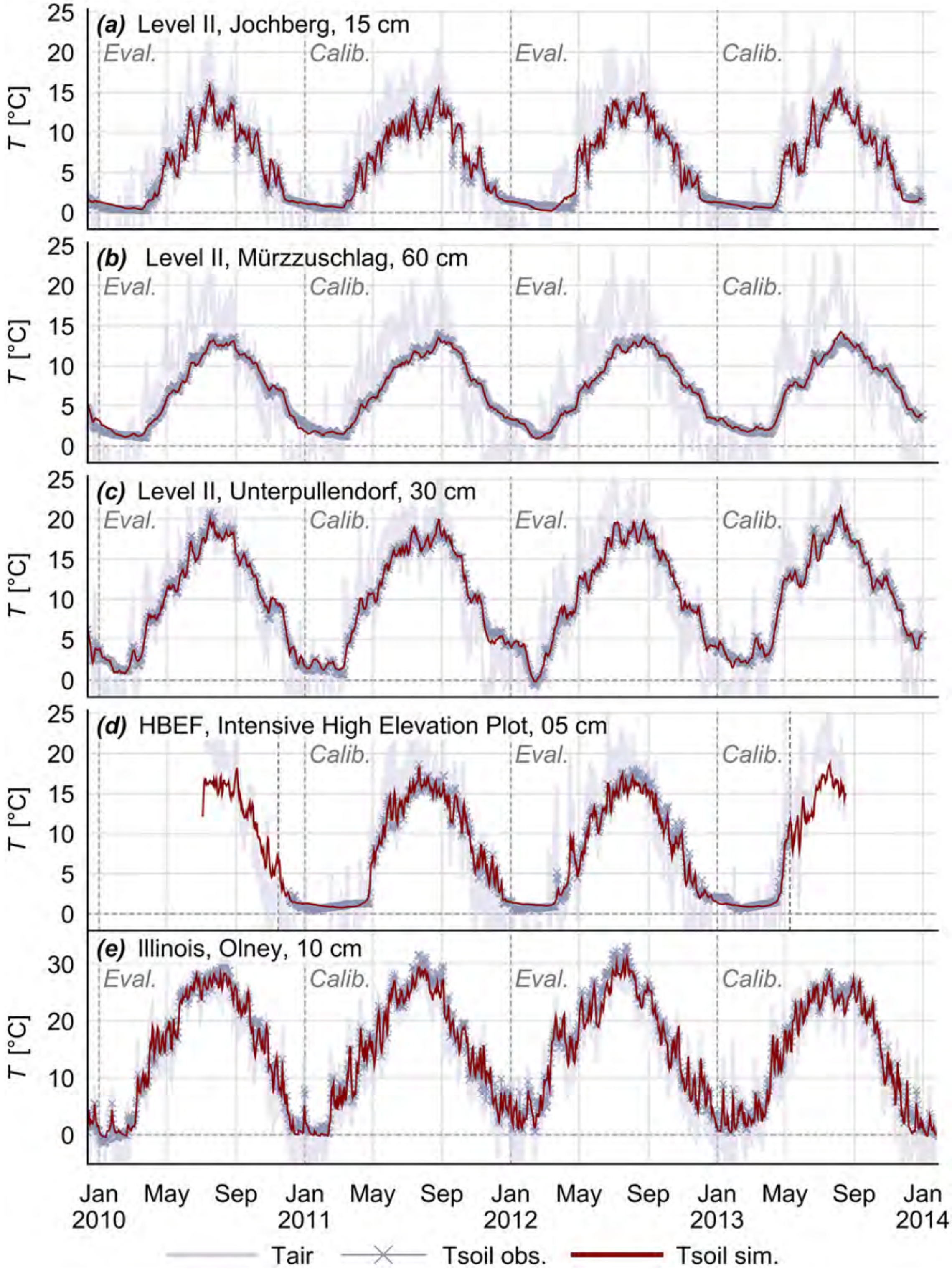

Fig. 3 Four years of observed air and soil temperature, overlaid with simulated T_{soil}. Calibration was performed on odd years, performance evaluation on even ones. Plot (**a**) and (**d**) clearly show the effect of snow cover on winter soil thermal regimes. In both cases the trend was successfully captured by the simulator. Also increasing phase shift and attenuation of the soil temperature wave with increasing soil depth (**b**) were captured. Stronger fluctuations of T_{soil} under open-field conditions (**e**), where the heat exchange might be dominated by radiation fluxes, did also not limit the simulators capability

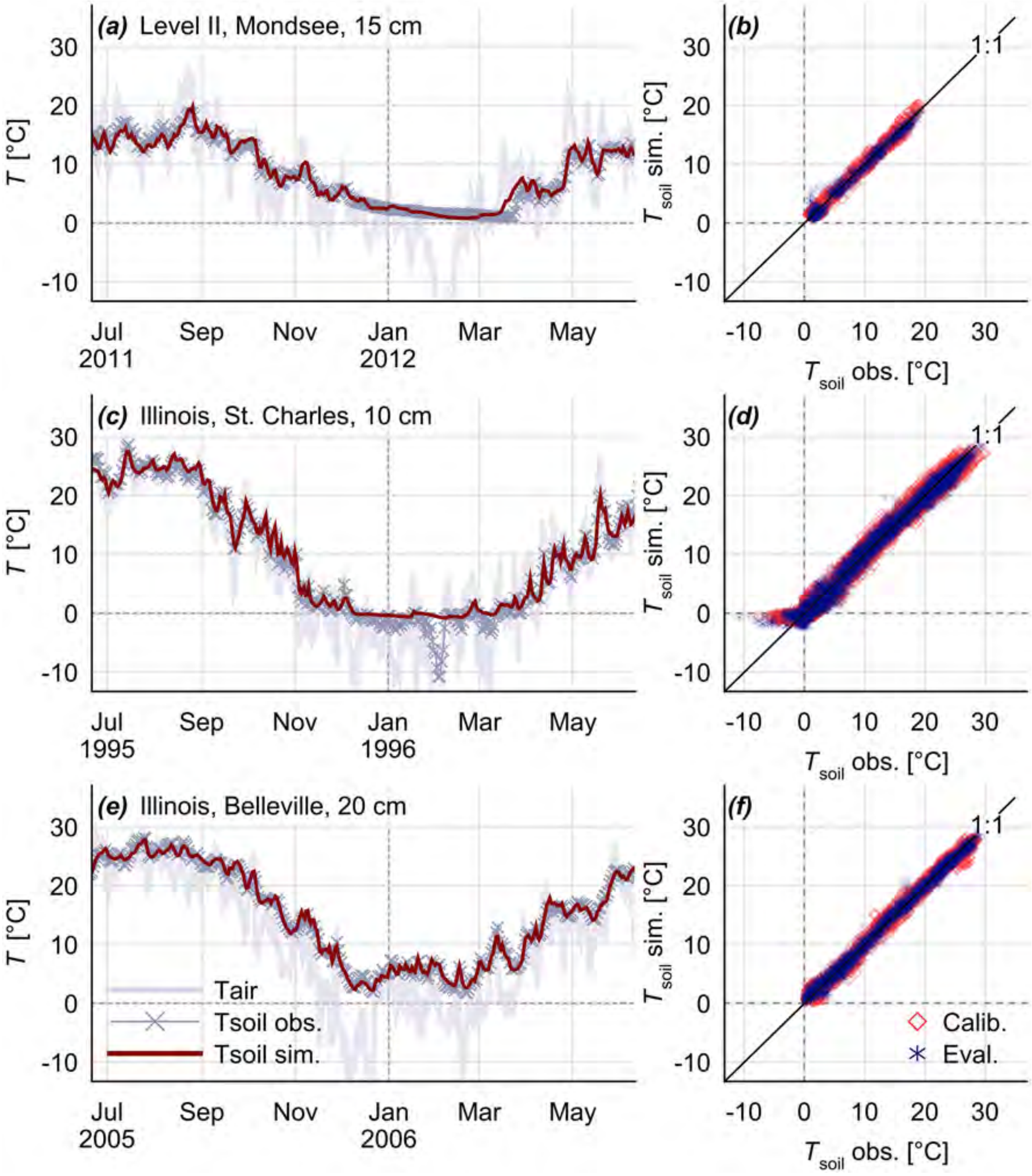

Fig. 4 One year section of observed and simulated T_{soil} time series plus the corresponding performance scatterplot. Note that the scatterplots cover the whole investigation timeframe! (**a**, **b**) winter snow cover decouples the course of air and soil temperature. The melting of the snowpack in the end of March causes T_{soil} to escalate, due to the ceasing insulation plus the abrupt decrease in surface albedo, making the soil susceptible for short wave radiation inputs, which are already considerable in early spring. As the snowpack is not modeled explicitly, the simulator fails to predict the exact time when T_{soil} rises in spring (**c**, **d**). Failure to predict a major soil frost event, due to limitations in the model structure: Temperature fluctuations in early winter indicate the absence of a snow pack. When in midwinter all latent heat is released due to the freezing of soil water, T_{soil} suddenly drops. In the formulation the transfer coefficient below the lower threshold temperature (T_0) remains constant. As a consequence, our formulation applies best, to sites where severe soil frost plays only a subordinate role (**e**, **f**)

Compared to forested locations, the biotic site components at the open field meteorological stations are kept intentionally constant. This enabled the successful prediction of T_{soil} over a long timeframe. On 2 sites in the northern part of the state (Freeport, St. Charles) we accomplished good results over 24 years of calibration and evaluation. But the best performance (evaluation NSE ≥0.99 over several years) was achieved on comparatively

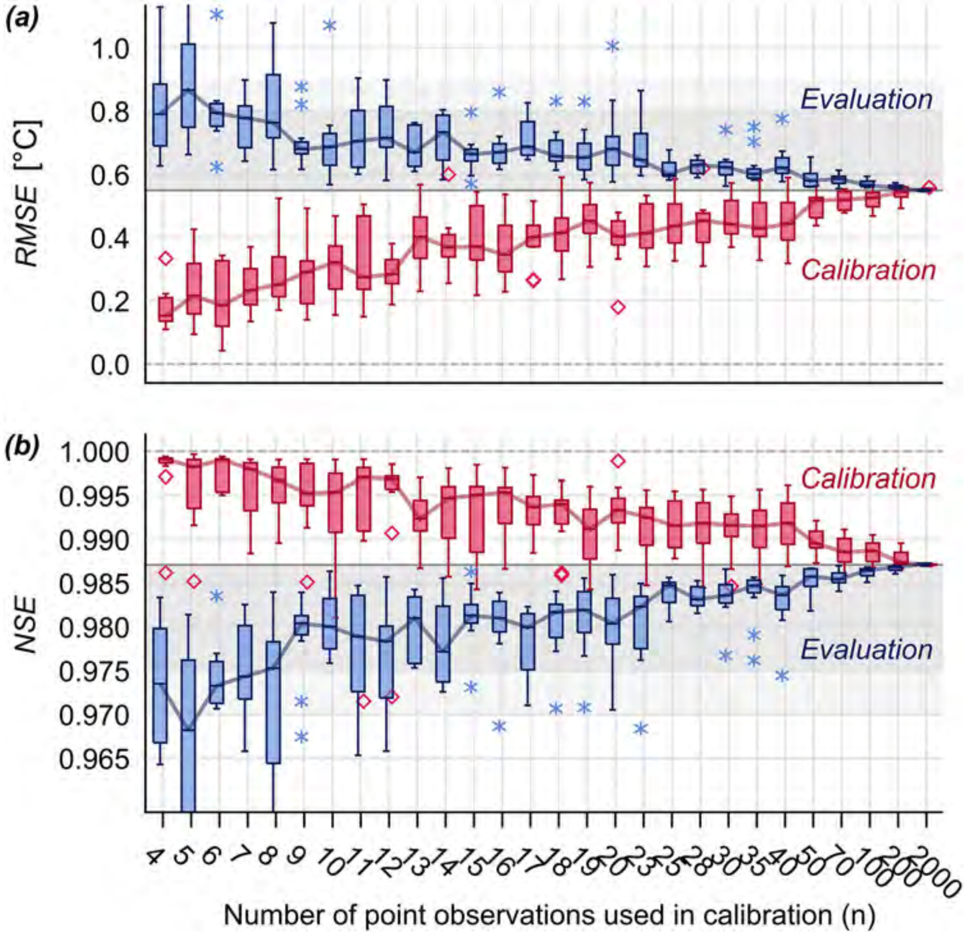

Fig. 5 Model optimization result for Klausen-Leopoldsdorf, 15 cm: to determine the amount of point observations, necessary to achieve sound model performance, the investigated time series was divided into *n* intervals of equal size, drawing one random point observation each. These *n* observations were used to optimize the model (simulated annealing). The remaining observations were used to validate model performance. For each *n*, the procedure was repeated 12 times with different random observations, to generate a distributed result. Performance measures shown are (**a**) root mean squared error, and (**b**) Nash–Sutcliffe efficiency. Both indices show high performance ($\mathrm{RMSE} \leq 0.9$ °C, $\mathrm{NSE} \geq 0.97$) with $n \geq 13$. For $n \geq 50$ there was only little difference in performance, compared to optimization utilizing the full calibration timeframe ($n = 2000$, *horizontal, grey line*)

warm locations, located at low elevations, in the south of Illinois (Belleville, Brownstown, Olney). In contrast to forested sites, open field sites, lack the attenuating properties of a dense canopy, or a thick litter layer. Especially for cold, but snow-free winters, these locations were prone to soil frost (Fig. 4c, St. Charles). Temperature fluctuations in early winter indicate the absence of a thick insolating snow pack. When in midwinter all latent heat is released, due to the freezing of soil water, T_{soil} suddenly drops. Due to the structure of the model, this behavior could not be tracked: In the presented formulation the transfer coefficient below the lower threshold temperature (T_0) remains constant at a reduced level, suppressing further soil cooling. This model limitation could be tackled by letting the transfer coefficient rise at temperatures below T_0. On the other hand, that would require the segregation of the effects of freeze/thaw processes and snow cover insulation, making the model again more complex and input data demanding.

The examination, to determine the minimum amount of point observations of soil temperature, necessary to yield suitable results, was performed on, an 11-years time series, of air and soil temperature at the Level II plot Klausen-Leopoldsdorf (15 cm depth). The time frame was divided in *n* sectors. Only one observation was selected randomly by sector. All other observations served in the evaluation. Disregarding single outlier runs, good results (NSE >0.97, RMSE < 0.9 °C) were achieved with $n \leq 13$. Having available 50 or more daily observations, there was only little difference to the result, compared to utilizing ~50 % ($n = 2000$) of the available data in the calibration process (Fig. 5).

Two considerations led to the implementation of decreasing transfer coefficients with decreasing soil temperature: (1) The heat release/consumption at the freeze/thaw transition (Beltrami 2001), and (2) the insulating effect of the winter snow cover. So intentionally, values for T_0 and T_1 were searched around 0 °C. Surprisingly, in most cases the optimization process led to T_1 values much higher, meaning that the attenuation of the transfer coefficient starts already at higher temperatures. The idea behind utilizing different responses for soil warming and cooling, was the assumption, that soil warming in spring is strongly driven by incoming solar radiation, which is accelerating the temperature rise.

As this model is primarily of an empirical nature, used parameters lack a specific meaning, in a strict physical sense. Nevertheless, it was noted that parameter values

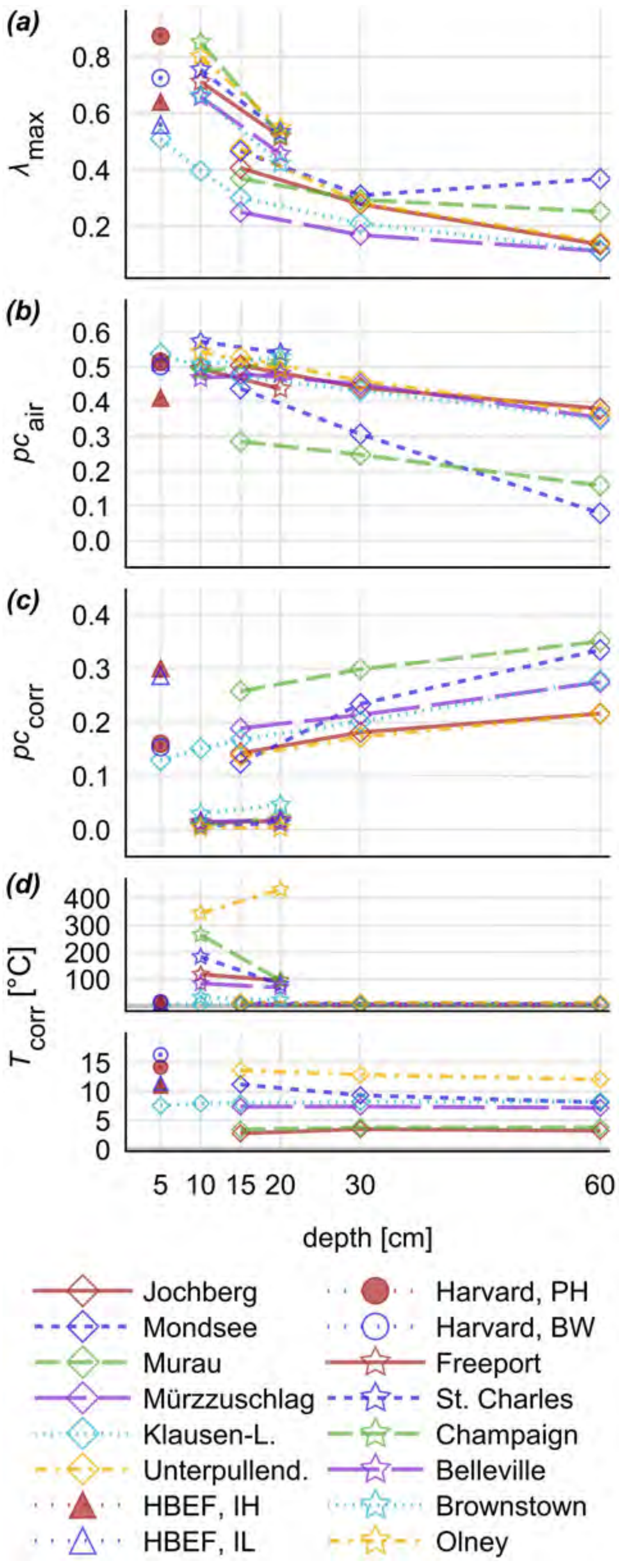

◀**Fig. 6** Four selected parameters and their change with increasing soil depth. **a** Transfer coefficient values showed a clear decreasing trend with increasing soil temp. **b** Also the fraction of the air temperature in the calculation of the environmental temperature showed, almost linear, decrement. **d** Where the correction temperature on forested sites was in a close range to the annual mean air temperature, the open field locations (*star symbol*) revealed much higher values. On the other hand, the relative weighting (**c**) of these temperatures was much smaller on non-forested sites. It is assumed, that on these locations, both parameters combined compensate for direct shortwave radiation inputs

were strongly affected by certain site characteristics: λ_{max} values clearly decreased with increasing soil depth (Fig. 6a). Meaning, the time demand, to compensate a fraction of the temperature difference between soil layer and air, rose with increasing soil depth. Also the relative partition of the correction temperature (pc_{corr}), in the calculation of the environmental temperature, increased in deeper soil layers (Fig. 6c). In contrast, the direct influence of air temperature (pc_{air}) showed a decrease downwards.

Investigated open field sites differed strongly from forest sites, in parameter values of the correction temperature (T_{corr}). Where on forest locations T_{corr} resided closely to the stands annual mean air temperature, open field sites revealed T_{corr} values, around and above 100 °C (Fig. 6d). On the other hand, their relative weight (pc_{corr}) in the calculation of the environmental temperature, is much lower than on forested sites. It is assumed, that in these cases, they correct for direct radiation energy inputs, which are obviously much higher without the presence of a shielding canopy. The reason that, even under such conditions, the simulator (which does not particularly address radiative heat flux) delivers good estimates of T_{soil}, might be found in the strong correlation between energy balance components, and the air temperature itself (Hock 2003).

Conclusion

The primary intention of this work was the provision of a tool, which enables the transformation of fragmentary records of forest soil temperature, into a complete time series of T_{soil}, using average daily air temperature as only input. In this specific case, the created time series is laying the base for the modeling of temperature dependent, biogeochemical soil processes.

To test the resilience of this model, it was applied to various locations and depths, covering a broad amplitude of site characteristics. The simulator delivered accurate predictions of the temperature of the topsoil, as well as of deeper layers. The high performance was not limited to the warm season. The combination of the insulating effect of the snow cover plus the effect of heat transformations at the freeze/thaw transition, on soil thermal regimes were captured sufficiently. The formulation was applied to forested, as well as open to field locations, where in the open field it failed to reproduce some major soil frost events. Bearing this limitation in mind, this simulator seems to be well applicable to other land use types.

The model parameters lack a specific meaning in a strict physical sense. Therefore, currently the parameterization requires at least a modest amount of T_{soil} observations, to yield sufficient results. A challenging impulse for future work, would be the attempt to derive model parameters, directly from more easily obtainable site characteristics. This also would enable the capability of the simulator to deal with a changing soil thermal regime, during stand development.

Acknowledgments This research was funded by the Austrian Science Fund (FWF, project number P23861-B16, granted to TW Berger) and the Commission for Interdisciplinary Ecological Studies (KIÖS) at the Austrian Academy of Sciences (project number 2010-05; granted to TW Berger). Level II data from Austrian sites was provided by the Austrian Research Centre for Forests. For the possibility to access air temperature data, we acknowledge the providers in the ECA&D project.

T_{soil} data from the HBEF were provided by Peter M. Groffman on 07/20/2015. We want to thank Jennifer L. Morse and Jorge Duran for their valuable field work. Air temperature records were provided by John Campbell and Amey Bailey on 07/20/2015. These data were gathered as part of the Hubbard Brook Ecosystem Study (HBES). The HBES is a collaborative effort at the Hubbard Brook Experimental Forest, which is operated and maintained by the USDA Forest Service, Northern Research Station, Newtown Square, PA. Significant funding for collection of these data was provided by the US National Science Foundation (Grants DEB 0949664—Ecosystem Studies, DEB 0423259 and DEB 1114804—Long-Term Ecological Research).

Further, we want to thank Jerry Melillo, Paul Steudler, Jacqueline Mohan, William Munger, Steven Wofsy, Emery Boose, Mark VanScoy, and all their collaborators, for the collection and the providing of air and soil temperature data, from the ecological research area at Harvard Forest.

Data from the open field sites, located in Illinois, were provided by the Water and Atmospheric Resources Monitoring Program, a part of the Illinois State Water Survey (ISWS) located in Champaign and Peoria, Illinois.

The Shuttle Radar Topography Mission, SRTM data product (Farr and Kobrick 2000) was retrieved from the online Data Pool, courtesy of the NASA Land Processes Distributed Active Archive Center (LP DAAC), USGS/Earth Resources Observation and Science (EROS) Center, Sioux Falls, South Dakota, https://lpdaac.usgs.gov/data_access/data_pool.

At last, we thank Mathias Mayer for his encouraging words on writing this article, and for providing a valuable tip.

References

Bailey AS, Hornbeck JW, Campbell JL, Eagar C (2003) Hydrometeorological database for Hubbard Brook Experimental Forest: 1955–2000, vol 305. US Department of Agriculture, Forest Service, Northeastern Research Station

Balisky AC, Burton PJ (1993) Distinction of soil thermal regimes under various experimental vegetation covers. Can J Soil Sci 73:411–420

Beltrami H (2001) On the relationship between ground temperature histories and meteorological records: a report on the Pomquet station. Glob Planet Change 29:327–348. doi:10.1016/S0921-8181(01)00098-4

Berbeco MR, Melillo JM, Orians CM (2012) Soil warming accelerates decomposition of fine woody debris. Plant Soil 356:405–417

Bergman TL, Incropera FP, Lavine AS (2011) Fundamentals of heat and mass transfer. Wiley

Betts AK, Ball JH, McCaughey JH (2001) Near-surface climate in the boreal forest. J Geophys Res Atmos 106:33529–33541. doi:10.1029/2001jd900047

Bilgili M, Sahin B, Sangun L (2013) Estimating soil temperature using neighboring station data via multi-nonlinear regression and artificial neural network models. Environ Monit Assess 185:347–358. doi:10.1007/s10661-012-2557-5

Bond-Lamberty B, Wang CK, Gower ST (2005) Spatiotemporal measurement and modeling of stand-level boreal forest soil temperatures. Agric For Meteorol 131:27–40. doi:10.1016/j.agrformet.2005.04.008

Boose E (2001) Fisher meteorological station (since 2001). Harvard Forest Data Archive: HF001

Brown SE, Pregitzer KS, Reed DD, Burton AJ (2000) Predicting daily mean soil temperature from daily mean air temperature in four northern hardwood forest stands. For Sci 46:297–301

Butler SM, Melillo JM, Johnson JE, Mohan J, Steudler PA, Lux H, Burrows E, Smith RM, Vario CL, Scott L (2012) Soil warming alters nitrogen cycling in a New England forest: implications for ecosystem function and structure. Oecologia 168:819–828

Campbell JL, Mitchell MJ, Groffman PM, Christenson LM, Hardy JP (2005) Winter in northeastern North America: a critical period for ecological processes. Front Ecol Environ 3:314–322. doi:10.1890/1540-9295(2005)003[0314:Winnaa]2.0.Co;2

Campbell JL, Ollinger SV, Flerchinger GN, Wicklein H, Hayhoe K, Bailey AS (2010) Past and projected future changes in snowpack and soil frost at the Hubbard Brook Experimental Forest, New Hampshire, USA. Hydrol Process 24:2465–2480. doi:10.1002/hyp.7666

Changnon SA, Angel JR, Kunkel KE, Lehmann CM (2008) Illinois Climate Atlas. Illinois State Water Survey. Prairie Research Institute of the University of Illinois, Urbana-Champaign

Davidson EA, Janssens IA, Luo YQ (2006) On the variability of respiration in terrestrial ecosystems: moving beyond Q(10). Glob Change Biol 12:154–164. doi:10.1111/j.1365-2486.2005.01065.x

Duran J, Morse JL, Groffman PM, Campbell JL, Christenson LM, Driscoll CT, Fahey TJ, Fisk MC, Mitchell MJ, Templer PH (2014) Winter climate change affects growing-season soil microbial biomass and activity in northern hardwood forests. Glob Change Biol 20:3568–3577. doi:10.1111/gcb.12624

Farr TG, Kobrick M (2000) Shuttle Radar Topography Mission produces a wealth of data. Eos Trans AGU 81:583

Gehrig-Fasel J, Guisan A, Zimmermann NE (2008) Evaluating thermal treeline indicators based on air and soil temperature using an air-to-soil temperature transfer model. Ecol Model 213:345–355. doi:10.1016/j.ecolmodel.2008.01.003

Hock R (2003) Temperature index melt modelling in mountain areas. J Hydrol 282:104–115. doi:10.1016/S0022-1694(03)00257-9

Hollinger SE, Reineke BC, Peppler RA (1994) Illinois climate network: site descriptions, instrumentation, and data management, vol 178. Illinois State Water Survey

Hu Q, Feng S (2003) A daily soil temperature dataset and soil temperature climatology of the contiguous United States. J Appl Meteorol 42:1139–1156. doi:10.1175/1520-0450(2003)042<1139:Adstda>2.0.Co;2

Kang S, Kim S, Oh S, Lee D (2000) Predicting spatial and temporal patterns of soil temperature based on topography, surface cover and air temperature. For Ecol Manag 136:173–184. doi:10.1016/S0378-1127(99)00290-X

Katterer T, Andren O (2009) Predicting daily soil temperature profiles in arable soils in cold temperate regions from air temperature and leaf area index. Acta Agr Scand B-S P 59:77–86 doi:10.1080/09064710801920321

Kim S, Singh VP (2014) Modeling daily soil temperature using data-driven models and spatial distribution. Theor Appl Climatol 118:465–479. doi:10.1007/s00704-013-1065-z

Kirkpatrick S, Gelatt CD, Vecchi MP (1983) Optimization by simulated annealing. Science 220:671–680. doi:10.1126/science.220.4598.671

Kisi O, Tombul M, Kermani MZ (2015) Modeling soil temperatures at different depths by using three different neural computing techniques. Theor Appl Climatol 121:377–387. doi:10.1007/s00704-014-1232-x

Körner C, Paulsen J (2004) A world-wide study of high altitude treeline temperatures. J Biogeogr 31:713–732

Lei SG, Daniels JL, Bian ZF, Wainaina N (2011) Improved soil temperature modeling. Environ Earth Sci 62:1123–1130. doi:10.1007/s12665-010-0600-9

Macdonald NW, Zak DR, Pregitzer KS (1995) Temperature effects on kinetics of microbial respiration and net nitrogen and sulfur mineralization. Soil Sci Soc Am J 59:233–240

Melillo J, Steudler P, Mohan J (1999) Prospect hill soil warming experiment at Harvard forest since 1991. Harvard Forest Data Archive: HF005. doi:10.6073/pasta/246c9bf827daa3a61d6a6dfb6b393b32

Melillo JM, Steudler PA, Aber JD, Newkirk K, Lux H, Bowles FP, Catricala C, Magill A, Ahrens T, Morrisseau S (2002) Soil warming and carbon-cycle feedbacks to the climate system. Science 298:2173–2176

Melillo J, Steudler P, Mohan J (2003) Barre woods soil warming experiment at Harvard forest since 2001. Harvard Forest Data Archive: HF018. doi:10.6073/pasta/dbb1bac50540a22cfdd6cd9a817274fd

Menne MJ, Durre I, Korzeniewski B, McNeal S, Thomas K, Yin X, Anthony S, Ray R, Vose RS, Gleason BE, Houston TG (2012a) Global historical climatology network—daily (GHCN-Daily), Version 3. NOAA National Climatic Data Center. doi:10.7289/V5D21VHZ

Neumann M, Schnabel G, Gärtner M, Starlinger F, Fürst A, Mutsch F, Englisch M, Smidt S, Jandl R, Gartner K (2001) Waldzustandsmonitoring in Österreich: Ergebnisse der Intensivbeobachtungsflächen (Level II). Forstliche Bundesversuchsanstalt Wien

Tank AMGK et al (2002) Daily dataset of 20th-century surface air temperature and precipitation series for the European Climate Assessment. Int J Climatol 22:1441–1453. doi:10.1002/joc.773

Menne MJ, Durre I, Vose RS, Gleason BE, Houston TG (2012) An overview of the global historical climatology network-daily database. J Atmos Ocean Technol 29:897–910. doi:10.1175/Jtech-D-11-00103.1

Mucina L, Grabherr G, Ellmauer T (1993) Die Pflanzengesellschaften Österreichs. Teil 3: Wälder und Gebüsche. Gustav-Fischer, Jena, Stuttgart, New York

Munger W, Wofsy S (1999) Canopy-atmosphere exchange of carbon, water and energy at Harvard forest EMS tower since 1991. Harvard Forest Data Archive: HF004. doi:10.6073/pasta/e89d6b8d2b175400e3072902e52280a1

Nash JE, Sutcliffe JV (1970) River flow forecasting through conceptual models part I—a discussion of principles. J Hydrol 10:282–290

Paul KI, Polglase PJ, Smethurst PJ, O'Connell AM, Carlyle CJ, Khanna PK (2004) Soil temperature under forests: a simple model for predicting soil temperature under a range of forest types. Agric For Meteorol 121:167–182. doi:10.1016/j.agrformet.2003.08.030

Rankinen K, Karvonen T, Butterfield D (2004) A simple model for predicting soil temperature in snow-covered and seasonally frozen soil: model description and testing. Hydrol Earth Syst Sci 8:706–716

Svensson M, Jansson PE, Gustafsson D, Kleja DB, Langvall O, Lindroth A (2008) Bayesian calibration of a model describing carbon, water and heat fluxes for a Swedish boreal forest stand. Ecol Model 213:331–344. doi:10.1016/j.ecolmodel.2008.01.001

Talaee PH (2014) Daily soil temperature modeling using neuro-fuzzy approach. Theor Appl Climatol 118:481–489. doi:10.1007/s00704-013-1084-9

Viterbo P, Beljaars A, Mahfouf JF, Teixeira J (1999) The representation of soil moisture freezing and its impact on the stable boundary layer. Q J Roy Meteor Soc 125:2401–2426. doi:10.1256/Smsqj.55903

Wagle P, Kakani VG (2014) Confounding effects of soil moisture on the relationship between ecosystem respiration and soil temperature in switchgrass. Bioenerg Res 7:789–798. doi:10.1007/s12155-014-9434-8

Zheng D, Hunt ER Jr, Running SW (1993) A daily soil temperature model based on air temperature and precipitation for continental applications. Clim Res 2:183–191

10.2 Ad Phenology and Water Balance: *The impact of rising temperatures on water balance and phenology of European beech (Fagus Sylvatica L.) stands*

https://link.springer.com/article/10.1007/s40808-019-00602-1

Modeling Earth Systems and Environment (2019) 5:1347–1363
https://doi.org/10.1007/s40808-019-00602-1

ORIGINAL ARTICLE

The impact of rising temperatures on water balance and phenology of European beech (*Fagus sylvatica* L.) stands

Klaus Dolschak[1] · **Karl Gartner**[2] · **Torsten W. Berger**[1]

Received: 27 November 2018 / Accepted: 6 May 2019 / Published online: 22 May 2019

Abstract

In this article, we outline the set-up and the application of an eco-hydrological box model, with the aim to describe the water balance of deciduous (*Fagus Sylvatica* L.) forest stands. The water balance model (WBM) uses standard meteorological parameters as input variables and runs on a daily time step. It consists of two modules. The aboveground module (1) comprises routines for fog precipitation generation, precipitation interception and snowfall/snowmelt dynamics. Covered belowground processes (2) are bypass flow, percolation, soil evaporation and transpiration, where the latter two processes are considered separately. Preceding to the WBM, a routine is introduced, specifying the intra-annual foliage dynamics of beech. Emphasis is also laid on the inter-annual variation of beech phenology. Leaf sprouting and leaf senescence are calculated as functions of day-length and air temperature. The WBM was applied to four European beech dominated forest stands in the northeastern part of Austria. They are located on a gradient of declining annual precipitation (from west to east). The two easterly sites are located close to the (dry) limit of the natural distribution of beech. Records of soil moisture were used for the adjustment of 26 parameters. On all sites the calibration process (simulated annealing) delivered good predictions of soil moisture (Nash–Sutcliffe efficiency ≥ 0.925). Then, the obtained parameterization was used to apply different scenarios of global warming. The temperature was increased step-wisely up to 4 °C. All scenarios were run (1) with present phenological conditions and (2) with phenology responding to higher temperatures. This way, we wanted to assign the effect of higher temperatures and longer growing seasons on the water dynamics of the forest stands. A warming of 1 °C corresponded roughly to an elongation of the growing season of 4.5 days, where the start of the growing season was affected more strongly than the end. Apparently, higher temperatures led to drier soils. The strongest change was observed in early summer, also amplified by an earlier start of the growing season. Rising temperatures led to lower export fluxes of liquid water, simultaneously increasing evapotranspiration (ET). The gain in ET was almost entirely assignable to increased soil evaporation. Drier soils led to a sharp depression of transpiration during summer months. This decline was compensated by the effect of elongated growing seasons. The risk of severe drought was increased by higher temperatures, but here the contribution of growing season length was negligible. Drier soils seem to hamper the stands' productivity. For all warming scenarios, the estimated increase of the gross primary production, caused by longer periods of assimilation, is nullified by the effect of soil water deficit in mid-summer.

Keywords Forest water balance · Box model · Soil drought · Climate change · Beech phenology · Simulated annealing

Introduction

Climate change is assumed to have a strong impact on Central European forest ecosystems. Over the last 140 years, South Europe and the Alps experienced a temperature increase of 2 °C (Mayer et al. 2005). Current climate estimations point to a further rise of the global surface temperature of 2 °C in the next 40 years (Field et al. 2014); it seems likely that the alpine region will experience a temperature elevation which will even be stronger (EEA 2015). Beech

---

Electronic supplementary material The online version of this article (https://doi.org/10.1007/s40808-019-00602-1) contains supplementary material, which is available to authorized users.

✉ Klaus Dolschak
klaus.dolschak@gmx.at

Extended author information available on the last page of the article

is a dominant tree species in Central and Western European forests (Dittmar et al. 2003); the natural distribution is associated to the Atlantic to Sub-continental Climate (Sutmöller et al. 2008). As a species with a broad eco-physiological amplitude, it seems adequately adapted to resist climate change in the (humid and cool) Atlantic areal of distribution (Kölling et al. 2007). Especially on the southern limit of the species' distribution a different picture is expected. There, the occurrence of beech is mainly restricted by the soil water availability (Ellenberg and Leuschner 1996). European Beech is a species which is particularly vulnerable to soil drought (Bolte et al. 2009). Dry and hot conditions have been known to restrict net primary production of beech forests significantly (Ciais et al. 2005). Higher temperatures are assumed to increase the frequency and intensity of soil drought due to the forcing effect on potential evapotranspiration (Bergh et al. 2003). In contrast to rising temperatures, annual precipitation sums are assumed to retain the present level, but there might be a shift in the seasonal pattern. Current estimations point towards increasing late-winter to spring precipitation, hand in hand with decreased precipitation during summer months (Geßler et al. 2007; Kunstmann et al. 2004), exacerbating soil water deficit.

Warmer conditions will lead to a temporal elongation of the growing season of beech (Vitasse et al. 2009). Under optimal conditions this would result in an increased productivity (Lindner et al. 2010). Under water limitation the opposite effect seems possible. High temperatures in spring favor growth at first. Later in the season they accelerate the soil water depletion, resulting in a sharp drop of carbon fixation by mid-summer (Dittmar et al. 2003; Kljun et al. 2007; Richardson et al. 2013).

A future increase of frequency and duration of drought periods during the growing season might alter the productivity, competitive and regenerative abilities of beech stands, especially on shallow soils (Geßler et al. 2007; Rennenberg et al. 2004). On these sites, it seems likely that beech stands will be replaced by drought resilient Oak-Hornbeam forest associations (Theurillat and Guisan 2001).

In this work, we set up a model describing the water balance of deciduous forest stands. The routing of modeled water fluxes is illustrated in Figure S1 of the supplementary. Due to a strong connection of processes such as light extinction, precipitation interception or the stands water demand to the stands leaf area (van Wijk and Williams 2005), we see the need to describe the temporal dynamics of the vegetation cover. Preceding to the WBM, a phenological routine is introduced, consisting of 2 elements: (1) the calculation of inter-annual variations of leaf emergence and leaf senescence, and (2) a quantitative measure, describing the stands seasonal development of the leaf area.

This way we assessed the soil moisture dynamics of four beech stands, which are located in the north-easterly part of Austria, close to the dry distribution limit of European beech. We analyzed the effect of climate change on the sites' water balance. In that context, possible changes in CO_2 air concentration or the precipitation pattern were neglected; the focus lay solely on the impact of rising temperatures on the stands' soil moisture regime. This way, we assessed temperature driven changes of the frequency and intensity of soil water deficit. At last we tried to identify factors which were influencing the stands' vulnerability and resilience towards soil drought.

Materials and methods

Study sites

The investigated forest stands are located in the north-easterly part of Austria in the foothills of the Northern Calcareous Alps (see Fig. 1b). The parent material for soil formation is Flysch, which consists of old tertiary and mesozoic sandstones and clayey marls of maritime origin. Due to high clay

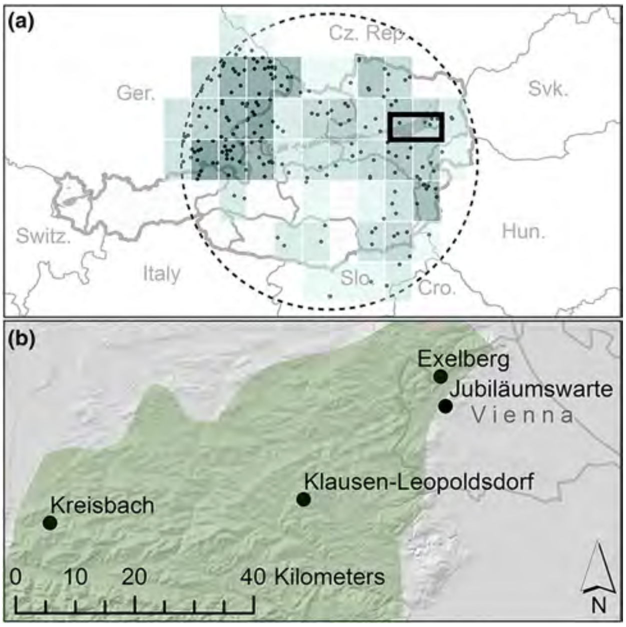

Fig. 1 **a** For calibration of the phenological model, PEP725 (Pan European Phenology Data) beech stands (small black dots) were accessed within a radius of 200 km centered to 47°42′00″N, 14°30′00″E. One average time series of air temperature was calculated, using data from the E-OBS gridded dataset (Tank et al. 2002b) (0.5° resolution, turquoise rectangles). The frequency of selected sites within one grid cell defines the relative weight, the cell receives in the calculation of the average; darker cells correspond to higher weightings. **b** Locations, used in the calibration of the WBM (black dots). All sites are beech dominated stands and share their geological bedrock (flysch). The green area represents the natural distribution of European Beech according to the Map of the Natural Vegetation of Europe (Bohn et al. 2004)

content, the saturated hydraulic conductivity is low, leading to frequent episodes of waterlogging. Therefore, the soil type can be classified as stagnic cambisol according to the WRB soil classification (IUSS Working Group 2006) throughout all studied sites. The mean annual temperature in the study area is approximately 9 °C. Precipitation declines from west to east, with average annual sums ranging from 820 mm (Kreisbach) to 652 mm (Vienna).

In the framework of the International Co-operative Programme on Assessment and Monitoring of Air Pollution Effects on Forests (ICP Forests), the Austrian Research Centre for Forests operates several intensively monitored forest sites (Level II) (Neumann et al. 2001). In addition to other environmental parameters, meteorological conditions are monitored continuously. Soil moisture (Campbell CS615 FDR probe) is recorded at 3 different depths (15, 30, 60 cm).

The model was originally set up on data from the Level II plot Klausen–Leopoldsdorf (KL), which is located in the Vienna Woods (48°07′16″N, 16°02′52″E), at an elevation of 510 m a. s. l. The research site is a pure beech (*Fagus sylvatica* L.) stand, which was planted in the late thirties of the last century. The site is facing NE with an inclination of 20%. The actual forest vegetation coincides with the potential natural one and can be classified as *Hordelymo-Fagetum* (Mucina et al. 1993). For a more detailed site description see Neumann et al. (2001).

The Kreisbach (KB) site, which is located south of St. Pölten (48°05′50″N, 15°39′50″E) at an elevation of 470 m a. s l., is a mixed European beech-Norway spruce (*Picea abies* L.) stand, with beech dominating. The stand is facing NNE with an inclination of 19%. The natural plant association can be classified as *Asperulo odoratae-Fagetum*. From 1998 to 2003 the site was monitored meteorologically within the framework of a special research program on Forest Ecosystem Restoration. Soil moisture records (Trase1 TDR probe) exist for 4 different depths (10, 20, 40, 55 cm). For a more detailed site description see Schume et al. (2003).

The third site (Jubiläumswarte, JU) is located within the municipal area of Vienna at the eastern edge of the Vienna Woods (48°13′12″N, 16°15′56″E), at an elevation of 440 m a. s. l. The site, which is a pure beech stand with an estimated age of 125-150 years, is facing SSE with an inclination of 15%. As a matured stand it is showing signs of collapse but also strong natural regeneration. Different to the other investigated sites, the bedrock contains calcareous material, reflected in higher base saturation and soil pH.

The Exelberg (EX; 48°14′40″N, 16°15′18″E) site is located in Lower Austria close to the border to Vienna, 2.8 km northwest of Jubiläumswarte. This site is also a pure beech stand. We estimated the stands' age approximately 100 years. The site is also facing SE with an inclination of 22%. Two years of bi-weekly observations of soil moisture exist for 10, 30 and 60 cm depth. The latter two sites are located at the dry distribution limit of beech (see Bohn et al. 2004). They receive significantly less precipitation than the first two. Due to their location at upper hill slopes and their exposition, we see them prone to soil drought.

Data sources

The WBM, which runs on a daily time step, uses standard meteorological data on a daily base as input. Time series of minimum (T_{min}, °C), mean (T_{mean}) and maximum (T_{max}) temperature, the daily averages of relative humidity (rH), global radiation (gR, wm^{-2}), and wind speed at 2 m above ground (u_2, ms^{-1}), as well as the observed 24-h precipitation sum (P_{obs}, mm) are required. The phenological module utilizes daily T_{mean} and T_{max}.

For gap filling purposes, data were accessed from the Austrian Meteorological Agency (ZAMG) as well as from the Austrian Hydrographic Service (eHYD). For the EX site, we accessed precipitation records from a private weather station. Missing data were replaced, using simple regression techniques, with data from highly correlated, neighboring stations.

For calibration of the phenological module, data were retrieved from the PEP725 database (PEP725 Pan European Phenology Data, data set accessed on 06/06/2015 at http://www.zamg.ac.at/pep725/). Two phenological stages were considered. (1) BBCH-11: leaf unfolding (LU) on the first visible leaf stalk, represents the onset of the growing season. (2) BBCH-94: autumnal leaf coloring (50% of leaves colored) (LC), marking the end of the growing season. In this work, phenological phases are calculated as functions of day-length and air temperature. Therefore, the gridded E-OBS dataset (a daily gridded observational dataset for meteorological parameters) was accessed (0.5°, regular grid), provided by the European Climate Assessment (ECA&D) (Tank et al. 2002a).

Due to strong site variations of phenological events, the set-up of the phenological model was conducted, utilizing multiple phenological sites within a radius of 200 km, centered to 47°42′00″N, 14°30′00″E (see Fig. 1a). The phenological dataset was scanned for outliers using Tukey's test. Parallel data was checked for month-mistakes (Schaber and Badeck 2002). Only time series with 10 or more annual observations were considered in the calculation. To overcome site specific effects, the influence of phenotypic plasticity (Capdevielle-Vargas et al. 2015), or divergences in the assessment of phenological stages (Estrella and Menzel 2006), the calibration of the model was performed on an assembled time-series. To generate this assembled time-series, we implemented the 3rd method which was proposed in Häkkinen et al. (1995). To each DoY of each time-series a site wise offset (O_s) was applied. The aim was minimizing the residual between site-wise time-series and the mean time-series over all sites:

$$\min_{O_s}\left[\sum_y\sum_s\left(\left(\mathrm{DoY}_{sy}-O_s\right)-\frac{\sum_s\left(\mathrm{DoY}_{sy}-O_s\right)}{n_y}\right)^2\right]. \tag{1}$$

To achieve this, we used the classical hill climber algorithm. 40,000 iterations were used to adapt O_s for all considered sites. The sum of squared residuals could be reduced to approximately 55% of its initial value. To ensure that the residual sum equals zero, the overall mean before and after the optimization was calculated; the difference between both means stated a second offset which was applied to DoY_{sy}:

$$o_n=-\frac{\sum_{sy}O_s}{n_{sy}}. \tag{2}$$

Parallel, a time-series of the average T_{min}, T_{mean} and T_{max} was calculated over all E-OBS grid cells, comprising selected phenological sites, whereat the number of sites within the cell defined the relative weighting the cell received in the calculation of the average.

Model description

Annual phenological key events

Beech can be considered a late flushing species (Vitasse and Basler 2013). By that, it is following a rather conservative strategy, aiming to decrease the risk of late frost exposure (Caffarra and Donnelly 2011; Körner and Basler 2010). There are several environmental signals involved, in the triggering of the start of the growing season. Of high relevance is the seasonal course of the photoperiod (Basler and Körner 2012), meaning the day length has to exceed a critical threshold in spring before bud burst might occur (Körner and Basler 2010). According to Laube et al. (2014), an environmental trigger which is weighted even more strongly, is the chilling demand, meaning winter temperatures, undershooting a threshold for a certain time, are promoting dormancy release in spring. Furthermore, leaf sprouting is accelerated by high spring temperatures (Caffarra and Donnelly 2011; Vitasse et al. 2009).

Compared to spring phenology, the environmental triggering of beech senescence is less understood (Estrella and Menzel 2006; Vitasse et al. 2009). Especially the role of temperature is discussed controversially. For European beech stands, Estrella and Menzel (2006) reported positive correlation of the August and September mean air temperature, with the date of leaf coloring. Surprisingly, the authors found also a negative correlation with temperature in May and June, meaning low average temperatures in late summer and high temperatures in late spring promote the temporal occurrence of leaf senescence. Whether the latter was a direct temperature effect, or the effect of (temperature correlated) drought during critical phenological stages, was not examined.

In this section, a model is presented, describing the onset of the growing season as function of daily air temperature. Assuming the chilling demand generally over-satisfied for central European forest stands (Fu et al. 2012), only the forcing effect of air temperature is considered.

A common approach to quantify the forcing effect of air temperature on spring development requires the definition of a threshold temperature; below this temperature no forcing is taking place, above the temperature forcing is assumed proportional to the temperature difference between actual and threshold temperature (Cannell and Smith 1983). To achieve a more gradual transition of the forcing response to air temperature, a piecewise combination of a first and second order polynomial is presented in this work. The full formulation of the function, which is optically resembling the shape of a hockey stick, is stated in the "Appendix" (Eqs. 18, 23, 24). Below the threshold temperature ($T_{0,\mathrm{LU}}$) the response is assumed 0. The onset is described with a 2nd order polynomial. A second key temperature ($T_{1,\mathrm{LU}}$) defines the transition from quadratic to linear response, where m_{LU} sets the forcing rate at $T_{1,\mathrm{LU}}$. Most approaches for predicting spring phenology as a function of air temperature make use the daily mean temperature. In this work, it was found that the average of daily T_{mean} and T_{max}, aiming to represent the average daytime temperature (T_{day}), displayed higher force of expression in the prediction of LU:

$$f_T=\mathrm{hockey}\left(T_{\mathrm{day}},T_{0,\mathrm{LU}},T_{1,\mathrm{LU}},0,m_{\mathrm{LU}}\right). \tag{3}$$

Analogue to Blümel and Chmielewski (2012), a day length term is included, accounting for the photoperiodic influence on spring development. The day length (*dl*, hours) was calculated as function of the day of the year (DoY) and the geographical latitude, analogue to Swift (1976). A model parameter in the exponent (x_{LU}) adds one degree of freedom. Preventing vast values in the photoperiod term, day length is normalized by dividing by 14 h:

$$f_{dl}=\left(\frac{dl}{14h}\right)^{x_{\mathrm{LU}}}. \tag{4}$$

The daily forcing is described as the product of a function of air temperature and day length:

$$f_{\mathrm{LU}}=f_Tf_{dl}. \tag{5}$$

The temperature accumulation starts with $\mathrm{DoY}_{0,\mathrm{LU}}$. LU is triggered after the accumulation of 10 forcing units:

$$Sf_{\mathrm{DoY1,LU}} = \sum_{\mathrm{DoY}\,=\,\mathrm{DoY}_{0,\mathrm{LU}}}^{\mathrm{DoY}_{1,\mathrm{LU}}} f_{\mathrm{LU,DoY}} = 10. \tag{6}$$

The calibration of the model was conducted on the assembled time-series, described in the previous section. The phenological data which used in this work was provided in discrete daily resolution, but calculating means over several sites led to non-integer values for the day of the year of the phenological event. A model, which is treating phenological events as discrete in time, cannot overcome the residual caused by the decimal places. To surmount this minor but unnecessary flaw, another function is introduced: The difference of the sum, necessary to trigger budburst and the sum of the day prior to budburst, divided by the difference of the sum, achieved on the budburst day and the prior day, minus a half day is calculated:

$$c_{\mathrm{LU}} = \frac{10 - Sf_{\mathrm{DoY1,LU\text{ - }1}}}{Sf_{\mathrm{DoY1,LU}} - Sf_{\mathrm{DoY1,LU\text{ - }1}}} - \frac{1}{2}. \tag{7}$$

A distinct exceeding of the temperature sum, necessary to trigger the event, on $\mathrm{DoY}_{1,\mathrm{LU}}$ will result in a negative value of c_{LU}, Therefore, $\mathrm{DoY}_{\mathrm{LU}}$ will be shifted to a slightly earlier point of time. A weak overshooting will result in a delay of the event. The DoY of leaf unfolding is finally calculated:

$$\mathrm{DoY}_{\mathrm{LU}} = \mathrm{DoY}_{1,\mathrm{LU}} + c_{\mathrm{LU}} \tag{8}$$

The approach for modeling the annual variability of the end of the growing season, is based on the findings of Estrella and Menzel (2006). A linear model is set up, utilizing averaged T_{mean} of 2 seasonal periods ($\mathrm{DoY}_{0,\mathrm{LC}} - \mathrm{DoY}_{1,\mathrm{LC}}$, $\mathrm{DoY}_{2,\mathrm{LC}} - \mathrm{DoY}_{3,\mathrm{LC}}$): (1) late spring and (2) late summer–early autumn. Within these periods, a parabolic function assigns weight (w_{LC}) to the observed T_{mean}:

$$w_{\mathrm{LC}} = \begin{cases} 0, & \mathrm{DoY} \le \mathrm{DoY}_{0,\mathrm{LC}} \\ 4h_{\mathrm{LC}}\frac{(\mathrm{DoY}_{1,\mathrm{LC}}-\mathrm{DoY})(\mathrm{DoY}-\mathrm{DoY}_{0,\mathrm{LC}})}{(\mathrm{DoY}_{1,\mathrm{LC}}-\mathrm{DoY}_{0,\mathrm{LC}})^2}, & \mathrm{DoY}_{0,\mathrm{LC}} < \mathrm{DoY} < \mathrm{DoY}_{1,\mathrm{LC}} \\ 0, & \mathrm{DoY}_{1,\mathrm{LC}} \le \mathrm{DoY} \le \mathrm{DoY}_{2,\mathrm{LC}} \\ 4\frac{(\mathrm{DoY}_{3,\mathrm{LC}}-\mathrm{DoY})(\mathrm{DoY}-\mathrm{DoY}_{2,\mathrm{LC}})}{(\mathrm{DoY}_{3,\mathrm{LC}}-\mathrm{DoY}_{2,\mathrm{LC}})^2} & \mathrm{DoY}_{2,\mathrm{LC}} < \mathrm{DoY} < \mathrm{DoY}_{3,\mathrm{LC}} \\ 0 & \mathrm{DoY} \ge \mathrm{DoY}_{3,\mathrm{LC}} \end{cases}, \tag{9}$$

Due to the fact that senescence dates correlate negatively with T_{mean} in late spring, the parabolic function in the first period yields negative values, with a minimum of h_{LC}. The weighted average T_{mean} (wA_{LC}) inside the temporal window is calculated. Figure S2 in the supplementary information states a graphical representation of the assessment of spring and autumn phenology:

$$wA_{\mathrm{LC}} = \frac{\sum_{i=\mathrm{DoY}_{3\mathrm{LC}}}^{\mathrm{DoY}_{0\mathrm{LC}}} T_{\mathrm{mean},i} w_{\mathrm{LC},i}}{\sum_{i=\mathrm{DoY}_{3\mathrm{LC}}}^{\mathrm{DoY}_{0\mathrm{LC}}} \left|w_{\mathrm{LC},i}\right|}. \tag{10}$$

The annual DoY of LC is then calculated in a linear equation:

$$\mathrm{DoY}_{\mathrm{LC}} = k_{\mathrm{LC}} wA_{\mathrm{LC}} + d_{\mathrm{LC}}. \tag{11}$$

The functions to determine LU and LC were optimized, using a combination of simulated annealing (Kirkpatrick 1984) and the Gauss–Newton algorithm. Performance criterion was the Nash–Sutcliffe efficiency (NSE) (Nash and Sutcliffe 1970):

$$\mathrm{NSE} = 1 - \frac{\sum_{i=1}^{n}\left(\mathrm{obs}_i - \mathrm{sim}_i\right)^2}{\sum_{i=1}^{n}\left(\mathrm{obs}_i - \overline{\mathrm{obs}}\right)^2}. \tag{12}$$

To express the model error in days, the root mean squared error is also calculated:

$$\mathrm{RMSE} = \left[n^{-1}\sum_{i=1}^{n}\left(\mathrm{obs}_i - \mathrm{sim}_i\right)^2\right]^{\frac{1}{2}}. \tag{13}$$

Water balance model

An exhaustive description of the setup and the formulation of the WBM can be found in the supplementary!

Model application

The simulator was parameterized, using time-series of observed soil moisture. We used records of different depths to calculate a mean time-series, aiming to reflect the integrated volumetric soil moisture over soil depth (z_{r}). Averages over a soil depth of 500 mm were calculated for all sites. Both canopy and the snowpack storage were initialized at 0 mm. Soil water storage was initialized at the product of soil depth and the water content at field capacity ($z_{\mathrm{r}}\theta_{\mathrm{fc}}$). The model ran a 200 day spin up, prior to the performance analysis timeframe. Twenty-six parameters (compare Table 3) were optimized by inverse modeling; a simulated annealing algorithm was applied. Performance criterion was the Nash–Sutcliffe efficiency (Eq. 12). The parameterization was performed over the entire investigation timeframe (Table 2).

Water stress assessment

The obtained parameterization was used to run the model over a reference climate period of 30 years. The timeframe was set from Jan 1983 to Dec 2012. Then, eight scenarios of climate warming were applied. Temperatures were increased from 0 to 4 °C in one degree steps. Four scenarios were run under the assumption that (1) phenology retains the values of the reference climate; four scenarios were run with (2) phenology responding to warmer conditions. This way, we wanted to quantify the influence of elongated growing seasons on the stands' water consumption and soil water deficit.

Different levels of water stress were calculated. The transpiration index (T_i) states the daily ratio between simulated actual transpiration and potential transpiration (transpiration which would occur under optimal root water supply) (Clausnitzer et al. 2011; Vilhar 2016). In our formulation, it corresponds to the water stress coefficient ($\mathrm{Kc}_{\mathrm{s,tree}}$) in the calculation of the actual transpiration rate:

$$T_\mathrm{i} = \mathrm{Kc}_{\mathrm{s,tree}} \tag{14}$$

A level of one corresponds to unlimited transpiration, a level of zero would correspond to a complete shutdown of transpiration. Investigating beech stands (Schwärzel et al. 2009) found indications of noteworthy water stress when T_i fell below 70%. Therefore, we set the threshold for (at least) moderate soil water deficit to 0.7. According to Bréda et al. (2006), xylem embolism occurs when stomatal conductance drops below 10% of its initial value. Therefore, a second stress level was calculated: If T_i falls below 0.1, we consider the stand affected by severe drought.

According to Granier et al. (1999), water stress occurs when the relative extractable water content (REW) drops below the critical value of 0.4. REW is calculated by normalizing theta to the interval from the wilting point to field capacity. The formulation, which is presented here, allows soil moisture below the wilting point (θ_{pwp}) and above field capacity (θ_{fc}). Therefore, REW can take values below zero and above 1!

$$\mathrm{REW} = \frac{\theta - \theta_{\mathrm{pwp}}}{\theta_{\mathrm{fc}} - \theta_{\mathrm{pwp}}} \tag{15}$$

Then, the number of days during the growing season with T_i or REW below the defined threshold was calculated. In this assessment, we considered the growing season as interval from the 25th of March (DoY = 84) to the 11th of November (DoY = 315). Years with more than 120 growing season days of $T_\mathrm{i} > 0.7$ were defined as dry years. The threshold for drought years was reached with a minimum of 31 growing season days with T_i below 0.1. At last, to gain information about the stands' photosynthetic activity, we estimated the gross primary production (GPP, $\mathrm{gm}^{-2}\mathrm{d}^{-1}$) as the product of water-use efficiency (WUE) and the transpiration rate:

$$\mathrm{GPP} = E_\mathrm{C}\mathrm{WUE} \tag{16}$$

To estimate the WUE, we relied on an empirical relationship, which was proposed by Tang et al. (2006). The water-use efficiency was calculated as function of the vapor pressure deficit (VPD):

$$\mathrm{WUE} = 4.4 + 15.69\mathrm{e}^{-5.94\mathrm{VPD}}. \tag{17}$$

Results and discussion

Timing of phenological events

Both, spring and autumn phenology showed high intra-annual plasticity. Nevertheless, after transforming the data to an assembled time-series, LU revealed a distinct pattern, with a recent trend towards an earlier onset of the growing season (see Fig. 2a–d). On the contrary to very high intra-annual plasticity, the year to year variations of the winsorized means of LC were smaller compared to LU. The reason no trend towards a delaying of senescence was observed, might be found in the counteracting effect of late spring and late summer temperatures.

The parameterization of the LU module led to a good fit between observed and modeled onset of the growing season (compare Table 1; NSE > 0.89, RMSE < 2 days). A very low modeled $T_{0,\mathrm{LU}}$ (< − 11 °C) seems to be non-meaningful in a plant physiological sense. On the other hand, the simulated effect of temperature forcing at cold conditions is partially nullified by low multiplier values from the day-length term, at the beginning of the forcing period, in early winter (see Fig. S5).

The regression approach, to predict the end of the growing season, utilizing the mean temperature of two temporal windows, was also suitable to reproduce the observed pattern to a sufficient degree (NSE > 0.73, RMSE < 2 days). The mechanism behind the acceleration of senescence by high temperatures in late spring was not elaborated in this work. Nevertheless, two explanatory assumptions are stated: High temperatures in spring point to an early onset of the growing season. This, and the high temperature itself might increase the water consumption, (1) inducing drought during critical phenological stages. (2) High temperatures in late spring might support the development of

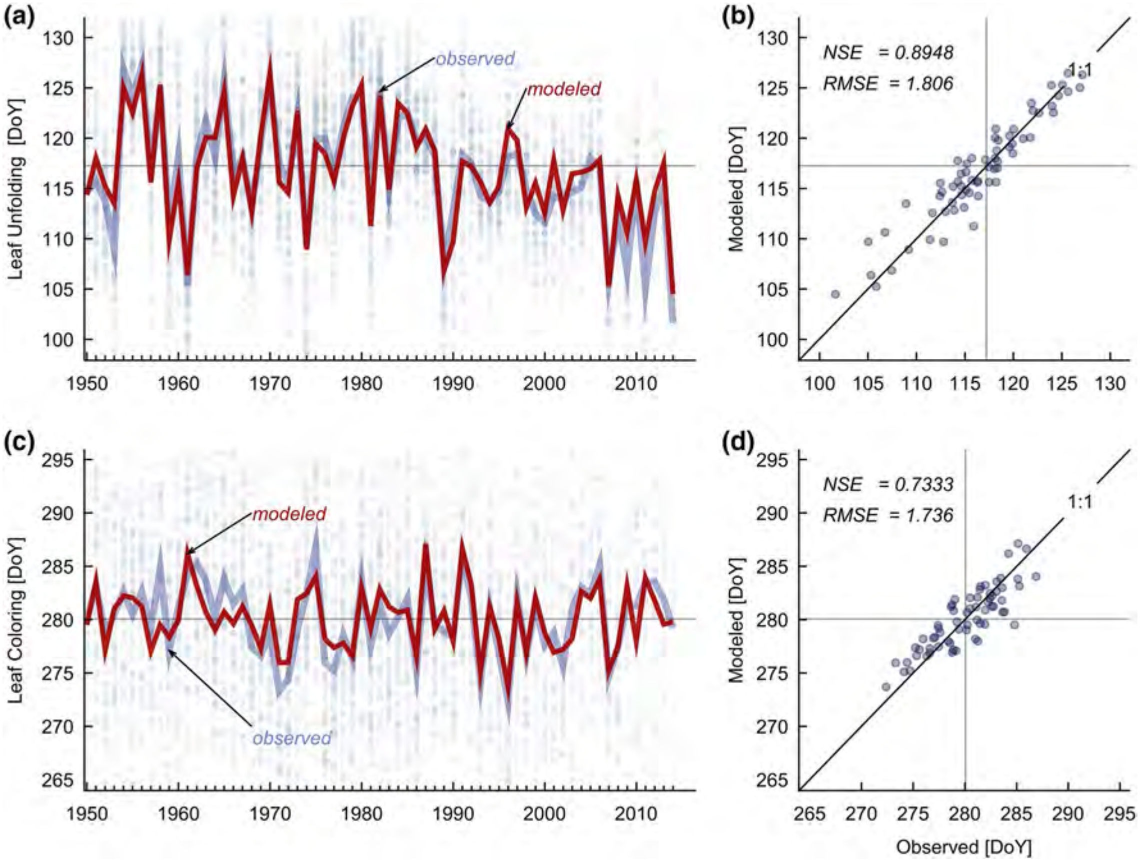

Fig. 2 **a**, **c** The model was fitted to an assembled time-series of annual DoYs (pale solid lines), which were calculated, if more than 10 annual observations (small dots) were available. Leaf unfolding and coloring data were processed analogously (**a**) where LU clearly shows a trend towards earlier onsets of the growing season in last decades, LC (**c**) reveals no such pattern. The reason for this might be found in the counteracting effect of late spring and late summer temperatures. **b**, **d** Observed assembled time-series mean of leaf unfolding and leaf coloring vs. the modeled timing of the event. Details about calculations of Nash–Sutcliffe efficiency (NSE) and root mean squared error (RSME in days) are given in the text

Table 1 Parameterization results of the phenological module

Leaf unfolding		Leaf coloring	
$DoY_{0,LU}$	4.353	$DoY_{0,LC}$	108.451
$T_{0,LU}$	– 10.820	$DoY_{1,LC}$	167.207
$T_{1,LU}$	30.747	$DoY_{2,LC}$	219.214
m_{LU}	0.362	$DoY_{3,LC}$	286.441
x_{LU}	2.921	h_{LC}	– 0.618
		k_{LC}	4.002
		d_{LC}	261.107
n	65	n	65
NSE	0.895	NSE	0.733
RMSE	1.806	RMSE	1.736

Optimization was conducted, using a combination of simulated annealing and the Gauss–Newton algorithm. Performance criterion was the Nash–Sutcliffe model efficiency

specific pest or pathogens, leading to stress induced, premature leaf coloring (see also Menzel et al. 2008).

Water balance

The approaches to describe fog precipitation, precipitation interception, as well as the responses of evapotranspiration and percolation to soil moisture, presented in this work are novel. Therefore, their parameterization cannot be relied on the literature data. Due to unavailability of direct measurements, they were deduced by model optimization, applying broad search ranges. In cases where literature values existed (e.g. degree day factors for snowmelt, field capacity), parameter values were searched in the close proximity of values stated in the literature. On both investigated sites, the optimization process lead to a good fit between the observed

Table 2 The model calibration was conducted, utilizing soil moisture records of the entire model timeframe

Site	Timeframe	*z* (cm)	*n*	NSE	RMSE
Kreisbach	04/14/1999–02/10/2003	00–50	1294	0.9262	0.0132
Klausen-Leopoldsdorf	10/01/2006–09/30/2013	00–50	2262	0.9303	0.0163
Exelberg	10/01/2009–09/30/2012	00–50	33	0.9148	0.0152
Jubiläumswarte	10/01/2009–09/30/2012	00–50	33	0.9225	0.0176

Optimization was performed, using a simulated annealing algorithm. Performance criterion was the Nash–Sutcliffe Efficiency

n number of utilized observations, *NSE* Nash–Sutcliffe Efficiency, *RMSE* root mean squared error (LL^{-1})

Table 3 Parameter optimization results for all 4 investigate sites

Parameter	Description	Unit	KB	KL	EX	JU
rH_0	Lower relative humidity threshold for fog precipitation	rH	99.99	99.99	94.34	93.93
f_c	Fog coefficient		0	0	0.516	0.494
DoY_{CC}	Canopy closure	DoY	221.4	222.9	173.3	180.5
l_{LC}	Duration of leaf senescence	Days	22.88	20.94	25.14	13.60
ID_{LAI}	Indeciduous fraction of leaf area at canopy closure		0.079	0	0	0
$C_{max,LAI0}$	Canopy interception capacity at $Kc_{LAI}=0$	mm	2.221	0.632	0.325	0.309
$C_{max,LAI1}$	Canopy interception capacity at $Kc_{LAI}=1$	mm	4.326	2.701	0.678	1.230
$K_{i,LAI0}$	Interception function shape parameter at $Kc_{LAI}=0$		4.354	3.777	2.665	2.832
$K_{i,LAI1}$	Interception function shape parameter at $Kc_{LAI}=1$		5.342	6.712	4.678	5.339
Kc_{canopy}	Crop coefficient for canopy evaporation		1.102	0.472	0.787	0.822
τ_{LAI0}	Maximum radiation transmittance coefficient at $Kc_{LAI}=0$		0.742	0.701	0.802	0.805
τ_{LAI1}	Minimum radiation transmittance coefficient at $Kc_{LAI}=1$		0.390	0.321	0.319	0.291
T_{snow}	Upper threshold temperature for snowfall	°C	1.388	0.203	1.706	1.509
T_{melt}	Lower threshold temperature for snowmelt	°C	1.972	1.508	1.897	0.938
DDF_{melt}	Degree day factor for snowmelt	mm $°C^{-1}$ day^{-1}	2.165	2.982	0.813	0.686
f_{by}	Water fraction, bypassing the soil box		0.362	0.083	0.437	0.112
k_{sat}	Saturated conductivity	LL^{-1} day^{-1}	0.071	0.038	0.017	0.021
θ_m	Shape parameter for percolation response		0.528	0.728	0.753	0.748
θ_{sat}	Saturated water content	LL^{-1}	0.502	0.520	0.369	0.420
θ_{fc}	Field capacity	LL^{-1}	0.344	0.392	0.285	0.362
θ^*	Upper threshold water content for evapotranspiration limit.	LL^{-1}	0.344	0.410	0.270	0.348
θ_{pwp}	Permanent wilting point, lower threshold for transpiration	LL^{-1}	0.189	0.228	0.085	0.155
θ_{res}	Residual water content, lower threshold for soil evaporation	LL^{-1}	0.008	0.003	0.012	0.003
ET_m	Shape parameter for evapotranspiration response		0.488	0.391	0.422	0.424
Kc_{tree}	Crop coefficient for vegetation at canopy closure		1.361	1.783	0.526	0.857
Kc_{ground}	Crop coefficient for soil evaporation		0.364	0.517	0.209	0.398

and predicted soil water content ($NSE < 0.92.5$); the simulator was capable to track the temporal dynamics of the daily average soil moisture (θ, L L^{-1}), over the whole investigation timeframe (Fig. S6) (Table 2).

In the following section, the parameterization of the WBM is discussed. For the parameter configuration of all 4 sites, see Table 3. On the sites KR and KL, the fog precipitation module had no improving effect on the models' performance. In both cases, the optimization process led to fog coefficient (f_c) values close to zero (see Table 3). The amount, fog is contributing to the total precipitation, seems insignificant at these locations. An explanation might be found in the sites relief; both investigated stands are located at lower hill slopes, partially shielded from (at least) two directions. A different picture was found on the EX and JU site; they are both located at upper hill slopes, close to the hill top, leaving them much more exposed to direct air flow.

The optimization process lead to relatively high parameters values, describing the maximum capacity of canopy storage (C_{max}). For a central European beech stand, Gerrits et al. (2010) reported a canopy C_{max} ranging from 0.4 mm for winter conditions to 0.9 mm in summer. In this work,

Table 4 Breakdown of modeled export fluxes, given as mean annual sums and in percent of the observed precipitation

Site	Kreisbach		Klausen-Leo.		Exelberg		Jubiläumswarte	
n (years)	30		30		30		30	
Unit	mm a^{-1}	%	mm a^{-1}	%	mm a^{-1}	%	mm a^{-1}	%
Precipitation (+ fog)	961.0	100	831.1	100	751.5	100	654.5	100
Fog	0	0	0	0	6.0	0.8	6.8	1.1
Canopy evaporation	202.8	21.7	88.4	10.8	54.4	7.4	68.4	10.7
Infiltration	480.8	49.7	656.4	79.1	386.1	51.5	492.4	75.7
Soil evaporation	106.6	11.6	127.1	15.6	100.1	13.8	189.0	30.1
Transpiration	189.1	19.8	246.3	29.8	174.4	23.5	180.9	27.6
Bypass flow	277.6	28.6	85.5	10	311.1	41.4	93.9	13.9
Percolation	185.1	18.4	283.0	33.7	111.8	14.6	122.9	18.6

the parameterization led to a maximum storage capacity of 4.3 and 2.7 mm for the KB and the KL site, respectively. For the beech stand mentioned above, Gerrits et al. (2010) calculated a litter layer storage capacity with a yearly average of 1.8 mm, temporally peaking in autumn (2.8 mm). So it seems possible, that high $C_{\max}$ might be explained by the contribution of the litter layer to precipitation interception. Soil moisture records, utilized in the calibration process, existed for a minimum depth of 10 cm and 15 cm, for Kreisbach and Klausen-Leopoldsdorf, respectively. It seems also plausible that the canopy interception module accounts for soil water storage/interception, caused by the topmost layer of the mineral soil. An alternative to explain high values for $C_{\max}$ arises from the assessment of precipitation on a daily time-step: The possibility of multiple storms during 1 day is neglected. In such a case, our formulation might underestimate canopy storage (compare Pearce and Rowe 1981). Here, high values for $C_{\max}$ would have a compensating effect. High values for the coefficient, scaling the reference evapotranspiration ($\mathrm{ET_O}$) to canopy evaporation ($\mathrm{Kc_{canopy}}$), could be explained by the low surface resistance of the wet canopy (Herbst et al. 2008). The combination of high $\mathrm{Kc_{canopy}}$ and high $C_{\max}$ values is leading to high interception evaporation (E_{I}) fluxes. On the KB site, deposition chemistry was monitored from the beginning of May 2002 to the end of October 2003 (Berger et al. 2008). In this course, also canopy evaporation fluxes were estimated as the difference between observed open area precipitation and the sum of throughfall and stemflow. A determined annual interception sum of 238 mm (26% of the open area precipitation) is in close resemblance to the estimate of the mean annual interception, presented in this work. On the KL site, throughfall was monitored in a bi-weekly interval from 2006 to 2010. For dormant and growing season, 5.8% and 11.9%, of the observed precipitation was intercepted by the canopy, respectively. For the same temporal interval, the simulation delivered canopy evaporation percentages of 8 and 11.9 for the dormant and growing season, respectively. For different beech stands, Peck and Mayer (1996) reported rainfall interception ranging from 5 to 48% of total precipitation, with a mean of 20%. On our investigated sites, modeled annual rainfall interception (canopy evaporation), was found on the low end of these estimates. Precipitation interception decreased from west to east, reaching its lowest value on the EX site (Table 4).

The calibration process lead to an unremarkable parameterization of the module, describing snow accumulation and snowmelt. Threshold temperatures for snowfall and snowmelt, as well as the degree day factors for snowmelt, were in the range of literature values. For a summary on threshold temperatures for snowfall, see Feiccabrino and Lundberg (2008), a summary on snowmelt degree-day factors for various catchments is given by Hock (2003).

On the KR forest location, an assessment of physical soil characteristics revealed a pore volume 52%, and a volumetric water content of 18.85% at 1 MPa (Schume et al. 2004). The parameterization for this site delivered values for saturation water content (θ_{sat}) and θ_{pwp}, which are located in the close vicinity of the measured ones.

For different beech stands, Peck and Mayer (1996) reported annual transpiration (E_{C}) sums ranging from 268 to 601 with a mean of 363 mm. Our estimations of annual E_{C} were below these values, on all sites (Table 4). Especially on the KR and KL plot, is seems possible that transpiration water fluxes were slightly underestimated in the simulation outcome (Table 4). On the KR plot, beech roots were found at a soil depth of 85 cm (Schmid 2002). On the KL plot, an assessment of the sites soil characteristics revealed medium to strong root penetration down to 65 cm soil depth (Neumann et al. 2001). Due to reasons of soil moisture data availability, only the topmost 50 cm of the mineral soil were considered in this work, neglecting the possible contribution of deeper soil layers to the trees' water supply.

On the KR and especially on the EX plot, the simulator delivered high relative fractions of bypass flow (Table 4).

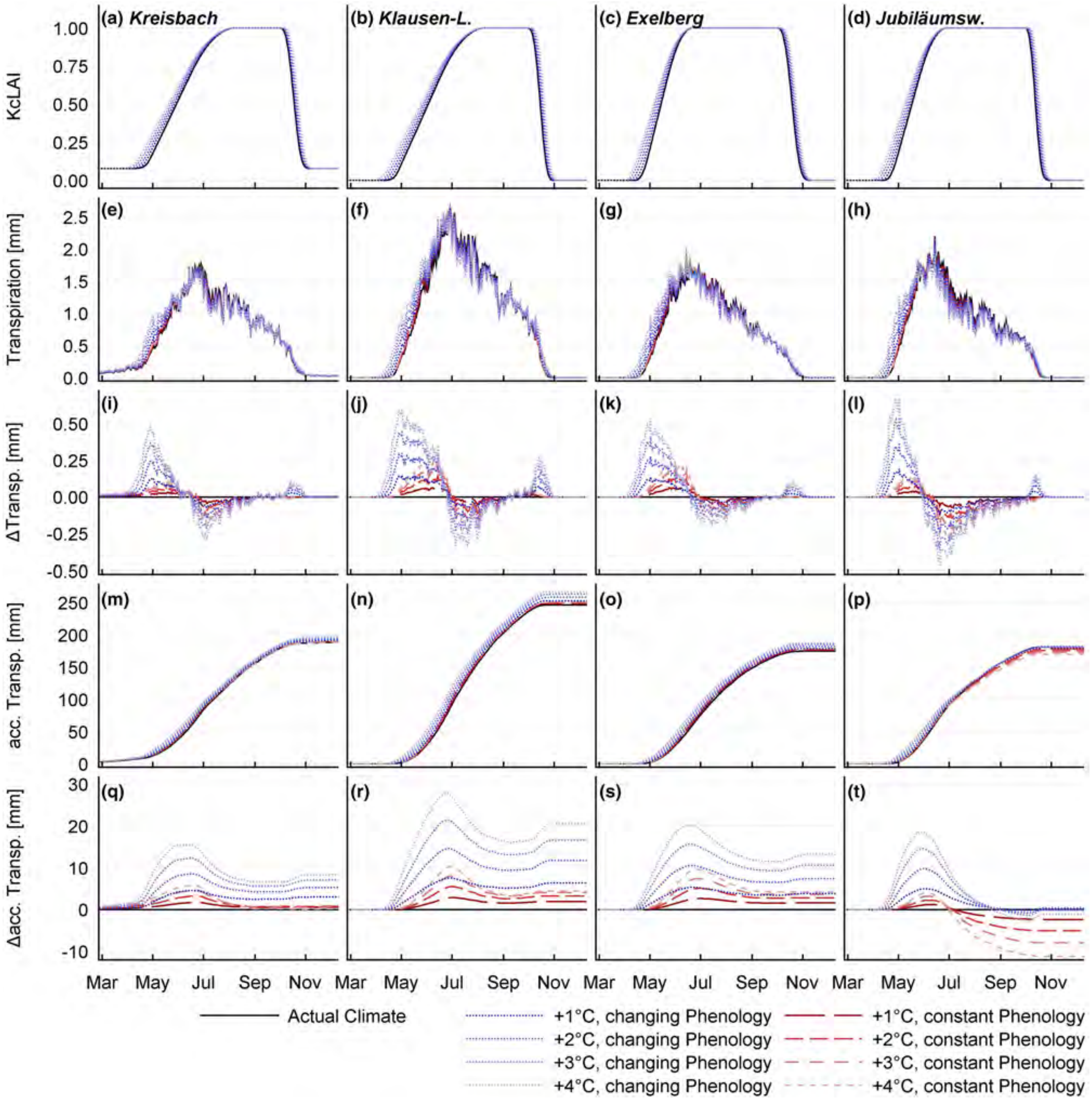

Fig. 3 Result of the temperature sensitivity analysis on day of year base. **a–d** Relative leaf area: One degree temperature rise corresponds roughly to an increase of 4.5 days in growing season length, whereat LU is affected more strongly than LC. **e–h** Mean daily transpiration for all 4 sites: Transpiration is modeled highest at the beginning of summer. The KL site experiences the highest transpiration rates. **i–l** Change of daily transpiration compared to the actual climate: The increase of transpiration at the beginning of the growing season caused by higher temperatures and earlier LU is followed by a marked decrease in summer, due to soil water depletion. **m–p** Accumulated transpiration: The KL site displays the highest annual sums. **q–t** Change of the accumulated transpiration compared to the present climate. Without consideration of elongated growing seasons, the JU site responds with a decline of transpiration due to soil drought in mid-summer. This decline is compensated by the effect of the elongated growing seasons

Analogue to the underestimation of E_C fluxes, the disregarding of the influence of deeper soil layers on the stands' water balance might result in an overestimation of bypass flow.

High transpiration rates during the growing season, in contrast to low evaporative water consumption during the leafless period of the year, are leading to a distinct seasonal pattern of soil moisture. Where in the growing season, θ

above field capacity occurs only exceptional, in the cold part of the year field capacity is rarely undershot, determining percolation through the soil profile as phenomenon of the dormant season (Fig. S7c,d).

Climate change assessment

Step-wisely increased temperatures led to a proportional elongation of the growing season. One °C roughly corresponded to an elongation of 4.7 days. The modeled relationship between warming and lengthening of the growing season was almost linear. All sites responded with a similar pattern (Fig. 3a–d). Spring phenology showed stronger reaction than autumn phenology. One °C warming corresponds to leaf unfolding, 3.5 days earlier. Regarding leaf senescence, the delaying effect of warmer late-summer temperatures was not fully compensated by the accelerating effect of high late-spring temperatures. A temperature increase of 1 °C corresponded to a delay of LC of 1.2 days.

The simulated temperature rise had a strong effect on the stands' water balance. Apparently, higher temperatures during the growing season led to drier soils (Fig. 4a–d). Gaseous water exports increased, while liquid exports decreased. Overall, the soil evaporation partition was affected positively, the percolation water fraction was affected negatively by warmer conditions (Fig. 5a–d). Increased ET was shifting soil moisture to lower levels, favoring the evaporation partition of ET, which is capable to deplete soil water at moisture levels below the wilting point, inducing severe drought.

Under current conditions, the KR and JU site experience frequent dry and drought years (Fig. 5i,l). Here, rising temperatures might lead to a drastic exacerbation of the situation. The reason, that the KR site (which is receiving the highest amount of precipitation) shows a similar behavior as the JU site (which is receiving the lowest annual precipitation sums), can be found in an unfavorable combination of high canopy evaporation rates with high bypass water fluxes (Table 4). At the end, only a small partition of the incoming water is available for plant consumption.

Under current conditions, drought is a rare phenomenon on the KL and EX site (Fig. 5f, g): The KL stand receives relatively high annual precipitation sums. Only a small percentage is lost by interception (Table 4). Paired with a high infiltration capacity, this has a beneficial effect on the stands' water supply. But also here, rising temperatures led to an increase of dry and drought years. Due to the favorable current state, the impact seemed to be less pronounced. It appears paradox, that the driest site experiences the lowest risk for severe soil drought, but the EX forest benefits from a very low modeled wilting point (see Table 3). This is enabling plant water supply at low soil moisture levels (Fig. S8). On this site, severe soil drought does only occur infrequently under present conditions and also rising temperatures lead to no significant increase of the drought risk (Fig. 4 s, w).

An earlier start of the growing season let to higher E_C water fluxes from spring to early summer (Fig. 3i–l). The effect was amplified by high rates of potential evapotranspiration during this period. Early LU had an intensifying effect on soil water stress in summer. As a consequence, the scenarios which considered changes in spring phenology experienced a drastic transpiration drop in mid-summer. On the contrary to soil water stress, extended growing seasons had almost no effect on the frequency and duration of severe drought. On all sites, there was a high probability for moderate soil water deficit ($T_i < 07$) during the entire growing season, with a weakly pronounced maximum at the beginning of summer. On the other hand, the risk for severe drought ($T_i < 0.1$) shows a very distinct peak at the end of August (Fig. 4q–t).

Longer growing seasons are assumed to widen the timeframe for potential C-assimilation (Gunderson et al. 2012; Vitasse et al. 2009). Without consideration of the growing season elongation caused by higher temperatures, all sites responded with decreased annual GPP due to water stress in mid-summer (Fig. 6e–h). In our simulation, prolonged growing seasons led to a marked increase of productivity at early stages of the growing season, followed by a significant depression from July to September (compare also Bergh et al. 2003). Growing season elongations were hardly sufficient to compensate for the productivity drop in mid-summer, caused by soil water stress. Only the EX site exhibits a net gain of GPP due to the combination of higher temperatures and longer growing seasons (Fig. 6o).

Falling in a time of high potential productivity, the extension at the start of the growing season had a stronger effect than the delay of autumn senescence (compare Gunderson et al. 2012).

Conclusion

In this work, a simulator is presented, aiming to depict the water fluxes and the phenological dynamics of beech forest stands. Covering forest sites dominated by deciduous trees, the formulation comprises routines for the inter- and intra-annual dynamics of the vegetation cover. A routine is introduced, calculating fog precipitation as a function of air temperature, relative humidity and wind speed. Furthermore, precipitation interception is calculated, utilizing a function based on the Langmuir isotherm. Soil processes (saturation excess overflow, percolation, soil evaporation, and transpiration) are described, utilizing a zero dimensional box model approach. Despite the strong simplification of the plant–soil system, this approach was sufficient to provide an accurate

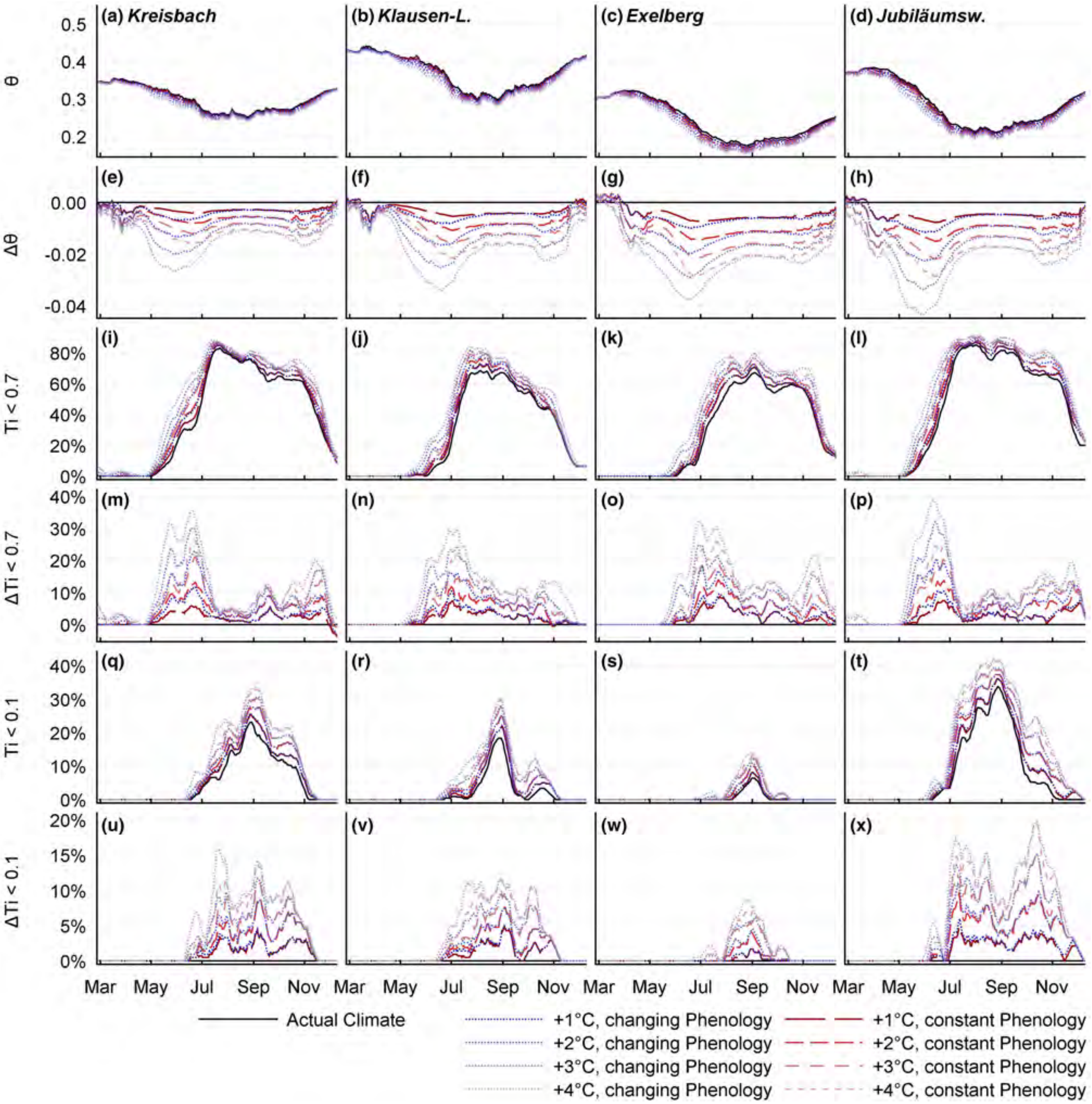

Fig. 4 Result of the temperature sensitivity analysis on day of year base. **a–d** Seasonal course of the relative water content: All sites display the same seasonal dynamics with lowest soil moisture during the growing season. The EX site appears to be strikingly drier than the other sites. **e–h** Changes of soil moisture compared to the present climate: All investigated forest stands are apparently getting drier. The KB and KL site seem to be affected slightly weaker than the other sites. The reduction of soil moisture is most pronounced at the beginning of summer, also amplified by an earlier LU. **i–l** Probability of water stress (defined as $T_i < 0.7$): On all sites, water stress is the usual soil state during the warm season. The highest probability is found in mid-summer. **m–p** Change of the water stress probability, compared to the present state. Warmer temperatures e.g. longer growing seasons increase the risk of soil water stress, especially in early summer. An earlier LU amplifies the probability of water stress, especially at the beginning of summer. **q–t** Risk of severe soil drought (defined as $T_i < 0.1$): All sites show the highest probability of severe drought at the end of August. Although the EX site appears to be the driest site, the risk for severe water stress is strikingly low. The reason can be found in the low wilting point (see Table 3, Fig. S8), allowing transpirative water consumption at low soil moisture. **u–x** Change of drought risk, compared to present conditions: Higher temperatures increase the risk of severe drought on all sites. The KB and JU site show the highest vulnerability. On these sites, a temperature rise of 4 °C more than doubles the probability for severe drought. On the other hand, the elongation of the growing season has almost no impact on the drought risk. The driest site (EX) exhibits the weakest increase in the risk of severe drought

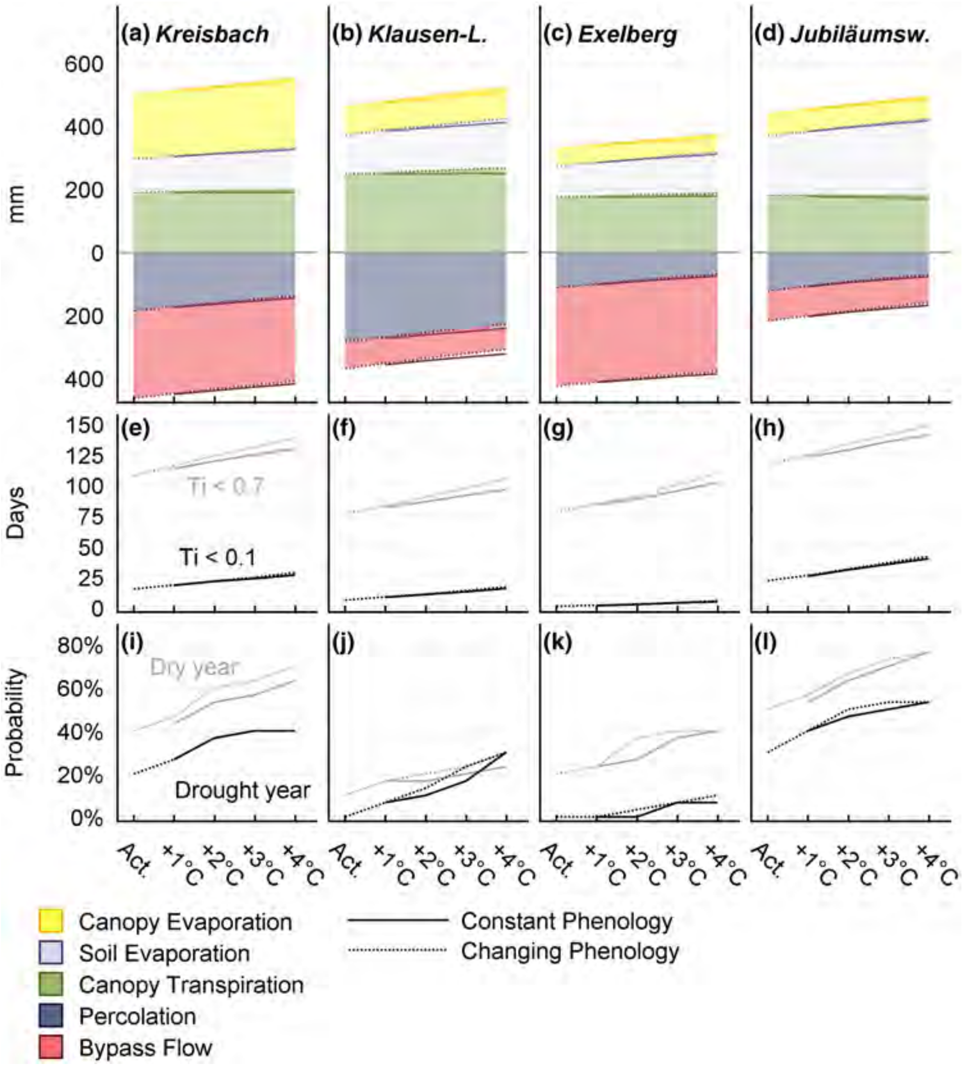

Fig. 5 **a**–**d** The influence of rising temperatures on the stands' annual export flux sums. Liquid and gaseous fluxes are displayed below and above zero, respectively. Warmer temperatures decrease the fraction of percolation, while (unproductive) soil evaporation rises. Although potential evapotranspiration rises, annual transpiration shows almost no response to higher temperature. The reason for this can be found in drier soils, which are favoring soil evaporation. **e**–**h** Days with water stress (defined as $T_i < 0.7$: grey line) and soil drought ($T_i < 0.1$: black line) within the growing season (from 25th March to 11th November): All sites display a distinct increase of dry days per year, with rising temperature. Except on the EX site, higher temperatures lead also to an increased frequency of drought days per year. In both cases, the effect of elongated growing seasons is almost negligible. **i**–**l** We define dry years as years with more than 120 days of $T_i < 0.7$ during the growing season; drought years are defined as years with more than 30 days of $T_i < 0.1$ during the growing season. Under current climate the risk for drought years does not exceed 20%, meaning drought years occur roughly every 5th year. On the KL and EX site, no year fulfilled the criteria for drought years, within the reference climate period. On the EX site, 4 °C warming lead also to no noteworthy increase of drought years. Under current conditions, the KB and JU site are facing the highest risk of severe soil water deficit. Considering an exacerbation due to rising temperatures, it seems possible that these stands might undergo future changes in species composition and productivity

prediction of the vertically integrated soil moisture on both investigated plots. The formulation, which's set up is exhibited in this article and the supplementary, it then used to assess changes in the water balance, caused by increasing temperatures.

Climate change might affect Central European forests in multiple ways. Along with the rise in temperature, the sites will face the effects of changing precipitation patterns, rising atmospheric CO_2 concentration, and the change of frequency, duration and intensity of extreme weather events. On the biotic side, the increased occurrence of pathogens will put even more pressure on forest ecosystems. In this work, we focused solely on the effect of rising temperatures

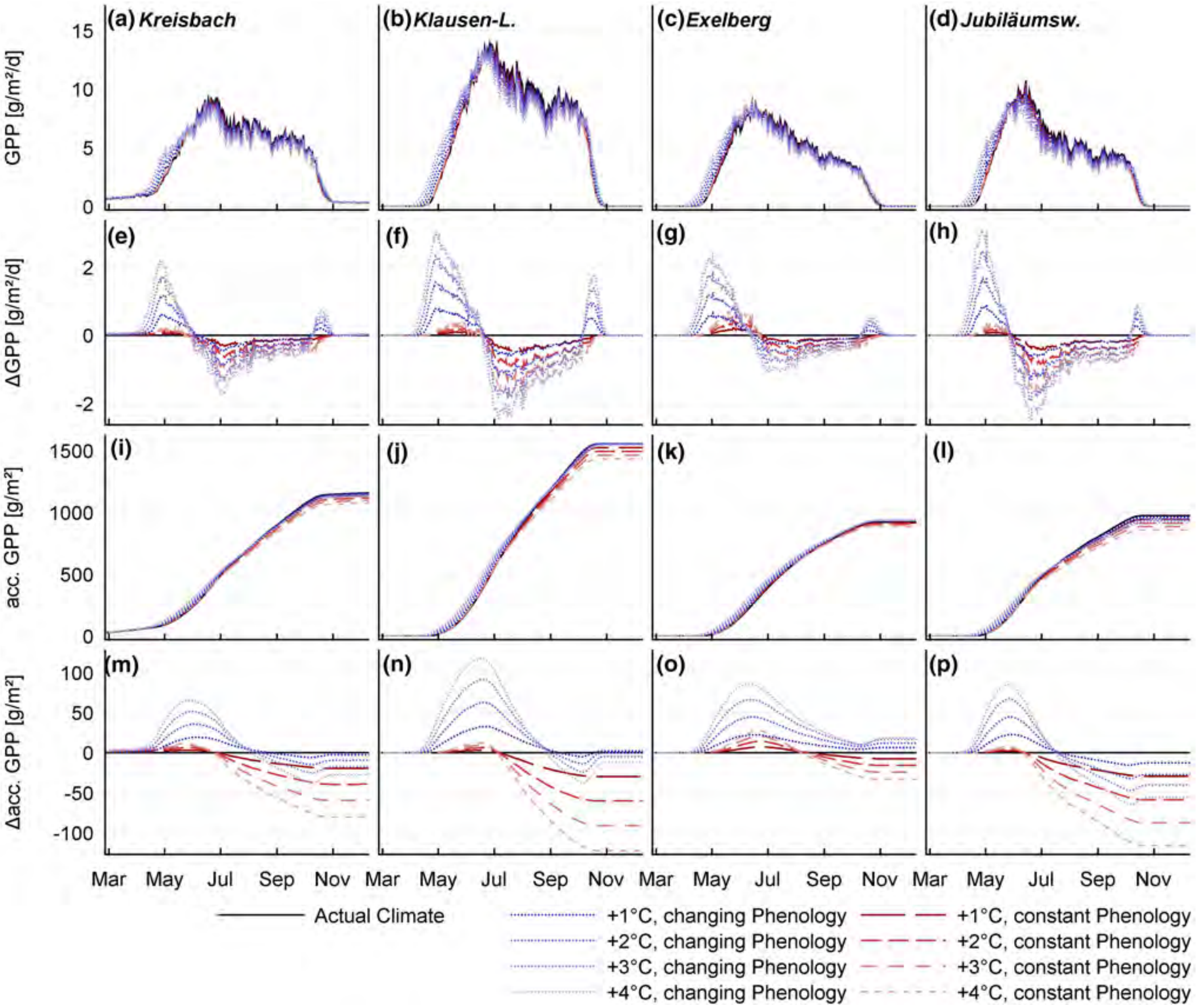

Fig. 6 Gross primary production on a day of year base: GPP was calculated as the product of transpiration water fluxes and the estimated water use efficiency. **a–d** GPP shows a pattern, very similar to transpiration. **e–h** Change of daily GPP compared to the reference scenario: Higher temperatures in spring and earlier LU accelerate the assimilation early in the season, before soil moisture deficit hampers primary production in mid-summer. **i–l** Accumulated GPP over the year: analogue to annual transpiration, the KL plot **j** shows the highest productivity. **m–p** Change of the accumulated primary production to the reference climate period: All warming scenarios show an advance in production in late spring, which dissipates in summer. Without consideration of a change in the growing season length, all warming scenarios respond with decreased annual assimilation. Due to a compensating effect of elongated growing seasons, rising temperatures lead to no net change of the stands' annual primal production. Again, the EX stand represents an exception. It appears paradox that the driest site seems to be also the only site, which might benefit from higher temperatures!

of the stands' water balance. The result of the simulation leads to the suggestion of mitigating measures.

To decrease the impact of drought on the forest stand, Bolte et al. (2007) point out the importance of a deliberate water resource management. They claim, that reduction in the shelterwood (1) decreases the overall water consumption of the stand and the (2) drought risk of overtopped trees. Our modeling work points out the opposite: A reduction of leaf area might lead to reduced water consumption by stand transpiration. On the other hand, unproductive soil evaporation is promoted by the increased aeration and light availability at the forest ground. At soil moisture approaching the wilting point, trees respond by actively shutting down transpiration. Only soil evaporation is capable to cause a noteworthy soil water depletion at soil moisture levels close to the wilting point, inducing severe drought. A dense canopy cover might help to counteract this, by suppressing evaporative fluxes from the soil. In that context, the strict differentiation between moderate soil water deficit and severe soil drought seems reasonable. Soil water deficit during the growing season seems to be a very common state on the investigated sites. It is clearly represented through our simulations that trees decrease their productivity during periods of water stress, but overall, they seem sufficiently adapted to such conditions. Only a strong increase in the frequency of moderate soil water stress might induce a shift in the composition towards species, with higher tolerance to soil water deficit. Severe drought on the other hand, might actively lead to severe damage of the stand (compare Barigah et al. 2013), resulting in more abrupt, or even catastrophic, changes in the appearance of the forest.

Acknowledgements Open access funding provided by Austrian Science Fund (FWF). This research was funded by the Austrian Science Fund (FWF, Project number P23861-B16, granted to TW Berger) and the Commission for Interdisciplinary Ecological Studies (KIÖS) at the Austrian Academy of Sciences (Project number 2010-05, granted to TW Berger). For her active support during the field campaign, we thank Pétra Berger. Level II data from Klausen-Leopoldsdorf was provided by the Austrian Research Centre for Forests. For the provision of meteorological and soil data from the Kreisbach site, which were generated within the framework of the Special Research Program 'Forest Ecosystem Restoration' (SFB 008), we thank Helmut Schume. For the possibility to access air temperature data, the providers in the ECA&D project are acknowledged. For the provision of temperature and precipitation records, we thank the operator of a private weather station, Thomas Huber. Al last, we thank the ZAMG and the Austrian Hydrographic Service (eHYD) for the provision of meteorological data, which was used for gap filling purposes.

Appendix

To achieve sigmoid shape transitions of a variables (x) response (y) inside a window (x_0 to x_1), the 'smoothstep function' (compare Dolschak et al. 2015) was applied in several cases. y_0 and y_1 state left and right threshold responses, respectively. The variable x has to be normalized into an auxiliary variable (t) inside the interval 0–1:

$$t = \frac{x - x_0}{x_1 - x_0}. \tag{18}$$

The transition is described using a third order polynomial:

$$y = \begin{cases} y_0, & x \le x_0 \\ y_0 + (y_1 - y_0)(3t^2 - 2t^3), & x_0 < x < x_1 \\ y_1, & x \ge x_1 \end{cases}. \tag{19}$$

In the article the smoothstep function is stated as:

$$y = \mathrm{smooth}(x, x_0, x_1, y_0, y_1). \tag{20}$$

To alter the shape of the transition, the latter function was modified, by introducing an exponent term:

$$y = \begin{cases} y_0, & x \le x_0 \\ y_0 + (y_1 - y_0)(3t^2 - 2t^3)^{\ln 0.5/\ln m}, & x_0 < x < x_1 \\ y_1, & x \ge x_1 \end{cases}. \tag{21}$$

The parameter m states the relative x position between x_0 and x_1 where the response (y) reaches 50% of the transition from y_0 to y_1. In the article the 'modified smoothstep function' is stated as:

$$y = \mathrm{msmooth}(x, x_0, x_1, y_0, y_1, m). \tag{22}$$

The description of the air temperature dependent forcing of spring phenology uses a combination of a second and first order polynomial. The variable, which is being transformed, has to be normalized to the interval x_0 to x_1, using Eq. 18.

$$y = y_0 + (y_1 - y_0)\begin{cases} 0, & x \le x_0 \\ t,^2 & x_0 < x < x_1 \\ 2t - 1, & x \ge x_1 \end{cases} \tag{23}$$

In the paper, the function, which is optically resembling the shape of a hockey stick, is stated as:

$$y = \mathrm{hockey}(x, x_0, x_1, y_0, y_1). \tag{24}$$

We calculate precipitation interception using a function, based on the Langmuir sorption isotherm. I states interception, $C_{\max}$ the maximum charge of the canopy, K_{i} the shape parameter and T throughfall:

$$I = \frac{K_{\mathrm{i}} C_{\max} T}{1 + K_{\mathrm{i}} T}. \tag{25}$$

Substituting Interception with the difference of precipitation (R) and throughfall yields:

$$R - T = \frac{K_{\mathrm{i}} C_{\max} T}{1 + K_{\mathrm{i}} T}. \tag{26}$$

Avoiding the intricacies of an implicit formulation, we solve the equation for throughfall:

$$T = \frac{\sqrt{K_{\mathrm{i}}^2 (C_{\max} - R)^2 + 2K_{\mathrm{i}}(C_{\max} + R) + 1} + K_{\mathrm{i}}(R - C_{\max}) - 1}{2K_{\mathrm{i}}}. \tag{27}$$

In the article this 3-argument function is stated as:

$$T = \mathrm{tru}(R, C_{\max}, K_{\mathrm{i}}). \tag{28}$$

References

Barigah TS et al (2013) Water stress-induced xylem hydraulic failure is a causal factor of tree mortality in beech and poplar. Ann Bot Lond 112:1431–1437

Basler D, Körner C (2012) Photoperiod sensitivity of bud burst in 14 temperate forest tree species. Agric Forest Meteorol 165:73–81. https://doi.org/10.1016/j.agrformet.2012.06.001

Berger TW, Untersteiner H, Schume H, Jost G (2008) Throughfall fluxes in a secondary spruce (*Picea abies*), a beech (*Fagus sylvatica*) and a mixed spruce–beech stand. Forest Ecol Manag 255:605–618

Bergh J et al (2003) Modelling the short-term effects of climate change on the productivity of selected tree species in Nordic countries. Forest Ecol Manag 183:327–340

Blümel K, Chmielewski FM (2012) Shortcomings of classical phenological forcing models and a way to overcome them. Agric Forest Meteorol 164:10–19. https://doi.org/10.1016/j.agrformet.2012.05.001

Bohn U, Gollub G, Hettwer C, Neuhäuslova Z, Raus T, Schlüter H, Weber H (2004) Map of the natural vegetation of Europe. Federal Agency for Nature Conservation, Bonn

Bolte A et al (2009) Adaptive forest management in central Europe: climate change impacts, strategies and integrative concept. Scand J Forest Res 24:473–482

Bolte A, Czajkowski T, Kompa T (2007) The north-eastern distribution range of European beech—a review. Forestry 80:413–429

Bréda N, Huc R, Granier A, Dreyer E (2006) Temperate forest trees and stands under severe drought: a review of ecophysiological responses, adaptation processes and long-term consequences. Ann Forest Sci 63:625–644

Caffarra A, Donnelly A (2011) The ecological significance of phenology in four different tree species: effects of light and temperature on bud burst. Int J Biometeorol 55:711–721. https://doi.org/10.1007/s00484-010-0386-1

Cannell M, Smith R (1983) Thermal time, chill days and prediction of budburst in *Picea sitchensis*. J Appl Ecol 1:951–963

Capdevielle-Vargas R, Estrella N, Menzel A (2015) Multiple-year assessment of phenological plasticity within a beech (*Fagus sylvatica* L.) stand in southern Germany. Agric Forest Meteorol 211:13–22

Ciais P et al (2005) Europe-wide reduction in primary productivity caused by the heat and drought in 2003. Nature 437:529–533

Clausnitzer F, Köstner B, Schwärzel K, Bernhofer C (2011) Relationships between canopy transpiration, atmospheric conditions and soil water availability—analyses of long-term sap-flow measurements in an old Norway spruce forest at the Ore Mountains/Germany. Agric Forest Meteorol 151:1023–1034

Dittmar C, Zech W, Elling W (2003) Growth variations of common beech (*Fagus sylvatica* L.) under different climatic and environmental conditions in Europe—a dendroecological study. Forest Ecol Manag 173:63–78

Dolschak K, Gartner K, Berger TW (2015) A new approach to predict soil temperature under vegetated surfaces. Model Earth Syst Environ 1:1–14. https://doi.org/10.1007/s40808-015-0041-2

EEA (2015) Global and European temperatures. http://www.eea.europa.eu/data-and-maps/indicators/global-and-european-temperature-1/assessment. Accessed 06 Feb 2016

Ellenberg H, Leuschner C (1996) Vegetation Mitteleuropas mit den Alpen, vol 1095. Ulmer, Stuttgart

Estrella N, Menzel A (2006) Responses of leaf colouring in four deciduous tree species to climate and weather in Germany. Clim Res 32:253–267

Feiccabrino J, Lundberg A (2008) Precipitation phase discrimination in Sweden. In: Pomeroy J (ed) 65th Eastern Snow Conference, Fairlee (Lake Morey), Vermont, USA, pp 239–254

Field CB et al (2014) IPCC, summary for policymakers climate change 2014: impacts, adaptation, and vulnerability Part A: global and sectoral aspects. In: Contribution of working group II to the fifth assessment report of the intergovernmental panel on climate change, pp 1–32

Fu YSH, Campioli M, Van Oijen M, Deckmyn G, Janssens IA (2012) Bayesian comparison of six different temperature-based budburst models for four temperate tree species. Ecol Model 230:92–100. https://doi.org/10.1016/j.ecolmodel.2012.01.010

Gerrits A, Pfister L, Savenije H (2010) Spatial and temporal variability of canopy and forest floor interception in a beech forest Hydrol Process 24:3011–3025

Geßler A, Keitel C, Kreuzwieser J, Matyssek R, Seiler W, Rennenberg H (2007) Potential risks for European beech (*Fagus sylvatica* L.) in a changing climate. Trees 21:1–11

Granier A, Bréda N, Biron P, Villette S (1999) A lumped water balance model to evaluate duration and intensity of drought constraints in forest stands. Ecol Model 116:269–283

Gunderson CA, Edwards NT, Walker AV, O’Hara KH, Campion CM, Hanson PJ (2012) Forest phenology and a warmer climate-growing season extension in relation to climatic provenance. Glob Change Biol 18:2008–2025

Häkkinen R, Linkosalo T, Hari P (1995) Methods for combining phenological time series: application to bud burst in birch (Betula pendula) in Central Finland for the period 1896–1955. Tree Physiol 15:721–726

Herbst M, Rosier PT, McNeil DD, Harding RJ, Gowing DJ (2008) Seasonal variability of interception evaporation from the canopy of a mixed deciduous forest. Agric Forest Meteorol 148:1655–1667

Hock R (2003) Temperature index melt modelling in mountain areas. J Hydrol 282:104–115. https://doi.org/10.1016/S0022-1694(03)00257-9

IUSS Working Group W (2006) World reference base for soil resources, vol 103. World Soil Resources Report, Rome, Italy

Kirkpatrick S (1984) Optimization by simulated annealing—quantitative studies. J Stat Phys 34:975–986. https://doi.org/10.1007/Bf01009452

Kljun N et al (2007) Response of net ecosystem productivity of three boreal forest stands to drought. Ecosystems 10:1039–1055

Kölling C, Zimmermann L, Walentowski H (2007) Klimawandel: was geschieht mit Buche und Fichte. AFZ-DerWald 11:584–588

Körner C, Basler D (2010) Phenology under global warming. Science 327:1461–1462. https://doi.org/10.1126/science.1186473

Kunstmann H, Schneider K, Forkel R, Knoche R (2004) Impact analysis of climate change for an Alpine catchment using high resolution dynamic downscaling of ECHAM4 time slices. Hydrol Earth Syst Sci Discuss 8:1031–1045

Laube J, Sparks TH, Estrella N, Höfler J, Ankerst DP, Menzel A (2014) Chilling outweighs photoperiod in preventing precocious spring development. Glob Change Biol 20:170–182. https://doi.org/10.1111/gcb.12360

Lindner M et al (2010) Climate change impacts, adaptive capacity, and vulnerability of European forest ecosystems. Forest Ecol Manag 259:698–709

Mayer H, Holst T, Brugger U, Kirchassner A (2005) Trends of the forest significant climate variables air temperature and precipitation in south-west Germany from 1950 to 2000. Allg Forst Jagdztg 176:45–56

Menzel A, Estrella N, Heitland W, Susnik A, Schleip C, Dose V (2008) Bayesian analysis of the species-specific lengthening of the growing season in two European countries and the influence of an insect pest. Int J Biometeorol 52:209–218

Mucina L, Grabherr G, Ellmauer T (1993) Die Pflanzengesellschaften Österreichs. Teil 3: Wälder und Gebüsche. Gustav-Fischer, Jena

Nash JE, Sutcliffe JV (1970) River flow forecasting through conceptual models part I—a discussion of principles. J Hydrol 10:282–290

Neumann M et al (2001) Waldzustandsmonitoring in Österreich: Ergebnisse der Intensivbeobachtungsflächen (Level II). Forstliche Bundesversuchsanstalt, Wien

Pearce AJ, Rowe LK (1981) Rainfall interception in a multi-storied, evergreen mixed forest: estimates using Gash's analytical model. J Hydrol 49:341–353

Peck A, Mayer H (1996) Einfluss von Bestandesparametern auf die Verdunstung von Wäldern. Forstwissenschaftliches Centralblatt vereinigt mit Tharandter forstliches Jahrbuch 115:1–9

Rennenberg H, Seiler W, Matyssek R, Gessler A, Kreuzwieser J (2004) Die Buche (*Fagus sylvatica* L.)–ein Waldbaum ohne Zukunft im südlichen Mitteleuropa. Allgemeine Forst-und Jagdzeitung 175:210–224

Richardson AD, Keenan TF, Migliavacca M, Ryu Y, Sonnentag O, Toomey M (2013) Climate change, phenology, and phenological control of vegetation feedbacks to the climate system. Agric Forest Meteorol 169:156–173

Schaber J, Badeck F-W (2002) Evaluation of methods for the combination of phenological time series and outlier detection. Tree Physiol 22:973–982

Schmid I (2002) The influence of soil type and interspecific competition on the fine root system of Norway spruce and European beech. Basic Appl Ecol 3:339–346

Schume H, Jost G, Katzensteiner K (2003) Spatio-temporal analysis of the soil water content in a mixed Norway spruce (Picea abies (L.) Karst.)—European beech (*Fagus sylvatica* L.) stand. Geoderma 112:273–287. https://doi.org/10.1016/s0016-7061(02)00311-7

Schume H, Jost G, Hager H (2004) Soil water depletion and recharge patterns in mixed and pure forest stands of European beech and Norway spruce. J Hydrol 289:258–274

Schwärzel K et al (2009) A novel approach in model-based mapping of soil water conditions at forest sites. Forest Ecol Manag 258:2163–2174

Sutmöller J, Spellmann H, Fiebiger C, Albert M (2008) Der Klimawandel und seine Auswirkungen auf die Buchenwälder in Deutschland. The effects of climate change on beech forests in Germany. Ergebnisse angewandter Forschung zur Buche 3:135–158

Swift LW (1976) Algorithm for solar-radiation on mountain slopes. Water Resour Res 12:108–112. https://doi.org/10.1029/Wr012i001p00108

Tang J, Bolstad PV, Ewers BE, Desai AR, Davis KJ, Carey EV (2006) Sap flux-upscaled canopy transpiration, stomatal conductance, and water use efficiency in an old growth forest in the Great Lakes region of the United States. J Geophys Res Biogeosci 111:1–12

Tank AMGK et al (2002a) Daily dataset of 20th-century surface air temperature and precipitation series for the European Climate Assessment. Int J Climatol 22:1441–1453. https://doi.org/10.1002/joc.773

Tank AMGK et al (2002b) Daily dataset of 20th-century surface air temperature and precipitation series for the European Climate Assessment. Int J Climatol. https://doi.org/10.1002/joc.773

Theurillat J-P, Guisan A (2001) Potential impact of climate change on vegetation in the European Alps: a review. Clim Change 50:77–109

van Wijk MT, Williams M (2005) Optical instruments for measuring leaf area index in low vegetation: application in Arctic ecosystems. Ecol Appl 15:1462–1470. https://doi.org/10.1890/03-5354

Vilhar U (2016) Comparison of drought stress indices in beech forests: a modelling study. Iforest 9:e1–e8

Vitasse Y, Basler D (2013) What role for photoperiod in the bud burst phenology of European beech. Eur J Forest Res 132:1–8. https://doi.org/10.1007/s10342-012-0661-2

Vitasse Y, Porte AJ, Kremer A, Michalet R, Delzon S (2009) Responses of canopy duration to temperature changes in four temperate tree species: relative contributions of spring and autumn leaf phenology. Oecologia 161:187–198. https://doi.org/10.1007/s00442-009-1363-4

Affiliations

Klaus Dolschak[1] · **Karl Gartner**[2] · **Torsten W. Berger**[1]

[1] Department of Forest- and Soil Sciences, Institute of Forest Ecology, University of Natural Resources and Life Sciences (BOKU), Peter Jordan-Straße 82, 1190 Vienna, Austria

[2] Department of Forest Ecology and Soil, Federal Research and Training Centre for Forests, Natural Hazards and Landscape, Seckendorff-Gudent-Weg 8, 1131 Vienna, Austria

10.3 Ad Sulfur Biogeochemistry: *Modeling the sulfur biogeochemistry of beech (Fagus Sylvatica L.) stands in the Vienna Woods*

https://link.springer.com/article/10.1007%2Fs40808-020-00770-5

Modeling Earth Systems and Environment (2020) 6:1557–1572
https://doi.org/10.1007/s40808-020-00770-5

ORIGINAL ARTICLE

Modeling the biogeochemistry of sulfur in beech (*Fagus sylvatica* L.) stands of the Vienna Woods

Klaus Dolschak[1] · **Torsten W. Berger**[1]

Received: 12 December 2019 / Accepted: 2 April 2020 / Published online: 12 May 2020

Abstract

In this article, we describe the setup and the application of a novel Sulfur Dynamics Model (SDM), with the aim to identify and quantify processes, which are crucial for the understanding of the biogeochemical sulfur (S) cycle of forest ecosystems. The simulator takes into account abiotic processes as well as biotic interactions between atmosphere, plant and soil. We applied the model to two Austrian beech stands where deposition of S and soil solution chemistry were monitored intensively over a two-year period. Under consideration of high historic loads and the more recent recession of atmospheric S deposition, we found a suitable model configuration where it was possible to assign both intra-annual fluctuations of the SO_4-S in soil solution and long-time trends in the stream discharge to specific S transformation processes. We identified the interplay of microbial immobilization (the microbial conversion of solute sulfate to organic soil S) and mineralization as key driver of short-term fluctuations in the soil solution. In the long term, the delayed release of historically accumulated S is driven mainly by the slow mineralization of S rich plant biomass, recalcitrant to decomposition. Adsorption and desorption processes seem to play only a negligible role on our investigated stands. We conclude that our proposed model which is based on the current understanding of S biogeochemistry is sufficient to describe S dynamics on the investigated forest stands. The code file (SAS) for all model functions will be provided by the authors after request.

Keywords Sulfur deposition · Occult deposition · Sulfur biogeochemistry · SO_4 soil solution · Nutrient balance model · Simulated annealing

Introduction

During the Twentieth century, Central European forest ecosystems received high loads of atmospheric S. Several reasons led to a sharp decrease in S emissions and accordingly deposition, starting in the late 1980s. From 1990 to 2016, sulfur emissions could be reduced by 81% in Austria (Umweltbundesamt 2018). This decrease was assignable to policy-driven shifts in the energy sector, mainly the reduction in the use of S-rich fossil fuel, coupled with the installation of end-of-pipe technology. With declining emission, also the deposition load to forest ecosystems decreased. In the period from 1984 to 2013 throughfall (plus stemflow) fluxes for an Austrian beech stand sank from 2.3 to 0.6 g m^{-2} $year^{-1}$ (Berger and Muras 2016). However, the observed drop was only poorly reflected in the catchment output of most forest sites (Alewell 2001; Alewell et al. 2001; Pannatier et al. 2011; Prechtel et al. 2001). Similar patterns were also reported from Northern America: The observed decline of acid deposition was, in most cases, not accompanied with a decline of acidifying agents in the stream output of the investigated catchments (Watmough et al. 2005). This was in strong contrast to the prediction of, at that time, state-of-the-art ecosystem simulators, which forecasted a relatively fast response of solution and stream chemistry after a change in the deposition regime. Likens et al. (2002) postulated 4 mechanisms, explaining a negative input/output balance of S: (1) the release of S by bedrock weathering, (2) a net release from the ion adsorber, (3) the excess mineralization of historically accumulated organic S or (4) the underestimation of dry S deposition. Studies of the isotopic composition of the atmospheric S input and the catchment S output clearly pointed toward an organic source (Novák et al.

✉ Torsten W. Berger
torstern.berger@boku.ac.at

[1] Department of Forest- and Soil Sciences, Institute of Forest Ecology, University of Natural Resources and Life Sciences (BOKU), Peter Jordan-Straße 82, 1190 Vienna, Austria

2000). Especially for catchments which received high historic loads of anthropogenic S, the isotopic composition of the stream discharge showed higher portions of ^{32}S than the atmospheric input. Plants and soil microflora generally prefer the lighter ^{32}S isotope toward the heavier, less abundant ^{34}S (Mitchell et al. 2001; Zhang et al. 1998). Sulfur, which was biologically incorporated into organic material during phases of high deposition, was now being released steadily, in form of SO_4-S by mineralization. Novák et al. (2000) state that a considerable amount of the atmospherically deposed S is cycled through the biosphere before being given off to the soil solution and the stream discharge. Ecosystem models such as MAGIC, SMART, SAFE or CHESS describe S storage and release based solely on sorption isotherms (compare Alewell 2001). They share their neglect in the possibility of biotic S cycling and the storage of S incorporated in an organic pool. In an attempt to model the stream chemistry of the output of a forested catchment in Germany with the MAGIC model, it was necessary to introduce an additional S source (968 mg m^{-2} yr^{-1}) to match the simulated with the observed stream discharge (Prechtel et al. 2003). Gbondo-Tugbawa et al. (2001) found that the introduction of a plant S uptake and a mineralization module considerably increased the performance of the PnET-BGC model in describing the SO_4-S output of a forested catchment.

In this work, we introduce a novel biogeochemical model to describe S dynamics of temperate deciduous forest stands. Besides the assessment of geochemical dynamics, we lay emphasis on biotic interactions: In addition to plant uptake, litterfall and the release of S via mineralization of plant organic material, we try to assess microbial immobilization (the microbial conversion of soil solution sulfate to organically bond S) in the forest soil as a crucial part of the biogeochemical S cycle. The model is applied to two beech stands in eastern Austria where deposition and solution chemistry were monitored closely over a two-year period. In this work, we try to answer the following questions:

- Is it possible to derive a model configuration that delivers a plausible representation of the current state of the investigated sites and of the observed temporal pattern in the soil solution?
- Does this model configuration provide insight, which biogeochemical processes are the key drivers of the observed intra-annual pattern in the SO_4-S soil solution?
- Furthermore, is the simulator, which is calibrated on data from a very narrow timeframe, capable to provide a reasonable perspective regarding the future development of the stands' S budget and balance? How long does it take for the stream discharge of S to decline to a pre-industrial level? Is a new steady state (balance between S input and S output) foreseeable within the model timeframe?

Materials and methods

Study sites

The investigated forest stands are located in the north-easterly part of Austria at the eastern edge of the Vienna Woods (see Fig. 1). The parent material for soil formation is Flysch, which consists of old tertiary and mesozoic sandstones and clayey marls of maritime origin. Due to a high clay content, the saturated hydraulic conductivity is low, leading to frequent episodes of waterlogging. Therefore, the soil type is classified as Stagnic Cambisol according to the WRB soil classification (IUSS Working Group 2006), throughout both studied sites. The mean annual temperature in the study area is approximately 9 °C. The average annual precipitation is 660 mm (Wien–Hohe Warte).

The first site Exelberg (E) is located in Lower Austria close to the border to Vienna (48°14′40″ N, 16°15′18″ E), at an elevation of 460 m a. s. l. This site is a pure beech stand. We estimated its age to approximately 100 years. The stand is facing SE with an inclination of 22%. The second site Jubiläumswarte (J) is located within the municipal area of Vienna at the eastern edge of the Vienna Woods (48°13′12″ N, 16°15′56″ E), 2.8 km southeast of E, at an elevation of 440 m a. s. l. The site, which is also a pure beech stand with an estimated age of 125–150 years, is also facing SE, with an inclination of 15%. As a matured stand, it is showing signs of collapse but also strong natural regeneration. In contrast to the E stand, the bedrock of the J site contains calcareous material, reflected in higher base saturation and soil pH. Both forest stands are located at upper hill slopes, close to the hilltop. Due to their southeasterly exposition they are very susceptible to direct air flow, coming from the urban area of Vienna. Further details about forest site, stand and soil characteristics are given in Hanousek et al. (2017).

Data sources

The simulator, which we outline in this work, runs on a daily timestep. Therefore, all input data must be provided in daily resolution. Sulfur enters and leaves the soil system mainly in aqueous solute form. To describe the short-term dynamics of S in the soil, we simulate water balance and water fluxes, using the formulation of the Water Balance Model (WBM) presented in the supplementary of Dolschak et al. (2019). We ran the WBM using meteorological input data from the weather station Jubiläumswarte (100 m distant from J) obtained from the Zentralantalt für Meteorologie und Geodynamik (ZAMG). The meteorological

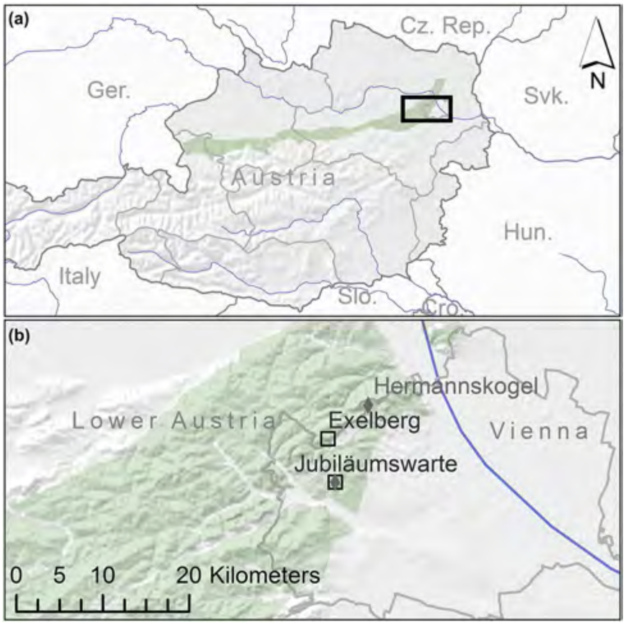

Fig. 1 **a** Location of the investigated sites in Lower Austria and Vienna. Both sites share the bedrock Flysch (darker band area, crossing Northern Austria) and several other site characteristics. **b** Both forest stands (squares) are located at upper hill slopes, close to the ridge, facing SE. Due to the sites' microrelief, in combination with the immediate proximity to the urban area of Vienna, they are deemed very susceptible for pollution-enriched air flow from south to easterly directions. Weather information and SO_2 data (diamonds) were obtained mainly from Jubiläumswarte and Hermannskogel

record of the mentioned station starts in 2011. For the timeframe before that year, we created a synthetic weather time series using neighboring stations with longer records; outside the timeframe with measured data, we applied a weather generator to create a synthetic record. We used the daily mean air temperature and snapshot measurements of soil temperature to generate a continuous record of soil temperature. The approach plus its parameterization is described in Dolschak et al. (2015). To determine the timing of the stands' phenological key events, we used the phenological module, which is also presented in Dolschak et al. (2019).

Both investigated sites were monitored from April 2010 to June 2012 in a biweekly interval. Precipitation water was collected in the open field (bulk precipitation), as well as after the passage through the canopy (throughfall). A funneling apparatus was installed on one tree per site to collect stemflow. Soil solution lysimeters were installed at 10, 30 and 50 cm soil depth, each in 5 replications per site. Snapshot measurements of soil moisture (TDR-Trase) and soil temperature were taken in the course of the biweekly sample collection. Water samples (precipitation and soil solution) were analyzed for SO_4-S content via ion chromatography (Dionex DX 500, USA).

Daily mean values of the aerial SO_2 concentration were obtained from the Umweltbundesamt (Wiener Umweltschutzabteilung—MA 22 Luftmessnetz), for the site Hermannskogel, ranging back to the year 1988. To extrapolate these data to the pre-industrial era, we used a time series of the estimated SO_4-S deposition, derived by Schöpp et al. (2003). This time series was normalized to a value of one for the period with existing data (compare Fig. 2b). Outside the timeframe, we multiplied the normalized estimate with the Day of Year (DoY) mean from the measured period. The data estimates range back to 1880. The dataset also comprises estimates for the near future. For our purposes, we chose the CLE (Current Legislation Emission) scenario. Outside the defined timeframe, we extended the time series, assuming static conditions before the first and after the last year of prognosis.

On both sites, bulk precipitation deposition of SO_4-S (open field) was sampled from April 2010 to June 2012 in a biweekly interval. To achieve a daily resolution, we prorated the collected amount proportionally to the measured amount of daily precipitation. For the extension of deposition to the time period before measured data were available, we used a similar approach as with the SO_2 air concentration (Fig. 2c).

Model description

Disregarding S inputs from dry deposition and gaseous losses, S enters and leaves the undisturbed forest ecosystem mainly in aqueous solute form SO_4^{2-} (Likens et al. 2002). Consequently, there is a strong link between biogeochemical S balance and the hydrologic balance. Also the S uptake by plants, the mineralization of S-containing biomass (Moyano et al. 2012; Sierra et al. 2015) as well as other microbially mediated S transformations in the soil are assumed to show a strong response to soil moisture (Aulakh et al. 2002; Janzen and Bettany 1987; Solberg et al. 2005). Therefore, an expedient description of the water balance seems crucial for modeling the S dynamics of a forest stand.

The simulator, which we outline in this article, works as an extension to the WBM; running the Sulfur Dynamics Model (SDM) requires the output of the WBM. Additional to that, the simulator requires daily information about SO_4-S inputs via wet deposition above the canopy. To calculate the amount of dry and occult deposition, the daily mean SO_2 air concentration is required. For the calculation of biological S transformations in the soil, the mean daily soil temperature of the soil is required. All other required input data are derived from the output of the WBM simulation. Fluxes, associated with the solute phase of S (canopy interception, snow dynamics, infiltration, bypass flow, percolation), are fully controlled by the associated water fluxes, defined

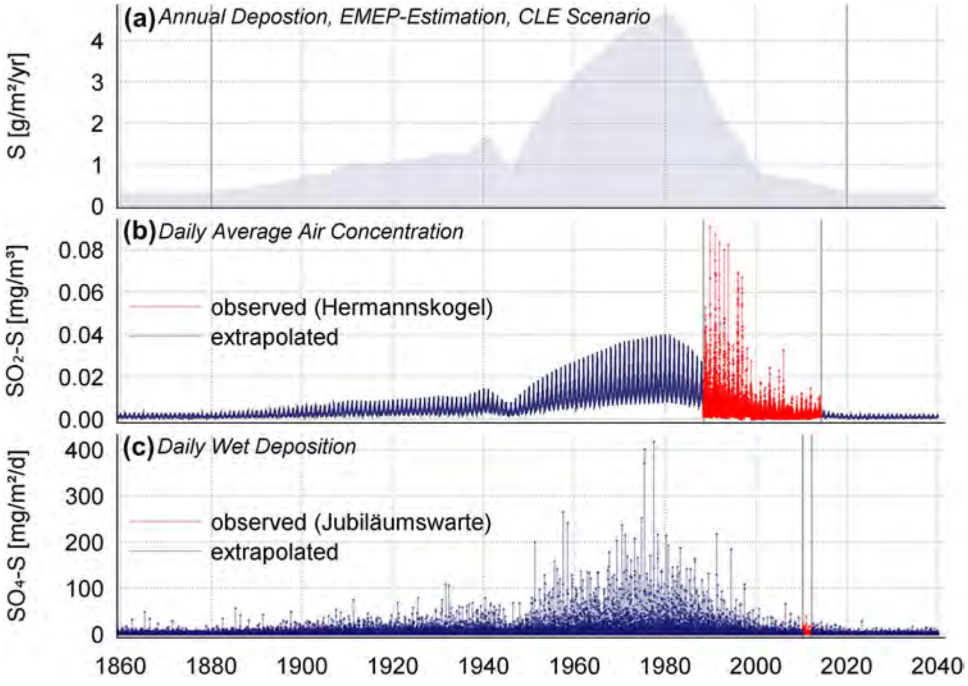

Fig. 2 Extrapolation of observed deposition data to the model timeframe. The model timeframe spans from 1770 to 2100. Observations of S deposition and air concentration were available only for the very recent past. **a** To extend our input data time series beyond the observed time frames we used a dataset of SO_4-S deposition estimates (EMEP), generated by Schöpp et al. (2003). The data estimates range back to 1880. The set also comprises estimates for the near future. For our purposes, we chose the Current Legislation Emission (CLE) scenario. Outside the defined timeframe, we extended the time series, assuming steady conditions. **b** Daily mean values of the aerial SO_2 concentration for the site Hermannskogel, were available, ranging back to the year 1988. Due to the fact that SO_2 concentrations exhibit a strong seasonal pattern, extrapolation was performed by calculating average values on a Day of Year base, which were then extended beyond the available timeframe. Here, the normalized EMEP time series served as a multiplier to scale the aerial concentration to historic/future conditions. **c** For daily wet deposition, we applied an approach, similar to the extension of the aerial concentration. Annual deposition sums where partitioned proportionally to daily precipitation events

through the WBM. All these processes are calculated, using the following scheme. The change in the content of the solute (mg/m^2) of the desired pool is defined as the product of content and the relative change of the water content of the pool during the timestep.

$$\frac{dCont}{dt} = Cont\frac{\frac{dWater}{dt}}{Water} \tag{1}$$

Analog to the WBM, the SDM can be divided into an aboveground and a belowground module. A flowchart of both formulations is given in Fig. 3. Only two aboveground processes are explicitly modeled in the SDM: occult (fog) deposition and dry (stomatal) deposition. We assume the SO_4-S concentration in fog precipitation proportional to the SO_2 concentration in the air. The amount of daily fog deposition (mg/m^2) is calculated as the product of fog precipitation (mm), the average daily SO_2-S air concentration (mg/m^3), multiplied with a specific enrichment factor.

$$occult = SO_2Sf_{\mathrm{occult}}FOG \tag{2}$$

The determination of stomatal deposition also utilizes data of the SO_2-S air concentration. As proxy for the degree of stomatal openness we use the soil moisture-dependent stress coefficient ($Kc_{\mathrm{s,tree}}$) (compare Dolschak et al. 2019). A value of one would correspond to fully opened stomata, whereas a value of zero would result in a complete shutdown of the stomatal gas exchange. The stands' relative leaf area (Kc_{LAI}) serves as proxy for the foliage surface (or the relative amount of stomata), exposed to sulfur dioxide. The function is stated as a product of the SO_2-S air concentration (mg/m^3), a specific enrichment factor, the stress coefficient, the relative leaf area and the daily mean wind speed (m/s), measured 2 m above ground.

$$dry = SO_2Sf_{\mathrm{dry}}Kc_{s,\mathrm{tree}}Kc_{\mathrm{LAI}}u_2 \tag{3}$$

Belowground and biotic S fluxes and transformations are stated as a system of five ordinary differential equations which are solved simultaneously using the 4th-order explicit Runge–Kutta scheme. The temporal dynamics of SO_4-S (*Sol*) in the soil solution are formulated, using the following equation. Infiltration (*Inf*) and the leaching (*Leac*) of

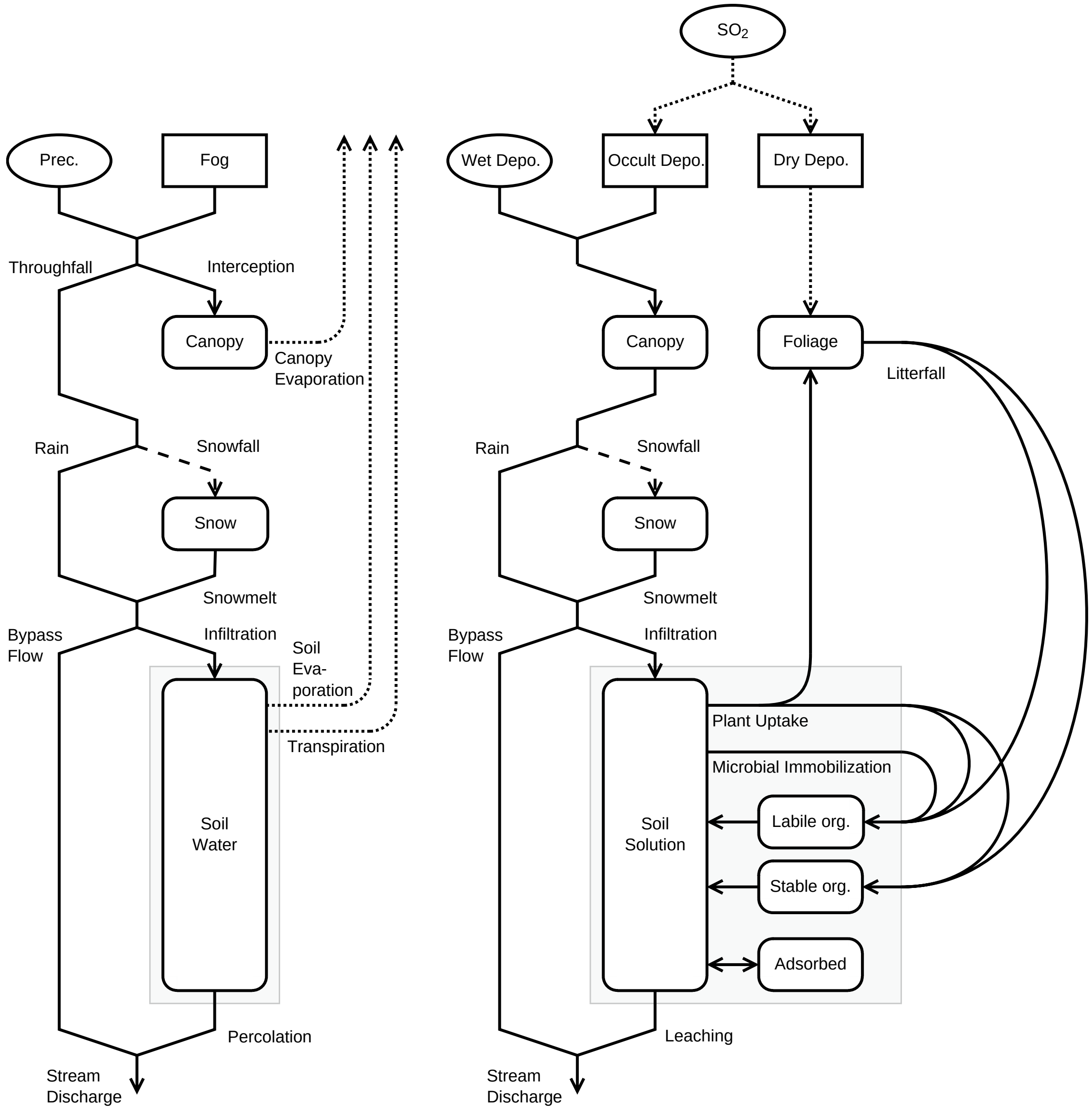

Fig. 3 Flowchart of the Water Balance Model (WBM, left) and the Sulfur Dynamics Model (SDM, right). A comprehensive description of the WBM is given in Dolschak et al. (2019). The WBM states the hydrologic framework for the SDM. All S fluxes, associated with the solute phase, are controlled by the WBM

sulfate-S are fluxes, driven by the WBM. M_{stable} and M_{labile} state the input to the soil solution via mineralization of the stabile organic and labile organic sulfur pool, respectively. U_{plant} and U_{micro} state the uptake of S by plants and soil microbes, respectively. *Ads* accounts for the adsorbed amount of SO_4-S.

$$\frac{dSol}{dt} = \left(Inf + M_{\text{stable}} + M_{\text{labile}}\right) - \left(Leac + U_{\text{plant}} + U_{\text{micro}} + \frac{dAds}{dt}\right) \tag{4}$$

Foliage S (*Fol*) dynamics are described as the difference of plant uptake, multiplied with a constant fraction, describing the partition of plant uptake, routed to the foliage, plus dry deposition input to the canopy, minus the autumnal litterfall loss of S. The simulator neglects the possibility of S washout from the canopy. The seasonal foliage S pool is the only explicitly defined biomass pool in the SDM. As our interest does not lie in tree growth, we do not assume a change in S storage during stand development. It could be claimed that living biomass S storage is incorporated in the labile as well as the stabile soil organic S pool.

$$\frac{dFol}{dt} = f_{\mathrm{fol}} U_{\mathrm{plant}} + dry - litter \tag{5}$$

In our model, two pools are used to describe the dynamics of organic soil sulfur: A stable pool accounts for recalcitrant organosulfur compounds, and a labile pool accounts for more transitory organic sulfur species. The first pool could be viewed as corresponding to carbon-bond S, and the second could be assigned to ester-bond sulfate (McGill and Cole 1981). As a simplification, we assume that microbial S immobilization is only contributing to the labile pool. The balance of the labile organosulfur pool can be stated as the difference of the labile partition of plant uptake, which is not routed to the foliage, and litterfall, plus the microbial S assimilation, and the loss via mineralization. As a simplification, we assume a steady-state forest with an unchanging S content in the living woody biomass.

$$\frac{dLabile}{dt} = f_{\mathrm{labile}} \left(\left(1 - f_{\mathrm{fol}} \right) U_{\mathrm{plant}} + litter \right) + U_{\mathrm{micro}} - M_{\mathrm{labile}} \tag{6}$$

The stable pool is formulated analog to the labile pool. The stabile fraction of plant uptake and litterfall is formulated as $1 - f_{\mathrm{labile}}$.

$$\frac{dStable}{dt} = \left(1 - f_{\mathrm{labile}} \right) \left(\left(1 - f_{\mathrm{fol}} \right) U_{\mathrm{plant}} + litter \right) - M_{\mathrm{stable}} \tag{7}$$

Sulfate adsorption is modeled using the Langmuir isotherm. M_{ads} and K_{ads} are site-specific model parameters, and *Conc* states the SO_4-S concentration in the soil solution. To express the kinetics of the process, it is coupled with a first-order decay function.

$$\frac{dAds}{dt} = \lambda_{\mathrm{ads}} \left(\frac{M_{\mathrm{ads}} K_{\mathrm{ads}} Conc\left[mg/L \right]}{1 + K_{\mathrm{ads}} Conc\left[mg/L \right]} - Ads \right) \tag{8}$$

The concentration of SO_4-S in the soil solution is calculated as the storage in soil solution, divided by the product of soil depth and soil moisture.

$$Conc\left[mg/L \right] = \frac{Sol\left[mg/m^2 \right]}{z_{\mathrm{r}} \theta} \tag{9}$$

We derive the lambda value from the process' half-life.

$$\lambda_{\mathrm{ads}} = -\frac{\ln 0.5}{HL_{\mathrm{ads}}} \tag{10}$$

The function stated below describes the response ($resp_{\mathrm{Q10}}$) of microbial S transformations to soil temperature. We use a base temperature of 8 °C that should resemble the annual average soil temperature at our investigated stands. The factor f_{Q10} describes the relative increase in the response when soil temperature rises by 10 °C.

$$resp_{\mathrm{Q10}} = e^{\frac{\ln f_{\mathrm{Q10}}}{10} \left(T_{\mathrm{soil}} - 8^{\circ} C \right)} \tag{11}$$

In the WBM, the autumnal decrease in the LAI inside the interval DoY_{LC}–DoY_{LE} (compare Dolschak et al. 2019) is described using the Smoothstep function (see Appendix). To define the relative amount of sulfur in the litterfall (litter) we first calculate the relative amount of daily litterfall (f_{litter}).

$$f_{\mathrm{litter}} = \begin{cases} 0, & DoY < DoY_{\mathrm{LC}} \\ 1 - \frac{LAI_{\mathrm{Kc,DoY}}}{LAI_{\mathrm{Kc,DoY-1}}}, & DoY_{\mathrm{LC}} \le DoY < DoY_{\mathrm{LE}} \\ 1, & DoY = DoY_{\mathrm{LE}} \end{cases} \tag{12}$$

To calculate the amount of sulfur in the litterfall biomass we multiply this value with the sulfur content in the foliage pool.

$$litter = f_{\mathrm{litter}} fol \tag{13}$$

The latter function describes the response ($resp_{\theta}$) of microbial S transformations to soil moisture (see Sverdrup et al. 2007). At soil moisture levels below (θ_0) and above a certain threshold (θ_3), we claim that all microbial transformations come to a halt ($resp_{\mathrm{opt}} = 0$). We assume optimal conditions ($resp_{\mathrm{opt}}$) at medium soil moisture between θ_1 and θ_2. In between θ_0 and θ_1 and accordingly in between θ_{moist} and θ_{drown} we assume linear transitions.

$$resp_{\theta} = resp_{\mathrm{min}} + \left(resp_{\mathrm{opt}} - resp_{\mathrm{min}} \right) \begin{cases} 0, & \theta \le \theta_0 \vee \theta < \theta_3 \\ \frac{\theta - T_0}{T_1 - T_0}, & \theta_0 < \theta \le \theta_1 \\ 1, & \theta_1 < \theta \le \theta_2 \\ 1 - \frac{\theta - T_2}{T_3 - T_2}, & \theta_2 < \theta \le \theta_3 \end{cases} \tag{14}$$

$$V_m = \frac{V_{\mathrm{max}} Conc\left[mg/L \right]}{K_{\mathrm{m}} + Conc\left[mg/L \right]} \tag{15}$$

We describe microbial S immobilization using the Michaelis–Menten equation.

$$V_{\mathrm{m,immobil}} = \frac{V_{\mathrm{max,immobil}} Conc\left[mg/L \right]}{K_{\mathrm{m,immobil}} + Conc\left[mg/\mathrm{L} \right]} \tag{16}$$

The maximal assimilation rate depends on soil temperature and soil moisture.

$$V_{\mathrm{max,immobil}} = V_{\mathrm{coeff,immobil}} resp_{\mathrm{Q10,immobil}} resp_{\mathrm{\theta,immobil}} \tag{17}$$

We describe the mineralization of stable organic S as first-order decay process, dependent on soil temperature and soil moisture.

$$M_{\text{stable}} = Stable\lambda_{\text{stable}} resp_{\text{Q10,mineral}} resp_{\theta\text{,mineral}} \tag{18}$$

The release of labile organic S (ester-bond) is also described as first-order decay process dependent on soil temperature and soil moisture. In addition, the rate of mineralization is also dependent on the SO_4-S soil solution concentration.

$$M_{\text{labile}} = Labile\lambda_{\text{sulfatase}} resp_{\text{Q10,mineral}} resp_{\theta\text{,mineral}} \tag{19}$$

The simulator comprises the effect of microbial sulfatase release on the kinetics of the labile organic S. A low SO_4 concentration in the soil solution promotes the microbial release of sulfatase, thus accelerating the mineralization release of ester-bond sulfate (Scherer 2009). This is implemented by making the process' half-life linearly dependent on the soil solution concentration. To set the linear dependence, half-lives are defined for 2 key solution concentrations (0 and 10 mg SO_4-S/L).

$$k_{\text{sulfatase}} = \frac{HL_{\text{sulfatase.10}} - HL_{\text{sulfatase.0}}}{10} \tag{20}$$

The linear equation takes the form:

$$HL_{\text{sulfatase}} = k_{\text{sulfatase}} C[mg/L] + HL_{\text{sulfatase.0}} \tag{21}$$

The half-life is used to calculate the lambda value of the first-order decay process.

$$\lambda_{\text{sulfatase}} = -\frac{\ln 0.5}{HL_{\text{sulfatase}}} \tag{22}$$

The S uptake of deciduous trees is mediated through two distinct active carrier systems (Herschbach and Rennenberg 2001). Kreuzwieser and Rennenberg (1998) postulate high affinity and low affinity uptake systems. Low sulfate level in the aqueous phase of forest soils points to the dominance of the high affinity system (Herschbach and Rennenberg 2001). We simulate the uptake of S beech trees using Michaelis–Menten kinetics. We assume that plant uptake is only taking place during the growing season.

$$U_{\text{plant}} = \begin{cases} \frac{V\max_{\text{,plant}} Conc[mg/L]}{K_{\text{m,plant}} + Conc[mg/L]}, & Kc_{\text{LAI}} > 0 \\ 0, & Kc_{\text{LAI}} = 0 \end{cases} \tag{23}$$

We also claim that plants only take up a certain amount of S during the season. After a certain demand is met (ACU_{starve}), plants start to throttle the uptake. After a second threshold is met (ACU_{sat}), plants shut down the uptake of S completely. We calculate the accumulated uptake on a Day of Year base.

$$ACU_{\text{DoY}} = \begin{cases} 0, & DoY = 1 \\ U_{\text{plant}} + ACC_{\text{DoY}-1}, & DoY > 1 \end{cases} \tag{24}$$

The transition of the demand is modeled under the usage of the Smoothstep function (see Appendix).

$$V\max_{\text{,plant}} = smooth\left(ACU_{\text{DoY}}[g/m^2],\ ACU_{\text{starve}},\ ACU_{\text{sat}},\ V_{\text{starve,plant}},\ V_{\text{sat,plant}}\right) \tag{25}$$

Model application

Before running the SDM, we define three target criteria, which mark a successful simulation:

- To bootstrap the SDM, we run a model spin-up, starting in the year 1770. As a primary requisite, the model must achieve steady-state conditions before atmospheric deposition starts to rise in 1880.
- The plots were sampled and analyzed in 2010, and the total S stock in forest floor and mineral soil (0–50 cm) was determined (E: 78.0 g/m^2, J: 102.6 g/m^2). The sum of all modeled soil S pools (adsorbed, stable organic, labile organic, soil solution) in 2010 has to be in a close range to the measured value.
- The simulator has to deliver a satisfactory reproduction of the observed timeline of the SO_4-S concentration in the monitored soil solution.

We define plausible ranges for our set of 25 parameters (Table 1). The SDM was calibrated via simulated annealing (Kirkpatrick 1984). Performance criterion was the Nash–Sutcliffe model efficiency (*NSE*; Nash and Sutcliffe 1970), a function, which is generally used to evaluate hydrologic models.

The code file of the model (written in Base SAS 9.4) is available after request to the authors. The file contains the code for all model functions which are utilized in the Water Balance Model (WBM) and the Sulfur Dynamics Model (SDM). The recommended citation is: *this publication: code file of the Water Balance Model (WBM) and the Sulfur Dynamics Model (SDM).*

Results and discussion

Evaluation

Soil solution chemistry was monitored in a biweekly interval, on each site in 15 replications (Fig. 4a, b). This enables the calculation of robust site wise mean SO_4-S soil solution concentrations per sampled event. The resulting timelines of both forest stands reveal a very similar pattern (Fig. 4c). The observed correlation gives a hint that sulfate solution chemistry might be driven by the same processes, on both stands.

Regarding the timeline of SO_4-S in soil solution, the SDM yields feasible results for both investigated stands:

The simulations capture the observed timeline to a satisfactory degree (Exelberg: $NSE = 0.78$, Jubiläumswarte: $NSE = 0.9$, compare Fig. 5f, g, Table 1). The SDM overestimates the amount of total soil-S, which was quantified in 2010. For the E and J plot, the observed mean of the total soil-S pool down to a depth of 50 cm was 78.0 g/m^2 and 102.6 g/m^2 (Hanousek et al. 2017). The SDM delivers an estimate of 103 and 128 g/m^2 (see Fig. 6c, d). Therefore, it overestimates both sites' pools, each by approximately 25 g/m^2. Given the fact that the presented model does not explicitly account for organic S, bond in living tree biomass other than foliage, one could argue that a portion of the modeled organic pool is contained in the aboveground plant tissue. For a beech-rich northern hardwood forest (Hubbard Brook Experimental Forest), Likens et al. (2002) give an estimate for the S, bound in aboveground living biomass, of 8.5 g/m^2 roughly. Subtracting 1.0e g representing foliage S this narrows the gap, reducing the overestimation to approximately 17.5 g/m^2.

Soil samples from both investigated sites were analyzed for S fractions by Hanousek et al. (2017). Additionally, they used material from a third site to create pooled samples. Adsorbed S was determined to a fraction of 6.4% of total soil S. The organic fraction accounted for 89%. Our modeling work delivers similar values. On both locations, adsorbed and organic fraction account for roughly 6.0% and 93.5% (Fig. 6c, d).

The organic fraction can further be divided into carbon-bonded S and ester-sulfates. For a nearby beech stand on similar bedrock the ester fraction was determined by Hanousek et al. (2017) via HI reduction (described in Kulhánek et al. 2011; Tabatabai 1996). The authors found that ester-sulfates account for approximately 38% of the entire organic fraction, which is in contradiction to Havlin et al.

Table 1 Parameter optimization results for the investigated sites

Abbrev.	Parameter and description	Unit	Exelberg	Jubiläum.
f_{occult}	Fog (occult deposition) enrichment factor		33922.35	15395.36
f_{dry}	Stomatal (dry) deposition factor		0.00	0.00
$\Theta_{0,\mathrm{mineral}}$	Mineralization, lower threshold Θ	$\mathrm{LL^{-1}}$	0.07	0.01
$\Theta_{1,\mathrm{mineral}}$	Mineralization, lower optimal Θ	$\mathrm{LL^{-1}}$	0.13	0.25
$\Theta_{2,\mathrm{mineral}}$	Mineralization, upper optimal Θ	$\mathrm{LL^{-1}}$	0.23	0.33
$\Theta_{3,\mathrm{mineral}}$	Mineralization, upper threshold Θ	$\mathrm{LL^{-1}}$	0.36	0.39
$\Theta_{0,\mathrm{immobil}}$	Immobilization, lower threshold Θ	$\mathrm{LL^{-1}}$	0.04	0.04
$\Theta_{1,\mathrm{immobil}}$	Immobilization, lower optimal Θ	$\mathrm{LL^{-1}}$	0.07	0.18
$\Theta_{2,\mathrm{immobil}}$	Immobilization, upper optimal Θ	$\mathrm{LL^{-1}}$	0.16	0.29
$\Theta_{3,\mathrm{immobil}}$	Immobilization, upper threshold Θ	$\mathrm{LL^{-1}}$	0.33	0.38
HL_{stable}	Half-life, stable soil-organosulfur, opt. Conditions	Years	54.71	67.34
HL_{labile}	Half-Life, Labile Soil-Organosulfur, opt. conditions	Days	21.99	13.00
$K_{\mathrm{m,immobil}}$	Immobilization, K_{m} parameter		1.81	1.05
$V_{\mathrm{m,immobil}}$	Immobilization, maximum rate, opt. conditions	$\mathrm{SO_4}$-S mg $\mathrm{m^{-2}}$	2.11	2.11
$f_{\mathrm{Q10,immobil}}$	Immobilization, Q10 Factor		2.37	2.77
$f_{\mathrm{Q10,mineral}}$	Mineralization, Q10 Factor		2.19	2.22
$V_{\mathrm{m,starve}}$	Plant Uptake, Maximum Rate at S Starvation	$\mathrm{SO_4}$-S mg $\mathrm{m^{-2}\ d^{-1}}$	0.11	0.07
$V_{\mathrm{m,sat}}$	Plant Uptake, Maximum Rate at S Saturation	$\mathrm{SO_4}$-S mg $\mathrm{m^{-2}\ d^{-1}}$	0.00	0.00
$K_{\mathrm{m,plant}}$	Plant uptake, Km parameter		1.16	0.95
$\mathrm{TC}_{\mathrm{starve}}$	Plant uptake, threshold uptake, starvation	$\mathrm{SO_4}$-S mg $\mathrm{m^{-2}y^{-1}}$	1141.79	913.76
TC_{sat}	Plant uptake, threshold uptake, saturation	$\mathrm{SO_4}$-S mg $\mathrm{m^{-2}y^{-1}}$	1367.79	2166.95
f_{labile}	Plant uptake, routed to labile soil-organosulfur		0.18	0.07
f_{fol}	Plant uptake, routed to foliage pool		0.74	0.82
HL_{ads}	Adsorption, half-life	Days	205.00	71.10
$K_{\mathrm{L,ads}}$	Adsorption, half-saturation concentration	$\mathrm{SO_4}$-S mg $\mathrm{L^{-1}}$	12.53	11.68
$K_{\mathrm{max,ads}}$	Adsorption, maximum charge	$\mathrm{SO_4}$-S mg $\mathrm{m^{-2}}$	6085.48	7057.02
	Initialization 1770, labile soil-organosulfur	$\mathrm{SO_4}$-S mg $\mathrm{m^{-2}}$	5054.55	6804.58
	Initialization 1770, stable soil-organosulfur	$\mathrm{SO_4}$-S mg $\mathrm{m^{-2}}$	51175.13	61845.05
	Plant uptake 2010	$\mathrm{SO_4}$-S mg $\mathrm{m^{-2}}$	1345.80	1245.00
	Litterfall 2010	$\mathrm{SO_4}$-S mg $\mathrm{m^{-2}}$	992.40	1017.40
NSE	Nash–sutcliffe index		0.78	0.90
$RMSE$	Root-Mean-Square Error		0.44	0.28

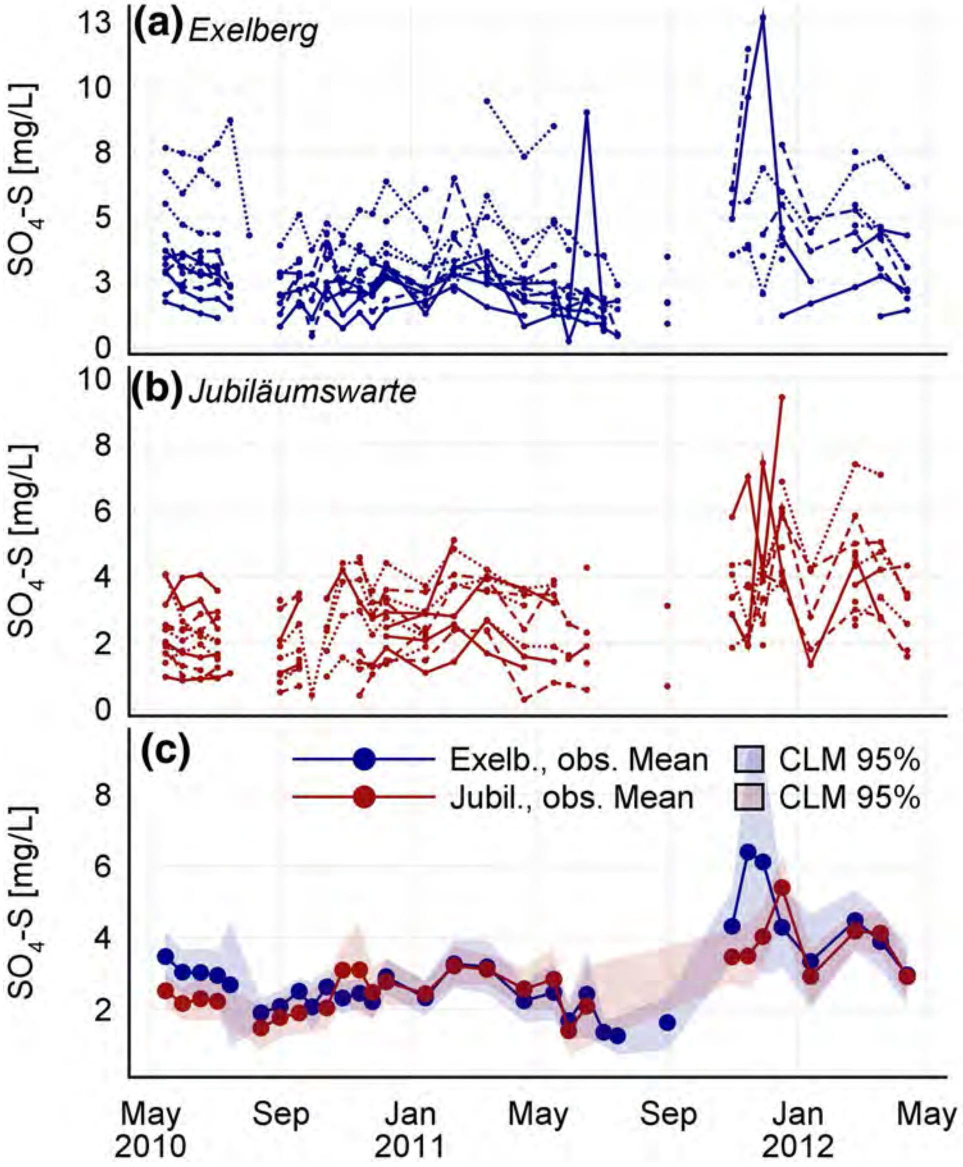

Fig. 4 **a**, **b** Time series of SO$_4$-S concentration, observed in soil solution. Each line represents one lysimeter. Eighteen lysimeters were installed per plot (6 repetitions and 3 depth classes). **c** To overcome the noise in the data, the SDM was fitted to site-wise mean concentrations. After calculating the mean, both sites reveal a very similar pattern regarding the temporal development of the soil solution concentration. This is leading to the assumption that soil S dynamics are controlled by over-regional drivers

(2005) who suggest that ester-sulfates account for the majority of organic soil S. Our hypothesis that labile soil organosulfur corresponds to ester-sulfates must be rejected: Accounting for only 3.5% (E) and 4.5% (J) or organic soil S, our simulated labile pool (June 2010) is even smaller than reported by Hanousek et al. (2017).

For a beech stand on similar bedrock, Berger et al. (2009) reported an annual litterfall S flux of 0.45 g/m^2. However, the S content in green foliage tissue was more than two times higher than in litter material, indicating translocation processes before leaf senescence. Our simulations exhibit values, of 1.0 g/m^2 per year. This overestimation could be explained by the neglect of plant-internal S translocations in the current version of the SDM.

Microbial S transformations

Compared to other soil S pools, the microbial S pool is small. According to Chowdhury et al. (1999), microbially bond S accounts only for 1–4% of total soil S. Nevertheless, it is of great importance regarding plant nutrition due to its labile nature. Kertesz and Mirleau (2004) describe the contribution of microbial activity to the plant S supply: Plants take up S primarily in form of inorganic SO$_4$ (Buchner et al. 2004). However, only a minor fraction of soil S is available in this form. As stated before, the majority is contained in organic material. Soil microbiota are responsible for the mineralization of organically bond S to inorganic sulfate. On the other hand, microorganisms are also driving the rapid immobilization of inorganic sulfate, first to relatively labile ester sulfates and furthermore, to more stable C-bonded S

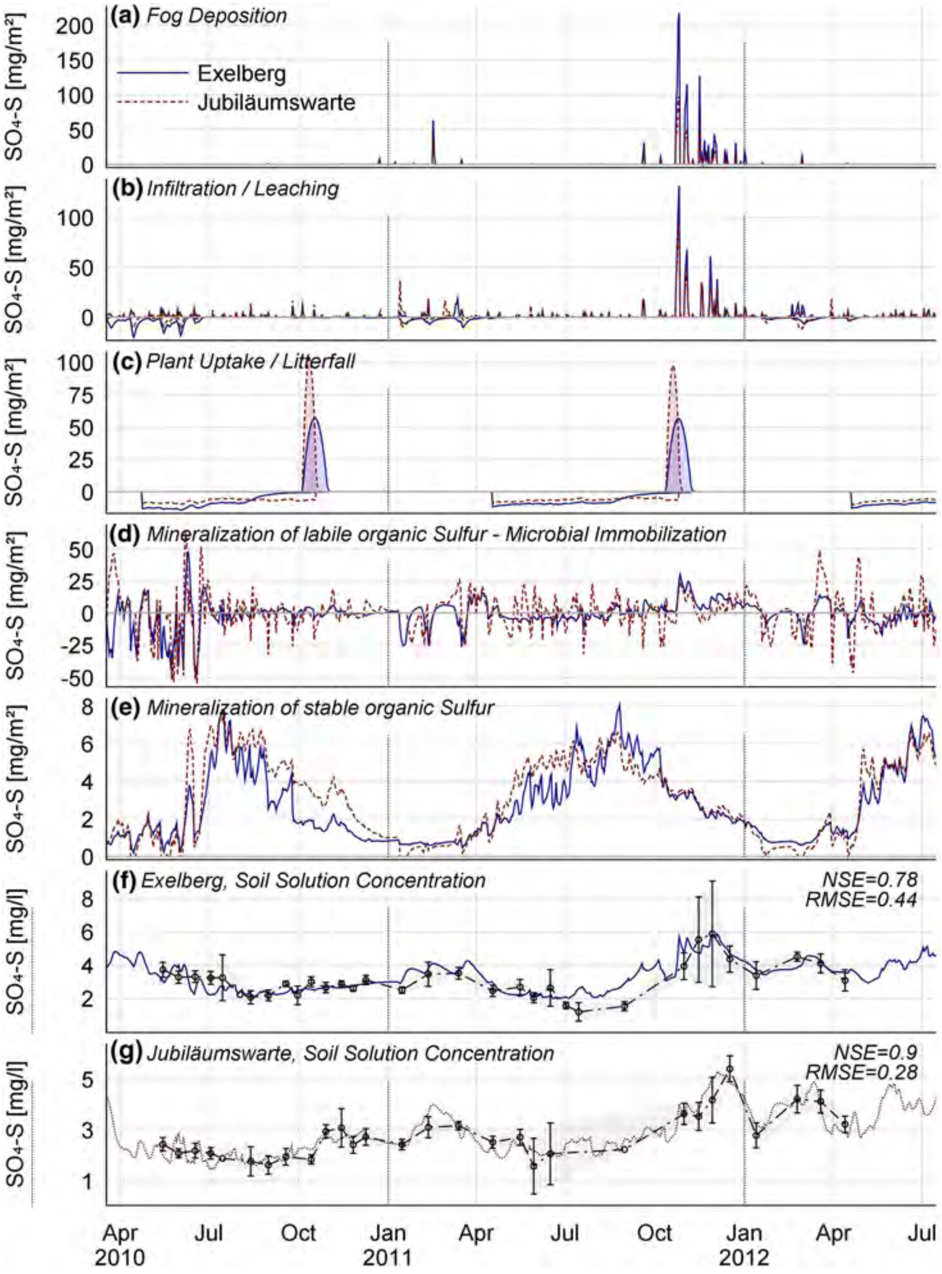

Fig. 5 S fluxes during two years of field campaign. **a** Both stands experience a prolonged fog event in the autumn of 2011. During this period, we measured occult deposition loads between 200 and 500 mg SO_4-S/m^2. The simulation outcome suggests much higher values: From mid-October to the end of December 2011, the simulator predicts occult deposition sums of 1800 and 900 mg SO_4-S/m^2, for the Exelberg and Jubiläumswarte site, respectively. **b** During the field campaign, atmospheric inputs were dominated by the occult deposition event in the fall of 2011. Due to the coupling with percolation, leaching of SO_4-S only takes place, when soil moisture is above water-holding capacity. This happens predominantly during the dormant season when evapotranspiration water fluxes are low. **c** We model plant uptake taking place only during the growing season. Because plant uptake is driven by their demand in our simulation, highest rates of S assimilation are achieved relatively early in the growing season. As the annual demand is met in late summer, plants start to throttle the uptake of S. During autumnal litterfall, the S, which is stored in leaf biomass, is transferred to the soil organic pool. **d** In this graph, we display the difference of mineralization of labile organosulfur and microbial immobilization. Positive values represent inputs to the soil solution meaning that mineralization is dominating. The erratic pattern is caused by shifted Θ optima for both processes (comp. Figs. 7, 8). Mineralization slightly favors higher Θ values than immobilization. **e** Mineralization is driven by substrate availability, Θ, and soil temperature. Maximal values are achieved at moderate Θ and high soil temperature (comp. Figs. 7, 8). **f**, **g** Observed and modeled timeline of the SO_4-S concentration in the soil solution. The dash-dotted line illustrates the stands mean concentration at given time, and the error bars display the 95% confidence limit for the mean. The calibration led to sufficiently good results for both investigated forest stands. Both sites exhibit a peak in the solution concentration in late autumn of 2011. This is assignable to (1) high input loads via fog deposition and (2) mineralization excess during this period

species (Ghani et al. 1993). In our formulation, S taken up by plants is routed to both stabile and labile organosulfur. In contrast to plant uptake, microbial immobilization contributes only to the labile pool. We describe mineralization and immobilization of the labile organic pool as temperature and moisture dependent. The soil moisture optima are slightly displaced (see Fig. 7): Immobilization is favored by dryer soil conditions. Immobilization also exhibits stronger response to warm conditions (compare Fig. 8). Kertesz and Mirleau (2004) see immobilization and mineralization as concurrent processes, occurring simultaneously in the soil. In our simulations, it is in fact the non-congruence of soil moisture and temperature response, which is driving a large portion of the observed fluctuations in the SO_4 soil solution, favoring net mineralization under cool and moist conditions and net immobilization under warm and slightly dryer conditions.

Occult deposition

During two years of field campaign, we captured a prolonged fog event in late autumn of 2011. There is a solid body of work, asserting that fog water is enriched in sulfate, compared to rainwater (see Fowler et al. 1989; Lange et al. 2003). Especially in mountainous regions, fog can contribute significantly to the hydrologic and nutrient balance (Klemm and Wrzesinsky, 2007). We monitored deposition (1) in the open and (2) below the canopy (throughfall) and in form of (3) stemflow. The accumulated S deposition sums clearly display significant S inputs via occult deposition during the captured fog event (compare Fig. 9). The observed discrepancy between open area deposition and throughfall plus stemflow deposition indicates an extra input of approximately 500 mg SO_4-S m^{-2}. For our modeling purposes, we deal with open area deposition as input. The derivation of fog precipitation is presented in Dolschak et al. (2019).To scale from the mean daily aerial SO_2-S concentration to the SO_4-S concentration in the fog precipitation water, we apply an enrichment factor (see Lange et al. 2003). From 22nd October to 5th December 2011, the simulation yields an input of 1330 and 620 mg SO_4-S m^{-2} in form of occult deposition for E and J. The spike in the soil solution at the end of 2011 (see Fig. 5a, f, g) is mostly assignable to fog deposition inputs. The observed and predicted high loads might be a result of the stands' local conditions: In the Vienna Basin, winter fog events often coincide with southeasterly currents. When passing over the urban area, the air becomes enriched with pollutants. At the edge of the Vienna Woods it is forced to rise, condensation starts. The forest stands, which are located at the upper hill slope, facing south to east, are acting as a first barrier for the enriched fog, making them susceptible for the interception of high loads of atmospheric S. For a detailed description see Auer et al. (1989).

Historic development and future prospect

Both stands display a strong rise in the total soil S pool during the Twentieth century (compare Fig. 6a, b). This can be assigned largely to the accumulation of stable organosulfur originating from plant residuals. Interestingly, the accumulation of stable S has not fully tapered off in the present decade. In an attempt, to predict the future S output of two German catchments with the MAGIC model (Cosby et al. 2001). Prechtel et al. (2003) found that for one catchment the observed SO_4 release could not be explained solely by adsorption/desorption processes in the soil. It was necessary to introduce an additional S source (968 mg m^{-2} yr^{-1}) to match the simulated with the observed stream output. The authors suggested an S release from decomposition of organic soil constituents. In our work, S from mineralization of stable organosulfur adds a relatively steady annual amount between 700 and 1300 mg (1980–2020) to the budget. However, in our simulations, only a limited fraction of mineralized S enters the stream output. As the availability of other S sources might dwindle in the future, this fraction could further decrease. Much rather than being exported, it might be rapidly incorporated into living biomass and be cycled through the biosphere again. On the other hand, the remaining fraction which is leaving the system via seepage might hinder the achievement of a balanced input/output for many decades. Prechtel et al. (2003) point out that the investigated catchments could reach pre-industrial conditions in a few decades. They also claim that knowledge of origin and behavior of the postulated organic sulfur is crucial for the prediction of future trend in the stream chemistry. In our work, a large organic S pool with modeled half-lives up to 67 years will allow only a slow temporal recession of the catchment S export over the coming decades (see Fig. 10): Pre-industrial conditions in the stream discharge as well as a steady-state equilibrium are not reached over the whole investigation timeframe. The modeled amount of SO_4-S, adsorbed in the soil, exhibits low variability over time. Simulated sorption is close to the modeled maximum sorption capacity on both sites ($K_{max,ads} = 6.1$ g SO_4-S m^{-2} Exelberg, 7.1 g SO4-S m^{-2} Jubiläumswarte). On both sites, these pools remain almost constant over the entire model timeframe (see Fig. 6a, b) and therefore does not contribute to the present output excess of S.

Mineralization of S-containing soil constituents shows a strong response to soil moisture and soil temperature. Mitchell and Likens (2011) state the importance of the water balance in controlling the S output of forested watersheds: Soil moisture affects the net stream discharge, mineralization, desorption and weathering of S-bearing minerals. High temperatures might also accelerate processes. On the other hand, due to increase in evapotranspiration, high temperatures might lead to dryer soil conditions (see also Dolschak

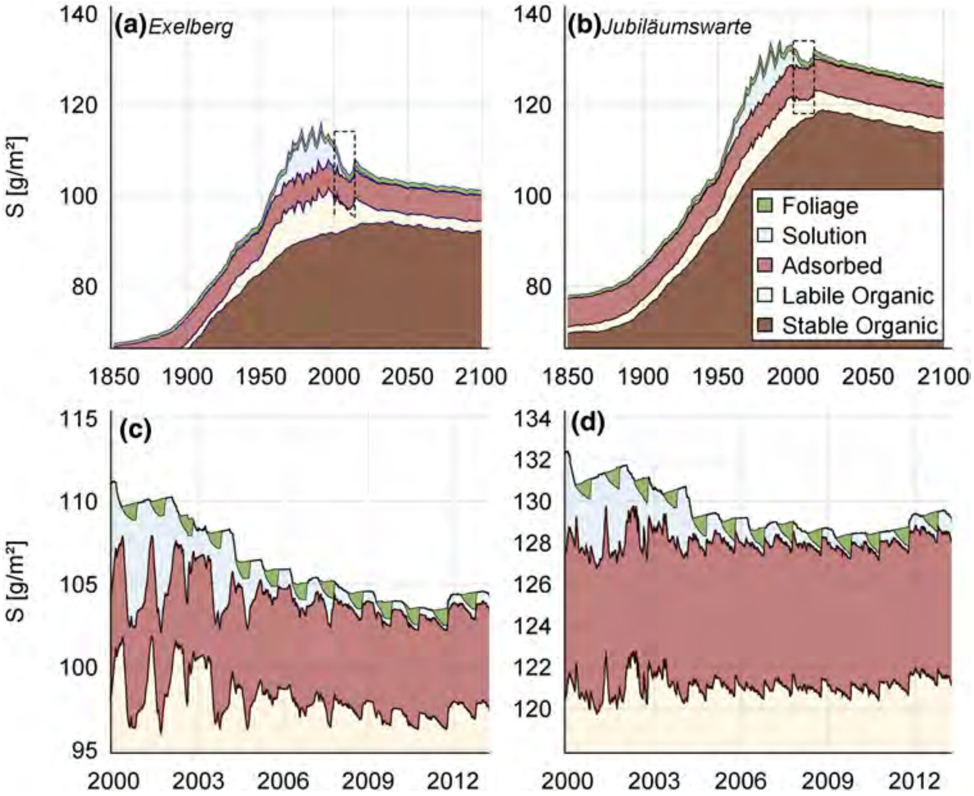

Fig. 6 Temporal development of S pools over the whole model timeframe (a, b) and focused on the recent past (c, d). **a**, **b** The model displays a rise in the stands' overall S stock, which is mainly assignable to the stable organosulfur pool (dark brown). Interestingly, this increase still has not tapered in the present decade. From the 1960s to the late 1980s S deposition peaked; high S loads are reflected in altered labile organosulfur and solute SO_4-S in the soil. The amount of SO_4-S, adsorbed in the soil, shows the lowest variability. Simulated sorption (E: 6.0 g, J 6.8 g) is during most periods close to the modeled maximum sorption capacity on both sites ($K_{\mathrm{max,ads}}=6.1$ g SO_4-S m^{-2} Exelberg, 7.1 g SO4-S m^{-2} Jubiläumswarte). We estimated both stands' total soil S pool in 2010. On the Exelberg site, an estimated amount of 78 g/m^2 corresponds to a simulated soil S pool of 103 g/m^2. The Jubiläumswarte soil S pool was estimated to 102 g/m^2 in June 2010 and 128 g/m^2 was simulated. Both sites exhibit two peaks of the total S pool: one at the end of the 1980s and one at the end of the monitoring period. The second peak might be caused by a high recurrence of deposition-rich fog events in this period. After 2020 both sites display a slow recession of S pools which does not reach steady state until the end of the prediction timeframe in 2100. **c**, **d** The model does not explicitly account for S, stored in non-green living plant biomass. The S uptake fraction, which is not assigned to foliage S, is routed to the soil organic S pool, where it is instantaneously exposed to mineralization. The simulated S content of foliage lies in the range of 1 g/m^2. S is modeled, to be taken up steadily during the growing season. Autumnal litterfall leads to a sharp increase in the soil organic S pools

et al. 2019) impeding release and the export of S. Hence, how a changing climate might affect the stands' S dynamics has yet to be explored.

Inactive modules

Stomatal deposition

We assume that plants take up S primarily over the roots. Additionally, it is possible that airborne SO_2 contributes to plant nutrition via the stomatal pathway (Rennenberg et al. 1990). We model stomatal deposition as a function of aerial SO_2 concentration, the relative leaf area, the stomatal degree of openness (see Dolschak et al. 2019) and the wind speed. The calibration process always leads to stomatal deposition rates close to zero. It seems possible that (1), under current atmospheric SO_2 concentration, stomatal uptake plays only a negligible role in plant nutrition or (2) the effect of stomatal uptake is comprised in other simulated modules.

Soil sulfatase activity

The SDM comprises the effect of microbial sulfatase release on the kinetics of the labile organic S. Deficits in the S supply (low SO_4-S solution concentration) promote the microbial release of sulfatase, thus accelerating the mineralization of organically bond sulfate (Scherer 2009). We implement this by introducing half-lives of the labile organic pool, linearly dependent on the soil solution concentration. Yet during model fitting, concentration-dependent half-lives did not improve the

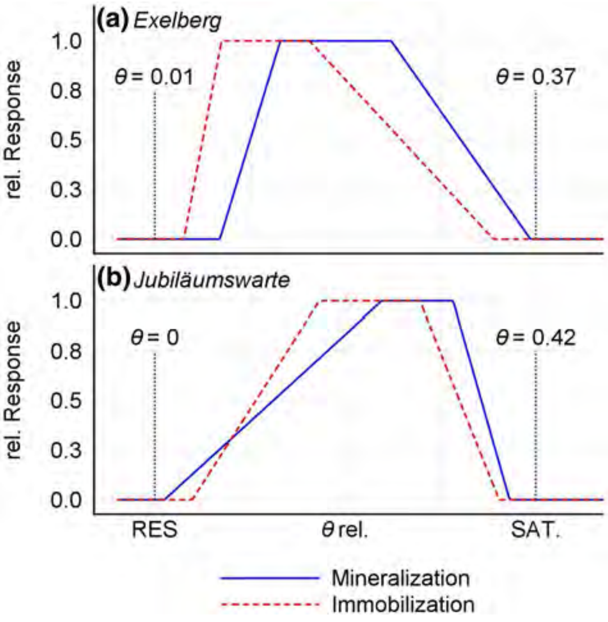

Fig. 7 Response of microbial S transformations to soil moisture (Θ). Θ is displayed on a relative scale, whereas 0 corresponds to the residual water content and 1 to soil saturation, respectively. The response of microbial processes to Θ was described using a piecewise linear function. On both sites, the calibration led to mineralization and immobilization optima at medium Θ where a balanced water and oxygen supply are given. The range of maximal immobilization rates is slightly shifted to drier soil conditions (compare Table 1). In our model simulations, the non-congruence between the moisture response of immobilization and mineralization is responsible for short-term fluctuations in the SO_4-S soil solution concentration

performance of the simulator. Comparable to stomatal deposition, it seems possible that (1) other modeled processes already cover the effect of microbial sulfatase release. It might also be thinkable that (2) the observed SO_4 supply in the soil solution is sufficiently high to fully meet the needs of soil microflora. Hence, the release of exo-enzymes might be initiated at solution concentrations much lower than observed.

Conclusion

The objective of this work lies less in the long-term perspective of acidification recovery of forest soils; our primary interest lies in finding a mathematical description of the forest plant–soil system, capable to reproduce observed temporal patterns of the SO_4-S in soil solution. Furthermore, we try to assign high-frequency fluctuations in the soil solution, observed on plot scale, to actual biogeochemical processes in the soil. After that, we venture a very cautious prognosis of the future development of the plant–soil system's S budget on the investigated forest stands.

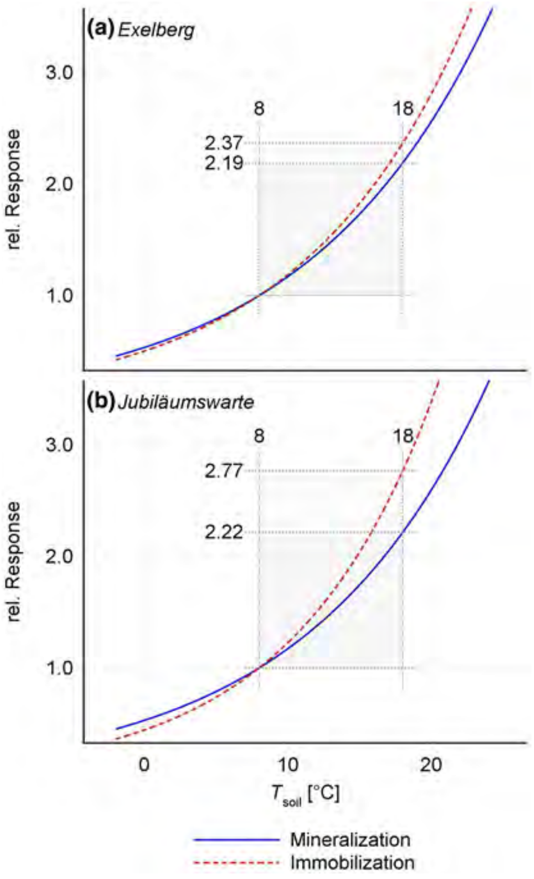

Fig. 8 Response of microbial S transformations to soil temperature. The effect of soil temperature was modeled, using the Q_{10} temperature coefficient. We set the base temperature to 8 °C, which is close to the annual mean soil temperature of the sites. The calibration process delivered similar Q_{10} factors for both forest stands, whereas the temperature sensitivity of immobilization was slightly higher than the sensitivity for mineralization (compare Table 1)

We identify microbial S transformations as important driver of the short-term dynamics in the soil solution. Yet on the long run, the mineralization of plant-originated soil organic S is responsible for the present input output imbalance. A large pool of historically accumulated organosulfur, which is decaying only very slowly, causes an output excess for decades or even centuries. Pre-industrial conditions in the stream discharge are not reached over the entire model timeframe. Besides that, occult deposition still contributes considerably to the supply of S to the forest.

For each plot, we deliver one set of parameters, which yields the best calibration result. We are aware that many different parameter configurations might lead to similar or even better outcomes. Nevertheless, the fact that it is even possible to find an adequate parameter set for each forest plot indicates that the current knowledge about forest soil S dynamics might be sufficient to describe the stands' dynamics to

Fig. 9 Accumulated SO_4-S deposition on both investigated stands. During late autumn 2011 both sites experience a sharp increase in throughfall deposition. This period coincides with a long-lasting fog event; occult deposition seems to be an important sulfate source during such events

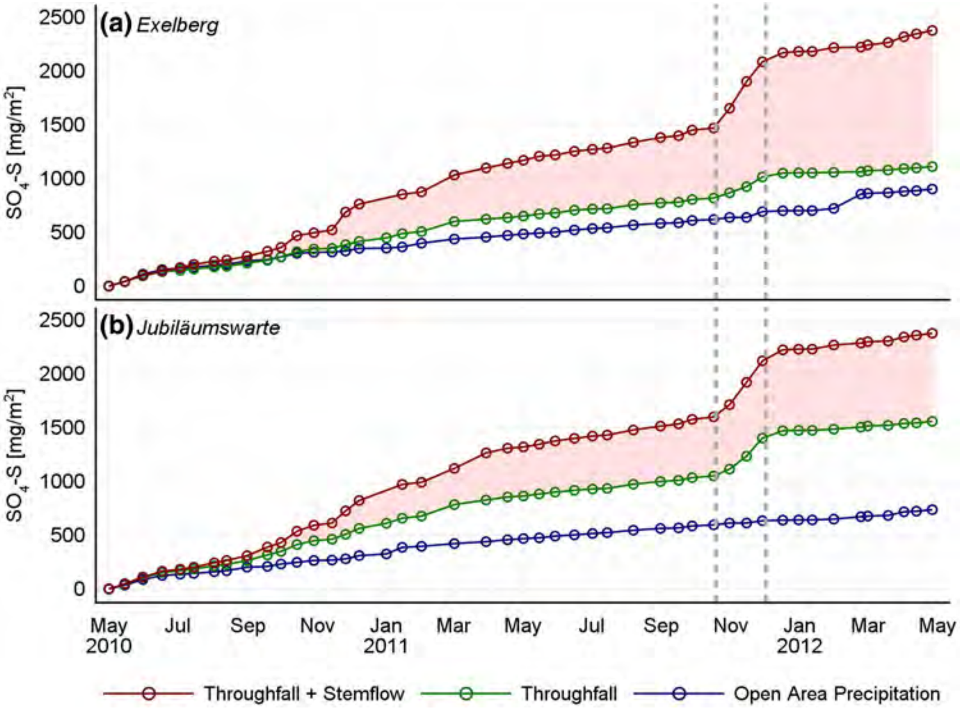

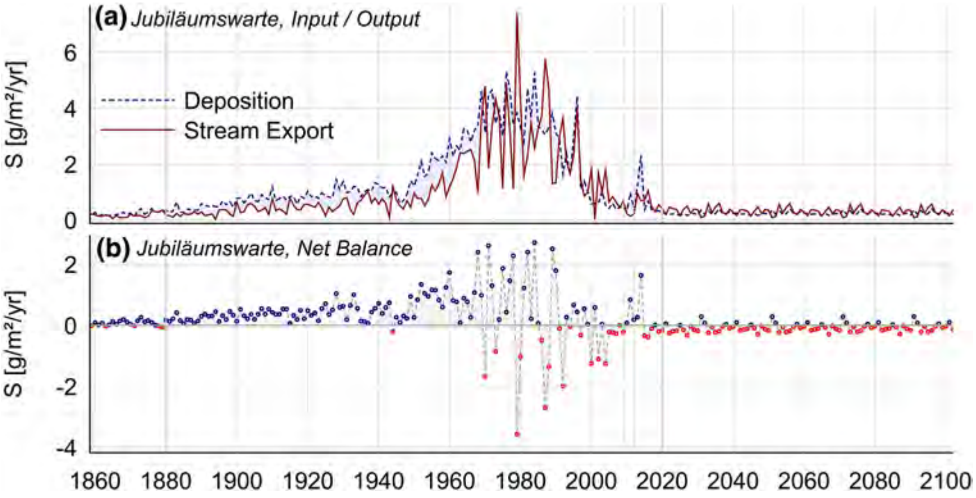

Fig. 10 Annual S input versus annual output (I/O) for the Jubiläumswarte site. After the spin-up period I/O is in steady state. With rising atmospheric deposition, the system shifts to input excess in the end of the Nineteenth century. Highest inputs are modeled around the year 1980. In the late 1980s, the system shifts to output domination for the first time. A second smaller peak of input excess around the year 2015 is caused by a frequent occurrence of fog events in this period. After 2020 the model predicts a steady recession of input and output with output moderately dominating inputs for the remaining time period. At the end of the investigation timeframe in the year 2100, the system has still not fully restored I/O equilibrium and stream discharge of SO_4-S remains slightly above the level of the pre-industrial era, ending in 1880

a satisfactory degree. At least in the short period that was monitored no unexplainable artifacts remain, requiring fundamental reconsideration of the assumptions about the workings of soil S dynamics. At this point, it seems like we cover all essential processes, necessary to illustrate a comprehensive picture of the stands' current S cycling.

The code file of the model will be provided by the authors after request

Filename: CODE_WBM_SDM.sas.

Title: Code file (Base SAS 9.4) for the WBM and the SDM.

Description: The file contains the code for all model functions which are utilized in the Water Balance Model (WBM) and the Sulfur Dynamics Model (SDM).

Recommended citation: *this publication: code file of the Water Balance Model (WBM) and the Sulfur Dynamics Model (SDM).*

Acknowledgements This research was funded by the Austrian Science Fund (FWF, project number P23861-B16, granted to TW Berger) and the Commission for Interdisciplinary Ecological Studies (KIÖS) at the Austrian Academy of Sciences (Project Number 2010-05, granted to TW Berger). Open access funding was provided by the University of Natural Resources and Life Sciences Vienna (BOKU). For her active support during the field campaign, we thank Pétra Berger. For the possibility to access air temperature data, the providers in the ECA&D project are acknowledged. We thank the ZAMG and the Austrian Hydrographic Service (eHYD) for the provision of meteorological data, which was used for gap filling purposes. For the provision of temperature and precipitation records, we thank the operator of a private weather station, Thomas Huber. We acknowledge the possibility to use records of SO_2 provided online by the Umweltbundesamt. We thank Wolfgang Schöpp, Maximilian Posch, Sophia Mylona and Matti Johansson for the possibility to use estimates for historic S deposition for our desired EMEP grid cells (Schöpp et al. 2003). Finally, we thank for anonymous critical comments for the improvement of this paper.

Appendix

To achieve sigmoid shape transitions of a variables (x) response (y) inside a window (x_0–x_1), the Smoothstep function (compare Dolschak et al. 2015) was applied in several cases. y_0 and y_1 state left and right threshold responses, respectively. The variable x has to be normalized into an auxiliary variable (t) inside the interval 0–1.

$$t = \frac{x - x_0}{x_1 - x_0} \tag{26}$$

The transition is described using a third-order polynomial.

$$y = \begin{cases} y_0, & x \le x_0 \\ y_0 + \left(y_1 - y_0\right)\left(3t^2 - 2t^3\right), & x_0 < x < x_1 \\ y_1, & x \ge x_1 \end{cases} \tag{27}$$

In the article, the Smoothstep function is stated as:

$$y = smooth\left(x,\ x_0,\ x_1,\ y_0,\ y_1\right) \tag{28}$$

References

Alewell C (2001) Predicting reversibility of acidification: the European sulfur story. Water Air Soil Pollut 130:1271–1276

Alewell C et al (2001) Are there signs of acidification reversal in freshwaters of the low mountain ranges in Germany? Hydrol Earth Syst Sci 5:367–378

Auer I, Böhm R, Mohnl H (1989) Klima von Wien: eine anwendungsorientierte Klimatographie. Beiträge zur Stadtforschung, Stadtentwicklung und Stadtgestaltung. Stadt Wien, Magistratsabteilung 18 - Stadtentwicklung und Stadtplanung, Vienna

Aulakh MS, Jaggi RC, Sharma R (2002) Mineralization-immobilization of soil organic S and oxidation of elemental S in subtropical soils under flooded and nonflooded conditions. Biol Fertil Soils 35:197–203

Berger TW, Muras A (2016) Predicting recovery from acid rain using the micro-spatial heterogeneity of soil columns downhill the infiltration zone of beech stemflow: introduction of a hypothesis. Model Earth Syst Environ 2(3):154

Berger TW, Untersteiner H, Toplitzer M, Neubauer C (2009) Nutrient fluxes in pure and mixed stands of spruce (*Picea abies*) and beech (*Fagus sylvatica*). Plant Soil 322:317–342

Buchner P, Takahashi H, Hawkesford MJ (2004) Plant sulphate transporters: co-ordination of uptake, intracellular and long-distance transport. J Exp Bot 55:1765–1773

Chowdhury MAH, Kouno K, Ando T (1999) Correlation among microbial biomass S, soil properties, and other biomass nutrients. Soil Sci Plant Nutr 45:175–186

Cosby BJ, Ferrier RC, Jenkins A, Wright RF (2001) Modelling the effects of acid deposition: refinements, adjustments and inclusion of nitrogen dynamics in the MAGIC model. Hydrol Earth Syst Sci Dis 5:499–518

Dolschak K, Gartner K, Berger TW (2015) A new approach to predict soil temperature under vegetated surfaces. Model Earth Syst Environ 1(4):1–14

Dolschak K, Gartner K, Berger TW (2019) The impact of rising temperatures on water balance and phenology of European beech (*Fagus sylvatica* L.) stands. Model Earth Syst Environ 5(4):1–17

Fowler D, Cape JN, Unsworth MH (1989) Deposition of atmospheric pollutants on forests. Philos Trans R Soc Lond B Biol Sci 324(1223):247–265

Gbondo-Tugbawa SS, Driscoll CT, Aber JD, Likens GE (2001) Evaluation of an integrated biogeochemical model (PnET-BGC) at a northern hardwood forest ecosystem. Water Resour Res 37:1057–1070

Ghani A, McLaren RG, Swift RS (1993) The incorporation and transformations of 35 S in soil: effects of soil conditioning and glucose or sulphate additions. Soil Biol Biochem 25:327–335

Hanousek O, Prohaska T, Kulhanek M, Balik J, Tejnecky V, Berger TW (2017) Fractionation of sulfur (S) in beech (*Fagus sylvatica*) forest soils in relation to distance from the stem base as useful tool for modeling S biogeochemistry. Model Earth Syst Environ 3:1065–1079

Havlin JL, Beaton JD, Tisdale SL (2005) Soil fertility and fertilizers an introduction to nutrient management. Pearson, Prentice Hall, Upper Saddle River

Herschbach C, Rennenberg H (2001) Sulfur nutrition of deciduous trees. Naturwissenschaften 88(1):25–36

IUSS Working Group, W., 2006. World reference base for soil resources. World Soil Resources Report, 103

Janzen HH, Bettany JR (1987) The effect of temperature and water potential on sulfur oxidation in soils. Soil Sci 144:81–89

Kertesz MA, Mirleau P (2004) The role of soil microbes in plant sulphur nutrition. J Exp Bot 55:1939–1945

Kirkpatrick S (1984) Optimization by simulated annealing—quantitative studies. J Stat Phys 34(5–6):975–986

Klemm O, Wrzesinsky T (2007) Fog deposition fluxes of water and ions to a mountainous site in Central Europe. Tellus Ser B Chem Phys Meteorol 59:705–714

Kreuzwieser J, Rennenberg H (1998) Sulphate uptake and xylem loading of mycorrhizal beech roots. New Phytol 140(2):319–329

Kulhánek M, Černý J, Balík J, Vaněk V, Sedlář O (2011) Influence of the nitrogen-sulfur fertilizing on the content of different sulfur fractions in soil. Plant Soil Environ 57(12):553–558

Lange CA, Matschullat J, Zimmermann F, Sterzik G, Wienhaus O (2003) Fog frequency and chemical composition of fog water—a relevant contribution to atmospheric deposition in the eastern Erzgebirge, Germany. Atmos Environ 37(26):3731–3739

Likens GE et al (2002) The biogeochemistry of sulfur at Hubbard Brook. Biogeochemistry 60:235–316

McGill W, Cole C (1981) Comparative aspects of cycling of organic C, N, S and P through soil organic matter. Geoderma 26(4):267–286

Mitchell MJ, Likens GE (2011) Watershed sulfur biogeochemistry: shift from atmospheric deposition dominance to climatic regulation. Environ Sci Technol 45(12):5267–5271

Mitchell MJ et al (2001) Use of stable isotope ratios for evaluating sulfur sources and losses at the Hubbard Brook Experimental Forest. Water Air Soil Pollut 130(1–4):75–86

Moyano FE et al (2012) The moisture response of soil heterotrophic respiration: interaction with soil properties. Biogeosciences 9:1173–1182

Nash JE, Sutcliffe JV (1970) River flow forecasting through conceptual models part I - A discussion of principles. J Hydrol 10(3):282–290

Novák M et al (2000) Sulfur isotope dynamics in two Central European watersheds affected by high atmospheric deposition of SOx. Geochim Cosmochim Acta 64:367–383

Pannatier EG, Thimonier A, Schmitt M, Walthert L, Waldner P (2011) A decade of monitoring at Swiss Long-Term Forest Ecosystem Research (LWF) sites: can we observe trends in atmospheric acid deposition and in soil solution acidity? Environ Monit Assess 174:3–30

Prechtel A et al (2001) Response of sulphur dynamics in European catchments to decreasing sulphate deposition. Hydrol Earth Syst Sci 5:311–325

Prechtel A, Armbruster M, Matzner E (2003) Modelling sulphate stream concentrations in the Black Forest catchments Schluchsee and Villingen. Hydrol Earth Syst Sci Discuss Eur Geosci Union 7(4):552–560

Rennenberg H, Brunold C, De Kok L, Stulen I (1990) Sulfur nutrition and sulfur assimilation in higher plants. SPB Academic Publishing, The Hague

Scherer HW (2009) Sulfur in soils. J Plant Nutr Soil Sci 172:326–335

Schöpp W, Posch M, Mylona S, Johansson M (2003) Long-term development of acid deposition (1880–2030) in sensitive freshwater regions in Europe. Hydrol Earth Syst Sci Dis 7(4):436–446

Sierra CA, Trumbore SE, Davidson EA, Vicca S, Janssens I (2015) Sensitivity of decomposition rates of soil organic matter with respect to simultaneous changes in temperature and moisture. J Adv Model Earth Syst 7:335–356

Solberg ED, Malhi SS, Nyborg M, Gill KS (2005) Temperature, soil moisture, and antecedent sulfur application effects on recovery of elemental sulfur as SO4-S in incubated soils. Commun Soil Sci Plant Anal 36:863–874

Sverdrup H, Belyazid S, Nihlgård B, Ericson L (2007) Modelling change in ground vegetation response to acid and nitrogen pollution, climate change and forest management at in Sweden 1500–2100 AD. Water Air Soil Pollut Focus 7(1–3):163–179

Tabatabai MA (1996) Sulfur. Methods of Soil Analysis Part 3. Chemical Methods. Soil Science Society of America, American Society of Agronomy, Madison

Umweltbundesamt (2018) Emissionstrends 1990–2016: Ein Überblick über die Verursacher von Luftschadstoffen in Österreich, Umweltbundesamt GmbH, Vienna

Watmough SA et al (2005) Sulphate, nitrogen and base cation budgets at 21 forested catchments in Canada, the United States and Europe. Environ Monit Assess 109(1–3):1–36

Zhang Y, Mitchell MJ, Christ M, Likens GE, Krouse HR (1998) Stable sulfur isotopic biogeochemistry of the Hubbard Brook experimental forest, New Hampshire. Biogeochemistry 41(3):259–275

11 Curriculum Vitae

PERSONAL DATA

Dipl.-Ing. Klaus Dolschak

📍 Seuttergasse 17/1/7, 1130 Vienna, Austria
✉ klaus.dolschak@gmx.at
☎ +43 676 7120699

Date of birth 22.09.1980 | Birthplace Graz | Nationality Austria

WORK EXPERIENCE

BILLA AG, Wiener Neudorf, Austria 01/2017 –
Data Scientist

UNIVERSITY OF NATURAL RESOURCES AND LIFE SCIENCES VIENNA, AUSTRIA 02/2012 – 06/2016
Research Assistant

FEDERAL RESEARCH AND TRAINING CENTRE FOR FORESTS, NATURAL HAZARDS AND LANDSCAPE AUSTRIA, VIENNA 11/2011 – 01/2012
Research Assistant

FEDERAL RESEARCH AND TRAINING CENTRE FOR FORESTS, NATURAL HAZARDS AND LANDSCAPE AUSTRIA, VIENNA 09/2011 – 10/2011
Internship

EDUCATION

UNIVERSITY OF NATURAL RESOURCES AND LIFE SCIENCES VIENNA, AUSTRIA 02/2012 – 06/2020
Doctoral Program (Wood and Forest Sciences)
Doctoral Thesis:

- *A modeling framework for temperate deciduous forest stands plus selected applications in drought assessment and sulfur (S) biogeochemistry at beech (Fagus sylvatica L.) stands in the Vienna Woods*

UNIVERSITY OF NATURAL RESOURCES AND LIFE SCIENCES VIENNA, AUSTRIA 02/2007 – 10/2010
Individual Diploma Study Program (Anthropogenic Ecosystems and Global Change)
Diploma Thesis:

- *Vergleichende Bodenuntersuchungen in reinen und gemischten Fichten- und Buchenbeständen auf Flysch und Molasse*

UNIVERSITY OF NATURAL RESOURCES AND LIFE SCIENCES VIENNA, AUSTRIA 10/2000 – 02/2007
Diploma Study Program (Agriculture)

LANGUAGES

German	mother tongue
English	quasi-fluently
Italian	basic knowledge

PUBLICATIONS

Dolschak, K., Jandl, R., & Ledermann, T. (2013). Coupling a forest growth model with a soil carbon simulator. Management Strategies to Adapt Alpine Space Forests to Climate Change Risks, 211.

Jandl, R., Breznikar, A., Lekše, M., Tomiczek, C., Schüler, S., Dolschak, K., & Zöscher, H. (2013). Case Study Carinthia/Slovenia–Productive Forests Affected by Climate Change (pp. 303-321). BoD–Books on Demand.

Dolschak K, Gartner K, Berger TW (2015): A new approach to predict soil temperature under vegetated surfaces. Modeling Earth Systems and Environment DOI: 10.1007/s40808-015-0041-2

Dolschak K, Berger TW (2019): The Impact of rising Temperatures on Water Balance and Phenology of European Beech (Fagus Sylvatica L.) Stands. Modeling Earth Systems and Environment DOI: 10.1007/s40808-019-00602-1

Dolschak K, Berger TW (2020): Modeling the sulfur biogeochemistry of beech (Fagus Sylvatica L.) stands in the Vienna Woods. Modeling Earth Systems and Environment DOI: 10.1007/s40808-020-00770-5

ORAL PRESENTATIONS

Dolschak, K, Berger, TW (2015): Modeling sulfur biogeochemistry of beech (Fagus sylvatica) stands at the Vienna Woods. 4th ICP Forests Scientific Conference, Ljubljana, SLOVENIA, MAY 19-20, 2015.